



Université
de Toulouse

THÈSE

En vue de l'obtention du

DOCTORAT DE L'UNIVERSITÉ DE TOULOUSE

Délivré par :

Université Toulouse 3 Paul Sabatier (UT3 Paul Sabatier)

Présentée et soutenue par :

NGUYEN Hong Hanh

Le mardi 28 octobre 2014

Titre :

Core-shell structures based on dendritic polymers sensitive to external stimuli:
applications to the synthesis of gold nano hybrid materials

ED SDM : Chimie macromoléculaire et supramoléculaire - CO044

Unité de recherche :

Laboratoire IMRCP UMR 5623

Directeur(s) de Thèse :

Dr. Jean-Daniel MARTY
Prof. Nancy LAUTH-DE VIGUERIE

Rapporteurs :

Dr. Delphine FELDER-FLESCH, IPCMS, Strasbourg
Dr. Min-Hui LI, Institut Curie, Paris

Autre(s) membre(s) du jury :

Prof. Fabien DELPECH, LCPNO, Toulouse
Dr. Jean-Christophe ROSSI, IBMM, Montpellier

Dành cho bố mẹ và em gái,

Dành cho Tấn,

Pour mes parents, ma sœur,

Pour Tan,

Remerciements - Lòi cảm ơn

En premier lieu, je tiens à exprimer ma plus profonde gratitude à mes directeurs de thèses Mme Nancy De Viguerie et M Jean-Daniel Marty pour avoir assuré la direction scientifique de ce travail de recherche, pour la confiance qu'ils m'ont accordée et leur soutien déterminant tout au long de ces trois années.

Je veux adresser mes plus vifs remerciements à l'ensemble des personnes qui m'ont fait l'honneur de juger ce travail. Plus particulièrement, je veux faire part de ma reconnaissance à Monsieur Fabien Delpech pour m'avoir fait l'honneur d'accepter de présider le jury, à Madame Min-Hui Li et Madame Delphine Delder-Flesh pour avoir bien voulu juger ce travail et en être les rapporteurs ainsi qu'à Monsieur Jean-Christophe Rossi pour m'avoir fait le plaisir d'accepter de participer au jury.

Je remercie Madame Monique Mauzac pour m'avoir accueillie au sein du laboratoire IMRCP ainsi que tous les membres du laboratoire des IMRCP. Je remercie Madame Anne Jonquière, mon encadrante de Master 2 qui m'a présenté cette opportunité de venir faire une thèse à Toulouse.

Je tiens à remercier mes collaborateurs pour leurs contributions à cette thèse : Annie Brûlet, Clara Valverde Serrano, Juliette Fitremann, Pierre Lavedan, Dominique Goudenèche, Bruno Payré, Corinne Routaboul, Pascal Saint-Aguet, Paul Château, Thomas Faure. J'ai beaucoup apprécié votre gentillesse et c'est un plaisir d'avoir travaillé avec vous. Je remercie également Anne-Françoise pour son aide et ses précieux conseils scientifiques. Je remercie Florence F. pour son aide administrative ainsi que pour sa gentillesse.

Je veux exprimer ma reconnaissance à Monsieur Christophe Mingotaud et l'ensemble de l'équipe IDEAS : Stéphane G., Clément, Véronique P., Jean-Claude, Christophe C., Barbara, Charles-Louis qui par leur bonne humeur et leur gentillesse ont rendu mes trois années de travail plus agréable.

Je remercie les collègues avec lesquels j'ai partagé de nombreux bons moments durant cette période de ma vie : Annas, Lacra, Alix, Aurélie(s), Baptiste, Ugo, Dan, Béatrice, Joris, Cécile, Ophélie, Lucie(s), Camille, Xuan, Stéphane L., Claire, Jean-Noël, Guillaume(s), Etienne, Dimitri,

Emmanuelle ... Je regrette de ne pas avoir profité de toutes les soirées et les apéros chez chacun ou au bord de la Garonne, mais les quelques soirées auxquelles j'ai participé resteront de très bons souvenirs en moi. Je remercie les amis qui ont fait un travail formidable pour mon pot de thèse !

Je suis comblée par le soutien et l'aide de mes amis vietnamiens à Toulouse ou au Vietnam: Bai, Chi, Mai, Hiep, Da, Hoan, Thu, Ly, Liem, Trang, Tham, Phuong Anh. Grace à vous, ces trois années sont passées très vite.

Véronique G. merci pour ta bonne humeur et pour ton aide, en plus d'être une collègue tu es devenue une bonne amie pour moi. Paty, ma belle, grâce à toi j'ai pu me rapprocher à la bande non-permanant du labo. Marie, je te remercie pour tout le temps qu'on a partagé, pour ton aide et pour ta gentillesse, tu es une fille formidable. Cette amitié tissée entre nous ne sera jamais perdue en moi.

Enfin, je pense à toutes les personnes qui me tiennent à cœur, sans eux je n'aurais pas pu finir cette thèse. Luyen, ma chérie, ma meilleure amie, je ne saurais pas dire combien tu comptes pour moi. Merci d'être à mes côtés et d'avoir toujours confiance en moi. Julien, tes grandes épaules ont supportées toutes mes tristesses, ma peine d'être loin de ma famille et le stress du travail. Merci de me donner ton amour, merci d'être là pour moi. Finalement, je tiens à remercier profondément ma famille qui m'a toujours accordé tout son amour et son soutien infini.

Con cảm ơn bố mẹ đã cho con có ngày hôm nay, đã luôn thương yêu và ủng hộ con. Cảm ơn em gái đã luôn gần gũi thân thiết với chị dẫu khoảng cách xa xôi. Con cảm ơn đại gia đình hai bên nội ngoại đã luôn ủng hộ và tự hào về con.

A la mémoire de ma grand-mère et Tấn.

Abbreviations

ATRP	Atom transfer radical polymerization
Au NPs	Gold nanoparticles
Au NRs	Gold nanorods
BPEA	2-((2-bromopropionyl)oxy)ethyl acrylate
CDI	1,1'-Carbonyldiimidazole
CGC	Critical gel concentration
CRP	Control radical polymerization
DB	Degree of branching
DCC	dicyclohexyl carbodiimide
DGL	Dendrigrft polylysine
DLS	Dynamique light scattering
DOX	Doxorubicin
DP	Dendritic polymers
DSC	Differential scanning calorimetry
HBP	Hyperbranched polymer
HBP(CL-co-BOD)	Hyperbranched Poly(ϵ -caprolactone-4,4-bioxepanyl-7,7-dione)
HBPL	Hyperbranched polylysine
HBPO	Hyperbranched poly(3-ethyl-3-oxetanemethanol)
HBPPA	Hyperbranched poly(phenylacethylene)
HOP	Hydrophobic oligopeptide
HPEE	Hyperbranched polyethylene
HPEG	Hyperbranched polyethylene glycol
HPEI	Hyperbranched Polyethylenimine
HPG	Hyperbranched polyglycerol
HPTAM	Hyperbranched poly(tertiary amino methacrylate)
HYPAM	Hyperbranched Polyamidoamide
LC	Liquid crystal
LCHBP	Liquid crystalline hyperbranched polymers
LCST	Lower critical solution temperature
LSPR	localized surface plasmon resonance
Mn	Number average molecular weight
Mw	Weight average molecular weight
NaBH ₄	Sodium tetrahydridoborate
NIR	Near infrared
NMR	Nuclear magnetic resonance
NMRP	Nitroxide-mediated radical polymerization
PAA	Poly(acrylic acid)
PAMAM	Dendrimer Polyamidoamide
PASA	poly(aspartic acid)
PCL	Poly(ϵ -caprolactone)
PDEGMA	poly(diethylene glycol methyl ether methacrylate)
PDI	Polydispersity index
PDI	Polydispersity index
PDMA	Poly(2-(dimethylamino)ethyl methacrylate)
PDMA	Poly(dimethylacrylamide)
PDMAEMA	N,N-dimethylamino-2-ethyl methacrylate

Abbreviations

PEG	Poly(ethylene glycol)
PEI	Poly(ethylene imine)
PEO	Poly(ethylene oxide)
PFG-NMR	Pulsed field gradient NMR
PIC	Polyion complex
PLL	Poly(L-lysine)
PLLA	Poly(L-lactic acid)
PMAA	Poly(methacrylic acid)
PNIPAM ou PNIPAm ou PNIPA	Poly(N-isopropylacrylamide)
POM	Polarized light optical microscopy
PPG	Poly(propylene glycol)
PPI	Poly(propylene imine)
ppm	Parts per million
PVA	Poly(vinyl alcohol)
PVCL	Poly(N-vinylcaprolactam)
PVME	Poly(vinyl methyl ether)
PVP	Poly(vinyl pyrrolidone)
PVP	Poly(vinylpyrrolidinone)
r.t.	Room temperature
RAFT	Reversible addition-fragmentation chain transfer
ROP	Ring opening polymerization
SANS	Small-angle neutron scattering
SAXS	Small-angle X-ray scattering
SCVP	Self-condensing vinyl polymerization
SEC	size exclusion chromatography
SERS	Surface-enhanced Raman scattering
SLS	Statistic light scattering
SRCSP	Stimuli-responsive core-shell polymers
T _c	Cloud point temperature

Table of contents

INTRODUCTION	1
CHAPTER 1. LITERATURE REVIEW	5
I. CORE-SHELL ARCHITECTURES BASED ON DENDRITIC POLYMERS	9
A. DENDRITIC POLYMERS	10
1. <i>Dendrimers</i>	10
2. <i>Hyperbranched polymers</i>	11
3. <i>Dendrigrfts</i>	12
B. CORE-SHELL DENDRITIC POLYMERS	13
1. <i>Core-first method</i>	15
2. <i>Coupling-onto method</i>	16
3. <i>Ionic interactions</i>	18
C. STIMULI-RESPONSIVE CORE-SHELL DENDRITIC POLYMERS	22
1. <i>Temperature responsive materials</i>	22
a. Solution of thermoresponsive polymers	23
b. Gels	26
c. Liquid crystalline materials	30
2. <i>pH responsive materials</i>	38
3. <i>Light and redox responsive materials</i>	42
4. <i>Conclusions</i>	44
II. NANO-HYBRID MATERIALS FROM POLYMERIC NANOSTRUCTURED SOFT- TEMPLATE	44
A. NANO-HYBRID MATERIALS	45
1. <i>Nanoparticles: some generalities</i>	45
a. Introduction	45
b. Gold nanoparticles	46
2. <i>Synthesis of nano-hybrid materials</i>	50
B. NANOPARTICLES STABILIZATION IN POLYMERIC AQUEOUS SOLUTION	50
1. <i>Introduction</i>	50
2. <i>In situ synthesis of nanoparticles</i>	52
3. <i>Stabilization of preformed nanoparticles</i>	57
a. Grafting from	57
b. Grafting to	57
4. <i>Stimuli-responsive nanohybrid</i>	59
5. <i>Conclusions</i>	62
C. NANOPARTICLES WITHIN GEL STRUCTURES	62
1. <i>Introduction</i>	62
2. <i>Ex situ synthesis of gel nanoparticles hybrids</i>	63
3. <i>In situ synthesis of nanoparticles</i>	64

4.	<i>Stimuli-responsive gel nanohybrid</i>	65
5.	<i>Conclusions</i>	67
D.	NANOPARTICLES AND POLYMERIC LIQUID CRYSTALS	68
1.	<i>Introduction</i>	68
2.	<i>Stabilization of preformed nanoparticles</i>	69
3.	<i>In situ synthesis of nanoparticles</i>	72
a.	Solvent mediated in situ formation of NPs/LC hybrids	73
b.	Solvent-free in situ formation of NPs/LC hybrids	73
c.	Effect of LC organization and structure on nanoparticle growth	75
4.	<i>Conclusion</i>	79
III.	OBJECTIVES OF THE PROJECTS	80
IV.	REFERENCES	82
 CHAPTER 2. THERMORESPONSIVE HYPERBRANCHED POLYMER: SYNTHESIS, CHARACTERIZATION AND APPLICATIONS FOR THE SYNTHESIS OF GOLD NANOSTRUCTURES		93
I.	INTRODUCTION	97
II.	SYNTHESIS AND CHARACTERIZATION OF THE HYPERBRANCHED POLYMERS CONSISTING OF THE PNIPAM SHELL AND HYPERBRANCHED POLYAMIDOAMINE CORE	98
A.	HYPERBRANCHED POLY(AMIDOAMINE)	98
1.	<i>Synthesis</i>	98
2.	<i>Characterization</i>	99
a.	NMR	99
b.	Quantification of number primary amine groups	99
c.	Determination of average molecular weights	102
d.	SANS measurements	103
B.	HYPERBRANCHED CORE-SHELL POLYMERS	104
1.	<i>Synthesis by CDI activated coupling</i>	104
2.	<i>Characterization of core-shell polymers</i>	105
a.	Evaluation of grafting efficiency	105
b.	Evaluation of grafting ratios	112
III.	PROPERTIES OF AQUEOUS SOLUTIONS OF HYPERBRANCHED POLYMERS	116
1.	<i>Behavior in diluted solution</i>	116
2.	<i>Thermoresponsive properties</i>	118
IV.	STABILIZATION AND IN SITU SYNTHESIS OF GOLD NANOCOMPOSITES	123
A.	EX SITU SYNTHESIS AND STABILIZATION OF GOLD NANOPARTICLES	124
1.	<i>Preformed Au NPs</i>	124
2.	<i>Stabilization of Au NPs by PNIPAM based hyperbranched polymer</i>	125

a.	Synthesis of Au NPs nanocomposite	125
b.	Salt adding effect	127
c.	Thermoresponsive properties	130
B.	IN SITU SYNTHESIS OF GOLD NANOPARTICLES	135
1.	<i>In situ synthesis of Au NPs by using NaBH₄ as reductant</i>	135
2.	<i>Architecture effect on the size of formed Au NPs</i>	135
V.	CONCLUSIONS	138
VI.	REFERENCES	138

CHAPTER 3. HYDROGEL-NANOCOMPOSITES BASED ON THERMOGELS OF HYPERBRANCHED POLYAMIDOAMINE AND POLY(N-ISOPROPYLACRYLAMIDE) CORE-SHELL POLYMERS 141

I.	INTRODUCTION	145
II.	SYNTHESIS AND CHARACTERIZATION OF THERMOGELS OF HYPERBRANCHED POLYAMIDOAMINE AND POLY(N-ISOPROPYLACRYLAMIDE) CORE-SHELL POLYMERS	147
A.	SYNTHESIS OF THE THERMORESPONSIVE HYDROGELS	147
1.	<i>Synthesis of polymers</i>	147
2.	<i>Synthesis of thermoresponsive hydrogels</i>	148
B.	CHARACTERIZATION OF THE HYDROGELS	148
1.	<i>Sol-gel transition</i>	148
2.	<i>Structure of the gels by cryo-SEM</i>	150
3.	<i>Rheological measurements</i>	152
4.	<i>UV following of thermoreversibility</i>	152
III.	IN SITU SYNTHESIS OF GOLD NANOPARTICLES IN THE GELS	153
A.	IN SITU SYNTHESIS OF AUNPS	153
B.	EFFECT OF AUNPS ON THE PROPERTIES OF THE HYBRID GELS	154
1.	<i>Structure of the gels</i>	154
2.	<i>Sol-gel transition</i>	155
a.	DSC	155
b.	Rheological measurements	157
3.	<i>Gel strength</i>	158
4.	<i>UV following of thermoreversibility</i>	159
IV.	CONCLUSIONS	159
V.	REFERENCES	160

CHAPTER 4. MESOMORPHIC IONIC HYPERBRANCHED POLYMERS: EFFECT OF STRUCTURAL PARAMETERS ON LIQUID-CRYSTALLINE PROPERTIES AND ON THE FORMATION OF GOLD NANOHYBRIDS	163
I. INTRODUCTION	167
II. SYNTHESIS AND CHARACTERIZATION OF THE HYPERBRANCHED-DODECYL SULFATE COMPLEXES	169
A. HYPERBRANCHED POLY(AMIDOAMINE)	169
B. MESOMORPHIC IONIC HYPERBRANCHED POLYMERS	169
1. <i>Synthesis</i>	169
2. <i>Characterization of the interaction between the core and the shell</i>	170
a) Interaction between the core and the shells by FT-IR	170
b) Interaction between the core and the shells by ¹ H NMR and 1D NOE experiment	171
3. <i>Quantification of functionalization degree</i>	172
4. <i>Behavior in solution and formation of aggregates</i>	174
a) Behavior in solution	174
b) Formation of aggregates	178
III. THERMAL AND MESOMORPHIC PROPERTIES	180
A. STUDY OF THERMAL PROPERTIES BY DSC AND POM	180
1. <i>Experimental conditions of DSC measurements</i>	180
2. <i>Phase transitions</i>	181
B. PHASE IDENTIFICATION OF HYPAM-DS100	183
1. <i>POM-SAXS-DSC studies for H4-DS100</i>	183
2. <i>FT-IR</i>	186
3. <i>Conclusion</i>	187
C. EFFECT OF STRUCTURAL PARAMETERS	187
1. <i>Effect of the core molar mass</i>	187
2. <i>Hydrophilic/hydrophobic composition balance</i>	191
3. <i>Effect of the nature of the core: Dendrimer vs hyperbranched core</i>	192
D. CONCLUSIONS	193
IV. IN SITU FORMATION OF GOLD NPS	194
A. SYNTHESIS OF AUNPS IN LC MATRIX	194
1. <i>Interaction between HAuCl₄ and the core HYPAM</i>	194
2. <i>Synthesis process</i>	195
B. MESOMORPHIC PROPERTIES OF HYBRID MATERIALS OF H4-DS100@AUNPS	196
C. MORPHOLOGY OF THE <i>IN SITU</i> SYNTHESIZED AUNPS WITHIN MESOPHASES OF H4-DS100	199

D.	THE EFFECT OF MOLECULAR ARCHITECTURE ON THE FORMATION OF GOLD NPS	201
V.	CONCLUSIONS	204
VI.	REFERENCES	205
	CHAPTER 5. POLYION COMPLEX BASED ON DENDRITIC POLYMERS	209
I.	INTRODUCTION	213
II.	FORMATION OF PICS BASED ON DENDRITIC ELECTROLYTES	214
A.	ASSOCIATION OF HYPERBRANCHED POLYAMIDOAMIDE POLYMERS AND POLY(ETHYLENE OXIDE)-B-POLY(ACRYLIC ACID) COPOLYMERS PEO6-PAA6.5	214
1.	<i>Characterization of formed PICS</i>	214
2.	<i>Stability of formed PICS</i>	218
B.	INFLUENCE OF THE STRUCTURAL PARAMETERS	220
1.	<i>Change of hyperbranched electrolytes</i>	220
2.	<i>Change of composition of block copolymers</i>	222
C.	PICS BASED ON DENDRIGRAFT POLYLYSINE	223
D.	PICS BASED ON PAMAM DENDRIMERS	224
E.	CONCLUSION	225
III.	THERMORESPONSIVE PICS	225
A.	THERMORESPONSIVE PICS BASED ON HYPERBRANCHED POLYAMIDOAMINE H4	226
1.	<i>Formation and stabilization of PICS</i>	226
2.	<i>Thermoresponsive properties</i>	227
B.	THERMORESPONSIVE PICS BASED ON DENDRIGRAFT POLYLYSINE DGL3	230
1.	<i>Formation and stabilization of PICS</i>	230
2.	<i>Stability of PICS colloidal solution</i>	230
3.	<i>Thermoresponsive properties</i>	232
IV.	CONCLUSION	236
V.	REFERENCES	236
	CONCLUSION	239
	EXPERIMENTAL SECTION	ES-1
	APPENDIX	A-1

Introduction

During the past decades, developments in the fabrication of stimuli responsive materials have opened new ways and possibilities towards novel technologies in a vast range of fields including high-tech electronics, medical diagnostics, cosmetics and many more. The interest behind the synthesis of such materials lies on their exclusive properties sensitive to external stimulus *e.g.* temperature responsive transporters in drug delivery.

Since nanotechnological applications depend on the structural properties and organization of nanoobjects, the driving force for nanoscience today is the development of new synthetic procedures, which allow to control over these properties. As a results, this instigated interest in the field of polymeric assembled structure. This project addresses the use of different assembled structures (lyotropic aggregates, hydrogels, liquid crystals) based on dendritic polymers for the synthesis of gold nanohybrid materials.

Although the synthesis of gold nanoparticles with control in size, shape and dispersion is one of the most investigated subjects in the last century, it is still a today's attracted topic especially in the context of emerging nanoscience and nanotechnology with nanoparticles. Dendritic polymers have high molecular weights, globular structures and a lot of intramolecular cavities, showing superb capability in the synthesis of monodispersed and ultra-stable nanoparticles. In addition, dendritic polymers can be modified to reach stimuli-responsive core-shell architectures which are able to regenerate self-assembled structures presenting ideal candidates for soft-templating of nanoparticles.

In the literature we find different kinds of core-shell structures based on dendritic polymers by both covalent and non-covalent grafting approaches. Nanohybrid materials may be formed by *in situ* synthesis of gold nanoparticles within host structures or *ex situ* method through doping of gold nanoparticles with host structures. **Chapter 1** is a literature overview, describing the above strategies. This account on prior research allowed us to evaluate the required improvements over existing systems and identify desired materials that have not yet been described. The principal objectives are disclosed in the closing section of this overview.

In **Chapter 2**, we address the synthesis of thermoresponsive core-shell polymers, their organization in diluted aqueous solution and their use as stabilizer for gold nanoparticles as well as medium for the *in situ* synthesis of the latter. **Chapter 3** will present the study on hydrogel states of these thermoresponsive core-shell polymers and their use as soft-template for the *in situ* synthesis of gold nanoparticles.

Chapter 4 covers the studies on liquid crystal phases resulted from ionic interaction between dendritic core and surfactants as well as their use as soft-template for the *in situ* synthesis of gold nanoparticles.

Chapter 5 gives an account on the formation of polyion complex based on dendritic core and ionic (thermoresponsive) copolymers and the studies on their responsiveness to external stimuli such as pH, ionic strength and temperature.

Finally a general conclusion will close this thesis.

Chapter 1

Literature Review

CONTENTS

I. CORE-SHELL ARCHITECTURES BASED ON DENDRITIC POLYMERS.....	9
A. DENDRITIC POLYMERS.....	9
1. <i>Dendrimers</i>	10
2. <i>Hyperbranched polymers</i>	11
3. <i>Dendrigrfts</i>	12
B. CORE-SHELL DENDRITIC POLYMERS	13
1. <i>Core-first method</i>	15
2. <i>Coupling-onto method</i>	16
3. <i>Ionic interactions</i>	18
C. STIMULI-RESPONSIVE CORE-SHELL DENDRITIC POLYMERS	22
1. <i>Temperature responsive materials</i>	22
a. Solution of thermoresponsive polymers.....	23
b. Gels.....	26
c. Liquid crystalline materials.....	30
i) Main characteristics of liquid crystalline materials	30
ii) Branched Polymeric liquid crystals.....	32
2. <i>pH responsive materials</i>	38
3. <i>Light and redox responsive materials</i>	42
4. <i>Conclusions</i>	44
II. NANO-HYBRID MATERIALS FROM POLYMERIC NANOSTRUCTURED SOFT-TEMPLATE	
44	
A. NANO-HYBRID MATERIALS	45
1. <i>Nanoparticles: some generalities</i>	45
a. Introduction.....	45
b. Gold nanoparticles	46
i) Properties of gold nanoparticles	46
ii) Synthesis methods of AuNPs	48
2. <i>Synthesis of nano-hybrid materials</i>	50
B. NANOPARTICLES STABILIZATION IN POLYMERIC AQUEOUS SOLUTION	50
1. <i>Introduction</i>	50
2. <i>In situ synthesis of nanoparticles</i>	52
3. <i>Stabilization of preformed nanoparticles</i>	57
a. Grafting from	57
b. Grafting to.....	58
4. <i>Stimuli-responsive nanohybrid</i>	59
5. <i>Conclusions</i>	62
C. NANOPARTICLES WITHIN GEL STRUCTURES	62


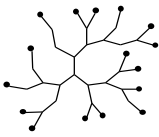
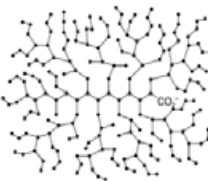
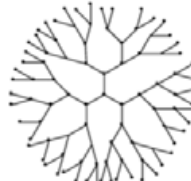
1.	<i>Introduction</i>	62
2.	<i>Ex situ synthesis of gel nanoparticles hybrids</i>	63
3.	<i>In situ synthesis of nanoparticles</i>	64
4.	<i>Stimuli-responsive gel nanohybrid</i>	65
5.	<i>Conclusions</i>	67
D.	NANOPARTICLES AND POLYMERIC LIQUID CRYSTALS	68
1.	<i>Introduction</i>	68
2.	<i>Stabilization of preformed nanoparticles</i>	69
3.	<i>In situ synthesis of nanoparticles</i>	72
a.	Solvent mediated in situ formation of NPs/LC hybrids.....	73
b.	Solvent-free in situ formation of NPs/LC hybrids.....	73
c.	Effect of LC organization and structure on nanoparticle growth.....	75
4.	<i>Conclusion:</i>	79
III.	OBJECTIVES OF THE PROJECTS	80
IV.	REFERENCES	82

I. Core-shell architectures based on dendritic polymers

A. Dendritic polymers

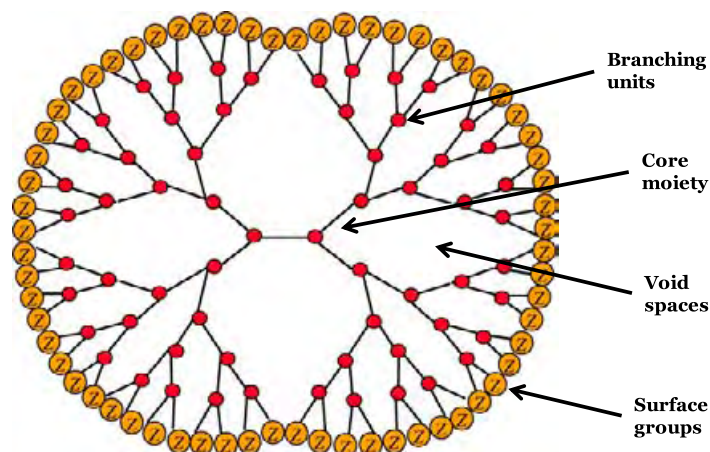
Polymeric materials can be designed to reach various compositions, architectures and functionalities. Among them, dendritic polymers have attracted considerable interest as nanomaterials over the past 30 years. This class of polymers offers significant different physical properties as well as chemical features compared to linear polymers but also to cross-linked polymer networks: they possess a globular form, a large number of surface functional groups, internal voids as well as high solubility, thermal stability, low viscosity. Dendritic polymers may be further subdivided into three categories based on their architectures: dendrimers, hyperbranched polymers and dendrigrafts [1]. Thank to these outstanding properties, dendritic polymers have been used as the key starting materials for the preparation of more complex polymer structures [2]–[5]. Table I.1 gives the main characteristics of the different families of dendritic polymers compared to their linear polymers counterpart.

Table I.1. Main features of hyperbranched polymers, linear polymers, dendrigraft polymers and dendrimers (adapted from [1])

Polymers	Linear	Hyperbranched	Dendrigraft	Dendrimer
Structure				
Topology	1D, linear	3D, ellipsoidal	3D, ellipsoidal	3D, globular
Synthesis	One-step, easy	One-step, cost-effective	Several steps	Multistep, laborious
Purification	Precipitation	Precipitation	Precipitation	Chromatography
Polydispersity Index	> 1.1	> 2.0	~ 1.1 (< 1.5)	1.0 (<1.05)
Degree of branching	0	0.4-0.6	0.6-0.7	1
Molecular cavity	No	Yes	Yes	Yes
Entanglement	Strong	Weak	Weak	Very weak
Viscosity	High	Low	Low	Very low
Functional group	At two ends	At linear and terminal units	At linear and terminal units	At terminal units

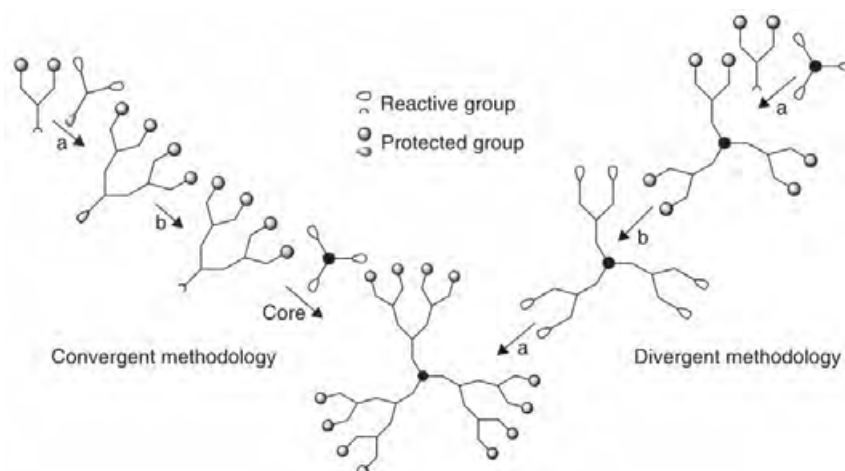
1. Dendrimers

Dendrimers are highly branched, star-shaped macromolecules with nanometer-scale dimensions. Dendrimers are defined by three components: a central core, an interior dendritic structure (the branches), and an exterior surface with functional surface groups (Scheme I.1).



Scheme I.1. Schematic representation of a dendrimer

The varied combination of these components yields products of different shapes and sizes with shielded interior cores that are ideal candidates for applications in both biological and material sciences. While the attached surface groups affect the solubility and chelation ability, the varied cores impart unique properties to the cavity size, absorption capacity, and capture-release characteristics. The perfect and ideally branched structure of dendrimers results in high molecular weight, monodispersed globular topology polymers, as well as high solubility, thermal stability and low viscosity. To achieve such elaborate dendritic structures requires lengthy and multistep synthesis using either a large amount of reagents to push reactions toward completion or extensive purification by chromatographic techniques to remove by-products. There are two defined methods of dendrimer synthesis, divergent synthesis and convergent synthesis (Scheme I.2).



Scheme I.2. Convergent and divergent methodologies for the synthesis of dendrimers [1]

2. Hyperbranched polymers

Efforts to mimic the structural features of dendritic architectures in a more synthetically efficient manner have resulted in the production of hyperbranched polymers (HBP). HBPs are typically produced by one-pot polymerization of AB_x monomers. Although the statistical nature of the polymerization results in polydisperse products and branching imperfection within structure, the methodology can deliver a three-dimensional topology analogous to that of dendrimers. As a consequence of the globular structure, hyperbranched polymers deliver many of the beneficial features of the dendritic structures such as high solubility, thermal stability, low viscosity, large number of surface functional groups as well as internal voids.

Degree of branching (DB) is a quantitative indication of the branching perfectness for hyperbranched polymers. Therefore, the DB value of dendrimers is 1. DB value of HBP is often between 0,4-0,6. Its value is evaluated from Equation I.1 and necessitate the knowledge of the number of dendritic, linear and terminal units involved in the polymer structure (noted d , l and t respectively) (Figure I.1)

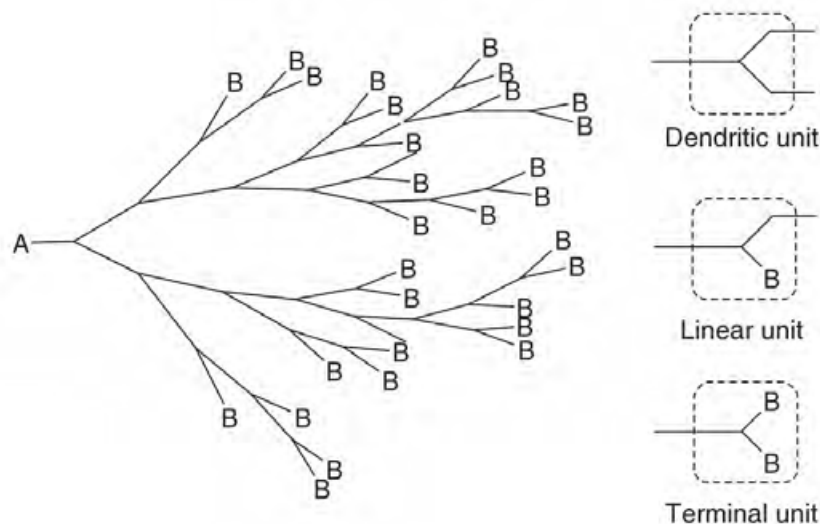
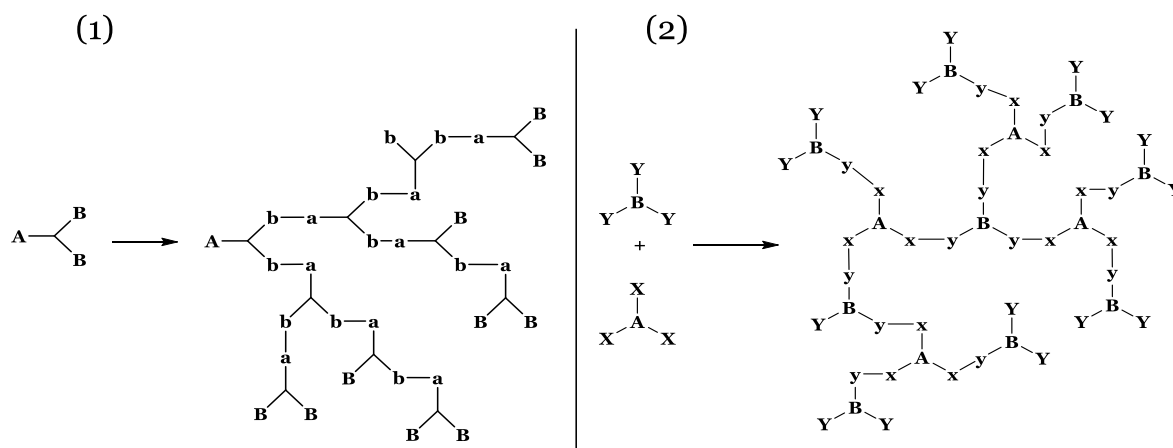


Figure I.1. Schematic architecture of the hyperbranched polymer prepared from an AB_2 monomer

$$DB = \frac{d + t}{d + l + t}$$

Equation I.1. Degree of branching, where d , l and t stand for the numbers of branched, linear and terminal units in the molecule, respectively.

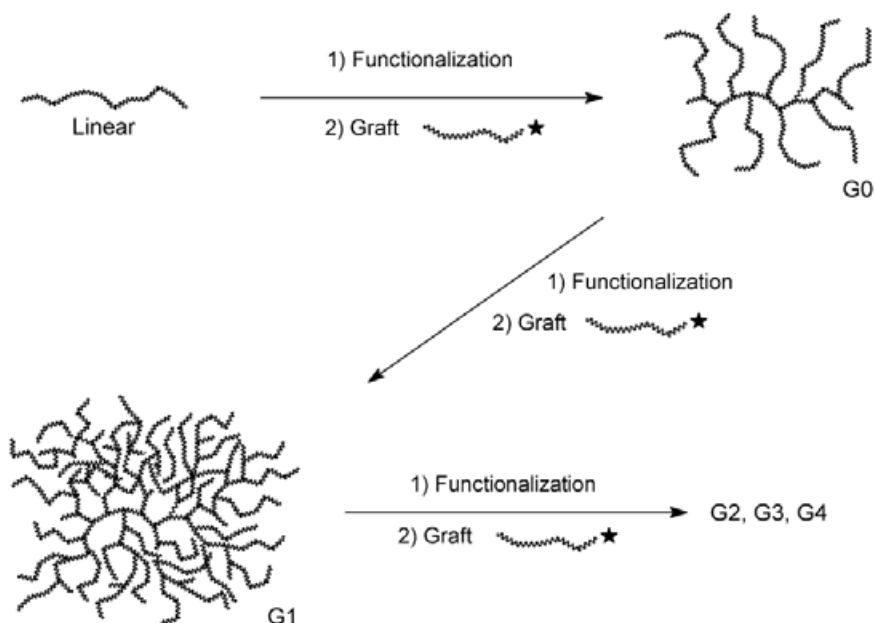
As depicted in Scheme I.3, two methodologies have been developed to prepare HBP *via* polymerization of monomers in one-pot reaction (bottom up ideology) using single-monomer AB_x ($x \geq 2$) or double/multiple-monomers (e.g. A_3+B_3) [6].



Scheme I.3. (1) Polycondensation of AB₂-type monomer; (2) Polycondensation of A₃+B₃-type monomers

3. Dendrigrrafts

The third class of dendritic polymers is the dendrigrraft systems, introduced simultaneously in 1991 as Comb-burst polymers by Tomalia et al. [7] and as arborescent polymers by Gauthier and Möller [8]. Multiple branching levels characterize the architecture of these molecules, in analogy to dendrimers and hyperbranched polymers. Dendrigrraft polymer synthesis follow a generation-based growth scheme similar to dendrimers, but use polymeric chains as building blocks. This leads to a very rapid increase in molecular weight per generation, and high molecular weight branched polymers can be produce in a few steps. The size of dendrigrraft polymers is typically 1-2 orders of magnitude larger than their dendritic counterparts, however, ranging from about 10 nm to a few hundred nanometers [9]. Since the grafting reaction is a random process, the branched structure bears similarities to hyperbranched polymers. Even though the architectures of dendrigrraft polymers are not as strictly defined as for dendrimers, the polydispersity index (PDI) achieved for these materials typically remain quiet narrow ($M_w/M_n \sim 1.1$) [9]. The three distinct synthetic methodologies are considered for the preparation of these materials: (1) divergent “grafting onto” methods based on a successive coupling reactions of polymer chains with a functionalized substrate polymer, (2) divergent “grafting from” methods using cycles of polymerization initiated from functional sites located on a substrate polymer, (3) convergent “grafting through” methods involving coupling of preformed polymer chains in a one-pot reaction. The “grafting onto” scheme has been by far the most widely applied for the preparation of dendrigrraft polymers, Scheme I.4 presents schematically this method.



Scheme I.4. General grafting onto scheme for the synthesis of dendrigraft polymers. [9]

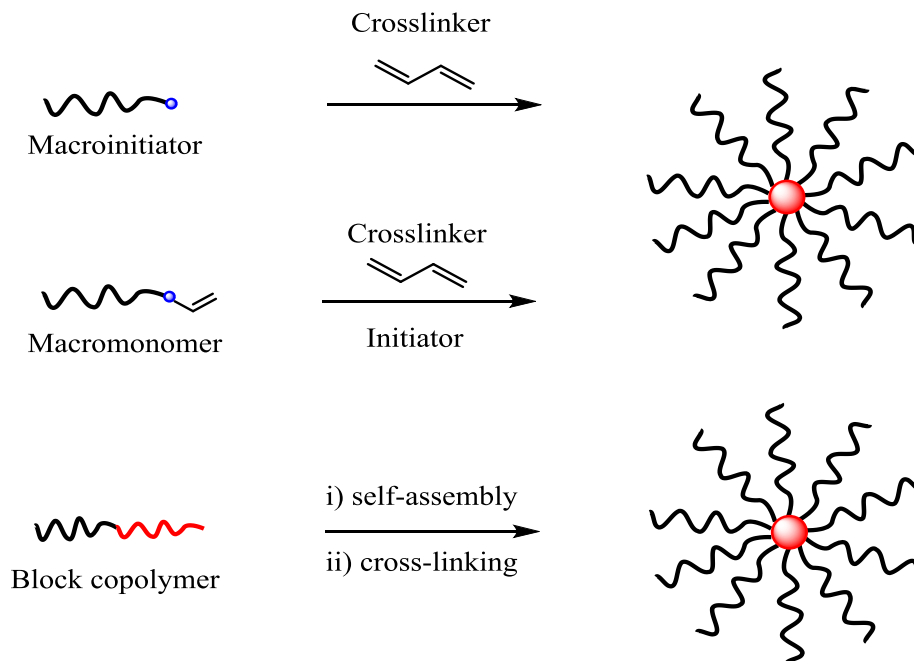
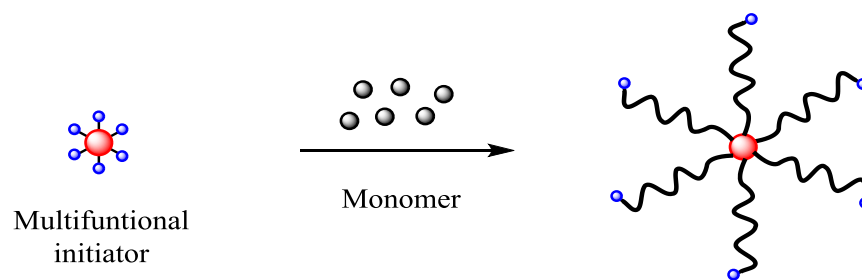
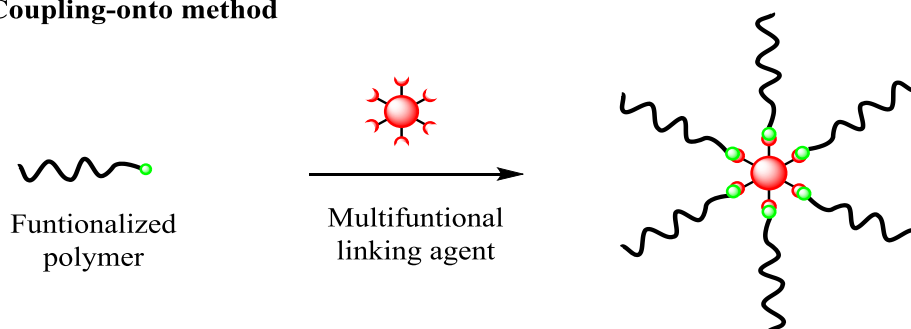
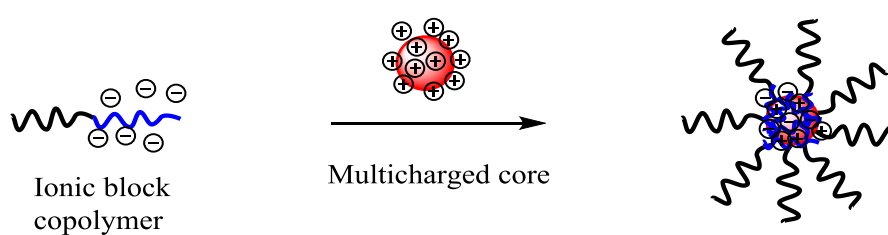
B. Core-shell dendritic polymers

Modification of dendritic core by an outer shell may be a requisite to access polymer structure with suitable properties (solubility, specific interactions,...) towards a chosen applications. Different strategies have been used to make core-shell structures from dendritic polymers: covalent grafting and non-covalent grafting. Scheme I.5 summarizes the common routes to make core-shell structures.

The synthesis of core-shell structures by covalent grafting had first been studied using ionic polymerization [10]. After the development of Control Radical Polymerization (CRP) core-shell polymers have been frequently synthesized using Atom Transfer Radical Polymerization (ATRP) [11], [12], Nitroxide-Mediated Radical Polymerization (NMRP) [13] or Reversible Addition-Fragmentation Chain Transfer (RAFT) [14]. Three main methods can be distinguished:

- the “core-first” method provides well-defined core-shell structure by growing arms from a multifunctional initiator [15], [16],
- the “arm-first” method lead to the formation of core-shell structures by crosslinking linear arm precursors using a crosslinker [17], [18],
- the “coupling-onto” method in which linear arm precursors are attached onto a well-defined multifunctional core combining coupling techniques such as click chemistry [19].

In this section, I will focus my attention to the “core-first” and the “coupling onto” methods using dendritic polymers as multifunctional cores. Since the “arm-first” method produce crosslinked core, they will not be discussed herein with respect to our project.

a) Arm-first method**b) Core-first method****c) Coupling-onto method****d) Ionic complexation**

Scheme I.5. Synthesis methodologies of polymeric core-shell structures [20], [21]

Besides covalent methods, non-covalent core-shell structures from ionic interactions between functional groups of dendritic polymers with ionic moieties such as ionic surfactants, or ionic block-copolymers is a very promising strategy to produce core-shell structures which avoid complicated chemical synthesis. This method will be also discussed in this section.

1. Core-first method

“Core-first” method concerns the polymerization of polymer shells by using dendritic polymers as macroinitiators *via* ATRP [11], [12], NMRP [13] and RAFT [14] techniques. Compared to the other two strategies (arm-first and coupling onto), the “core-first” strategy has the advantage of offering a more precise control over arm number by tailoring the number of functionality of the multifunctional initiators [22]. A variety of multifunctional initiators have been successfully developed to suit each of the above CRP techniques for “core-first” synthesis of core-shell polymers from various monomer stocks. Because of their high and controllable number of functionalities, multifunctional dendritic initiators (i.e., dendrimers and hyperbranched polymers bearing multiple initiating sites) are particularly valuable for synthesis of star polymers having high tunable arm numbers (as high as 20 and higher) [23], [24]. Some selected examples from the literature for this method are given in Table I.2.

Table I.2. Typical examples of core shell structures obtained from core first method.

Core	Shell	Synthesis way	Application	Ref
Hyperbranched polyethylene (HPPEE)	Hyperbranched polyglycerol (HPG)	ROP	unimolecular transporters for hydrophobic compounds in water: pyrene and Nile red	[26]
Dendrigraft Poly Styrene	Deuterated poly(ethylene oxide) PEO	ROP [27]		[28]
Hyperbranched polyethylene glycol (HPEG)	PLLA	ROP		[29]
HPEI	Poly(ϵ -caprolactone) (PCL)	Sn(Oct) ₂ -catalyzed ROP [30]	Encapsulation of polar and non-polar guest: pyrene, Methyl orange, Methylene blue, methacrylic acid and thio-michler's ketone	[31]
Hyperbranched Poly(ϵ -caprolactone-4,4-bioxepanyl-7,7-dione) HBP(CL-co-BOD)	N,N-dimethylamino-2-ethyl methacrylate (PDMAEMA)	RAFT	Biodegradable core-shell materials	[32]

Crosslinked of 2-(5-Norbornene)methyl Methacrylate	Thiobenzoate-Capped PS	RAFT	[33]
HPEE	Polyethylene	Ethylene living polymerization	[23]

ROP: Ring Opening Polymerization, see abbreviation section for the name of polymer

2. Coupling-onto method

The “coupling onto” method consists of attaching linear polymer arms onto a multifunctional core by coupling techniques. The advantage of this method is the ability to prepare well-defined arms using CRP techniques. Coupling technique such as click chemistry or Michael reactions etc ... are then used to anchor the well performed shell to the dendritic core. Nevertheless, coupling yields reported in the literature are often less than 70%. Some selected examples from the literature for this method are given in Table I.3.

Table I.3. Typical examples of core shell structures obtained from coupling-onto method

Core	Shell	Application	Ref
Hyperbranched Polyethylenimine (HPEI)	oligosaccharide shells (Reductive amidation [34])	Drug carrier for B vitamins, estradiol derivative, pantoprazol	[35] [36]
HPEI	Hydrophobic oligopeptide (HOP)-PEG	Drug carrier for hydrophobic compounds	[37]
HPEI	PS	Drug delivery	[38]
HPEI-cationic core	Polymethylmethacrylate (PMMA)	Behavior in organic solution	[39]
HPEI	C16 D1-C16 ^a D2-C16 ^b	Guest encapsulation	[5]
HPEI	C16 D1-C16 ^a D2-C16 ^b	In situ synthesis of gold NPs and their application for the catalytic reduction of 4-nitrophenol by NaBH ₄	[40]
HPEI	Alkyl chain-PEO (DCC activation coupling)	Stabilization of gold NPs	[3]
Hyperbranched polyglycerol (HPG) HPG-aromatic groups	PEG	Drug carrier : pyrene	[41]
Hyperbranched Polyglycerol (HPG)	PEG Biphenyl-PEG (Click	Encapsulation of hydrophilic and	[4]

	chemistry)	hydrophobic drug: pyrene, beta-carotene, nimodipine	
HB Poly(β -cyclodextrin)	PEG (Click chemistry)	Drug release	[42]
HB Poly β -cyclodextrin (hydrophobic)	Methoxy polyethylene glycol (Click chemistry)	Controlled release of guest molecules: levofloxacin lactate and rhodamine B	[43]
HB Poly Lysine	Fatty acid	Template and stabilizing agent for Ag, Au, Pd NPs	[44]
HB Poly(phenylacetylene)s (HBPPAs)	Polystyrene (Click chemistry)		[45]
HB Poly(1,3-diether)	Polar inner imidazolium cation shell and non-polar outer n-alkyl shell	Transport and dispersion of water-soluble dyes and functionalized graphene nanosheets from aqueous phase into nonpolar fluids	[46]
HB Poly(3-ethyl-3-oxetanemethanol) (HBPO)	PEG - DNA	cell uptake, excellent fluorescence properties, and smart targeting capability	[47]
HB Polyamylopectine	cholesteryl chloroformate	Fluorescence properties	[48]
Hyperbranched conjugated polymer HCP	PEG (acylhydrazone connection)	Self-assembly properties	[49]
^a 2,2-bis(hydroxymethyl)propionic acid (BHP)-based generation 1 dendron with two palmitate tails(D1-C16); ^b the generation 2 dendron with four palmitate tails (D2-C16)			

Combined coupling-onto and core-first methods were also employed efficiently to produce core-multi shell structures, examples are given in Table I.4.

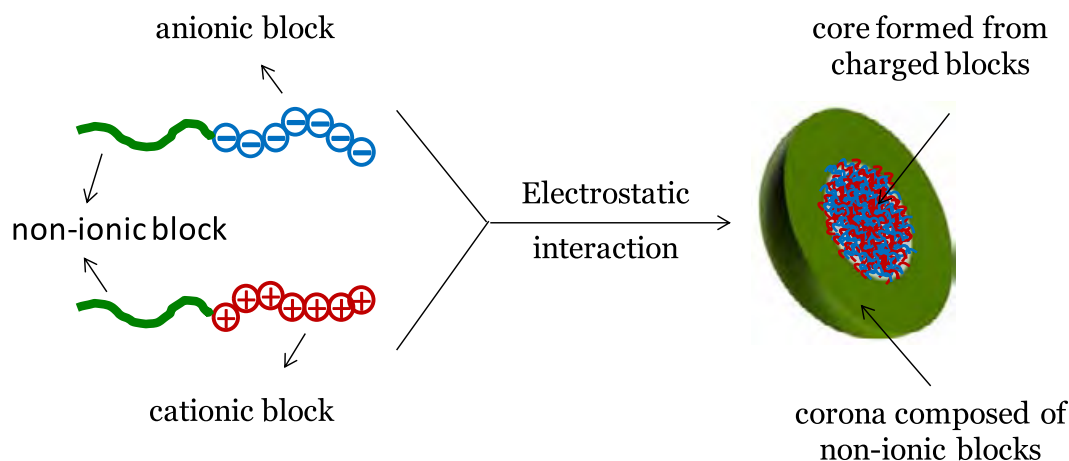
Table I.4. Typical examples of core shell structures obtained from combined coupling-onto and core-first methods.

Core	Shell	Synthesis way	Application	Ref
HB poly(2-(dimethylamino) ethyl methacrylate)	PS	RAFT-SCVP Menschutkin click reaction	Drug delivery	[50]
HPG PEI	PLA DNA	DCCsuccinimide Ionic interaction	Gene delivery	[51]
Boltorn H40	PLA-PEG	1, Grafting from PLA 2, Coupling onto DCC	Drug loading	[52]

Boltorn H40	Polycaprolactone PLC – Adenine PEG- Uridine	1, ROP (Grafting from) 2, self assembly interaction thanks to A-U recognition	Drug delivery (Doxorubicin)	[53]
Hyperbranched poly(tertiary amino methacrylate)s (HPTAM)	PEG or tert-Butyl Acrylate (PtBA) or Alkyl chain	Click chemistry RAFT Click chemistry		[54]
Dendritic Boltorn® H40	PLA-PEG-Folic acid	ROP DCC activation coupling	Tumor targeted drug delivery of doxorubicin	[25]
HPEI	PCL inner shell - crosslinked methacrylate	radical-crosslinked	Encapsulation of polar and non-polar guest: pyrene, Methyl orange, Methylene blue, methacrylic acid and thio-michler's ketone	[31]
	PCL-PEG	ROP + coupling onto by DCC		

3. Ionic interactions

Oppositely charged polyelectrolytes are capable of co-assembly, directed by multivalent ionic interactions. The supramolecular architectures that result are often referred to as PolyIon Complexes (PICs). As depicted in Scheme I.6, oppositely charged polyelectrolyte blocks complex to form the PIC core, while the hydrophilic blocks expose to the solution provide solubility and stability under physiological conditions. The structures, properties and functions of PICs are strongly governed by electrostatic forces. Many factors and strategies influencing polyion complex morphology have been investigated. Mixing oppositely charged polyelectrolytes with a 1:1 charge ratio generally forms precipitates or aggregates in solution. However, if one polyelectrolyte is in large excess, it will envelop the counter polyelectrolyte and the assembly remains soluble [55]. Since the electrostatic interactions are mediated both by water molecules and ions, addition of salts can suppress complexation through a shielding effect. This shielding effect can play a key role in PIC formation. Additionally, pH, concentration and morphology of the polyelectrolytes all influence the assembly. Thus PIC formation is tunable; the nature of the supramolecular architecture can be controlled by various conditions such as ionic strength, pH of solution, and mixing ratios of electrolytes [56].



Scheme I.6. Concept of the formation of PIC micelles from a pair of oppositely charged block copolymers.

Whereas a great number of polymeric micelle systems have been prepared using block copolymers, very little examples have been reported about dendritic polymer based PICs. Ionic dendrimers, ionic hyperbranched polymers and dendrigrafts with ionic side chains are globular and rigid-rod shaped polyelectrolytes. Unlike linear polyelectrolytes, their ionic segments have reduced degrees of freedom, when mixing with block copolymers that are composed of neutral hydrophilic and polyelectrolyte blocks yields PIC aggregates with a core-shell structure.

Kataoka and coworkers reported the formation of PICs through oppositely-charged electrostatic interactions of ionic dendrimers (DP) and block copolymers of poly(ethylene glycol)-block-poly(L-lysine) (PEG-*b*-PLL) or poly(ethylene glycol)-block-poly(aspartic acid) (PEG-*b*-PASA). As shown in Figure I.2, the dendrimer, bearing a porphyrin group in its central core, can be negatively or positively charged. The PIC micelles prepared from negatively-charged DP and positively-charged PEG-*b*-PLL had a spherical shape with a diameter of approximately 64 nm (measured by DLS) containing an average of 38 DP molecules (by SLS) in physiological saline solution. It is showed that the PIC micelles consisting of cationic DPs and PEG-*b*-PASA showed a higher stability against NaCl concentrations than those of PLL₂₇-PEG-*b*-PASA up to 1500 mM, 10 times higher than the physiological concentration. The authors explained this fact by the assumption that the PIC from a rigid dendrimer may produce a smaller entropy gain upon dissociation than that from a flexible PLL homopolymer. In addition, in the case of the PIC micelles consisting of cationic DP-PEG-*b*-PASA or anionic DP-PEG-*b*-PLL, the complexation between DPs and block copolymers might be accomplished by the formation of hydrogen bonds between carboxylic acid and primary amine groups after proton transfer from the acid to amine [57].

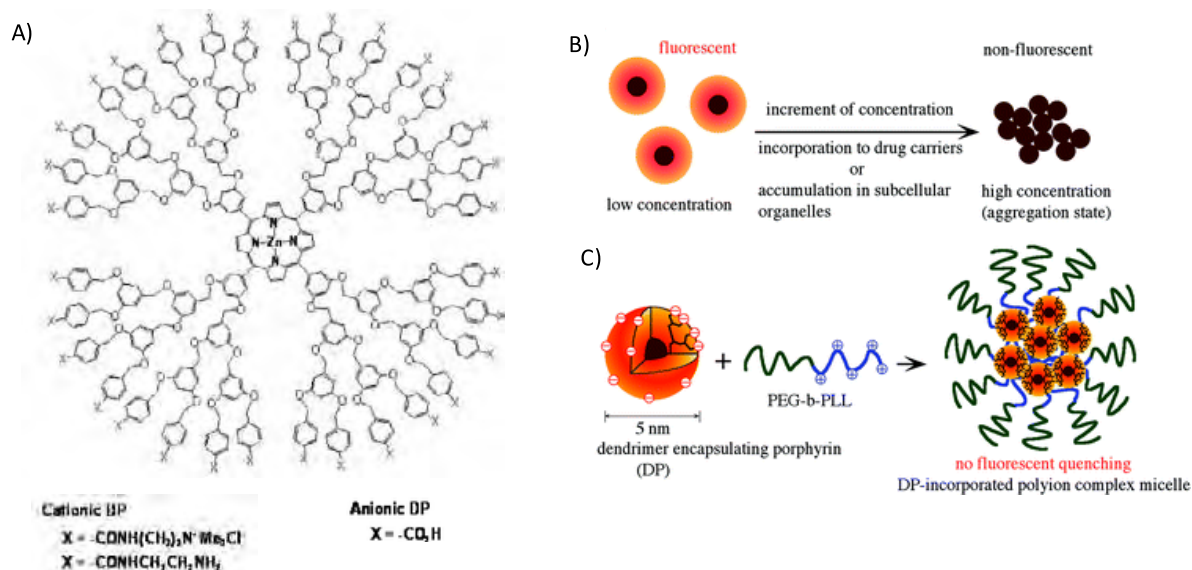


Figure I.2. (A) Chemical structures of dendrimers encapsulating porphyrin with ionic peripheral groups (DPs); (B) Conventional photosensitizers form aggregates at a high concentration, resulting in their self-quenching; (C) Formation of DP-incorporated polyion complex (PIC) micelles through electrostatic interactions between anionic DPs and poly(ethylene glycol)-block-poly(L-lysine) (PEG-*b*-PLL) copolymers. The dendritic structure of DP can sterically prevent aggregation of the center porphyrin, thus there is no fluorescent quenching of the center porphyrin. [57]

Moreover, the PIC micelles of anionic DP-PEG-*b*-PLL showed pH-dependent structural changes. The hydrodynamic diameter and the apparent molecular weight of the micelles remained constant in the pH range from 6.4 to 8.5. However, when the pH was below 6.4, the PIC micelles showed a gradual increase in the diameter and apparent molecular weight, and finally underwent precipitation at pH 5.6. Under acidic pH conditions, the carboxylic acid groups of DP might be considerably protonated, leading to diminution of the electrostatic interaction between anionic DP and PEG-*b*-PLL, thus the well-defined core-shell structure may become more obscure and a merging of the micelles may take place. The similar pH-dependent structural changes of the PIC micelles were also observed for the system of cationic DP bearing 32 primary amino groups-PEG-*b*-PASA. Such a pH-responsive behavior of the micelles allows their effective accumulation in solid tumors in response to a low pH condition in the tumor tissue (\sim pH 6.5) or an intracellular acidic endosomal compartment (\sim pH 5.0) while their stable circulation in the bloodstream is expected. The PIC micelles of anionic DP-PEG-*b*-PLL also showed the enhancement of photocytotoxicity and the capacity of cellular uptake. [57]

Riguera et al. reported (Figure I.3) supramolecular assembly of anionic PEG-dendritic block copolymers with PLL leading to spherical PIC micelles of ca. 25 nm, low dispersity, and remarkable stability against dilution (5 times), and ionic strength (up to 0.5 M NaCl). Freeze drying led to only a small reduction in size (to ca. 20 nm) by DLS, with no effect on dispersity. Interestingly, the core-shell architecture of these PIC micelles, with a segregated core (network of polyions) surrounded by a palisade of flexible and hydrophilic PEG, was confirmed by ^1H NMR. Thus, the dendritic block signals in the micelles showed only an intensity of about 20% [normalized to the terminal methoxy (PEG) signal] when

compared to the free block copolymer, suggesting more dense packing and decreased solvation within the core. The authors believed that the steric stabilization imparted by the PEG corona, along with the size and narrow distribution of the PIC micelles, should result in longer circulation times, improved biocompatibility, and enhanced ability to extravasate into the disease sites [58].

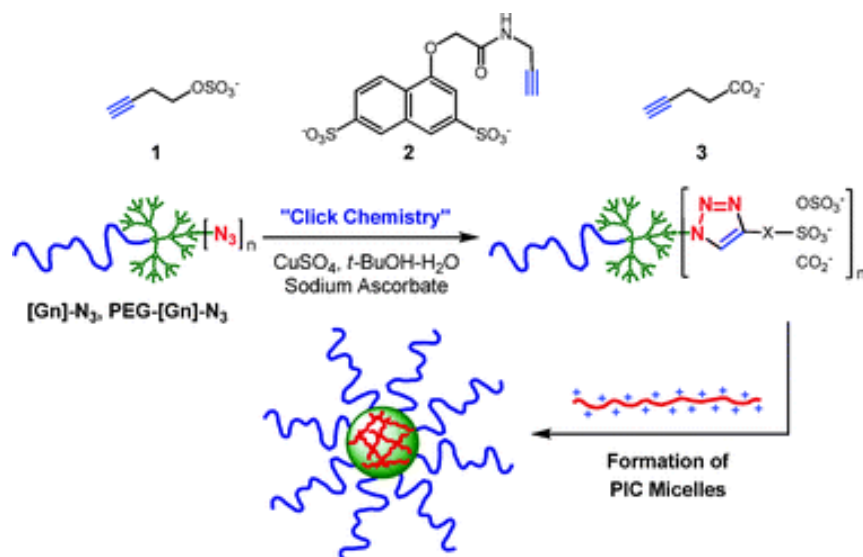
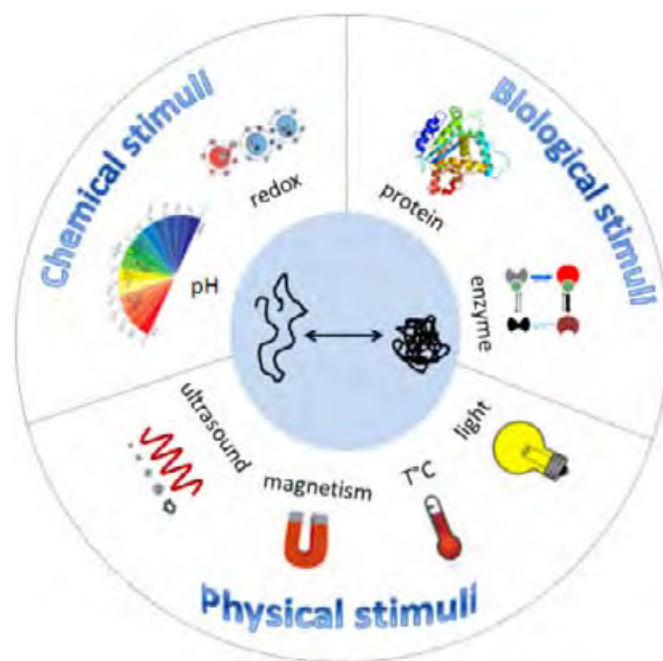


Figure I.3. Supramolecular assembly of anionic PEG–dendritic block copolymers with PLL [58].

Dendritic polymers can also complex with small ionic moieties such as fatty acid and surfactant forming solid state assemblies that possess liquid crystal properties. This issue will be discussed below (section liquid crystals).

C. Stimuli-responsive core-shell dendritic polymers

During the past decades the stimuli-responsive polymers became a very important field of research. Stimuli-responsive polymers are able to undergo significant property changes as a reply to relatively small external or internal variations of the environmental conditions (stimuli). The nature of the environmental stimulus can be classified into three categories: physical, chemical and biomedical stimuli (Scheme I.7). The response of the material can have miscellaneous forms: a change in shape, dimension or organization of the polymer material, altering its mechanical, optical or electrical properties as well as changes in permeability [59]. Some examples of stimuli can be mentioned: temperature responsive, pH-responsive, photo-responsive, redox-responsive and other types.



Scheme I.7. Three categories: physical, chemical and biomedical stimuli

1. Temperature responsive materials

Temperature responsiveness is one of the most studied stimuli in literature. Three different families of polymer based on dendritic structures (i.e, solution of polymer, gel networks, liquid crystalline materials) presenting structural change as a function of temperature can be distinguished and will be described in the next sections. Table I.5 gives an overview of some of the systems described in literature.

Table I.5. Examples for temperature responsive core-shell polymers

Diluted solution			
Core	Shell	Synthesis way	Ref
Multi-HPBPEA : 2-((2-bromopropionyl)oxy)ethyl acrylate (BPEA)	PNIPAM	Grafting from ATRP	[60]
HBPoly(β -cyclodextrin)	P(DEAEMA-b-PVCL-b-PDMAEMA)	Triple RAFT Grafting from	[61]
Boltorn H40	P(PDEA-PDMA)	RAFT Grafting from	[62]
Boltorn H40	P(PNIPAM-PDMA)	RAFT Grafting from	[63]
Hyperbranched polyglycerol (HPG)	Crosslinked PDMA-PNIPAM	DCC activation coupling	[64]
Hydrogels			
Core	Shell	Synthesis way	Ref
PEG star	PNIPAM	Core-first, anionic polymerization	[65]
PDMA star block	PDEGMA	Core-first, ATRP	[66]
β -cyclodextrin	(PNIPAM-b-PDMA)	Core-first RAFT	[67]
Multi block $m(\text{PDMA}_p\text{-PNIPAM}_q)$	PNIPAM	RAFT	[68]
Liquid crystals			
Core	Shell	Synthesis way	Ref
methylated hyperbranched PEI	mesogen-containing carboxylic acid	Ionic interaction	[69]
PAMAM or PPI or PEI or methylated PEI	aromatic-based carboxylic acid	Ionic interaction	[70]
PAMAM, PPI	alkanoic acids	Ionic interaction	[71]
hyperbranched polylysine (HBPL)	sodium alkyl sulfate	Ionic interaction	[72]
PAMAM	fatty acid	Ionic interaction	[73]

a. ***Solution of thermoresponsive polymers***

Table I.6 shows some examples of polymers showing a thermo-responsiveness in water. The most common of these is poly(*N*-isopropylacrylamide) (PNIPAM). PNIPAM has a low critical solution temperature, LCST of around 32 °C, a very useful temperature for biomedical applications since it is close to the body temperature (37 °C). The low critical solution temperature-type phase transition of PNIPAM in aqueous solutions is a very well-known phenomenon that has been widely reported in the literature. At low temperature, PNIPAM chains are soluble in water and take a coiled conformation in order to maximize their hydrogen bonds with water molecules. Crossing the transition temperature, the chains

start to undergo a sharp coil-to-globule transition in water, changing from hydrophilic state to hydrophobic one. Adjustment of the LCST of PNIPAM has been achieved by copolymerizing with hydrophilic or hydrophobic monomers rendering the overall hydrophilicity of the polymer higher or lower respectively.

The LCST of a polymer is the critical temperature below which the polymer is miscible with the solvent for all compositions. Determining LCST of a polymer in a solvent requires a phase diagram. In the literature, the term LCST is often used confusedly with the term cloud point temperature (T_c). At one defined concentration, crossing the T_c makes the polymer become immiscible with the solvent.

Table I.6. Polymers showing a low critical solution temperature (LCST) in water [74]

Polymer	T_c (°C)
Poly(N-isopropylacrylamide), PNIPAM	~ 32
Poly(vinyl methyl ether), PVME	~ 40
Poly(ethylene glycol), PEG	~ 120
Poly(propylene glycol), PPG	~ 50
Poly(methacrylic acid), PMAA	~ 75
Poly(vinyl alcohol), PVA	~ 125
Poly(vinyl pyrrolidone), PVP	~ 160
Poly(silamine)	~ 37
Poly(N-vinylcaprolactam), PVCL	~ 30

Hence different thermoresponsive polymers were used to obtain stimuli-responsive core-shell polymers (SRCSPs). These ones have gain more and more interest over the last decades due to their unique properties compared to their linear copolymer counterparts. The branched structure for instance has influence on the responsive behavior of these polymers such as changing the cloud point (T_c) [20].

Plummer and coworker's have studied the effect of polymer architecture and the presence of end groups derived from RAFT agent on four-arm star PNIPAM compared the the linear one. The four-arm star polymer was prepared by core-first approach using hydrophobic RAFT agent which bearing four trithiocarbonate reactive groups. The T_c transitions of star PNIPAM were significantly depressed by the presence of the hydrophobic star core and possibly the benzyl end groups. The star polymers exhibited increasing chain density with increasing molecular weight above the T_c , while the opposite trend was observed for linear PNIPAM and indicates that the star polymers are able to collapse to form a denser globule as a result of the star architecture. A significant decrease in R_H was observed below the T_c for star and linear PNIPAM using pulsed field gradient NMR (PFG-NMR) and was attributed to the formation of n -clusters. The star polymers showed increasing n -cluster contributions with increasing molecular weight, while the linear PNIPAM showed the opposite trend. Successful application of a scaling law to the linear PNIPAM data indicated

that the average size of the clusters was $n = 6$. Star polymer data did not obey a scaling law; the hydrophobic star core may inhibit n -cluster formation in the lowest-molecular-weight stars. [75]

Cai and Liu [60] reported a novel amphiphilic core–shell unimolecular nanoparticles synthesized from inimer 2-((2-bromopropionyl)oxy)ethyl acrylate BPEA *via* ATRP in three steps as depicted in Figure I.4. Firstly, a hyperbranched hydrophobic core (HPBPEA) was synthesized by self-condensing vinyl polymerization (SCVP) of BPEA. Then HPBPEA were crosslinked using ethylene dimethacrylate (EGDMA) as crosslinking agent giving multi-HPBPEA. Lastly multi-HPBPEA-*g*-PNIPAM was synthesized by multi-HPBPEA core initiating ATRP of NIPAM. The SEC-MALLS measurements showed that the molar mass of the HPBPEA, the cross-linked multi-HPBPEA core and the grafted core-shell structure multi-HPBPEA-*g*-PNIPAm increased from 4700 to 201 000 and 410 000 g.mol⁻¹. The transition temperature of PNIPAm shell for multi-HPBPEA-*g*-PNIPAm was found equal to 27.6 °C from DSC measurement. Fluorescent spectra of 8-anilino-1-naphthalenesulfonic acid /multi-HPBPEA-*g*-PNIPAm evidenced that the core of multi-HPBPEA-*g*-PNIPAm could encapsulate hydrophobic guest molecules. Moreover, it is found that multi-HPBPEA-*g*-PNIPAm can efficiently encapsulate and release a hydrophobic drug such as nifedipine.

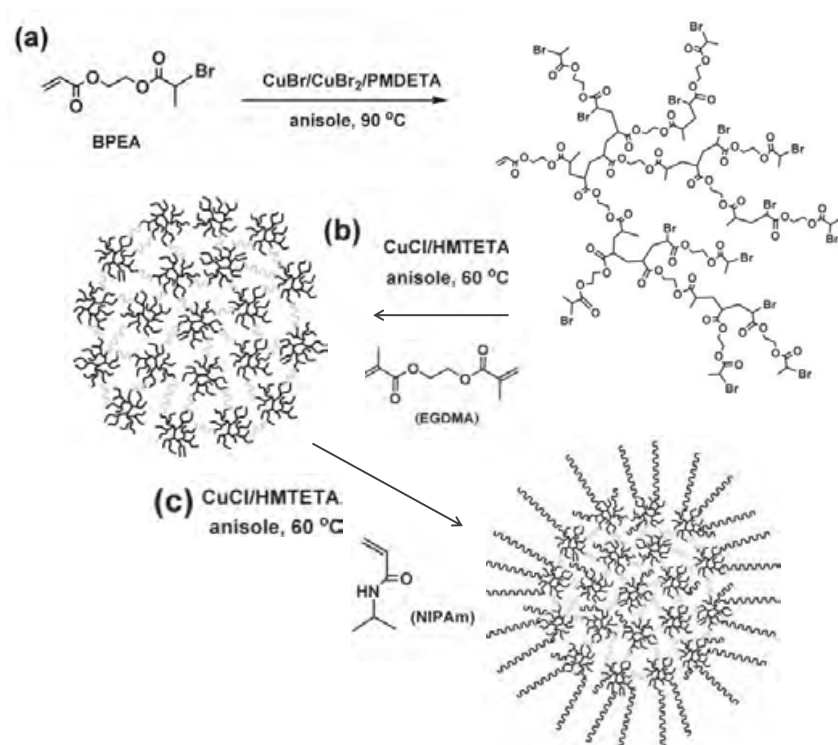


Figure I.4. Synthesis scheme of Multi-HPBPEA- *g*-PNIPAm by ATRP, adapted from ref [60]

The combination of two polymers with different T_c behaviors (can lead to the formation of dendritic unimolecular micelles that exhibit two-stage thermally induced collapse with increasing temperature [62] [63]. Hence, as illustrated in Figure I.5, the synthesis of such structures was obtained from a Boltorn H40-based macro-RAFT agent, PNIPAM as an inner shell and poly(2-(dimethylamino)ethyl methacrylate) (PDMA) as an outer shell.[63] T_c of these polymers are 23 and 40°C respectively.

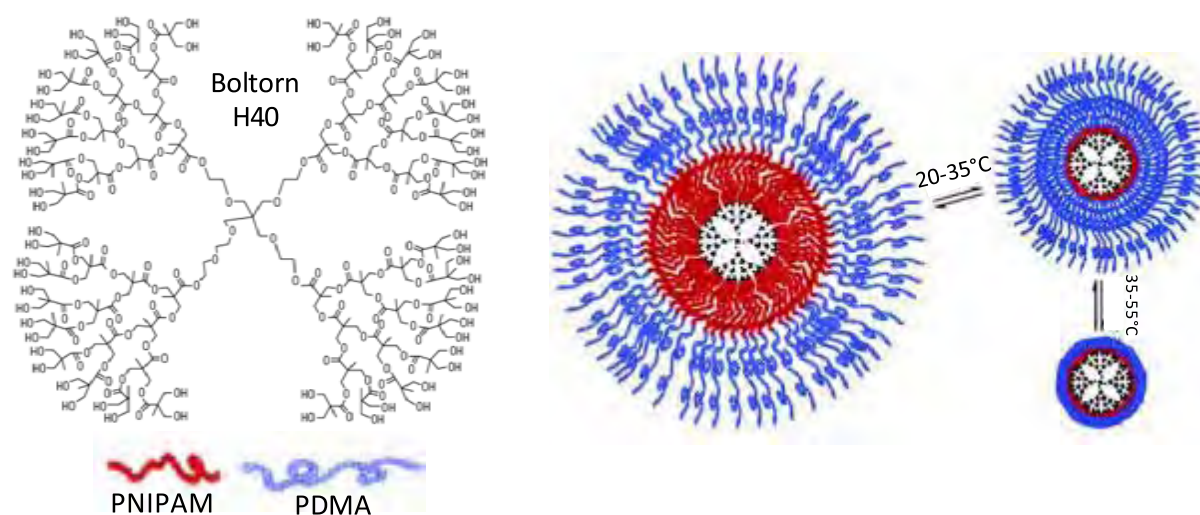


Figure I.5. Schematic illustration of the thermally induced collapse of H40-PNIPAm-PDMA upon heating through the cloud points of PNIPAM and PDMA [63]

b. *Gels*

Gels are three-dimensional polymeric networks. Two main categories of gels can be distinguished: physical gels and covalently linked gels. The latter, as the name suggests, are based on polymer chains that are linked together through covalent bonds at points that are called crosslinks. That is why this type of gels may also be referred to as crosslinked gels or covalently linked networks [76]. Physical gels, on the other hand, are formed by the physical entanglement of polymer chains and/or micelle ordering in solution and not from covalently linked polymer chains [77]. Both of these gels, crosslinked or physical, have the ability to swell in a solvent depending on their compatibility with the solvent. However when a physical gel is in the appropriate solvent and it is given enough time and space it will dissolve in the solvent, whereas crosslinked gels will not. Hydrogels are polymer networks that can bind a large amount of water or biological fluids.

Stimuli responsive gels have been extensively study due to their ability to dramatically change one of their properties (volume, hydrophobicity, rheological properties...) as a function temperature, pH... Hence, in the case of thermo-responsive polymers, covalently linked networks exhibit a change in their degree of swelling in response to temperature, whereas physical gels show a sol-gel transition [78]: Sol phase is defined as a flowing fluid, whereas gel phase is non-flowing on an experimental time scale. Moreover, the gel phase appears above a critical gel concentration of the polymer. This one is commonly inversely related to the molecular weight of the polymer employed. The development of physical junctions in the system is regarded as one of the prerequisites in determining gelation, which must be sufficiently strong with respect to the entropically driven dissolving forces of the solvent. The determination of the boundary between the sol and gel phases depends on the experimental method. A simple test-tube inverting method was employed to roughly determine the phase boundary [79]. When a test tube containing a solution is tilted, it is defined as a sol phase if the solution deforms by flow, or a gel phase if there is no flow. The flow is a function of time, tilting rate, amount of solution, and the diameter of the test tube. Considering the time–temperature superposition principle in polymer deformation, the test

parameters should be fixed before determining the sol–gel boundary. When gelation is induced by temperature, the endothermic peak during heating obtained from differential scanning calorimetry (DSC) determines the transition temperature as well as the enthalpy of gelation. Recently, a dynamic mechanical analysis was used to determine the sol–gel transition in a more reproducible manner. An abrupt change in the storage modulus or viscosity reflects the sol–gel transition.

Physical gel typically consists generally of block copolymers where the stimuli responsive blocks are used to form the temporary crosslinking points, i.e., the responsive block is switched insoluble by increasing its hydrophobic interactions. It is noted that physical gels can be formed by low molecular weight gelators too; however these systems are not within the scope of this thesis, thus will not be discussed herein.

Diblock and star-shaped block copolymers AB, A(B)₂, A(B)₄, and A(B)₈, where A is the central hydrophilic star-shaped PEG block (molecular weight (Mw) per arm 2000–2460 g.mol⁻¹) and B is the temperature-responsive NIPAM oligomer block (Mw 1900–2400 g.mol⁻¹), have been synthesized Figure I.6. These were reported to form a somewhat viscoelastic gel upon heating (gelation temperature 26–33 °C) when the typical polymer concentration was > 20 wt%, and the resulting gels showed no syneresis. This process was reversible without hysteresis. Based on differential scanning calorimetry (DSC) and dynamic mechanical analysis, the gelation mechanism was observed to be micellar aggregation for the AB diblock copolymer. It was found to be a strong associative network formation for the other polymer architectures *via* hydrophobic interactions of collapsed NIPAM oligomer blocks. The polymer architecture influenced the resulting gel strengths and A(B)₄ showed the highest gel strength of 860 Pa yield stress. [65]

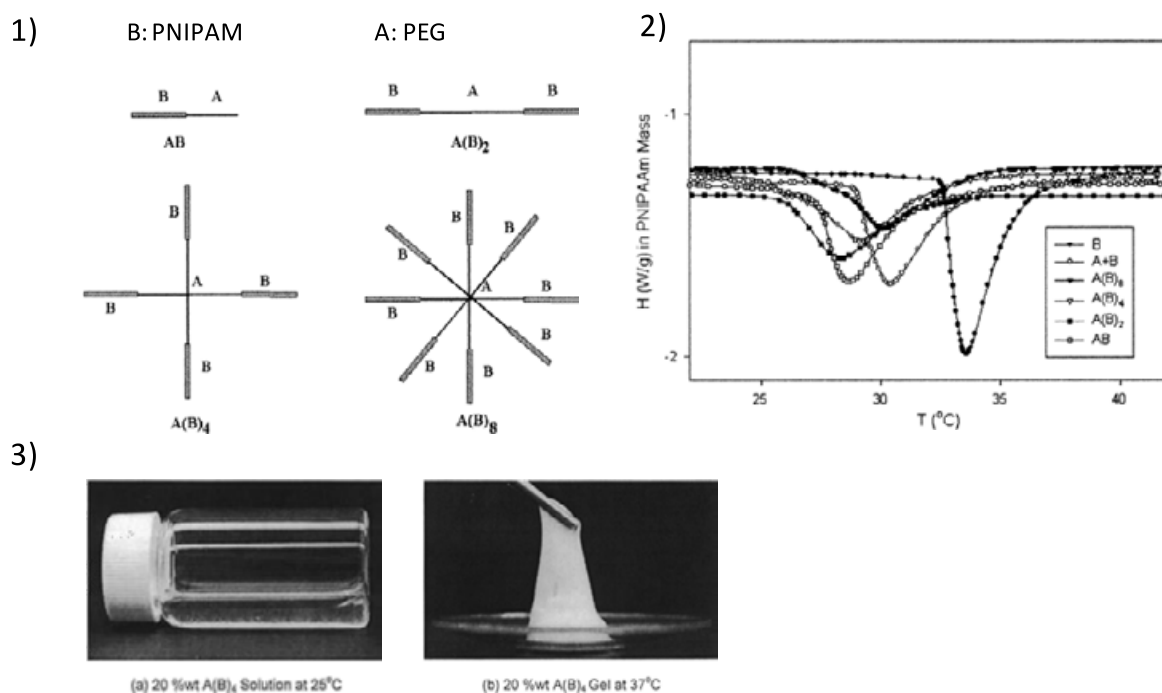


Figure I.6. 1) Schematic structure of PEG-(PNIPAM)_x, x= 1, 2, 4, 8; 2).Endotherme of 20 wt % aqueous solutions of PNIPAM, (PNIPAM)_x-PEG. 3) material images at 25 and 37°C [65].

A series of smart hydrogels based on dual stimuli responsive star-block copolymers responding to pH and temperature were prepared *via* ATRP employing the core-first method (Figure I.7). This four-branch star copolymer consists of poly(2-(dimethylamino)ethyl methacrylate) (PDMA) inner blocks and outer blocks comprised of poly(di(ethylene glycol) methyl ether methacrylate) (PDEGMA) (Figure I.7).

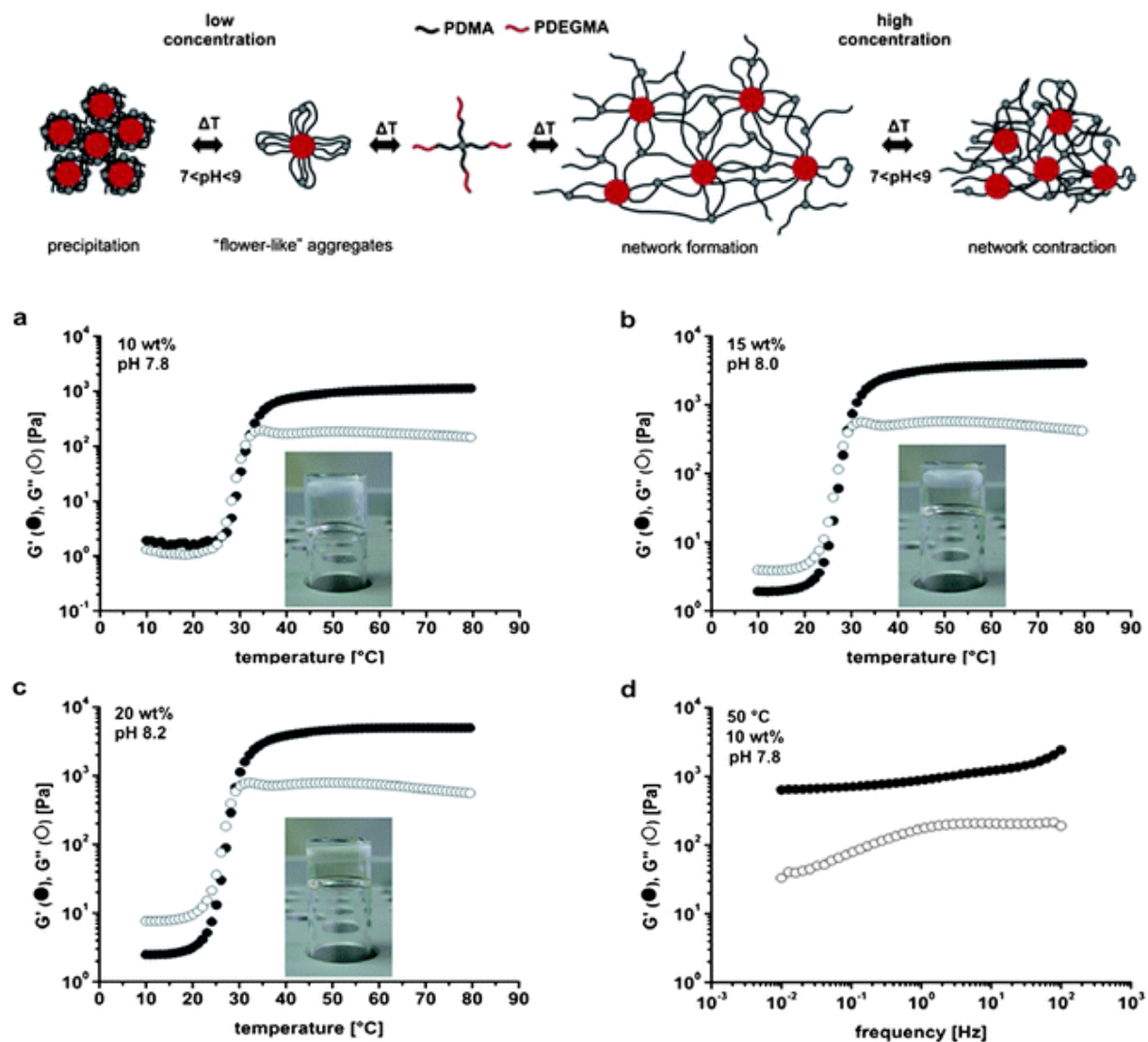


Figure I.7. Aggregation and network formation of dual temperature and pH responsive star-block copolymers in dependence on concentration. Temperature-dependent storage and loss moduli for (DMA₁₃₀DEGMA₁₄₀)₆ in (a) a 10 wt% solution at pH 7.8, (b) a 15 wt% solution at pH 8.0, and (c) a 20 wt% solution at pH 8.2 and (d) isothermal frequency sweep at 50 °C for the 10 wt% sample. Insets depict digital photographs of tube-inversion experiments of the respective samples at 50 °C. [66]

The gelation behavior of these block copolymer stars is analyzed by rheology in dependence on block length, arm number (4 or 6) and polymer concentration. At pH8, tube inversion revealed that all stars formed free-standing hydrogels from 15%wt except the one with the lowest PDEGMA fraction. The star with the highest PDEGMA fraction forms free-standing gels even at concentration 10%wt. Study of temperature dependent gelation by

rheology shows that with increasing temperature both moduli increase and at 30°C, the transition temperature of PDGEMA, the solution crosses into the gel state. G' exceeds G'' and reaches a plateau with $G' > 1\text{kPa}$, indicating a strong gel. The gel strength is influenced by both molar fraction of DEGMA units ($f(\text{DEGMA})$) and the arm number of the star. The arm number determines the number of the possible crosslinking points so that a higher arm number means more crosslinking and thus a stronger gel. The effect of the arm number is more pronounced, as 6-arm star with the lowest $f(\text{DEGMA})$ forms stronger gel than the 4-arm star with a higher $f(\text{DEGMA})$ at all concentration measured. This suggests that the concentration of crosslinking points is more important than the strength of the hydrophobic interactions. However, when the gels are prepared at $\text{pH} \approx 9$ they exhibit significantly reduced gel strength and thus a drop of the moduli upon heating over the transition temperature of PDMA can be observed. At $\text{pH} 9$, the PDMA chains are less stretched because the PDMA blocks are less protonated leading to a decrease of the effective volume fraction of the stars, making the gels at high pH softer compared to the gels at lower pH values. To further prove the versatility of the system, the inner PDMA blocks were quaternized to form a strong polycation. Further advantages of a quaternized block are the possibilities to incorporate nanoparticles or to introduce a light sensitivity through multivalent counterions. During the quaternization the temperature and pH responsiveness of the inner block is lost but so are the restrictions on the solution pH value. The increased effective volume fraction of the quaternized diblock stars leads to a significant decrease in the critical gelation concentration. [66]

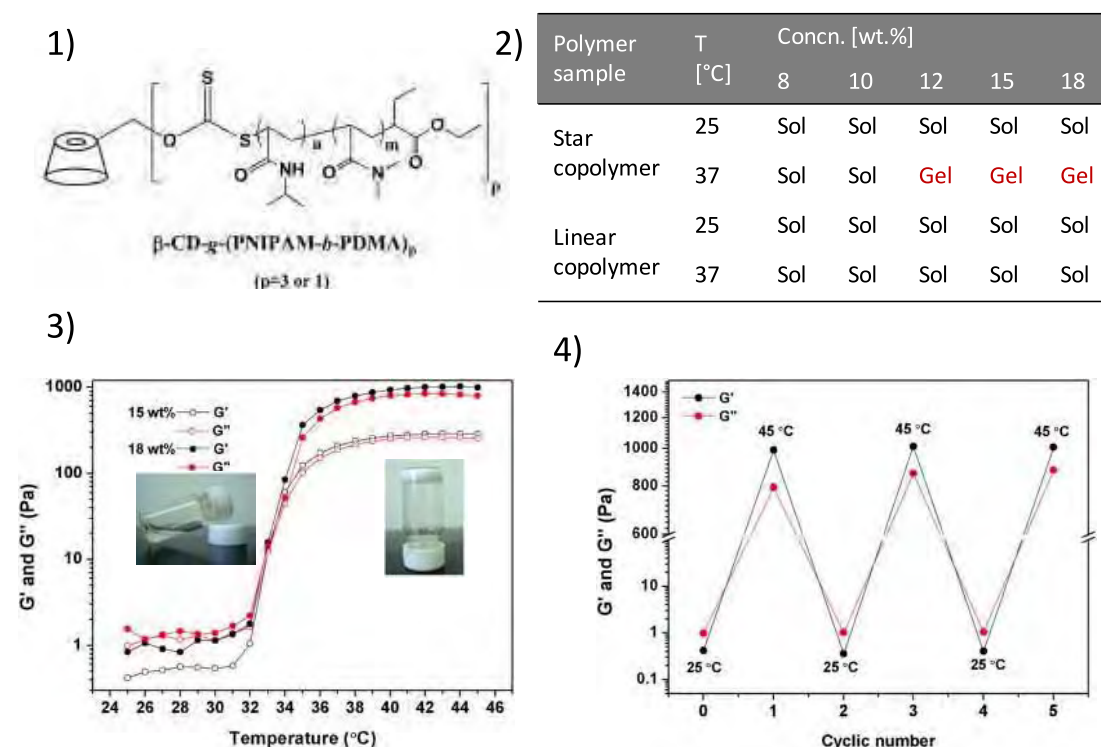


Figure I.8. 1) $\beta\text{-CD-}g\text{-(PNIPAM-}b\text{-PDMA)}_x$, $x=1$ or 3 . 2) Gelation behaviors of $\beta\text{-CD}$ -based star-shaped and linear copolymers in aqueous solution at 25 and 37 °C. 3) Storage modulus (G') and loss modulus (G'') for 15 and 18 wt% aqueous solution of star-shaped copolymer as a function of temperature. 4) Reversible sol–gel transitions cycled by alternative heating and cooling. [67]

Temperature responsiveness was introduced in a hydrogel system composed of a star copolymer β -CD-*g*-(PNIPAM-*b*-PDMA)₃ with a biocompatible β -Cyclodextrin (β -CD) core (Figure I.8). The star polymer was synthesized *via* RAFT polymerization. By simply heating and cooling, the star polymer exhibited robust sol–gel and gel–sol transitions. Above the cloud point, the gelation of the star-shaped polymer was ascribed to two reasons: the collapsed PNIPAM chains and the star-shape architecture. For the linear counterpart, gelation did not occur because there was only one-arm PDMA block in the copolymer, which was inadequate to ensure the occurrence of intermicelle bridging. [67]

c. **Liquid crystalline materials**

i) Main characteristics of liquid crystalline materials

The liquid crystalline state, also referred as mesophase, is the fourth state of matter that intermediates between that of a solid and a liquid. Liquid crystalline materials are generally classified into two categories, thermotropic and lyotropic mesophases (Figure I.9).

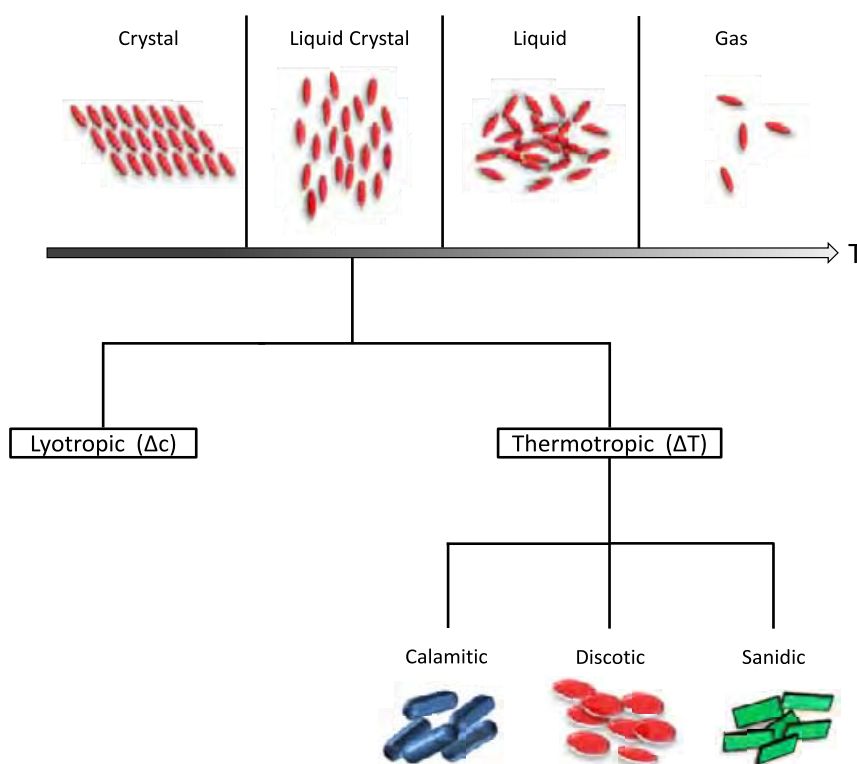


Figure I.9. The liquid crystal state as the fourth state of matter. The liquid crystal state is classified into two groups; the lyotropic phase which is solvent-dependant and the thermotropic phase which depends solely on temperature. The latter can be further classified according to the molecular shape: calamitic, discotic and sanidic. [80]

For mesomorphism to occur, molecules should constitute high geometrical anisotropy such as rods or discs. Depending on this geometry, the system passes through one or multiple mesophases as it transits from the highly ordered crystalline state with long range

orientational and positional order to the disordered isotropic liquid state (or *vice versa*). Transitions through these mesophase can occur *via* two processes. The first is the case of thermotropic liquid crystal phases, which are brought by a change in temperature, while the second is the lyotropic phase, which occurs in the presence of a suitable solvent. The latter is also affected by a change in concentration. The fundamental unit of a liquid crystal is called a mesogen. At this point it is also important to mention that some mesogens can exhibit both lyotropic and thermotropic phases, known as amphotropic. Since this thesis project concerns only thermotropic liquid crystals, we will focus our attention on this subject.

Thermotropic liquid crystals can be further subdivided according to the molecular shape of the constituent molecule. Figure I.10 shows the three sub-divisions; calamitic (rod-like), discotic (disk-like) and sanidic (board-like) mesogens. In Figure I.11 we show some examples of the three types of thermotropic-phase-forming LCs. Calamitic mesogens are often composed of a rigid aromatic-based core and one or two flexible alkyl or alkoxy chains. Commonly reported disk-like mesogens, are generally made of six flexible chains attached to a rigid core. Sanidic mesogens can be composed of either rod-like or disk-like mesogens that adapt a board-like structure. Other molecular anisotropies such as bent-core geometries [81] can also be found in literature but will not be discussed within this text.

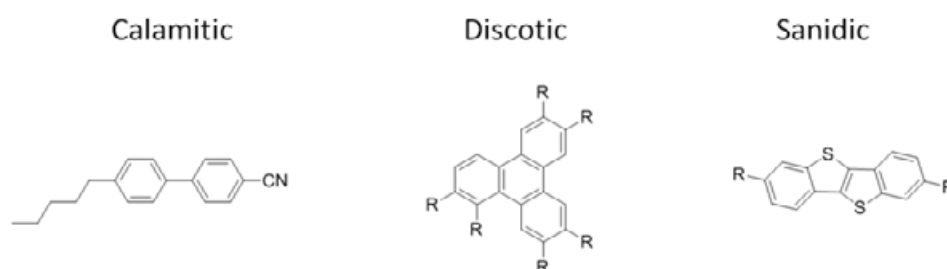


Figure I.10. Some selected examples of calamitic, discotic and sanidic mesogens.

A large number of thermotropic liquid crystals are composed of rod-like molecules. They can be simply classified into three groups; nematic, cholesteric and smectic (Figure I.11). The nematic phase (*N*) is characterized by a high degree of long-range orientational order, but no long-range translational order. This phase differs from the isotropic in that all mesogens spontaneously orient along a common direction characterized by the director n [82]. The preferred direction usually varies throughout a nematic liquid crystal but when uniformly aligned the LC is said to be optically uniaxial, positive and strongly birefringent.

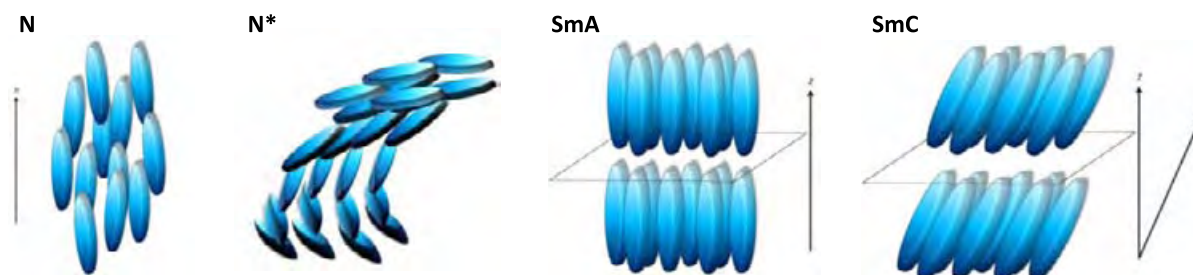


Figure I.11. Schematic representation of the structural order in the main thermotropic LC phases formed by rod-like mesogens. From left to right; the nematic (uniaxial) **N**, chiral nematic **N***, smectic-A **SmA** and smectic-C **SmC**.

The twisted version of the nematic phase is known as chiral nematic (N^*). A spontaneous twist in the structure of the nematic phase is brought about by the presence of optically active molecules that spontaneously results in a continuous helical distortion, about an axis normal to the director n . The orientation of the twist may be left- or right-handed depending on the molecular conformation. Elongated rod-like molecules commonly form the smectic liquid crystalline phase. From a structural point of view, the most prominent difference to nematics, smectic phases exhibit a stratified structure. This gives the system a degree of positional order of the molecules' center of mass. The arrangement of molecules within a layer can be different leading to the two most important smectic modifications. In the first case the mesogens are aligned with their longer molecular axes perpendicular to the layer plane; the smectic-A phase (SmA). While the second type is the smectic-C (SmC) which is essentially, a tilted form of the smectic-A, *i.e.* the molecules are inclined with respect to the layer normal. Although some smectic phases (*e.g.* SmA) can have fluidic properties, they are much more viscous than nematics. There are several different other types of smectic phases including chiral versions and ones with additional positional ordering, however they will not be discussed herein. For further reading refer to the *Handbook of Liquid Crystals: Vol.1., Fundamentals* [83].

The organization of disk-like structure mesogens (or discogens) generally fall under one of two main distinct categories, the nematic and the columnar (Figure I.12). The former is formed by disc-like molecules which have an orientational order but no long-range translational order (N_D). Whereas the columnar, is made up of stacked discogens in an aperiodic fashion that form columns in a two-dimensional lattice (*e.g.* N_{Col} or Col_h). The discotic nematic phase is however optically negative (for definition see annex), unlike the classical nematic exhibited by calamitic mesogens.

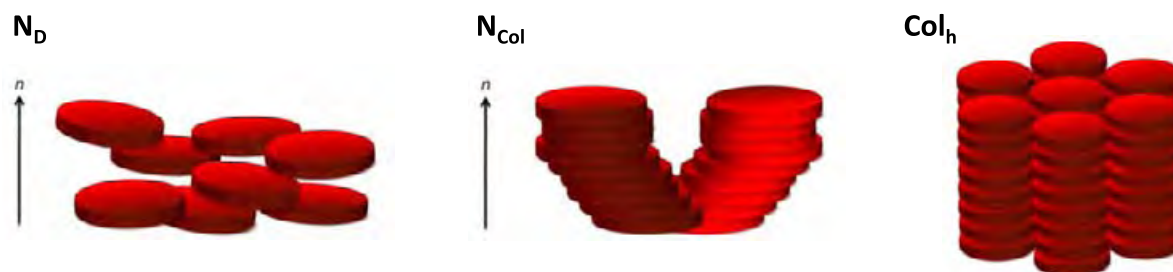


Figure I.12. Schematic representation of some different thermotropic LC phases formed by discotic-like mesogens; discotic nematic N_D , columnar nematic N_{Col} and hexagonal columnar Col_h .

ii) Branched Polymeric liquid crystals

Research on polymers forming liquid crystal phases has been an important field of polymer science for several decades. The most common structures forming such LC materials are given in Figure I.13. The monomer units consist of low molar mass calamitic or discotic mesogens which either form part of the main chain in the polymer backbone or attached as side groups. The nature of the mesophase is largely dependent on various factors, the most important being the type of mesogen, the spacers and the backbone itself. In the case of repeating calamitic units, nematic-, smectic- or cholesteric-like mesophases are generally

observed [84]. For polymers containing discotic liquid crystal units, different kinds of mesophases can be formed including the hexagonal columnar, smectic nematic and columnar nematic. Although the first reports on LC dendrimers date back to the 90s [85], [86], more important developments in this area only commenced in the second half of the last decade [87], [88]. Therefore liquid crystal dendritic structures have recently found an important place within this research area. This modern and promising field has led us to the investigation of liquid crystalline hyperbranched polymers (LCHBPs).

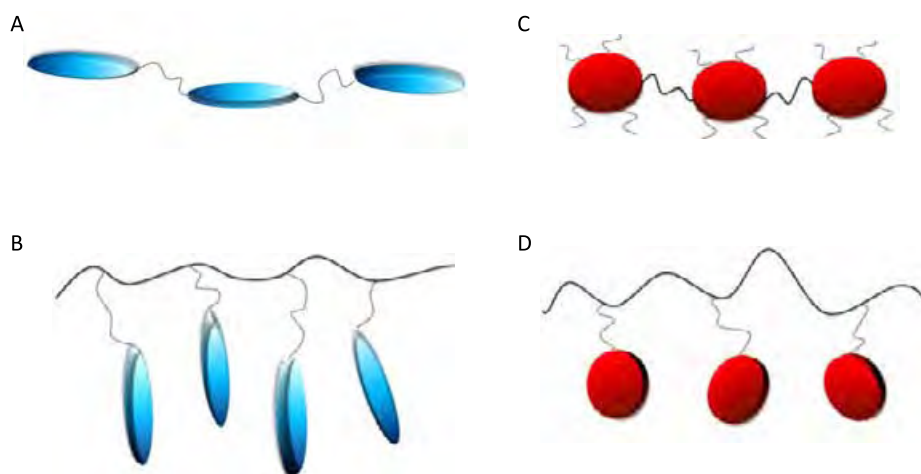


Figure I.13. Structures for the most common liquid crystal polymers. The mesogens can be of a rod-like (calamitic) or disc-like nature. These units can be attached to the polymer backbone (A and C) or as side groups (B and D).



Figure I.14. Schematic representation of the two general classes of liquid crystal hyperbranched polymers; main-chain (A) and side-chain (B).

As for the traditional LC polymers discussed above, the structural features of LCHBPs are also classified into two groups; main-chain and side-chain (Figure I.14). The mesogenic units in the former are introduced during the polymerization process and forms part of the branching units, whereas for side-chain LCHBPs, mesogenic units are found at the terminal zones of the structure. The attachment of mesogens can occur *via* covalent or non-covalent interactions. According to the literature, the first examples of LCHBPs were reported by Percec *et al.* with the formation of “willow-like” dendrimers consisting of aligned mesogenic

units that form the nematic phase [89], [90]. Shortly after, Bauer and co-workers reported on the synthesis of hyperbranched polymers with terminal chiral groups exhibiting cholesteric and smectic phases [91]. Hyperbranched polyglycerols with LC properties induced by mesogenic end groups was published by Sunder *et al.* The latter claim that complete mesogen functionalization of the end groups is not necessary for LC phase formation and broad nematic phases with low viscosities can be easily achieved using such LCHBPs [92].

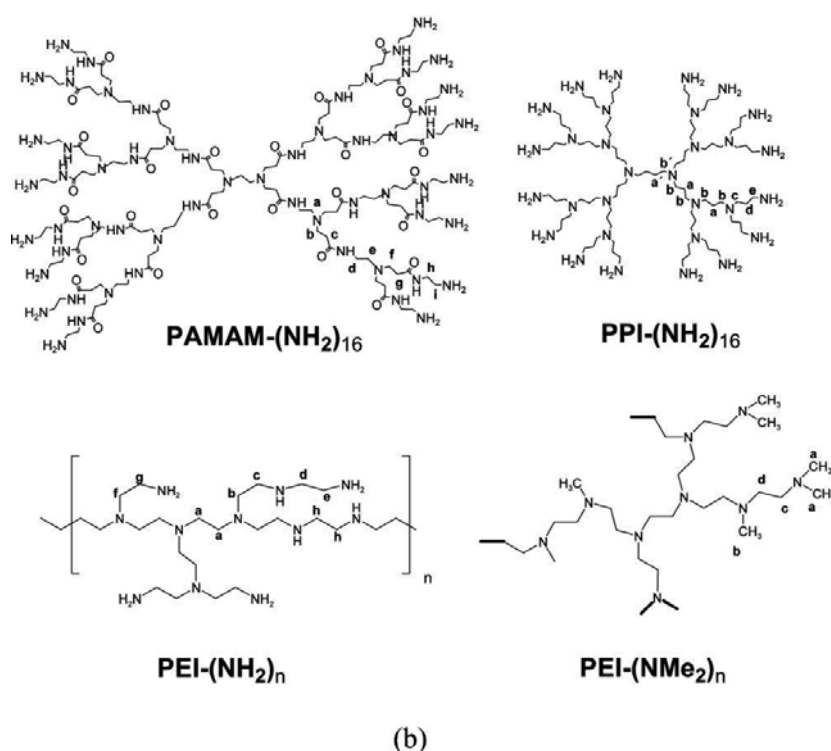
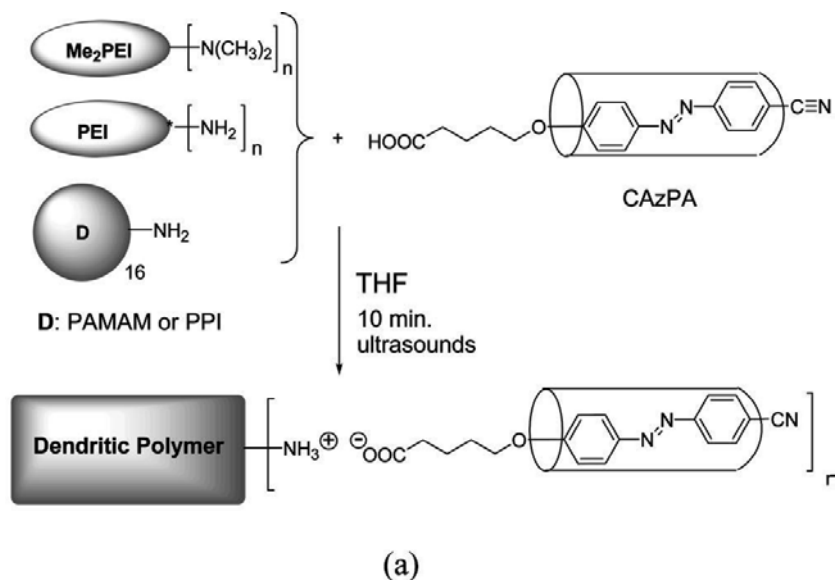


Figure I.15. The synthetic route to ionic dendritic complexes containing carboxylic acid-containing mesogens together with the structures for the dendrimers and HBPs used. Reprinted from Marco *et al.* [70]

The synthesis of LCHBPs by attachment of mesogenic entities *via* non-covalent interactions was recently demonstrated by Chen and co-workers [69]. Complexation of methylated hyperbranched PEI with carboxylic acid -containing mesogens was achieved by proton transfer forming the first ionic LCHBP with a nematic order. Authors claim that the nematic phases are rather unusual for LC polymers and have the potential in optoelectronic applications. Developments in this field was recently reported by Serrano *et al.* where the synthesis of ionic LC complexes was made possible by self-assembly of dendrimers or HBPs with an aromatic-based carboxylic acid (Figure I.15) [70]. The straightforward synthesis and photosensitive properties makes these dendritic complexes attractive for various optical applications.

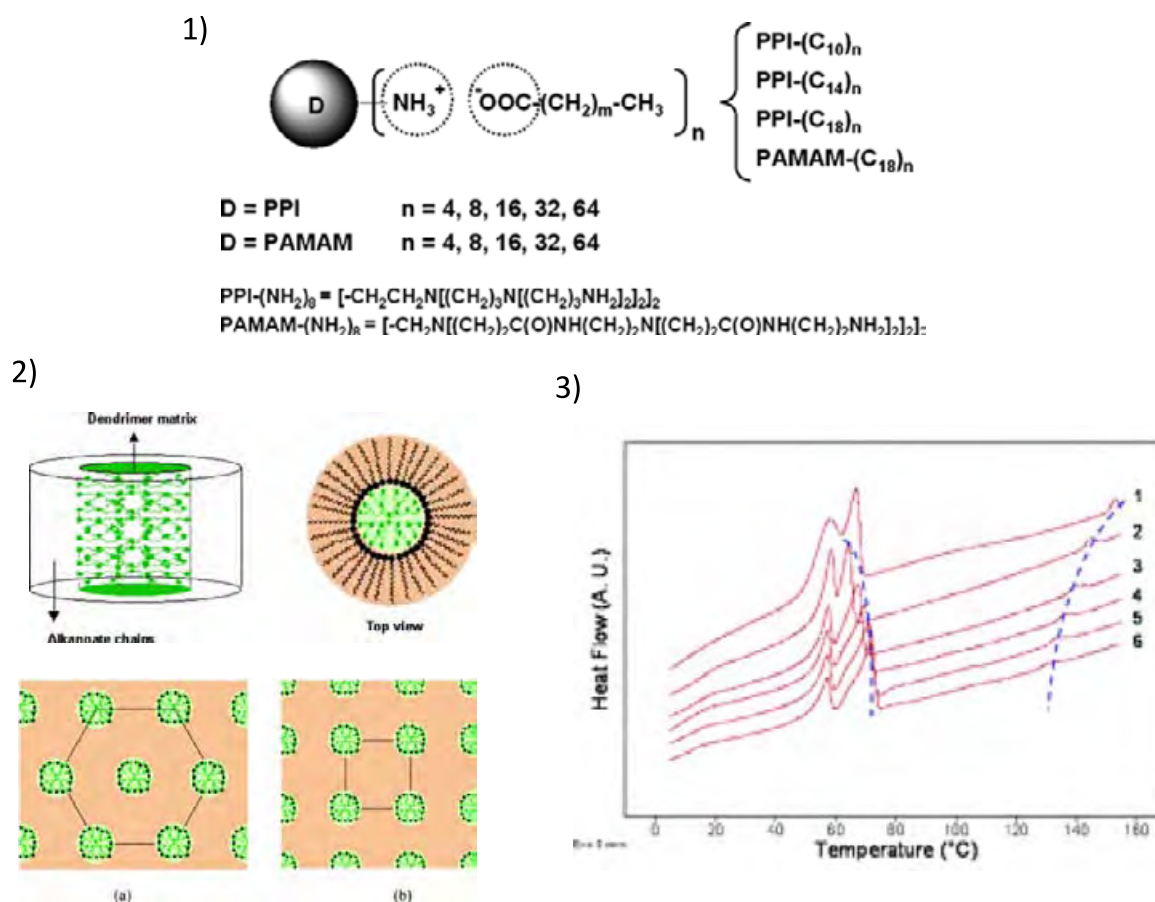


Figure I.16. 1) Ionic dendrimers, 2) Molecular model for the ionic dendrimers with a columnar mesomorphism, and schematic representation of the molecular organization in a columnar mesophase: (a) hexagonal; (b) tetragonal, 3) Evolution of the six consecutive DSC heating scans of PAMAM-(C18)16. [71]

Shortly latter, Serrano and co-workers [71] described a simple non-covalent dendrimer system which exhibit thermotropic liquid crystal behavior (Figure I.16). This system is achieved by converting the dendrimer surface from hydrophilic ($-\text{NH}_2$) to hydrophobic (alkyl chains). The method is based on the formation of ion pairs between *n*-alkanoic acids and the terminal amine groups of PAMAM and PPI dendrimers. The ionic dendrimers obtained do not have aromatic (pre)mesogenic groups in their structure, which

indicates that the ionic interaction plays a key role in the formation of a thermotropic lamellar mesophase and the enhancement of the thermal stability. The results reported indicate that these systems tend to assemble in smectic LC phases, as happened for covalent LC dendrimers. The exception to this trend is found for PPI-derived dendrimers of the fifth generation, which self-assemble into a columnar supramolecular structure.

Canilho and coworkers [72] describes solid-state structure of polyelectrolyte complexes generated from hyperbranched polylysine (HBPL) and various anionic, sodium alkyl sulfate surfactants (Figure I.17). HBPL–surfactant complexes were found to form liquid crystalline phases, whose thermal stability and structure depended both on the molecular weight of the HBPL as well as on the nature of the anionic surfactant. Depending on the surfactant alkyl chain length, liquid crystalline phases with short range liquid-like order, columnar hexagonal packing or lamellar ordering were observed. By combination of small-angle X-ray scattering (SAXS), differential scanning calorimetry (DSC), and cross-polarized light optical microscopy (POM), the exact structure of the LC phases, as well as their region of thermal stability, could be identified. HBPL–sodium dodecyl sulfate LC phases showed thermotropic behavior and underwent two transitions with increasing temperature. First, at lower temperatures, an order–nematic transition was observed. Upon further temperature increase, a second transition from a nematic to an isotropic phase was observed. Structural models for these different LC phases are proposed.

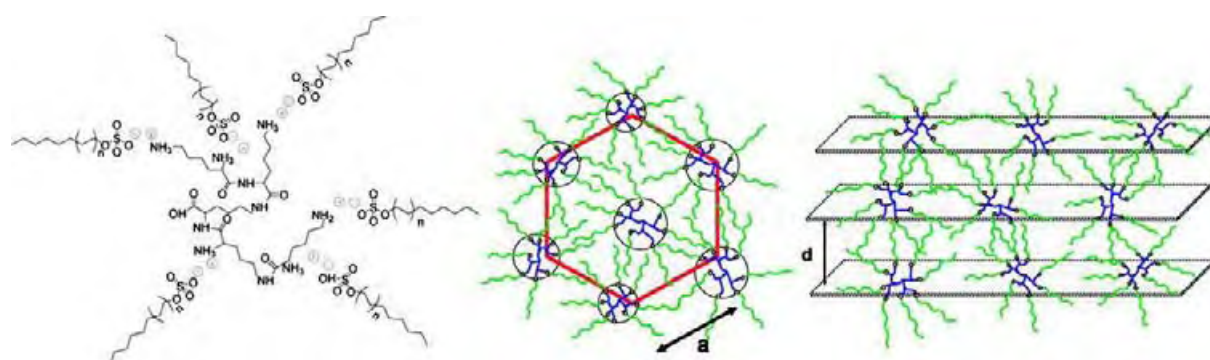


Figure I.17. Molecular structure of the HBPL-surfactant complex, schematic structure of hexagonal and lamellar phases [72]

Most recently Serrano describes ionic liquid-crystal PAMAM dendrimers by functionalization of the amine groups (inner and outer) of generations 0 to 4 functionalized with fatty acids of different length (Figure I.18). These amphiphilic dendrimers are capable to self-assemble both in bulk, generating mesomorphic materials, and in water. On the one hand, segregation between different nature moieties, namely, the hydrophilic PAMAM matrix and the hydrophobic fatty acid chains, is responsible for the supramolecular organization of these materials in the liquid crystal state. Smectic A mesomorphism was found for all of the compounds and rectangular columnar mesophase is displayed for the highest generation compound at low temperature. [73]

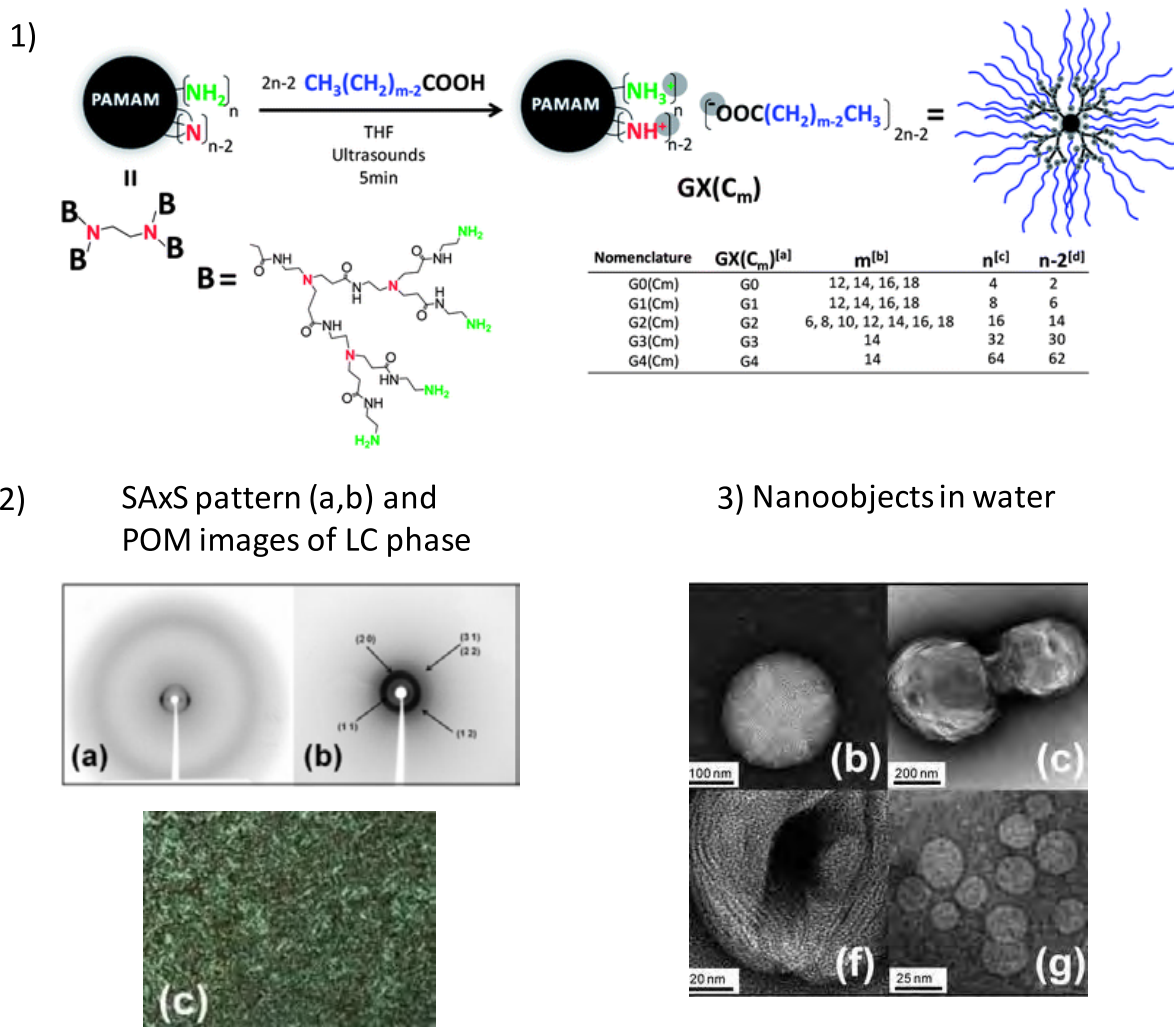


Figure I.18. 1) Schematic synthetic route, chemical structure of PAMAM (G1-4) and nomenclature for the ionic dendrimers. In the table: [a] generation, [b] number of carbon atoms of the acid, [c] terminal primary amine groups (in green) and [d] inner tertiary amine groups (in red). The subscript $(2n-2)$ points out that acid has been added to theoretically functionalize all amine groups of the dendrimeric core. 2) SAXS pattern and POM images of LC phase, 3) Representative TEM images of samples stained with uranyl acetate. [73]

Together with the mentioned literature above, a few other examples of hyperbranched liquid crystals can be found in literature. However, the domain is quite recent and the development for such materials geared towards important applications is an exciting challenge. For further reading, the tutorial review from Serrano and co-workers [93] was published regarding specifically about liquid crystal dendritic structures.

2. pH responsive materials

In the case of pH-sensitive polymers, the key element of the system is the presence of ionizable weak acidic or basic moieties. Upon ionization, the coiled chains extend dramatically responding to the electrostatic repulsions of the generated charges (anions or cations). However, complete ionization on polyelectrolytes is more difficult due to electrostatic effects exerted by other adjacent ionized groups especially when considering adsorbed polymer systems. As a result, the hydrodynamic volume of the polymer drastically increases. This transition between tightly coiled and expanded state is influenced by any condition that modifies electrostatic repulsion, such as ionic strength and type of counterions. The transition from collapsed state to expanded state has been explained by changes in the osmotic pressure exerted by mobile counterions neutralizing the network charges. The pH value at which this transition occurs could be tuned either by choosing the chemical nature of the polymer or by incorporating hydrophobic moieties in a controlled way. When ionizable groups become neutral – non-ionized – and electrostatic repulsion forces disappear within the polymer network, hydrophobic interactions dominate. The introduction of more hydrophobic moieties can offer a more compact conformation in the uncharged state and a sharper phase transition. pH-responsive polymers contain either weakly acidic (e.g., carboxylic acid) or basic (e.g., amine) groups, these either release protons or accept free protons, respectively, in response to environmental pH. For example, poly(acrylic acid) (PAA) has a dissociation constant pK_a of 4.25 and above this pH the carboxylic group becomes ionized (Figure I.19). This leads to electrostatic repulsion between the chains that can then associate with water to cause swelling. In addition, other polymers show an inverse behavior. The cationic polyelectrolyte poly(*N,N*-dimethylaminoethyl methacrylate) (PDMAEMA) shows ionized behavior at low pH values. Charge status in these materials is readily reversed by returning the pH of the solution.

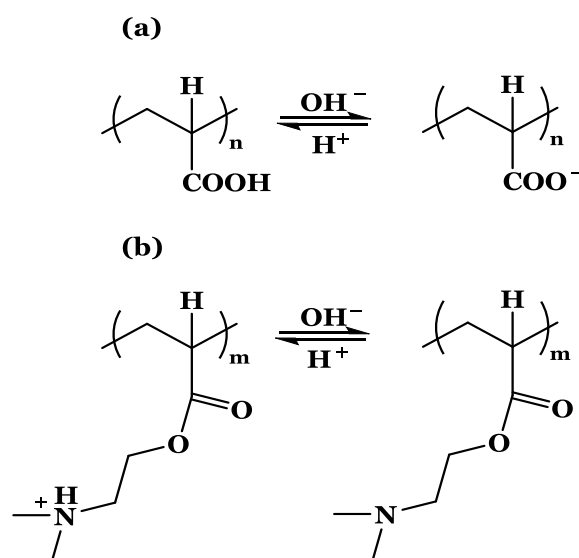


Figure I.19. Structures of pH-responsive polyelectrolytes (a) PAA and (b) PDMAEMA.

The most commonly used polymers with anionic groups are poly(acrylic acid) (PAA) [94] or poly(methacrylic acid) (PMAA) [95] and polysulfonamides (derivatives of *p*-benzene sulfonamide) [96]. The latter present a pK_a that narrowly varies from 3 to 11, depending on

the electron removing nature of the substituent on the nitrogen. An opposite behavior is shown by cationic polyelectrolytes, for example poly(2-aminoethyl methacrylamide) (PAEMAM), poly(2-aminoethyl acrylamide) (PAEAM), poly[N,N'-dialkyl aminoethyl (meth)acrylates] (PDMAEMA and PDMAEA) [97], poly(lysine) (PL) [98], [99], poly(ethylenimine) PEI [100], [101] have also been used.

Some of the dendritic structures based on these pH responsiveness polymers are reported in Table I.7.

Table I.7. Examples for pH responsive core-shell polymers

Core	Shell	Synthesis way	Application	Ref.
Hyperbranched Polyglycerols (HPG)	Amino ligand or PEG and Amino ligand or Aminoligand-b-PEG	Click chemistry Coupling onto	Copper ions carriers	[102] [103]
Hyperbranched polyethylenimine (HPEI)	Polylysine-PEG	1, ROP 2, grafting from	Encapsulation of insulin	[104]
HPEI	poly(l-glutamic acid) (PLG) inner shell, and a poly(ethylene glycol) (PEG) outer shell	-Grafting from PLG polymerization, then, coupling onto PEG	Encapsulation of crystal violet, hydrochloride doxorubicin	[105] [106]
HPEI covalently derived with dense carboxylic acids	PS	Coupling onto		[107]
HPEI	Brush-like polyacrylic acid mPAA-PS PS	Ionic interaction Coupling onto	highly charge-selective separation of ionic dyes	
HPEI-with beta-cyclodextrin inserted in the core	PEO : PolyEthylene oxide	EDC activated coupling reaction	Encapsulation of hydrophobic guest	[108]
HPG	DOX PEG	acid-sensitive hydrazone linker Michael reaction with maleimide	Release of doxorubicin	[109]
HBPolyther (PEOM)	N,N-dimethylamino-2-ethyl methacrylate	ATRP	Drug carrier : Congo red dye	[110]

	(PDMAEMA)			
hyperbranched poly(amidoamine) (HPAMAM)	PEG	pH-sensitive acylhydrazone bonds	nanoreactor for the formation in aqueous solution of CdS quantum dots	[111]
HPEI	PEO-PS	Succinic anhydride activation coupling Then: nitroxide-mediated living radical polymerization of styrene	Encapsulation and vectorization of drugs in different solvents	[112]
HPEI	PEG	Succinimide anhydride coupling		[113]

Nowag et al. present core-shell structures comprising hyperbranched polyglycerol (hPG) as cores (Figure I.20). The shells comprise a tri- or dimethylethylene diamine ligand as inner shells following by PEG outer shells (CMS). Alternatively, the ligand and PEG chains are both anchored directly to the HPG core (CRS) by click chemistry. These polymers have a high binding affinity for copper ions and were able to release these ions at low pH. It is demonstrated that the exact architecture of the core-shell system is a paramount parameter to control the maximum loading, the strength of complexation, and the release profile of copper into the solution. The CMS structure proved to be the most promising structure for Cu^{2+} complexation and release. [103].

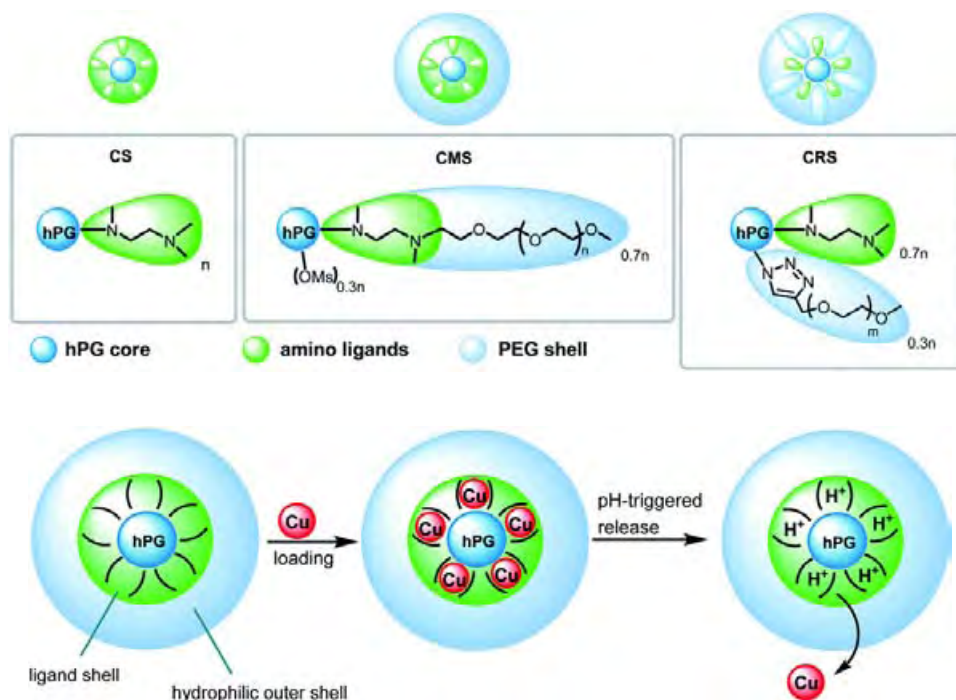


Figure I.20. Schematic structure of hyperbranched polyglycerol–ligand-PEG core-shell structure. [103]

Tian et al. reported triple-shell architectures consisting of poly[(*N,N*-diethylaminoethyl-methacrylate)-*block*-(*N*-vinylcaprolactam)-*block*-(*N,N*-dimethylaminoethyl methacrylate)] triblock copolymers, obtained by sequential reversible addition–fragmentation chain transfer polymerizations, using a terminal-modified hyperbranched poly(β -cyclodextrin) core as a macro chain transfer agent (Figure I.21).[25]

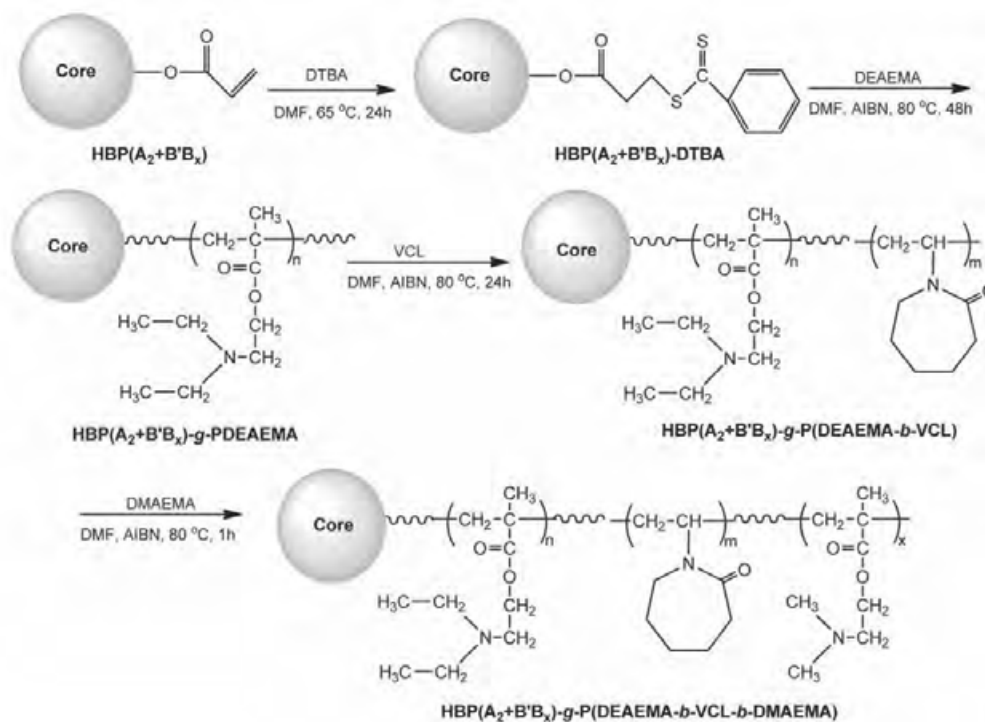


Figure I.21. Synthesis scheme of triple-shell architectures by sequential RAFT polymerizations. Adapted from ref [61].

Firstly, the HBP(A₂+B'_x)-DTBA carrying dithiobenzoyl groups as a macro CTA was synthesized based on the Michael addition reaction between the sulfhydryl groups of DTBA and the double bonds from allyl groups. Then, three sequential RAFT polymerizations were carried on using this macroinitiator. Polymers with increasing molar mass polymers were synthesized as confirmed from SEC-MALLS measurement (molar masses were estimated to 94000, 169000 and 226000 g.mol⁻¹). Furthermore, the triple-shell architectures possess one pH-responsive from the PDEAEEMA block at pH 12.5 aqueous solution under room temperature, followed by a double-temperature-response based on P(VCL-b-DMAEMA) block copolymers between 33 and 36 °C at pH 12.5. Furthermore, this kind of triple-shell structure is more stable than that of a single or double-shell structure during the process of phase transition. The above results can be further confirmed by investigating the controlled release behaviors of metronidazole as a model drug from the hyperbranched poly(β -CD) core–triple-shell architectures under different pH and temperature conditions. DLS and TEM characterizations were not performed to characterize the size and the shape of the obtained core-multishell structure.

3. Light and redox responsive materials

In drug delivery, researchers have begun to focus on incorporating redox-responsive degradable linkages to such as disulfide bonds into the macromolecular vehicles where core-shell structures were largely employed. The cleavage of disulfide bond in the delivery vehicles could be mediated by thiol/disulfide exchange reactions with small redox molecules like glutathione, either alone or with the help of redox enzymes.

Pang et al. reported a bioreducible amphiphilic multiarm hyperbranched copolymer based on H40 core, PLA inner-shell and PEG outer-shell with disulfide-linkages between the hydrophobic and hydrophilic moieties as unimolecular micelle for intracellular drug release triggered by glutathione in tumor cells (Figure I.22). The synthesis process was carried out by ring-opening polymerization (ROP) of LA using H40 as a macroinitiator and Sn(Oct)₂ as a catalyst, and then following by coupling mPEG-SS-COOH to H40-star-PLA-OH by DCC activated coupling reaction. Doxorubicin (DOX) was encapsulated into these reductive unimolecular micelles. In vitro release studies revealed that under the reduction-stimulus, the detachment of PEG outer-shell in DOX-loaded micelles resulted in a rapid drug release. [114]

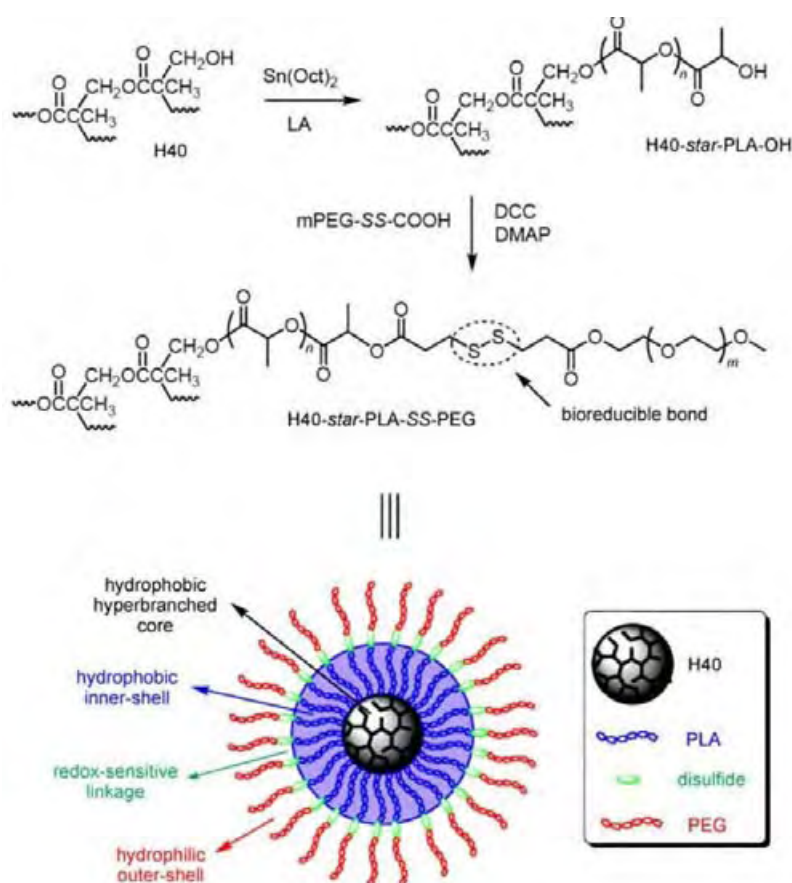


Figure I.22. Detailed synthetic route and illustration of unimolecular micelle structure of H40-star-PLA-SS-PEG. [114]

You et al. present the approach for preparing the dually responsive core-shell nanostructure: Michael-addition polymerization of triamine (B, 1-(2-aminoethyl)piperazine, AEPZ) with double molar bisacrylamide (A, *N,N'*-cystamine bisacrylamide, CBA) forms

hyperbranched polymer with redox-sensitive disulfide bonds in the backbone and vinyl terminals, then the amino-ended poly(*N*-isopropylacrylamide) (PNIPAM-NH₂) was directly added into the above polymerization mixture, the vinyl terminals further reacted with PNIPAM-NH₂ *via* Michael-addition reaction, thereby linking temperature-responsive shell to the redox-sensitive hyperbranched core (Figure I.23). Consequently the dual stimuli-responsive core-shell nanostructure (the core is responsive to redox agent and the shell is responsive to temperature) was obtained simply *via* one-pot approach [115].

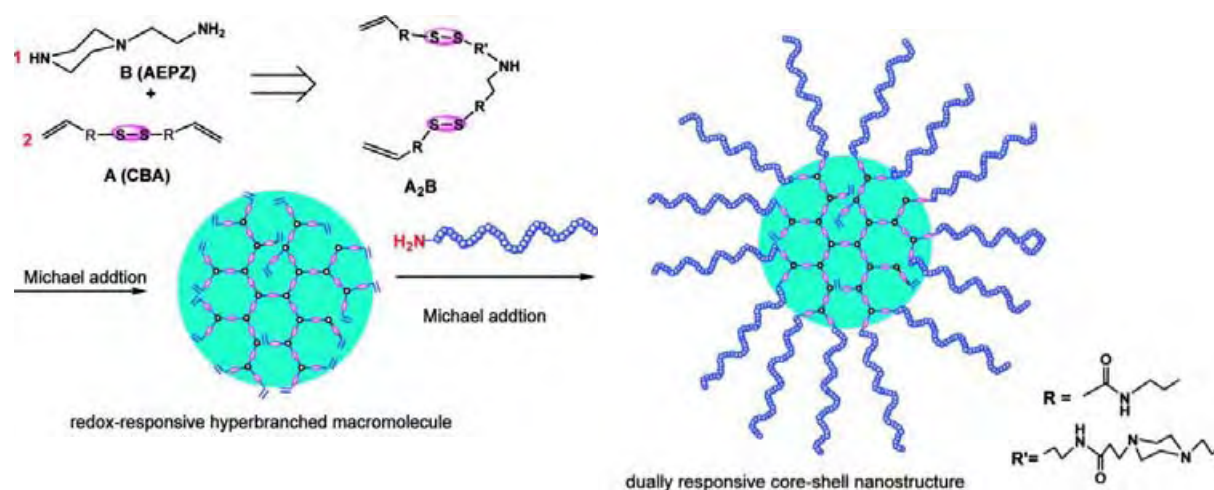


Figure I.23. One-pot synthesis for preparing a redox-responsive HBP core PNIPAM shell structure. [115]

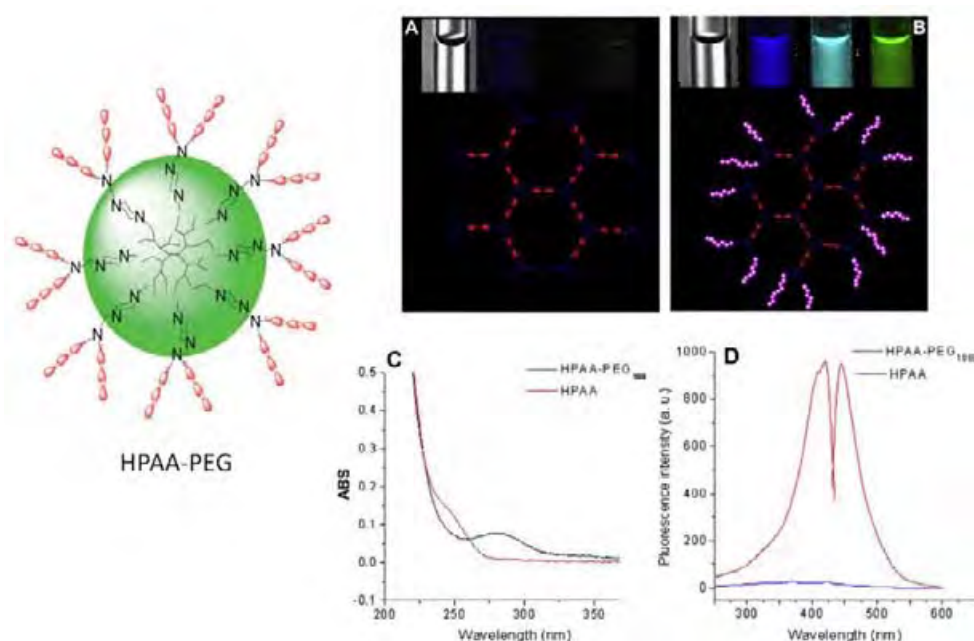


Figure I.24. Optical fluorescence microscope images of aqueous solutions of HPA (A) and HPA-PEG188 (B) in a capillary (from left-to-right, the first, no filter was used, and then the light filters used are BFP (380 nm), CFP (435 nm) and GFP (489 nm)); absorption spectra of HPA and HPA-PEG188(C); and fluorescence excitation and emission spectra of HPA and HPA-PEG188(D). [116]

Concerning photosensitive core-shell polymers, Di Wang et al. have reported that hyperbranched poly(amido amine)s (HPAA) show weak photoluminescence, however, they have shown strong emission after short polyethylene glycol (PEG) chains have been linked onto HPAA macromolecule *via* Michael addition reaction (Figure I.24). The authors claimed that the PEG shell around HPAA change the microenvironment and surface charge density of HPAA in solution, hence highly intensify the photoluminescence. [116]

4. Conclusions

Through this section, we have reviewed the stimuli-responsive core-shell polymers based on dendritic core by core-first, coupling to and ionic interaction approaches. We can see that the core-shell architecture have an important impact on the stimuli responsiveness of the systems in solution. Furthermore, wide range of self-assembly structure (liquid crystals, micelles or unimolecular micelles, hydrogels ...) can be generated from dendritic based core-shell structures. Their internal structures can be modulated by changing architectures and chemical compositions of the starting polymers. These self-assembled structures can be induced by external stimulus such as temperature, pH, light, redox potential. Most of the reported application of those systems concerns their use as drug carrier whose release response to an external stimulus. Those systems were also taken into account to have access to stimuli responsive inorganic/organic hybrid materials. This interesting subject will be explored in the following sections.

II. Nano-hybrid materials from polymeric nanostructured soft-template

In recent years, there has been a considerable interest in the development of metal- and semiconductor-based nanomaterials, in part for their unique optical, electronic and catalytic properties and also because nanometer-size structures are appropriate for interfacing with biomacromolecules (proteins, DNA, and so forth) and probing intracellular environments [20], [117], [118]. Dendritic polymers have high molecular weights, globular structures, intramolecular cavities and a large number of chemical functions showing superb capability for the synthesis and stabilization of monodispersed nanoparticles [119]. In this section, we will discuss the different approaches for the stabilization and the *in situ* formation of nanoparticles from branched polymer structures presented in the first part of this chapter.

A. Nano-hybrid materials

1. Nanoparticles: some generalities

a. *Introduction*

Physicists predicted that nanoparticles in the diameter range 1–10 nm (intermediate between the size of small molecules and that of bulk metal) would display electronic structures, reflecting the electronic band structure of the nanoparticles, owing to quantum-mechanical rules. The resulting physical properties are neither those of bulk metal nor those of molecular compounds, but they strongly depend on the particle size, interparticle distance, nature of the protecting organic shell, and shape of the nanoparticles.

In recent years, there has been a considerable interest in the development of metal- and semiconductor-based nanomaterials, in part for their unique optical, electronic and catalytic properties and also because nanometer-size structures are appropriate for interfacing with biomacromolecules (proteins, DNA, and so forth) and probing intracellular environments (Figure II.1). The chemical methods have conspicuous advantages in controlling the size and shape of NCs, which would seriously influence the properties. On the other hand, NCs show aggregation tendency because of strong interactions between each other owing to colossal surface energy, resulting in poor change of performance. Thus, besides the size and shape, dispersibility and stability of NCs are also crucial for their performance, functions, and real applications.

Because the sizes of nanomaterials are comparable to the sizes of biomolecules such as proteins, they can be designed for biomedical applications such as devices for diagnosis, drug delivery, and therapy.

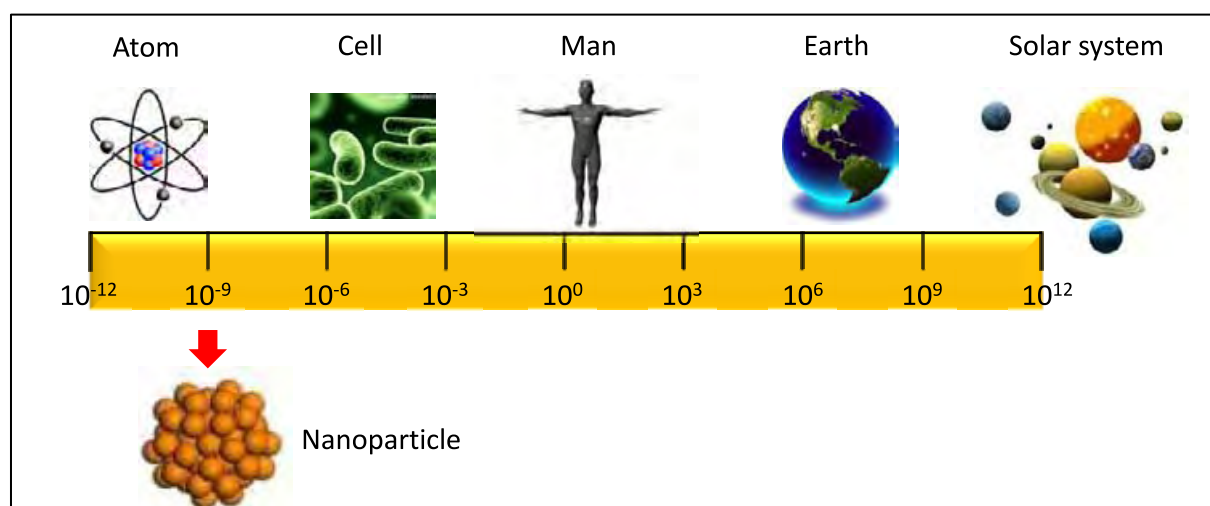


Figure II.1. Characteristic size of nanoparticles.

b. **Gold nanoparticles**

i) Properties of gold nanoparticles

Gold nanoparticles (AuNPs) are the most stable metal nanoparticles, and they present fascinating aspects such as their assembly of multiple types involving material sciences, the behavior of the individual particles, size-related electronic, magnetic and optical properties (quantum size effect), and their applications to catalysis and biology. Their promises are in these fields as well as in the bottom-up approach of nanotechnology, and they will be key materials and building block in the 21st century.

Michael Faraday first observed that the colloidal gold solutions have properties that differ from the bulk gold [120]. Hence the colloidal solution is either an intense red color (for particles less than 100 nm) or a dirty yellowish color (for larger particles) [120]. These interesting optical properties of these gold nanoparticles are due to their unique interaction with light [121]. In the presence of the oscillating electromagnetic field of the light, the free electrons of the metal nanoparticles undergo an oscillation with respect to the metal lattice. This process is resonant at a particular frequency of the light and is termed the localized surface plasmon resonance (LSPR) (Figure II.2). After absorption, the surface plasmon decays radiatively resulting in light scattering or nonradiatively by converting the absorbed light into heat. Thus for gold nanospheres with particle size around 10 nm in diameter have a strong absorption maximum around 520 nm in aqueous solution due to their LSPR (Figure II.3). These nanospheres show a Stokes shift with an increase in the nanosphere size due to the electromagnetic retardation in larger particles.

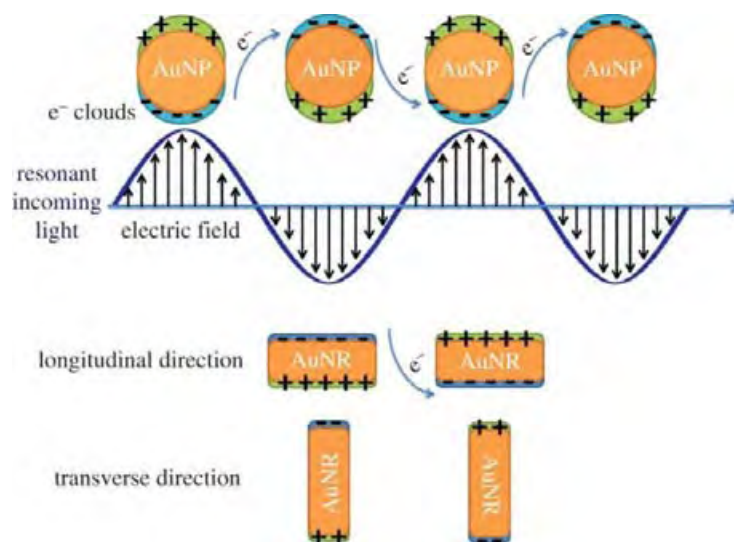


Figure II.2. Surface plasmon oscillations in spherical gold nanoparticles (AuNPs) and gold nanorods (AuNRs). [122]

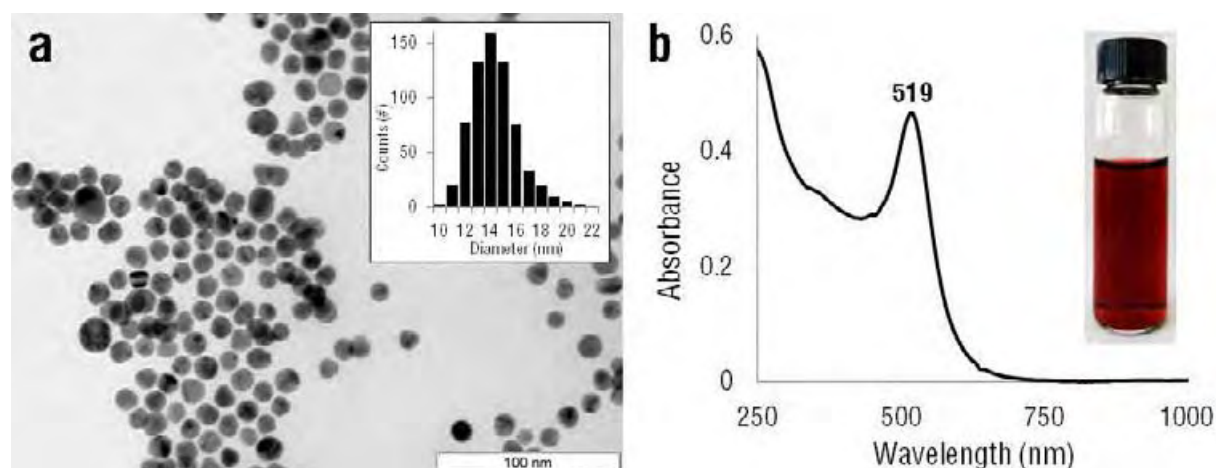


Figure II.3. (a) TEM image (scale bar = 100 nm) and size distribution histogram (Inset) showing an average diameter of 14.35 ± 1.97 nm. (b) UV-Vis spectrum of the synthesized gold nanoparticles with a characteristic surface plasmon resonance band at 519 nm and a representative photograph of the same nanoparticles (inset). [123]

Moreover, the properties and applications of colloidal gold nanoparticles also depend upon its shape. Figure II.4 shows that the difference in color of the particle solutions is more dramatic for rods than for spheres [124]. For example, the rod-shaped nanoparticles have two resonances: one due to plasmon oscillation along the nanorod short axis and another due to plasmon oscillation along the long axis, which depends strongly on the nanorod aspect ratio, that is, length-to-width ratio. When the nanorod aspect ratio is increased, the long-axis LSPR wavelength position red shifts from the visible to the near infrared (NIR) and also progressively increases in oscillator strength. For example, rodlike particles have both transverse and longitudinal absorption peak, and anisotropy of the shape affects their self-assembly. Due to these unique optical properties, gold nanoparticles are the subject of substantial research, with enormous applications including biological imaging, electronics, and materials science. Thus to develop gold nanoparticles for specific applications, reliable and high-yielding methods including those with spherical and non spherical shapes have been developed over the period of years. [125]

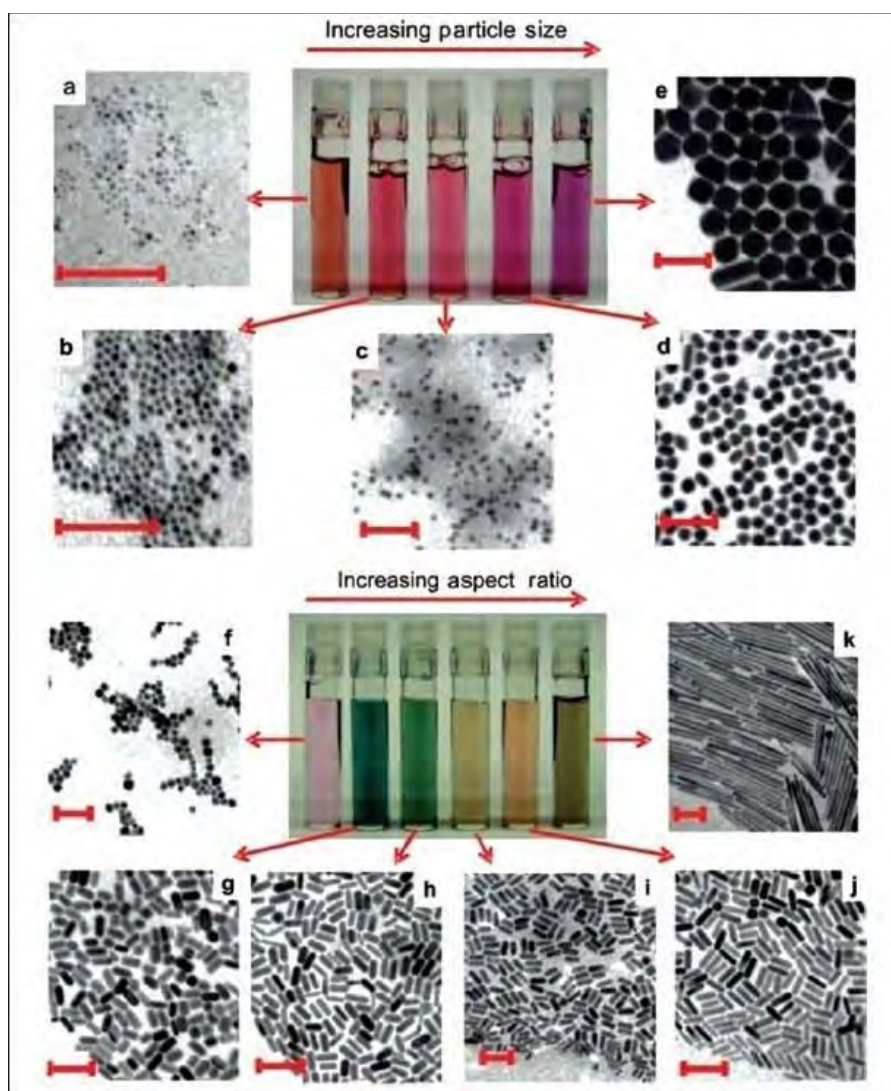


Figure II.4. Photographs of aqueous solutions of gold nanospheres (upper panels) and gold nanorods (lower panels) as a function of increasing dimensions. Corresponding transmission electron microscopy images of the nanoparticles are shown (all scale bars 100 nm). The difference in color of the particle solutions is more dramatic for rods than for spheres. This is due to the nature of plasmon bands (one for spheres and two for rods) that are more sensitive to size for rods compared with spheres. For spheres, the size varies from 4 to 40 nm (TEMs a-e), whereas for rods, the aspect ratio varies from 1.3 to 5 for short rods (TEMs f-j) and 20 nm(TEM k) for long rods. [124]

ii) Synthesis methods of AuNPs

The synthesis of gold nanoparticles has been developed using either physical methods (thermolysis, photochemistry, sonolysis, radiolysis ...) or chemical ones. We will focus on the latter ones in the following.

The most popular way to produce AuNPs is the reduction of metal salts. Among all available methods, the most commonly used are Turkevich and Brust methods [126] [127]. Citrate and cetyl trimethylammonium bromide (CTAB) were used respectively in those methods. These methods also necessitate the use of stabilizing agents that enable to control

especially in the context of emerging nanoscience and nanotechnology with nanoparticles which leads to an exponentially increasing number of publications. This thesis project has devoted to this research topic through exploring a relatively new approach: the use of various polymeric assembly systems as soft template for the synthesis of AuNPs and gold nanohybrids. In the following sections, I will focus my attention on the literature of this topic. When needed nanohybrids issued from different inorganic parts (Pt, Ag, ...) will be also discussed.

2. Synthesis of nano-hybrid materials

The nanoparticles (NPs) are usually coated with an organic or inorganic layer that provides solubility, long-term colloidal stability and functionalization. Nanohybrids adopt some characteristics from the components that compose it; synergistic effects can also produce properties not present in any of the parts. In general, two methodologies have been adopted for the synthesis of nanohybrid materials: *in situ* synthesis of NPs or post-modification of preformed NPs (Figure II.7). Polymeric self-assembled structures appear as fascinated candidates for these subjects.

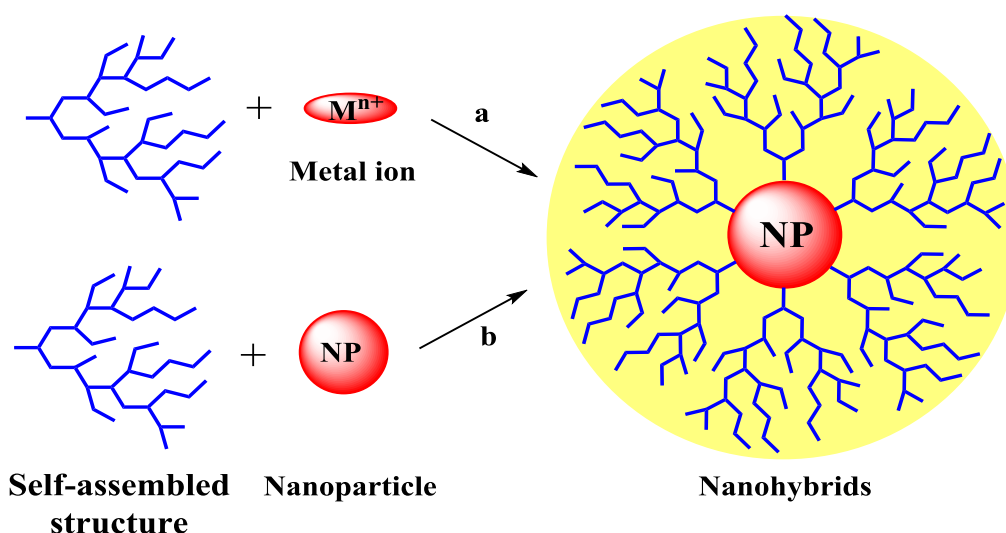


Figure II.7. Two methodologies of nanohybrid synthesis: a) *in situ* synthesis of NPs, b) post-modification of preformed NPs (*ex situ* method)

B. Nanoparticles stabilization in polymeric aqueous solution

1. Introduction

Dendritic polymers possess excellent attributes of three-dimensional topology, low viscosity, good solubility, and plenty of modifiable terminal groups. The combination of nanocrystals NCs and dendritic polymers (DPs) to form nanohybrids cannot only endow NCs with multifunctionality, uniform dispersibility, and splendid solubility but also can impact extra properties to dendritic polymers. Nanohybrids (NHBs) can be obtained by three approaches: *in situ* synthesis of NCs with the present of dendritic polymers, grafting from (i.e., DPs grow from the surface of as-prepared NCs), and grafting to (the original ligand of

NCs is replaced with DPs). Various DPs including hyperbranched poly(amidoamine), polyethylenimine, polyglycerol, polyester, polyamide, polyurethane, and poly(3-ethyl-3-hydroxymethyloxetane), as well as sorts of NCs such as metals (e.g., Ag, Au, Pd, Pt, and Rh), quantum dots (e.g., ZnO, CdS, CdTe, CdSe, and SnO₂), magnetic oxides (e.g., Fe₃O₄), rare earth compounds, and so forth, have been used to obtain NHBs. Here, we mainly focus our attention on the synthesis of nanohybrids composed of DPs and gold NPs. Highlighted examples of dendritic/gold nanohybrids were reported in Table II.1.

Table II.1. Selected examples for synthesis of gold-dendritic polymer nanohybrid by grafting to and *in situ* method

Grafting to method							
Hyperbranched polymers	End groups or shell	M _w (*10 ³ g.mol ⁻¹)	Synthesis method	AuNPs size (nm)	T _{synthesis} (°C)	Reaction time	Ref
Poly(ethylene glycol methacrylate) (PEGMA)	trithiocarbonate and alkyne	25.8, 53.7, 34.4, 153.2	Grafting to (ligand exchange)	17-18	Room temperature (R.T).	12h	[137]
Hyperbranched polyglycerols (HPGs)	OH, NH ₂	7.1, 11.6, 13.1, 14.5	Grafting to (ligand exchange)	13.5	R.T.	48h	[138]
Hyperbranched polyglycerol HPG	NIPAM	4.9, 10.4, 22.5	Grafting to (ligand exchange)	12	R.T.		[139]
<i>In situ</i> method							
Hyperbranched polymers	End groups or shell	M _w (*10 ³ g.mol ⁻¹)	Reductants	AuNPs size (nm)	T _{synthesis} (°C)	Reaction time	Ref
Hyperbranched poly(amidoamine)s HPAMAMs	methyl ester terminals COOCH ₃	3.3	without external reductant	Spherical ~ 4.0	R.T.	Several days	[140]
Hyperbranched polyglycidol	Mono-pyrene and OH	3.2	without external reductant	Spherical 4.5-35.5	60°C	6h	[141]
Hyperbranched polyester Boltorn G2, 3, 4	OH	1.7, 3.6, 7.3	hydrazine	1.8 - 420	R.T.	24h	[142]
Hyperbranched poly(amine-ester)	OH	1.6, 3.7, 6.6	D-glucose	24.2, 18.3, 13.6	R.T.		[143]
Hyperbranched polyethylenimine	palmitamide (C16) chains	1.8, 10.0, 25.0	NaBH ₄		R.T.	10 min	[144]
HPAMAMs	OH	16.5, 20.8	NaBH ₄	5	R.T.	2 days	[145]
Hyperbranched poly(amidoamine) (HYPAM)	NH ₂	13.6, 30.3	NaBH ₄	4	R.T.		[146]
	Gluconamide	116.2	NaBH ₄	4	R.T.		

2. *In situ* synthesis of nanoparticles

The three-dimensional structure of hyperbranched polymers (HBP) provides large amount of nanocavities both intra- and inter-molecule, which can be used as boxlike container to encapsulate metal ions. In the presence of HBPs and metallic cations, metal and metal-contained nanocrystals (NC) could be obtained by the addition of a reducing agent. Furthermore, HBP possess abundance of functional groups, and some of them can complex with metal ions and then stabilize resulting NC *via* multivalence mode of interactions. Various HBP have been used as templates to prepare series of NC. In the case of gold nanoparticles, control the size of the *in situ* synthesized AuNPs when changing the molecular weight of the HBP or changing the ratio between the [HBP]/[Au], as well as the interaction of metal precursor with the HBP.

Li et al. reported the utilization of a mono-pyrene terminated hyperbranched polyglycidol (mPTHP) as a building block to fabricate one dimension (1D) mPTHP and mPTHP/Au NP nanostructures by one-pot reactions in aqueous environments with no additional reducing agents, surfactants and organic solvents (Figure II.8). Upon simply mixing Au(III) ions and mPTHP at room temperature, mPTHP nanofibers and nanotubes were fabricated *via* Au(III) induced self-assembly processes. By simply elevating the reaction temperature from room temperature to 60 °C, Au NPs were *in situ* generated within mPTHP assemblies through an analogous polyol process. The involvement of NaBr provided an alternative way to obtain mPTHP/Au NP nanotubes with Au NP belts centered around their inner surfaces and mPTHP/Au NP pseudo-nanotubes with double-line Au NP chains linearly aligned along their inner surfaces. Moreover, the size of the resultant Au NPs could be controlled from 4.5 to 35.5 nm, depending on the Au(III) concentration. [141]

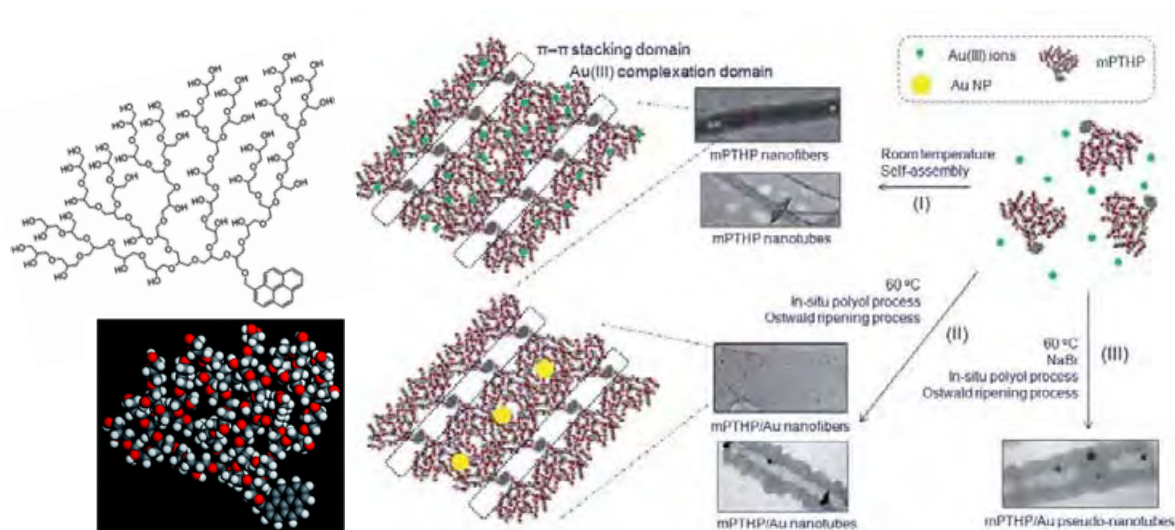


Figure II.8. Schematic illustration for the generation of 1D mPTHP self-assemblies and mPTHP/Au NP hybrid nanostructures with tunable spatial distribution of Au NPs. Ref [141]

Shi et al. reported a methyl ester-terminated hyperbranched polyamidoamine (HPAMAM-COOCH₃) as nanoreactors and reductants to prepare Au NPs with small particle size (Figure II.9). The authors suggested that HPAMAM-COOCH₃ bound AuCl₄⁻ through their internal amines, whereas the external methyl ester groups prevented the aggregation of

polymers, thus non-aggregated AuNPs around 4nm sequestered by HPAMAM-COOCH₃ were obtained. Benefiting from the repulsive interactions among the ester groups, HPAMAM-COOCH₃ nanoreactors were proved to be effective in controlling the size of Au and Ag NPs. [140]

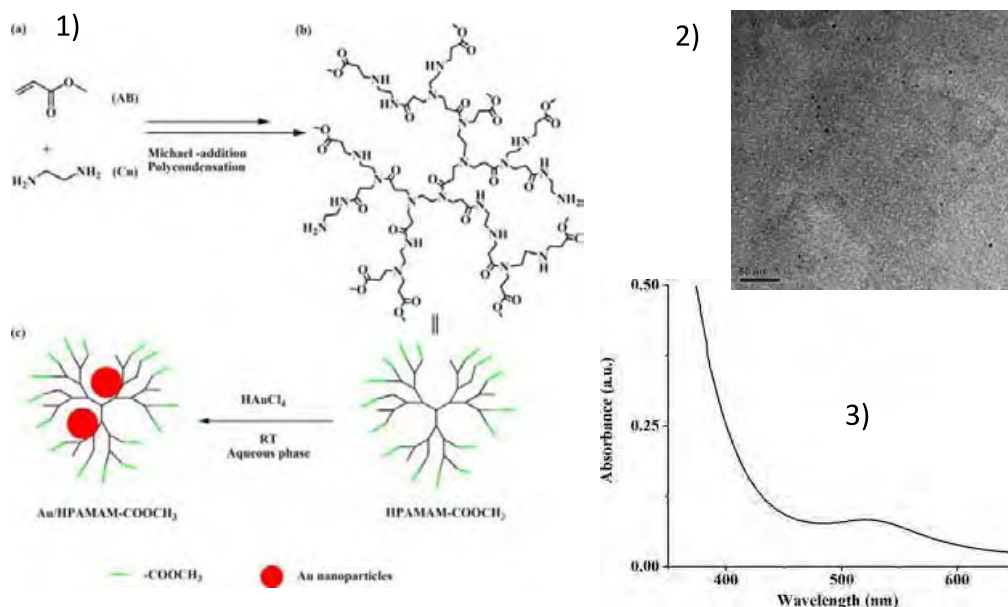


Figure II.9. 1) Schematic illustration for (a,b) the synthesis of HPAMAM-COOCH₃ and (b,c) the preparation of Au NPs using HPAMAM-COOCH₃ nanoreactors and reductants. 2) TEM image of Au NPs prepared within HPAMAM-COOCH₃. 3) UV-Vis spectrum of Au NPs prepared within HPAMAM-COOCH₃ nanoreactors and reductants. [140]

Sekowski et al. described a comprehensive investigation on the synthesis and characterisation of hybrid materials based on gold nanoparticles assisted with pseudo G₂, G₃ and G₄ generations of hyperbranched polyesters (HBP) (Boltorn H₂₀, H₃₀, H₄₀). Nanoparticles (NPs) were obtained *via* a wet chemical method by mixing HBP polymers and a gold precursor in N,N'-Dimethylformamide (DMF) followed by reduction by hydrazine (Figure II.10). The system has been evaluated with two HBP: Au molar ratios 1:1 and 1:10. Well-defined and novel HBP-AuNPs hybrid materials were obtained mainly as a result of the interaction between the peripheral hydroxyl groups of HBP and the gold nanoparticles. In the hybrid nanomaterials synthesis process, volcano-nanorings structures were obtained on solid substrate during the reaction of HBP-G₄-OH₆₄ (Boltorn H₄₀) with gold nanoparticles. These novel nanostructured hybrid materials could be used in medicine as specific nano-containers for different drug molecules. [142]

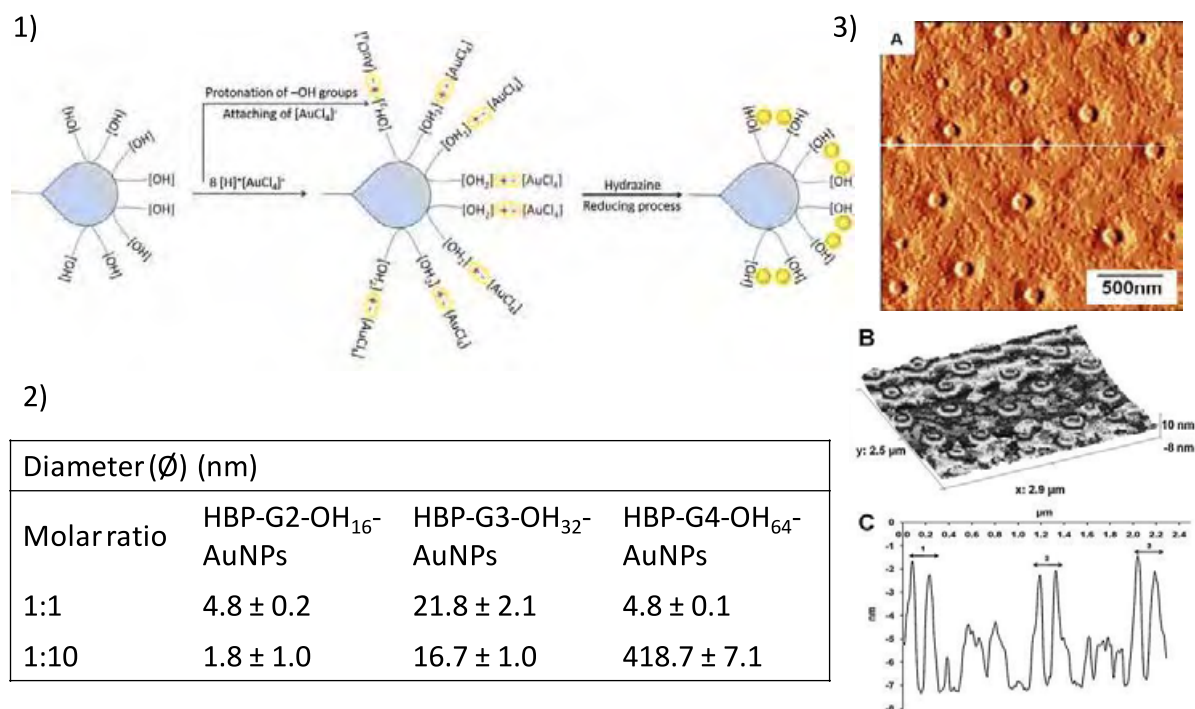


Figure II.10. 1) Mechanism of fabrication of hybrid materials based on hyperbranched polyester HBP polymers and gold nanoparticles, 2) Diameters (\varnothing) of synthesized HBP-AuNPs hybrid nanoparticles, 3) “Volcano-rings” structures of HBP-G4-OH₆₄-AuNPs (molar ratio 1:10). [142]

Zhang et al. reported a series of different generation hyperbranched poly(amine-ester) with hydroxyl as terminal group as protectants to *in situ* synthesize gold nanoparticles using D-glucose as reducing agent (Figure II.11). The results of UV-Vis absorption spectroscopy, TEM and SEM images showed that the mean diameter were 24.3 ± 2.6 nm, 18.2 ± 2.1 nm, and 13.6 ± 1.5 nm corresponding to the different generation hyperbranched poly(amine-ester), and the synthesized gold nanoparticles were almost monodisperse with a narrow size distribution. This study show the control over size of AuNPs by changing the molar weight of the hyperbranched template [143].

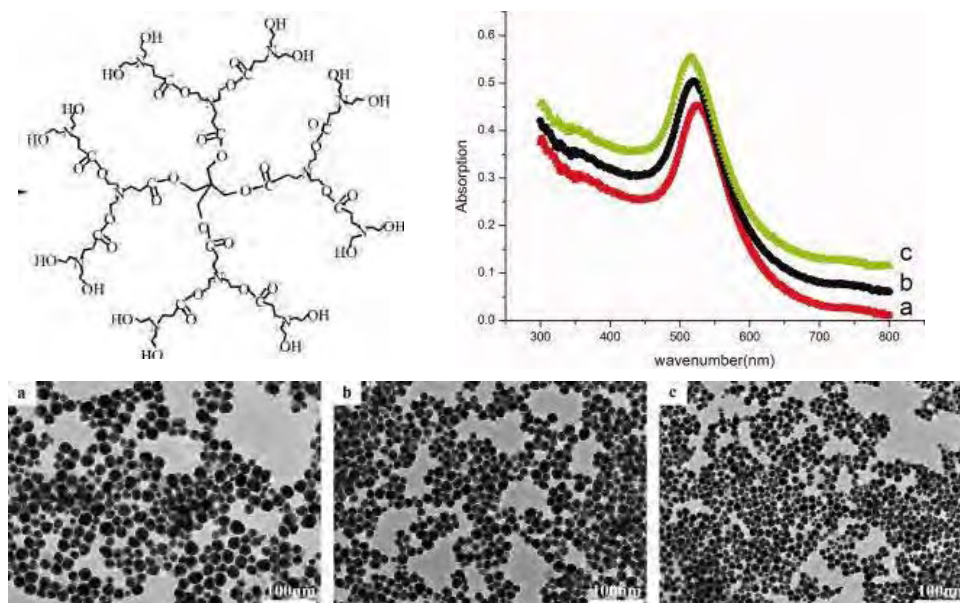


Figure II.11. UV-Vis spectra of gold nanoparticles encapsulated with G3 HPAE (526 nm, curve a), G4 HPAE (523 nm, curve b), and G5 HPAE (519 nm, curve c), respectively. Bottom: TEM images of gold nanoparticles encapsulated with G3 HPAE (a), G4 HPAE (b), and G5 HPAE (c), respectively. [143]

Hu et al. showed that amphiphilic palmitic acid modified hyperbranched and linear polyethyleneimine (HPEI and LPEI) polymers could be successfully used as stabilizers in preparing organo-soluble AuNPs with spherical shape. Increasing the feed ratio of polymer to HAuCl_4 and using the capping polymers with higher C16 density were two effective methods to get the smaller AuNPs with relatively lower polydispersity (Figure II.12).

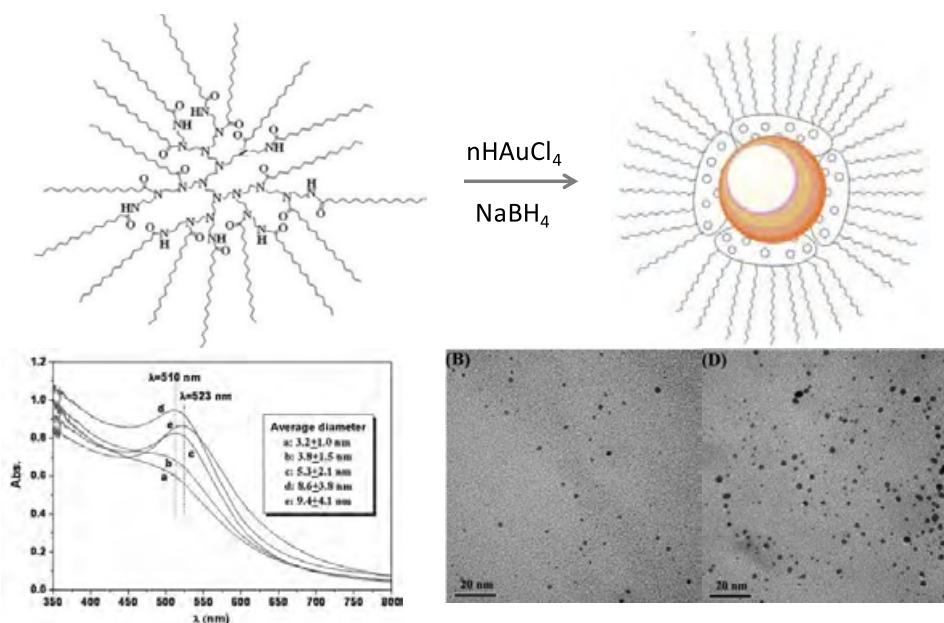


Figure II.12. Illustration of the preparation of organo-soluble AuNPs using amphiphilic hyperbranched polymers as the stabilizers. The typical TEM images of the AuNPs stabilized by (B) the amphiphilic hyperbranched polymer (HPEI₂₅K-C160.73, $[\text{N}]/[\text{Au}] = 10$); (D) the amphiphilic linear polymer (LPEI₁₅K-C160.73, $[\text{N}]/[\text{Au}] = 10$). [144]

When the molecular weight of the used amphiphilic polymers reached a certain limit, the molecular weight and the morphology of the amphiphilic polymers had almost no effect on the size of the formed AuNPs. All the organo-soluble AuNPs could be used as the efficient catalysts for the biphasic catalytic reduction of 4-nitrophenol by NaBH_4 . The k_{app} of the composites had well correlation with the molecular weight of used amphiphilic polymers, and was less relevant to the morphology of the polymers. The organo-soluble AuNPs could be conveniently recovered and reused many times. The structure of the capping polymers had obvious effect on the lifetime of the AuNPs catalysts in the catalytic reduction of 4-nitrophenol. [144]

Jiang et al showed that hyperbranched poly(amidoamine)s with high density tertiary nitrogen coated gold nanoparticles greatly enhanced photoluminescence than the HBP alone (Figure II.13). The hyperbranched polymers with a flexible nature have a non-rigid plane, while the existence of gold nanodots in the interior of the hyperbranched polymer make its non-rigid plane become rigid, which causes the fluorescence intensity of HPAMAMs-OH to be raised and the red shift of emission peak. The other reason for the enhancement of fluorescence intensity of HPAMAMs-OH may be on account of the nanogold. Some literature reports that fluorescence occurs only when the size of the metal nanoclusters is sufficiently small (<5 nm). The luminescence maximum moves to lower energy or disappears with increased core size, and only the smaller nanodots were observed to luminesce. The luminescence from gold nanodots is thought to arise from transitions between the filled d band and sp conduction bands. Because two components (HPAMAMs-OH and nano gold) have a good biocompatibility, and the complex with nano gold encapsulated in the interior of the HPAMAMs-OH provides better stability as a composite photoluminescence nano-material. [145]

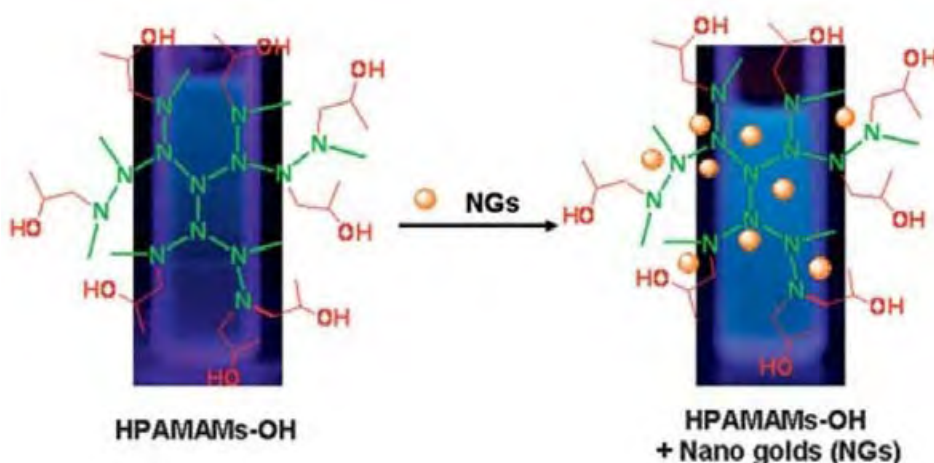


Figure II.13. The structural representation of HPAMAMs-OH encapsulated with nano gold (NG). [145]

Pérignon et al. synthesized, in a single step reaction hyperbranched polymers poly(amidoamine) HYPAM, they were then used to prepare water stable gold nanoparticles (Figure II.14). The open architecture of the HYPAM hyperbranched polymers facilitates the interactions between metal ions and polymer functional groups. Nevertheless, it maintains a control on the gold nanoparticles formed after reduction by sodium borohydride.

Nanoparticles of ca. 4 nm were indeed obtained and stabilized in solution by the hyperbranched polymer. The average size of the nanoparticles could be easily adjusted by changing the $[\text{HAuCl}_4]/[\text{polymer}]$ or $[\text{NaBH}_4]/[\text{HAuCl}_4]$ ratios. The stability of the nanoparticles in water was mainly influenced by the molecular weight of the polymer core and the pH of the solutions. HYPAM functionalized by D-gluconolactone influences rather the stability of the nanoparticles than their size. Indeed, the presence of D-gluconolactone prevents the aggregation promotion by salts in aqueous solution. [146]

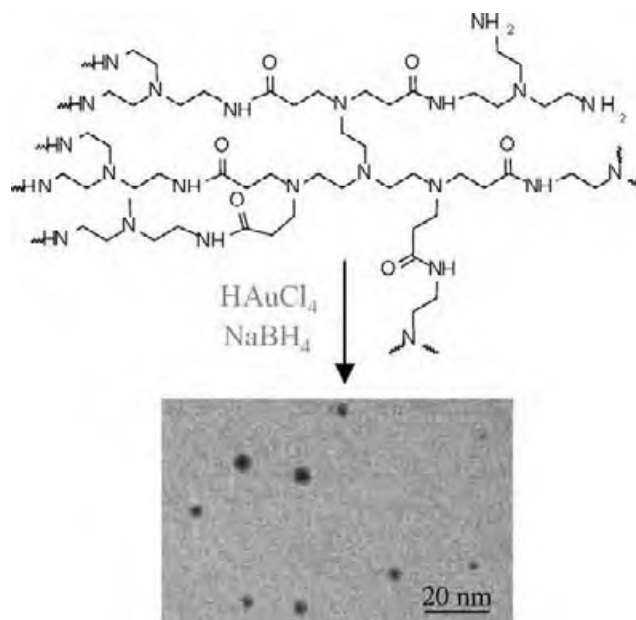


Figure II.14. *In situ* synthesis of gold nanoparticles in presence of hyperbranched polyamidoamine (HYPAM) using NaBH_4 as reductant with corresponding TEM images. [146]

3. Stabilization of preformed nanoparticles

a. *Grafting from*

Compared with the “*in situ*” strategy, “grafting from” allows to prepare nanocrystals (NCs) with the traditional methods, affording more uniform dispersibility. Then, the properties of NCs such as solubility, biocompatibility, and surface functionality can be tuned by surface modification with desired dendritic polymers (DPs). In this regard, *in situ* growth of DP onto quantum dot (QD) surfaces is of particular interest and significance. The obtained NCs *via* the “grafting from” strategy normally show uniform dispersibility and high grafting density of HPs. However, the intrinsic properties of the resulting NC would change more or less due to the harsh chemical reaction. In some cases, for example, the fluorescence of QD will be quenched during the polymerization. Besides, the DPs that can be used to grow *in situ* from NCs are quite limited, which is unfavorable for tailoring the structure and properties of resulting nanohybrids.

b. **Grafting to**

“Grafting to” strategy broadens the scope of optional DPs, at the same time retains the advantages of “grafting from” method. I will give some examples from the literature concerning the synthesis of gold NPs by “grafting to” method.

Dey et al. reported chemically identical polymers tailored by RAFT polymerization to have multiple branches ranging from 1 to 9, thereby having 2–18 end groups that exhibit a strong affinity for gold (Figure II.15). Each of these linkers was capable of mediating the assembly process of gold NPs. This report explores the role of the polymeric linker architecture, specifically the degree of branching of the tailored polymer in determining the formation, morphology, and properties of the hybrid nanoassemblies. The degree of branching of the linker polymer, in addition to the concentration and number of anchoring groups, strongly affected the self-assembly process. The assembly morphology shifts primarily from 1D-like chains to 2D plates and finally to 3D-like globular structures, with increase in degree of branching of the macromolecular linker. The hot-spot density, and thus the surface-enhanced Raman scattering (SERS) enhancements increased as a function of morphology, from 1D chains to 2D-like plates and finally be highest with 3D globular structures. [137]

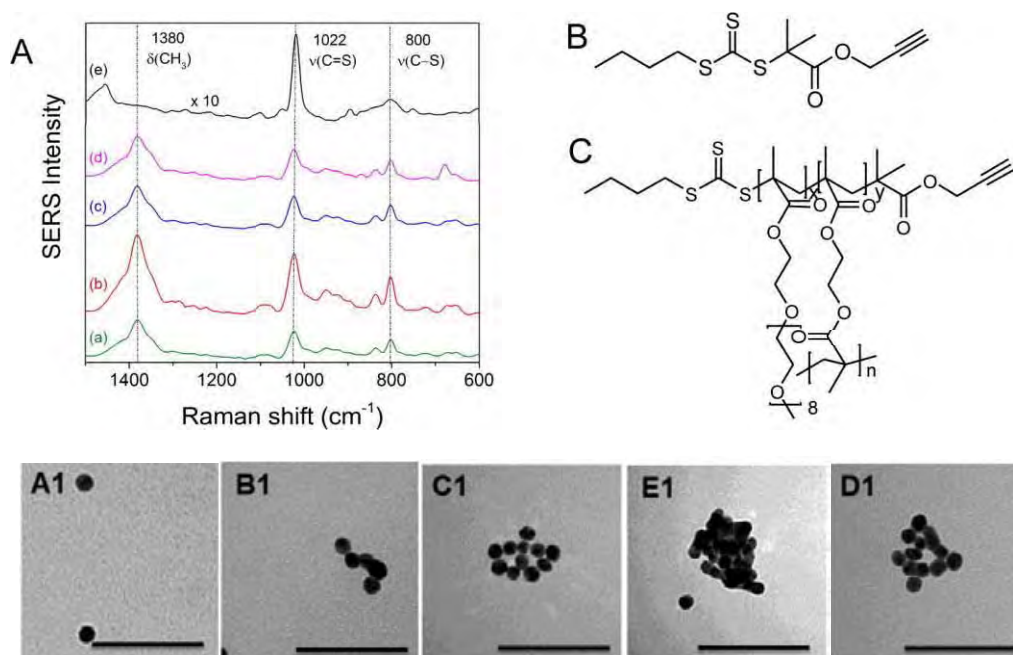


Figure II.15. (A) SERS spectra of linker polymer of the assemblies of (a) P1 hybrids, (b) P4 hybrids, (c) P5 hybrids, (d) P9 hybrids, and (e) RAFT agent. (B) Chemical structure of RAFT agent. (C) Chemical structure of linker polymer $n = 0$ for P1, $n = 3$ for P4, $n = 4$ for P5, and $n = 8$ for P9 polymer. Bottom: Typical TEM micrographs of row-wise: (A) citrate-stabilized gold NPs, (B) P1 regime II nanoassemblies, (C) P4 regime II nanoassemblies, (D) P5 regime II nanoassemblies, and (E) P9 regime II nanoassemblies. [137]

Zill et al. reported the preparation of an alkyne-containing hyper-branched polyglycerols (Figure II.16). Thus, these clickable HPGs were covalently linked to a broad range of compounds and materials using standard click chemistry. Especially, amine

functionalized HPG by click chemistry was used to coat 13.5 ± 1.1 nm diameter, citrate-capped gold NPs. Functionalization of the NPs was confirmed by an increase of hydrodynamic diameter of 2.7 nm and a change in surface effective charge (zeta potential) from -30.2 ± 0.6 mV to -0.01 ± 4 mV for HPG-capped NPs. NPs exhibited enhanced stability to salt-induced aggregation compared to citrate-capped NPs, this enhanced stability likely involves a steric protection of the NP surface that is independent of solution ionic strength, thus mimicking the classic PEG NP coating. [138]

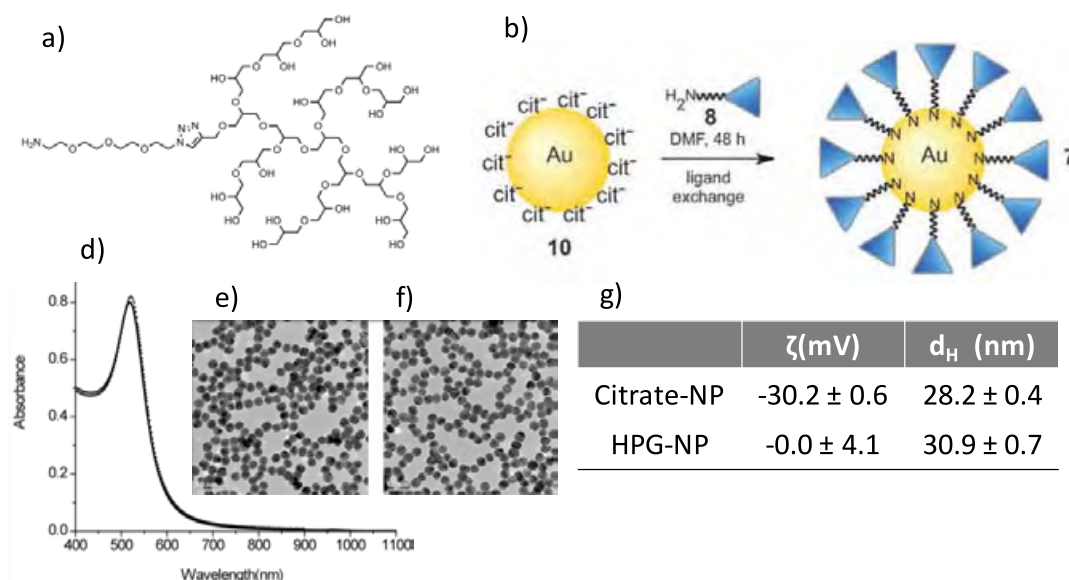


Figure II.16. a) amine functionalized HPG, b) synthesis of HPG coated gold nanoparticles, d) UV-vis spectra of citrate capped gold NPs (solid line) and HPG capped nanoparticles (dashed line), e) TEM images of citrate capped gold NPs, f) TEM images of HPG capped gold NPs, g) Zeta potential and hydrodynamic diameter value of citrate capped gold NPs and HPG capped gold NPs. [138]

4. Stimuli-responsive nanohybrid

Thermoresponsive gold nanoparticles can be obtained by coating NPs with thermoresponsive polymers or *in situ* synthesis in thermoresponsive polymer solution. The thermoresponsive characteristic of the polymers can be impacted by interaction with NPs. Inversely, interaction with the polymers along with the thermoresponsive properties can change the optical properties of the nanoparticles. The paragraph below is meant to give some of the few examples described in literature concerning the synthesis of gold nanoparticles hybrids based on thermoresponsive hyperbranched polymers as stabilizers or soft-template medium.

Thermosensitive Au nanoparticles with tunable lower critical solution temperature have been prepared by coating the nanoparticles with a thermo- and pH-responsive hyperbranched polyelectrolyte (Figure II.17). The obtained values of transition temperatures of HPG-NIPAM show a strong dependence on molecular weight and pH since the HPG-NIPAM polymers possess tertiary amine groups in their structures so the pH of the solutions can affect the hydrophilic–hydrophobic balance in the polymers by changing their charge density. The HPG-NIPAM-coated nanoparticles became highly stable in concentrated salt

solutions (e.g., 1.0 M NaCl) compared to the original nanoparticles. Similar to HPG-NIPAM, the transition temperatures of the coated nanoparticles are also dependent on solution pH and temperature. Upon increasing of the temperature to 35 °C, the surface plasmon band of the coated gold nanoparticles became broader and further red-shifted by 50 nm with a concomitant change in solution color from clear red to opaque purple. Figure I.17.2.d demonstrates that aggregation of these nanoparticles caused either by temperature or pH variation is completely reversible over multiple cycles, thus revealing the robust nature of this hyperbranched polymer coating. The transition temperatures of the polymer-encapsulated nanoparticles are slightly lower (3–9 °C) than that of the pure polymer. This finding could result from the significant reduction in conformational freedom of the HPG-NIPAM polymers after immobilization on the gold nanoparticle surfaces because binding on the nanoparticles imposes an additional boundary for the polymers to collapse, towards the nanoparticle core. [139]

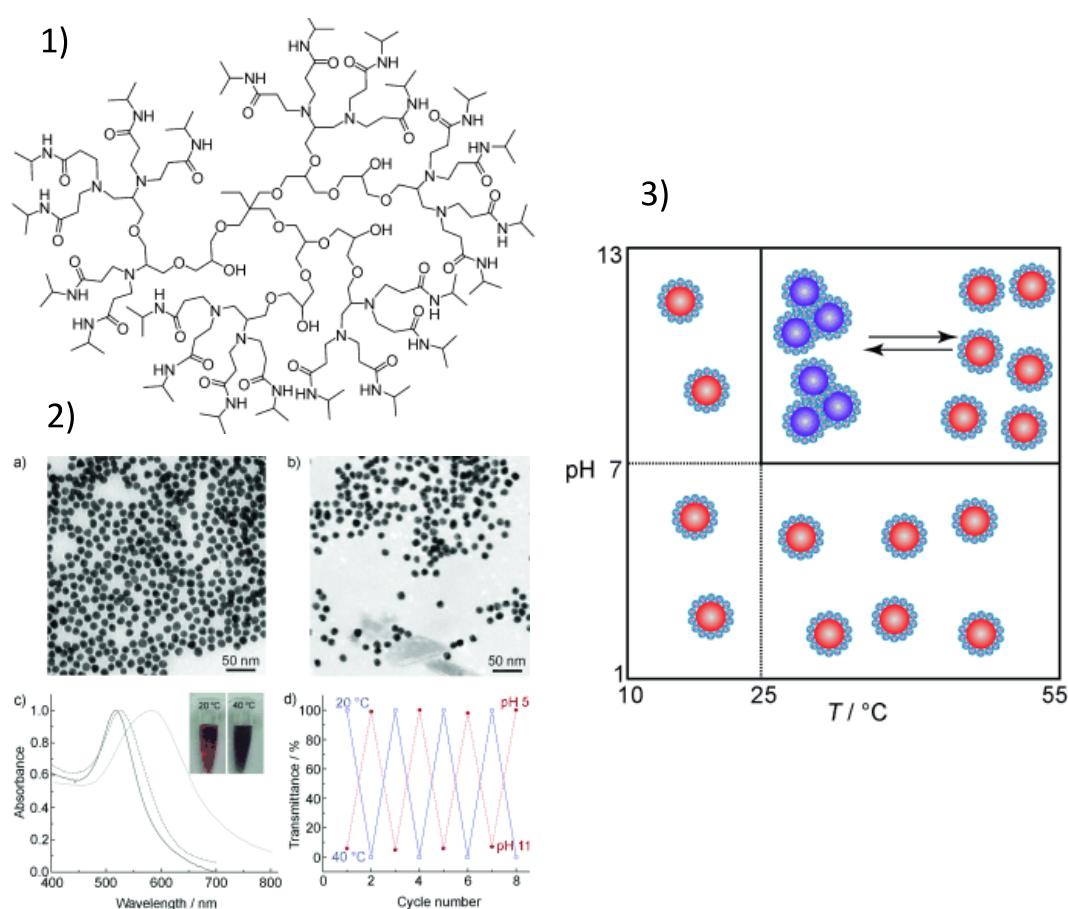


Figure II.17. 1) Chemical structure of HPG-PNIPAM, 2) TEM micrographs of gold nanoparticles before (a) and after (b) coating with HPG₇₆-NIPAM. c) UV/Vis absorption spectra of the original gold nanoparticles (solid line), gold nanoparticles coated with HPG₇₆-NIPAM at 20.0 °C (dashed line), gold nanoparticles coated with HPG₇₆-NIPAM at 40.0 °C (dotted line); inset: photographs of aqueous solutions (pH 9.0) of HPG₇₆-NIPAM-coated gold nanoparticles at 20 °C and after heating up to 40.0 °C. d) Changes of transmittance during both pH variation cycles between 20 pH 5 and 11 and heating–cooling cycles between 20.0 and 40.0 °C, 3) Illustration of effects of pH and temperature on dual-responsive Au nanoparticles coated with HPG-NIPAM. [139]

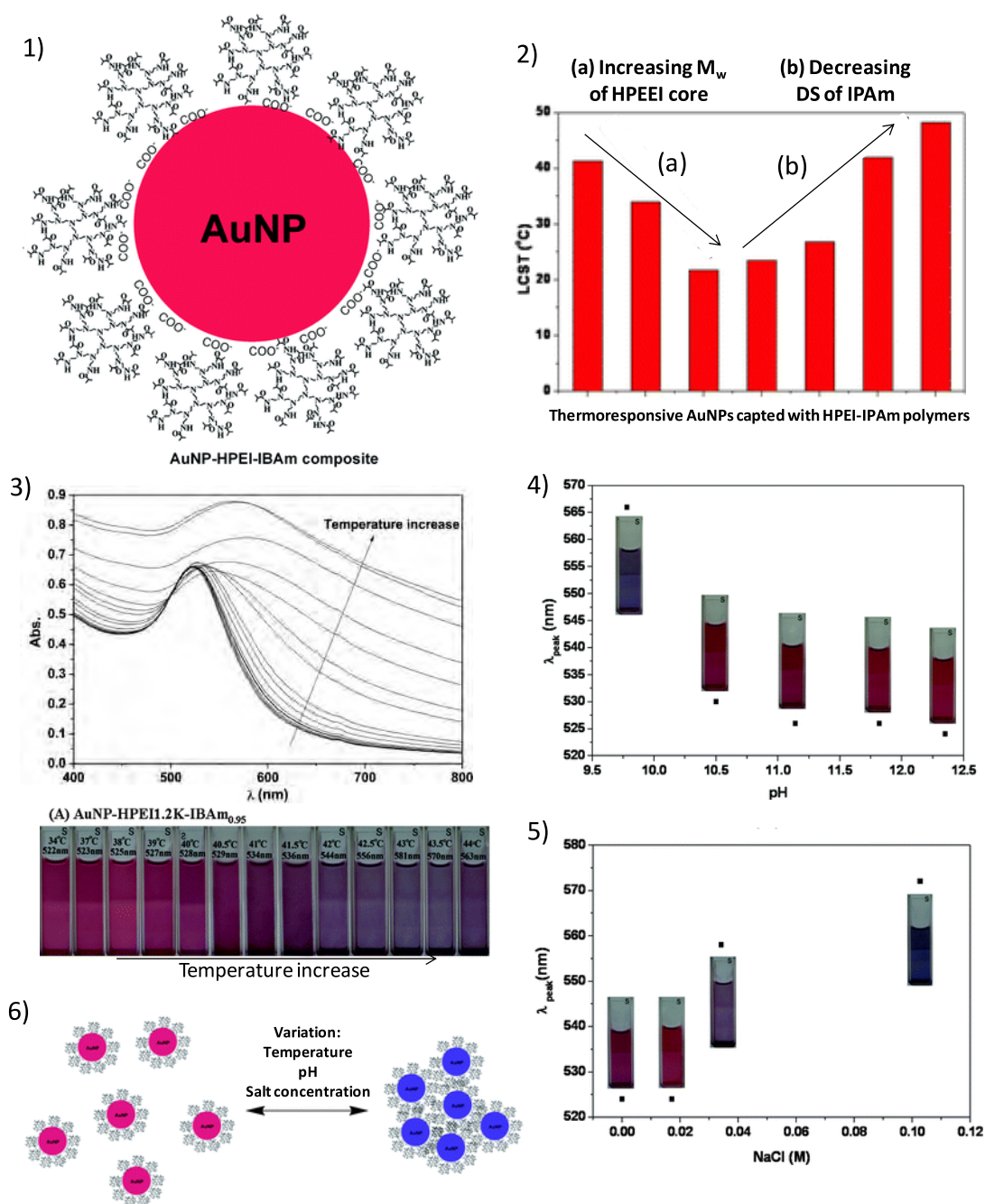


Figure II.18. 1) Thermo-responsive AuNPs capped with hyperbranched polyethyleneimine terminated with isobutyric amide groups, 2) transition temperatures of thermo-responsive AuNPs modulated by changing the molecular weight of the HPEI core and the degree of substitution (DS) of the capping HPEI-IBAm, 3) Typical UV-vis absorbance spectra of the composite of AuNPs with HPEI-IBAm polymers (HPEI10K-IBAm_{0.95} was used here) in function of temperature with corresponding solution images, 4) The λ_{peak} variation of the AuNP-HPEI1.2K-IBAm_{0.95} composite in the presence of 0.034 M NaCl versus pH at 39 °C, 5) The λ_{peak} variation of the AuNP-HPEI1.2K-IBAm_{0.95} composite at pH = 9.8 versus NaCl concentration at 38 °C, 6) illustration of stimuli-responsive AuNPs. [147], [148]

Liu et al reported thermo-responsive AuNPs with transition temperatures conveniently adjustable over a broad range through the non-covalent interaction between

thermoresponsive HPEI-IBAm polymers and the citrate-protected 14 nm diameter AuNPs. Upon raising the temperature above the transition temperature the surface plasmon resonance (SPR) peaks of the obtained thermo-responsive AuNPs red-shifted sharply in a narrow temperature range, accompanied by a color transition from transparent red to transparent purple–red until turbid red, which made them suitable to be used as sensitive colorimetric sensors for detecting environmental temperature variation. The solutions of the thermo-responsive AuNPs were very stable during many heating–cooling cycles. Moreover, the temperature range of sensitivity of the obtained thermo-responsive AuNPs could be tuned by modulating the molecular weight of core or degree of substitution of the thermo-responsive polymers employed or lowering the pH of the solution (Figure II.18). Furthermore, the solution colors of the thermo-responsive AuNPs were also sensitive to pH and NaCl concentration variation, as a result of which they could also be used as colorimetric sensors for detecting the variation of pH and salt concentration [147], [148].

The obtained thermo-responsive AuNPs could be used as recyclable responsive catalysts for the reduction reaction of 4-nitrophenol by NaBH_4 . As far as the thermo-responsive catalysts were concerned, reducing the molecular weight of the HPEI core, lowering the DS values and increasing the concentrations of the capping HPEI-IBAm polymers or the gold resulted in the acceleration of the reaction. By choosing the right capping HPEI-IBAm polymers, the reaction was faster than that catalyzed by AuNPs without capping polymers. The reaction rate was accelerated by elevating the reaction temperature at first, but reached a plateau or decelerated upon raising the temperature close to the T_c of the thermo-responsive AuNPs catalysts. Moreover, the obtained thermo-responsive AuNP catalysts could be recovered by heating the temperature above their transition temperatures and be recycled at least six times with more than 95% conversion. [147], [148]

5. Conclusions

Through this review, we can see that hyperbranched polymers and their derivatives show huge capacity to encapsulate and stabilize gold nanoparticles by three approaches: *in situ* synthesis and *ex situ* : grafting to and grafting from. Every coin has two sides, the “grafting to” strategy also has some disadvantages such as the incomplete removal of original ligands, change of NC properties during an exchange reaction, and so on. So, each of the above three strategies has its own merits and demerits requiring careful choice for the most proper one to synthesize the desired NCs in actual experiments and applications. Thermo-responsive Au NPs with tunable transition temperature have been prepared by *in situ* and *ex situ* methods. Hyperbranched polymers appear as efficient candidates for the synthesis of thermo-responsive nanohybrids. Up to date, ends groups modified hyperbranched polymers were used for the stabilization of gold NPS, but core-shell structure seems to be rarely exploited for this purpose.

C. Nanoparticles within gel structures

1. Introduction

Natural characteristics, such as soft, flexible, elastic and wet nature, make hydrogels an indispensable engineering material for many advanced material designs. The combination

of the hydrophilic nature and stabilizing effects of polymeric chains on the metal nanoparticles make hydrogels an excellent candidate as a soft template for both metal nanoparticle preparation and as a reactor in the catalysis of various reactions. Hydrogels are favorite for the *in situ* synthesis and encapsulating of metal nanoparticles and as a reaction vessel. Both *in situ* and *ex situ* synthesis approach will be given in this section. Furthermore, some examples of thermoresponsive gel nanohybrids will also be given in this section. As only few examples of hyperbranched related systems are described in the literature and in order to describe the main features of those hydrogels, the examples which are given also concern more conventional linear polymer.

2. *Ex situ* synthesis of gel nanoparticles hybrids

Wang et al reported the synthesized of gold nanoparticles using agarose as a reducing agent with a good dispersion of metal nanoparticles throughout the support. AuNP sizes were about 20-40 nm by adjusting the quantity of H₂AuCl₄ compared to agarose. The hybrid material was then used as template for the formation of Au-TiO₂ nanohybrids (Figure II.19). [149]

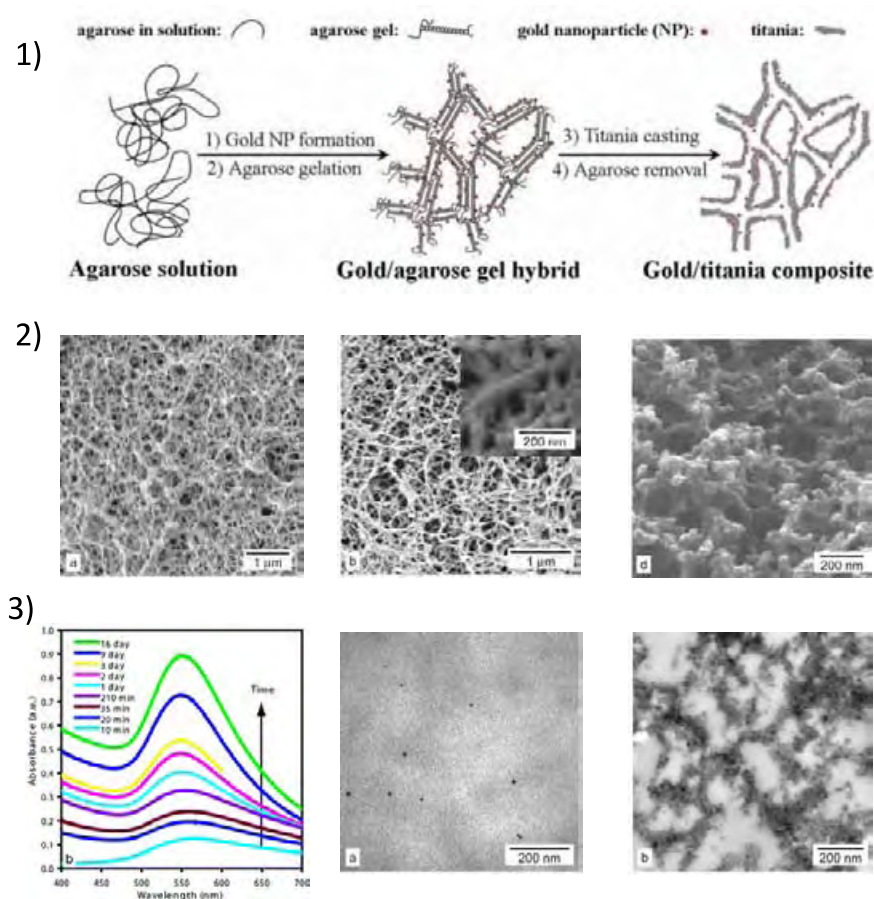


Figure II.19. Schematic of the Au/TiO₂ method A synthesis procedure, 2) SEM images of (a) the critical point dried agarose gel; (b) the Au nanoparticle/agarose hybrid from method B (0.50 mM initial Au concentration), inset at higher magnification; (d) the final Au nanoparticle/TiO₂ structure from method B (0.50 mM initial Au concentration). UV-vis spectra of method A (0.25 mM initial Au concentration) as a function of time, TEM images of (a) the Au/agarose hybrid, and (b) the Au/TiO₂ composites [149]

Vemula and John reported the use of urea based gelators as reductants for the formation of AuNPs, as the gelation occurred, the nanohybrid gels were obtained. Formation of gels in presence of AuNPs did not change the basic morphology of the gel (Minimum gelation concentrations, Tgel). More interestingly, the edges of all gel platelets were decorated with GNPs as we can see in a) and b) of Figure II.20.

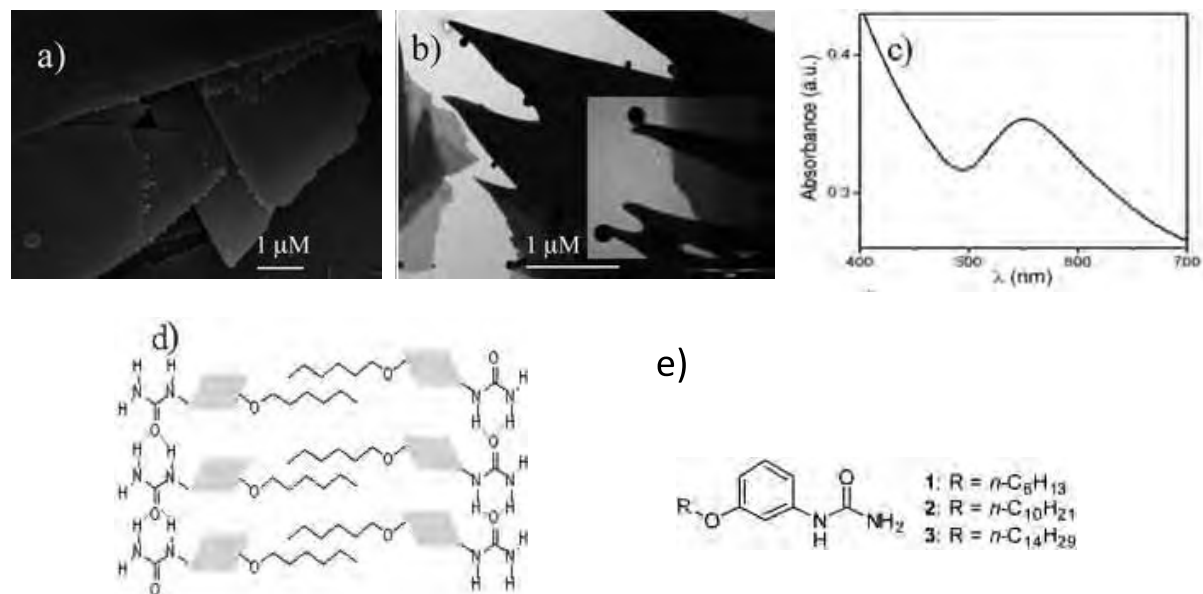


Figure II.20. SEM image of xerogels prepared from gels of a) 2 in water and sheets with GNPs. TEM image of b) hydrogel of 1 with GNPs (inset magnified range), c) UV-vis spectra of GNPs embedded hydrogel of 3, d) Possible molecular arrangement of hydrogels, e) gelators with different alkyl chains [150]

3. *In situ* synthesis of nanoparticles

Similarly, Faucher et al. reported the synthesis of gold nanoparticles by reduction of HauCl_4 within agarose hydrogel using NaBH_4 as reducing agent where they form percolating networks upon partial dehydration and shrinkage of the gel. [151]

Mohan et al. reported hydrogel networks based on N-isopropylacrylamide (NIPAM) and sodium acrylate (SA) prepared by redox-polymerization in the presence of N,N'-methylenebisacrylamide (MBA) (Figure II.21). Highly stable and uniformly distributed silver nanoparticles have been prepared using these hydrogel networks as a carrier *via in situ* reduction of silver nitrate in the presence of sodium borohydride as a reducing agent. The hydrogel network facilitate the narrow dispersion of silver NPs and the network chains also assist in digestive ripening of such particles without aggregation. It was shown that the MBA cross-linker concentration in the preparation hydrogel networks determines the size of the Ag NPs. The size of the Ag NPs decreased from 21 nm to 3 nm when cross-linker concentration increased from 4.5mM to 13mM. The hydrogel hybrid with different sizes of silver nanoparticles (3 nm) can be effectively employed as antibacterial material. [152]

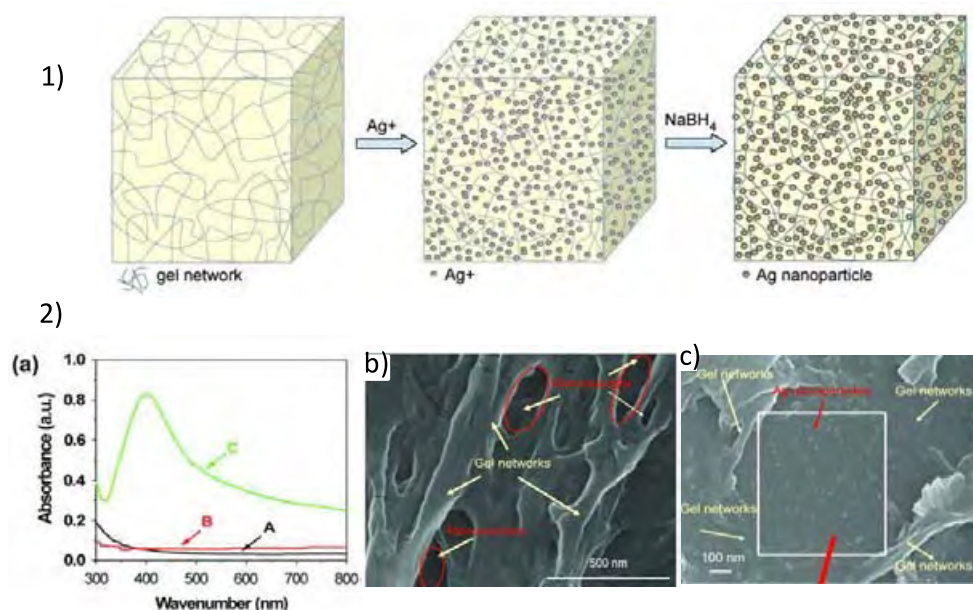


Figure II.21. Schematic representation for the Ag nanoparticles formation in the hydrogel network, 2) a) UV spectra of (A) hydrogel, (B) AgNO_3 and (C) hydrogel Ag nanoparticle hybrids, b) SEM of pure hydrogel and (c) Ag nanoparticle grown in 4.50 mM MBA-crosslinked hydrogel network nanoreactor. [152]

Table II.2. Highlighted examples of nanohybrid gel-nanoparticles

Gelators	Reductant	NPs	Size (nm)	Ref
PNIPAM crosslinked gel	Ex situ (seed-growth, citrate reductant)	Au	2.7, 13, 18	[153]
agarose	In situ Polysaccharide agarose	Au	20 -40	[149]
agarose	In situ NaBH_4	Au	5-8nm	[151]
Pnipam-co-PSA (Sodium acrylate)	In situ NaBH_4	Ag	21.1, 6.6, 4.4, 2.7	[152]
Urea based hydrogel	In situ (amino group)	Au	11-15	[150]

4. Stimuli-responsive gel nanohybrid

Embedding AuNPs in thermoresponsive hydrogels should enable to create “smart” material systems through the advantages of both thermoresponsive materials and metal nanoparticles. Cross-linked hydrogels have been used to produce thermoresponsive nanohybrids. In this case thermoresponsive characteristic consists the swelling and deswelling of the cross-linked gels. To the best of our knowledge, physical hydrogels have not been applied for this subject. This section is meant to give some brief examples of both chemical and physical thermoresponsive hydrogel nanohybrids.

Kazimierska et al. reported: Gold NPs of various sizes in the range from 2.7 to 18 nm in diameter were synthesized and introduced to crosslinked poly-N-isopropylacrylamide (NIPA) polymeric gels during the polymerization process (Figure II.22). The presence of polymeric matrix does not affect the size and the shape of gold particles. However, surface plasmon resonance for gold in NIPA gels is slightly shifted toward longer wavelengths comparing to the neat colloidal suspension. The temperature of the volume phase transition for neat and gold modified NIPA gels was the same: $32.0 \pm 0.6^\circ\text{C}$. [153]

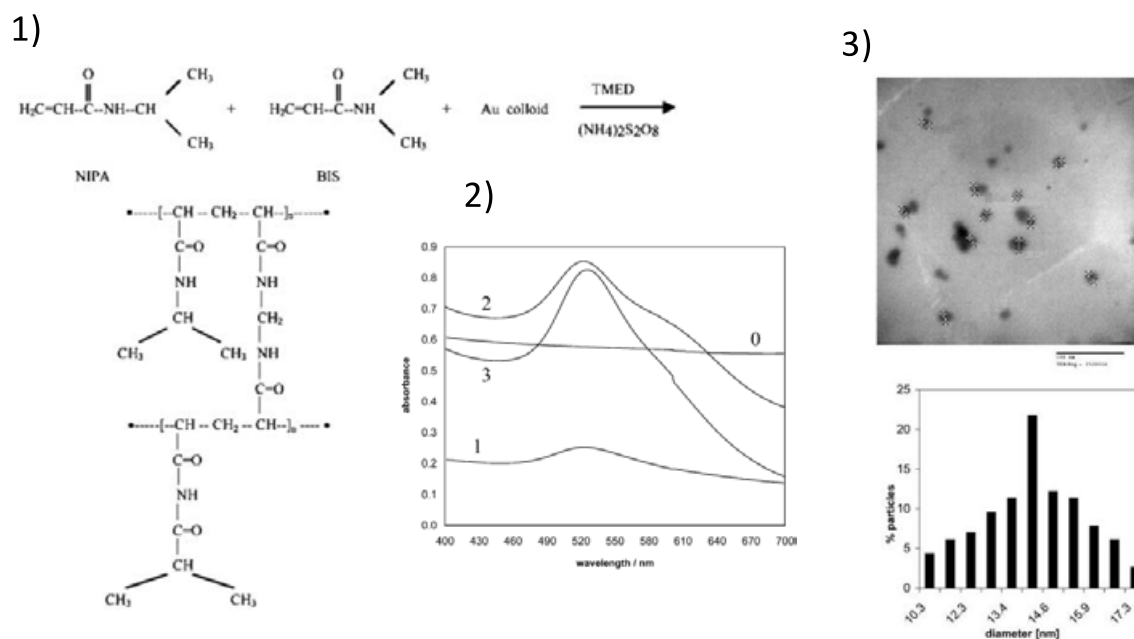


Figure II.22. Schematic synthesis of poly-N-isopropylacrylamide cross-linked with N,N'-methylenebisacrylamide, 2) UV-vis spectra of colloidal gold particles incorporated into NIPA gel (spectra collected before drying). Au particles size: 0) neat NIPA gel without gold, (1) 2.7 nm, (2) 13 nm, (3) 18 nm, 3) TEM image and size distribution of 13 nm Au particles in the NIPA gel. [153]

Pong et al. reported the changes in the structure and thermoresponsive behavior of poly(N-isopropylacrylamide) (PNIPAm) hydrogels when gold nanostructures were synthesized *in situ* within the hydrogel matrix. Firstly, crosslinked PNIPAm hydrogels were synthesized using NIPAm and 0.00–3.50% (w/w versus NIPAm) of N,N'-methylenebisacrylamide (MBAm) and/or N,N'-cystaminebisacrylamide (CBAm) as cross-linking agents. The hydrogels were soaked in potassium tetrachloroaurate to introduce gold ions. The hydrogels containing Au^{3+} were then immersed in a sodium borohydride solution to reduce the gold ions. Infrared spectroscopy, UV-visible spectroscopy, and equilibrium swelling were used to examine the structural/physical differences between gels of different compositions; UV-visible spectroscopy and mass measurements were used to observe the kinetics and thermodynamics of the hydrogel volume phase transition. These studies revealed several differences in the physical characteristics and thermoresponsive behavior of hydrogels based on cross-linker identity and the presence or absence of gold nanostructures. Hydrogels with gold nanostructures and high CBAm and low MBAm content have equilibrium swelling masses 3–20 times their native analogues. In comparison, gold-containing hydrogels with high MBAm and low CBAm content have swelling masses that are

equal to their native analogues. Additionally, the gold-containing PNIPAm hydrogels cross-linked with only CBAm have a deswelling temperature of ~ 40 °C, ~ 8 °C above the samples cross-linked with only MBAm. Varying the CBAm content and introducing gold enables tuning of the deswelling temperature. [154]

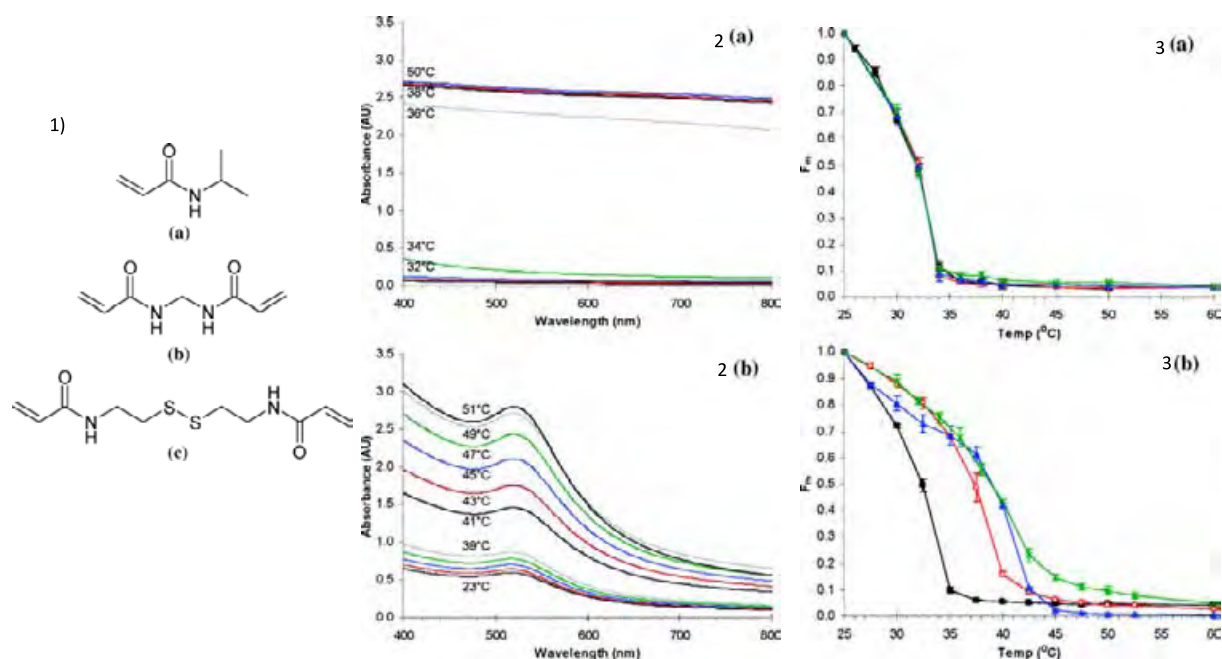


Figure II.23. 1) Structures of (a) *N*-isopropylacrylamide, (b) *N,N'*-methylenebisacrylamide, and (c) *N,N'*-cystaminebisacrylamide. 2) Temperature-dependent UV-visible spectra of 3.50M/3.50°C hydrogels. Spectra of (a) native hydrogels were recorded at 25, 30, 32, 34, 36, 38, 40, and 50 °C and (b) gold-containing hydrogels were recorded at 25, 30, 35, 37, 39, 41, 43, 45, 47, 49, and 51 °C. Absorbance values for each hydrogel type increase with temperature, and several spectra have been labeled. 3) Fractional mass change of (a) native and (b) gold-containing 3.50M/0.00°C (■), 1.75M/1.75°C (°), 0.00M/3.50°C (▲), and 3.50M/3.50°C (×) hydrogels over the temperature range of 25–60 °C. Error bars on data represent the standard deviation from a minimum of three separate hydrogel samples. [154]

5. Conclusions

The combination of metal nanoparticles with host hydrogels of different characteristics is a strategically significant way of creating novel composite materials with extraordinary properties. The utilization of environmentally benign hydrogel networks for metal nanoparticle preparation provides two advantages: firstly as a template, the hydrogel network prevents nanoparticle aggregation, and secondly, provides an adapted media as flexible reactor for catalysis or various reactions. Thermoresponsive hydrogels has been used for preparing metal nanocomposites however physical hydrogels remain largely unexplored for such application.

D. Nanoparticles and polymeric liquid crystals

1. Introduction

Liquid crystals (LCs) have been extensively exploited in display technologies throughout the past decades. However, they play also an important role in numerous sectors including organic transistors, sensory, light modulators, bio-medical applications and more. By no surprise, due to their organization at the molecular level, LCs have also found an important place in nanosciences. In recent years, intimate mixtures of LCs and nanostructures have aroused great interest in the scientific community in order to obtain materials that manifest simultaneous nanoparticle-related properties and liquid crystalline behaviour. [82], [155]

First studies have involved the doping of LC materials with preformed nanoparticles. As trivial as it may sound, a homogeneous material involving nanoparticles (NPs) and LCs is not in any way straightforward to obtain. Indeed, the insertion of NPs can disrupt the LC order and can generate various types of defects e.g., hyperbolic hedgehogs, Saturn rings or boojums.... Those defects were taken in good account to generate anisotropic colloidal structures. The incorporation in a homogeneous way of NPs within a LC medium often requires surface modification of the former. For this reason, many studies have proposed the coating of NPs with LC ligands, by using for instance ligand exchange processes. Doping of LCs with NPs was found to improve the physical properties of LCs and can give rise to applications in various technologies such as highly-sensitive LC-based sensors. In addition, liquid crystals exhibit a certain amount of order by nature, which can be exploited either to organize NPs in two- or three- dimensions or as templating agents. [82], [155]

Alternatively to this *ex situ* strategies to obtain NPs embedded in LCs media, direct growth of NPs within a LC phase was also reported. This pathway requires the doping of a LC by an adequate precursor that will be *in situ* modified (reduction, oxidation, hydrolysis...) to obtain NPs. This strategy presents also several issues concerning the compatibility of a chosen precursor with a LC phase and the way the precursor can be directly modified *in situ* without disrupting LC order. These issues have been circumvented by the use of lyotropic LC mesophases which have been used to obtain nanostructured silica materials useful in a wide range of applications. In contrast, thermotropic materials have been scarcely reported [82], [155].

This section will focus on the use of liquid crystalline polymers in order to obtain intimate structures of NPs and LCs. We will first describe the doping of NPs in LC media and in a second section, the direct growth within a LC matrix. This overview is meant to give an insight into hybrids incorporating different types of nanoparticles, e.g. metallic or metallic oxides, and different types of liquid crystals.

2. Stabilization of preformed nanoparticles

The *ex situ* procedure to get hybrid liquid crystalline polymer-nanoparticle composites is usually preferred when monodispersed nanoparticles with definite shape and dimensions are necessary for precise practical applications, i.e. solar cells or optical sensing devices or actuation, which can take advantage from the collective behavior of ordered NPs.

One of the most delicate points of this approach is the homogeneity of the dispersion. Above all when high NPs weight fractions are necessary, it is very important that nanoparticle-nanoparticle interactions are somewhat balanced by nanoparticle-polymer interactions. For this reason, in order to obtain a more intimate mixture, the most used strategy is to make inorganic nanoparticle more compatible to the liquid crystalline polymer matrix. This can be achieved by using mesogens which are functional groups able to interact with NPs or surrounding the NPs with liquid crystalline ligands. This is true whichever the NPs used. The NP choice usually depends on the wished application. The liquid crystal polymer is then accordingly tailored.

Shandryuk et al. reported about the dispersion inside a side-chain liquid crystal polymer of CdSe spherical quantum dots (QDs) [156] and CdS nanorods [157], which share with LCs the anisotropic character. In both cases they chose a poly[4-(n-acryloyloxyalkoxy)]benzoic acid with a smectic C-type phase as the presence of alkoxybenzoic acid functionalities should insure the interaction with the inorganic fillers. In the case of CdSe, the interaction between the QDs and the polymer is clearly shown by infrared analysis: upon increasing concentration of CdSe, the intensities of bands related to the carbonyl group (ν_{CO}) decreased while new bands relative to carboxylate anions appeared. X-ray scattering spectra showed a change of the interlayer spacing due to the presence of CdSe NPs, so the authors suggested a composite nanostructure where polymer layers alternate with QDs highly packed layers (Figure II.24). The LC polymer-nanoparticle interactions were also proved by the change in the thermal behavior of the LC in the composite. Till 20 wt% QDs the LC-Isotropic transition temperature dropped by some degrees and the associated transition enthalpy decreased. At 40 wt% QD content the LC transition disappeared. The quantity of NPs in a LC matrix is a limiting factor, so it must be carefully chosen in order to preserve the liquid crystalline properties of the final materials. The optical properties of these materials were characterized [158] and confirmed the good insertion of the NPs inside the liquid crystal matrix.

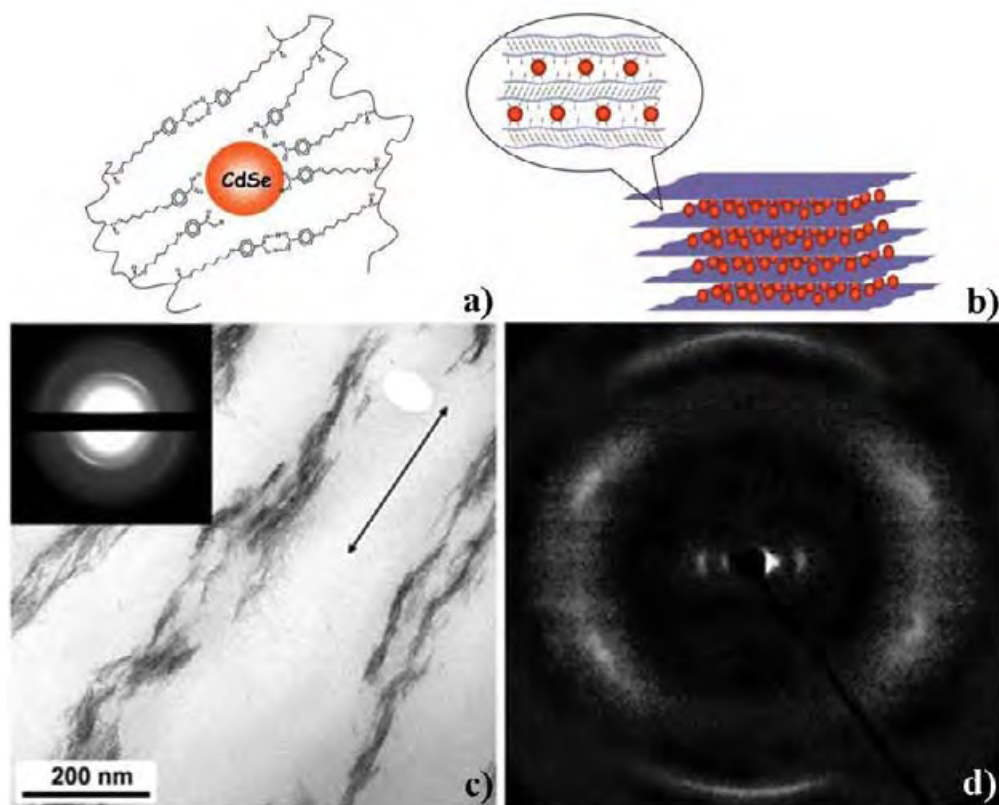


Figure II.24 Schematic representation of a) a side-chain LC polymer stabilizing CdSe NPs *via* alkoxy benzoic functionalities and b) the localization of CdSe between polymer nanolayers [156]. c) TEM images and d) X-ray pattern (right) of uniaxially oriented films of the liquid crystal polymer with CdS nanorods [157].

The case of the CdS nanorods described by the same authors is less straightforward [157]. The IR spectra of the composite showed no sign of the presence of the trioctylphosphine oxide (TOPO) ligands used in the nanorods synthesis, suggesting that they have been replaced by the functional groups in the polymer. As for the spherical NPs, when nanorods were incorporated in the polymer matrix, the number of H-bonded dimers in the composite decreased. The X-ray analysis showed only a change of 0.5 nm in the interlayer spacing, which is quite small. Moreover, the LC thermal behavior was just slightly influenced by the presence of the nanorods. The authors then concluded for weak interactions between the nanorods and the LC matrix. Nevertheless, they exist and TEM images showed 100-200 nm low density domains of nanorods evenly distributed in the matrix. They compared the LC matrix with an amorphous one made up of norbornene-methyl methacrylate copolymer without functional groups. They found a significant phase separation with bigger and much denser domains. Interestingly, the uniaxial stretching of the composite films caused the formation of wire-like structures oriented as the LC groups in the sense of the deformation (Figure II.24), thus confirming an interaction between the nanorods and the mesogens. This same interaction was responsible for the optical properties of the composites: CdS nanorods emission peak in the LC matrix and a homogeneous solution were nearly the same, whereas it was red-shifted in the amorphous matrix.

In the examples reviewed above the liquid crystal character is exploited in order to

organize the inorganic filler: the NP localization and organization is a key factor for sensing and authors care about their good dispersion and they underline the importance of a specific interaction for the successful mixture. The necessity to adapt the NP content is also discussed. In the same way, when doped liquid crystalline block copolymers are proposed for hybrid photovoltaic devices [159], [160], the NP concentration, location and order must be cared with as they directly influence the performances of the device. More precisely, in this kind of application the main issue is to obtain highly ordered nanostructures and big interfacial area where the semiconductor NPs are ideally located. Liquid crystalline block-polymers are ideally suited to favor oriented ordered domains and the LC matrix-nanoparticle interface is crucial. Besides, a quite important NP content is necessary in order to guarantee sufficiently high current density but at the same time it is limited by the disruption of the liquid crystalline order. In these examples a good compatibility is even more essential.

ZnO QDs were dispersed in a liquid crystal donor-acceptor copolymer poly[3-(6-(cyanobiphenyloxy)thiophene)-alt-4,7-(benzothiadiazole)], P3HbpT-BTD [159] (Figure II.25.a). The composite films were prepared with high dopant content, 1:3 wt% P3HbpT-BTD: QDs, by spin-coating highly concentrated dichlorobenzene solutions and annealing them at different conditions. The authors observed a relation between the annealing conditions, the composite film microstructure and the device performances. In particular, films annealed in the mesomorphous state achieved power conversion efficiencies comparable to the better values in the literature (ca. 2%). X-ray diffraction and TEM images showed highly ordered ZnO domains and well developed interpenetrating network if annealing was conducted in the liquid crystal state; on the contrary films annealed in the crystalline or isotropic state were characterized by extensive ZnO aggregation. In this way, the enhanced charge separation and transport efficiency could be attributed to the well-ordered percolated network.

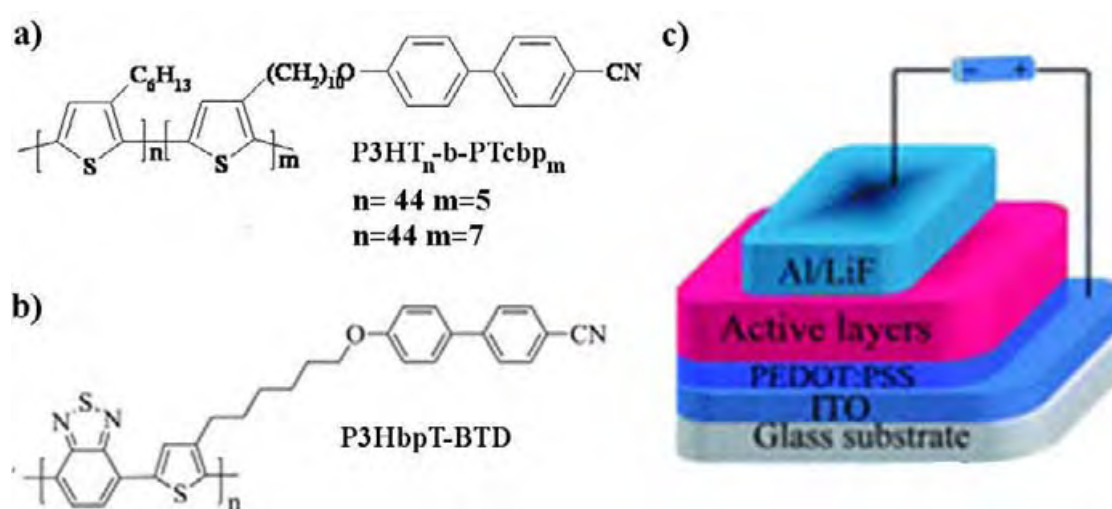


Figure II.25. Chemical formula of the a) polythiophene-b-poly{3-[10-(4'-cyanobiphenyloxy)-decyl]thiophene} (P3HT-b-PTcbp) [160] and b) poly[3-(6-(cyanobiphenyloxy)thiophene)-alt-4,7-(benzothiadiazole)], P3HbpT-BTD [159] used in the active layer of a hybrid solar cell device schematized in c) [159].

The performances of such kind of device were improved by the same authors by allowing a more intimate mixture of the liquid crystalline polymer and inorganic NPs [160]. As already said, in order to have good charge separation, the NPs must ideally be located at the heterojunction. This situation is more likely achieved if the polymer possesses groups allowing cooperative interactions with the QDs. At this purpose, the authors compared the power conversion efficiencies of hybrid solar cells formed by conjugated rod-rod diblock copolymers containing cyanobiphenyl mesogenic pendants, polythiophene-b-poly{3-[10-(4'-cyanobiphenyloxy)-decyl]thiophene} (P₃HT-b-PTcbp) (Figure II.26.b), as electron donors and by ZnO or CdS QDs as electron acceptors. They fabricated devices where the QDs surfaces were modified or not with liquid crystalline ligands, 4'-hydroxy-[1,1'-biphenyl]-4-carbonitrile (cbp). The role of the liquid crystalline ligands is to guarantee a better miscibility with the polymer thanks to the intermolecular interactions arising from their similar structure. All the devices containing liquid crystalline ligands on the QDs possessed better power energy conversion. The authors attributed the improved performances to the improved order of the active layer due to the presence of liquid crystalline moieties on the conducting polymer and to the better nanoparticle dispersion, showed by TEM images, when liquid crystalline cbp are present on QDs surface (Figure II.26).

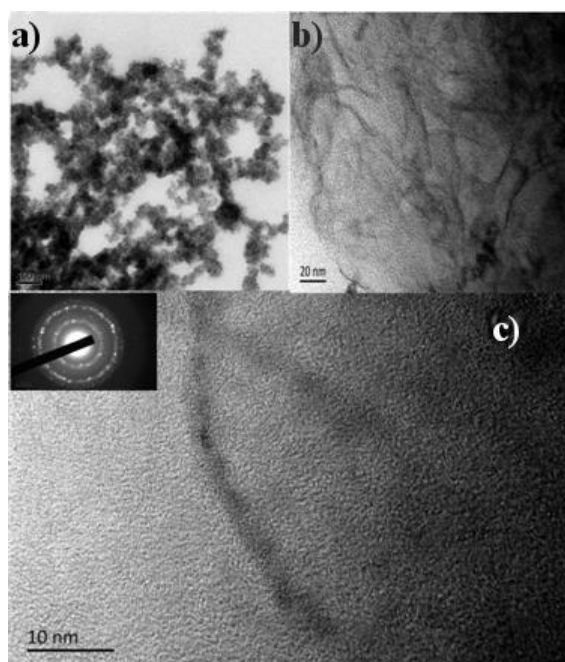


Figure II.26. TEM images of a) P₃HT-b-PTcbp/ZnO, and b) P₃HT-b-PTcbp/cbp@ZnO. c) HRTEM images of the self-assembly of cbp@ZnO in the corresponding areas of P₃HT-b-PTcbp/cbp@ZnO. The polymers concentration was 10 mg/mL, the polymer:ZnO ratio 1:2. [160]

3. *In situ* synthesis of nanoparticles

As previously mentioned, successful hybridization of NPs within a liquid crystalline medium depends on several factors including NP size/concentration, chemical compatibility, topological defects and so on. For this reason, research groups in this field started focusing on the possibility of growing NPs directly within the LC instead of using preformed particles.

Nevertheless, the direct synthesis of NPs in LCs generally presents several difficulties:

- i) The first one concerns the retention of the liquid crystalline phase upon addition of the NP precursor that could disrupt the LC phase.
- ii) The second one concerns the development of an *in situ* procedure to generate NPs within a LC medium. For this, in order to avoid the diffusion of additional reactants within the LC medium, most studies involve the *in situ* reduction of metal precursors *via* oxidation of the LC medium in order to obtain the desired NPs. In other cases, sputtering or electrodeposition techniques were used. Alternatively the diffusion of small molecules in a gas phase (water, dihydrogen) has been also reported.
- iii) Lastly, if the interactions between the formed NPs and the LC phase are poor, segregation of the formed NPs may occur.

Another advantage of this *in situ* synthesis is that the LC anisotropic medium may induce a morphology-controlled growth of NPs, *i.e.* control over size and shape. Whereas this last approach has been often reported in the case of lyotropic liquid crystals, the use of thermotropic liquid crystals is seldom found in literature. For this specific purpose, the use of LC polymers has demonstrated its better efficiency than the use of small LC molecules. That will be discussed in the following.

a. ***Solvent mediated in situ formation of NPs/LC hybrids***

In order to get homogeneous dispersions of inorganic NPs in liquid crystalline polymer matrixes, another possibility is the *in situ* synthesis of the NPs. Zadoina et al. adapted the synthesis of Co NPs starting from bis(bis(trimethylsilyl)amido)cobalt(II), $\text{Co}[\text{N}(\text{SiMe}_3)_2]_2$, in the presence of long chain carboxylic acid and amine ligands [161]. They successfully obtained spherical and/or rod-like Co NPs inside a silicone based liquid crystalline polymer. The precursor decomposition was carried under 3 bar H_2 in toluene solution varying the ratio between the Co precursor, the carboxylic acid side-chain groups on the polymer and the hexadecyl amine. For low content of the acid ligand, anisotropic NPs started to form, and a majority of nanorods formed when hexadecyl amine was added in the solution at Co: acid ligand:amine ligand ratio 1:0.16:1. All the obtained NPs were well dispersed inside the matrix which retained its mesomorphous character; the ferromagnetic properties of Co NPs were also verified. By using a similar strategy, Domracheva et al [162] have prepared superparamagnetic $\gamma\text{-Fe}_2\text{O}_3$ nanoparticles from oxidation of a second generation polypropylene imine LC dendrimer – iron (II) complex in THF solution. NPs with an average diameter of about 2.5 nm encapsulated within the LC dendrimer were obtained. After removal of the solvent, those particles presents a liquid crystalline columnar as identified from X-ray diffractometry measurements. The electron magnetic resonance spectra of those NPs within the LC phase were then compared to the one of bulk $\gamma\text{-Fe}_2\text{O}_3$. Electron magnetic resonance spectra demonstrated that, in contrast to bulk $\gamma\text{-Fe}_2\text{O}_3$, LC NPs possessed enhanced effective magnetic and uniaxial anisotropy induced by the particle surface and shape effect.

b. ***Solvent-free in situ formation of NPs/LC hybrids***

Lee and Jin [163] have first reported the growth of metallic NPs inside a thermotropic

LC based on polymeric materials. A polyester matrix polymer consisting of hydrophilic PEG branches attached to a hydrophobic aromatic polyester backbone was used for his purpose (Figure II.27.A). This structure tends to organize in smectic like domains with the PEG branches occupying the inter-layer domains. Gold nanoparticles were obtained in a two-step procedure: first an aqueous solution of HAuCl_4 was allowed to diffuse into hydrophilic domains. Then, these gold ions were reduced to Au NPs upon the addition of a hydrazine solution as shown on TEM micrographs in Figure II.27.B. Mesomorphic properties of the LC/NP hybrid were not discussed.

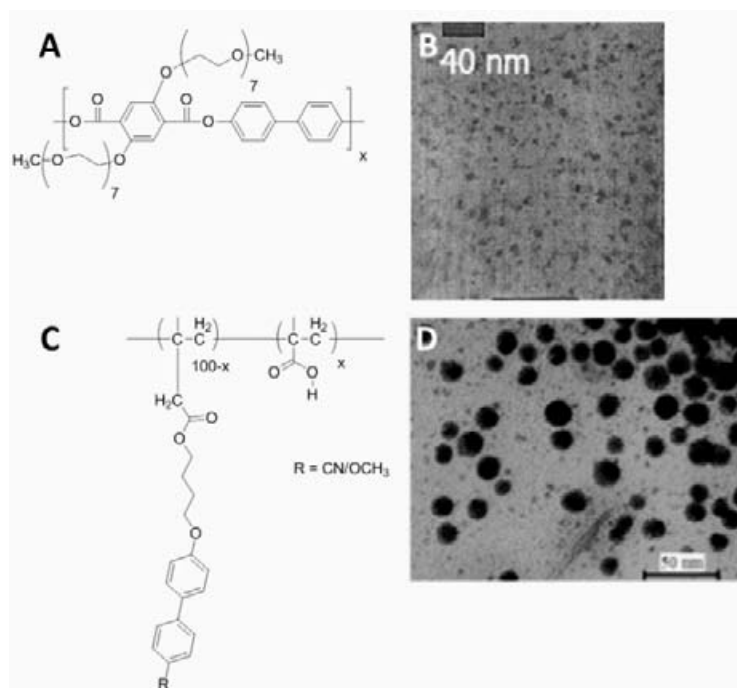


Figure II.27. Structure of DiPEG-BP LC polymer (A) and TEM micrograph of Ag NPs within (B) (Adapted from ref [163]). Molecular structure of side chain LC polymer used by Barmatov et al. [164] incorporating cyanobiphenyl or methoxybiphenyl mesogens (C) and TEM micrograph of Ag NPs synthesized within (D).

The procedure used to form the NPs necessitates the addition of a limited quantity of water to the liquid crystal materials in order to introduce the NP precursor and the reducing agent. Therefore a partial disruption of the mesomorphic order at localized sites during the nanocomposite preparation could occur. To avoid this, Barmatov et al. [164] used a different strategy that involved direct reduction of metal precursor within the LC matrix. LC polymer with cyano- or methoxy- biphenylmesogenic side-fragments was used in this study (Figure II.28.C and Table 1). A silver-olefin complex is first mixed with a solution of polymer in THF and the solvent is then evaporated. After heating, Ag^+ ions are reduced by olefin ligands inducing the formation of isotropic Ag NPs with average sizes in the range 5-30 nm (Figure II.27.D). As NPs presented large size distribution the control over the NP morphology is somehow limited. Moreover the presence of NPs has a strong and negative influence on the mesophase stability: the composites based on cyanobiphenyl mesogens presented no more mesomorphic properties above 2 wt% silver content whereas the ones based on methoxybiphenyl entities remained relatively stable up to 15 wt% of silver NPs. The drastic decrease of mesophase stability in the first case is thought to be related to the strong

interactions between terminal cyano groups and silver surfaces disturbing significantly the packing of the mesogenic groups and resulting in the rapid loss of LC behavior.

c. ***Effect of LC organization and structure on nanoparticle growth***

Until now, the examples we have discussed generally focused on the incorporation of NPs in LCs to form LC nanocomposites. However, not much attention was given to the control of NP morphology using the LC as a template. First attempts have involved the use of mixture of ionic liquids and NPs precursors presenting mesomorphic properties leading after reduction to gold, copper or silver nanoparticles [165], [166]. In both cases particle size and thickness can be tuned by varying the reaction temperature: while nanospheres were obtained in isotropic conditions, anisotropic structures (copper platelets, leaf-like Au nanostructures) were obtained in LC state. However, none of those examples have shown a direct relation between the LC structure and the morphology of the synthesized NPs as rather large NPs were obtained. A clear correlation between LC phase and NP size and shape can be found in a recent paper of Mallia et al. [167]. The system involves amphiphilic low-molecular-weight mesogens, which are capable of reducing the metallic salt without the need of external reducing agent. The gold ions interact with ammonium groups in the liquid crystal molecule. The control of size and shape was obtained by either varying the concentration of the gold chloride precursor or by the LC phase.

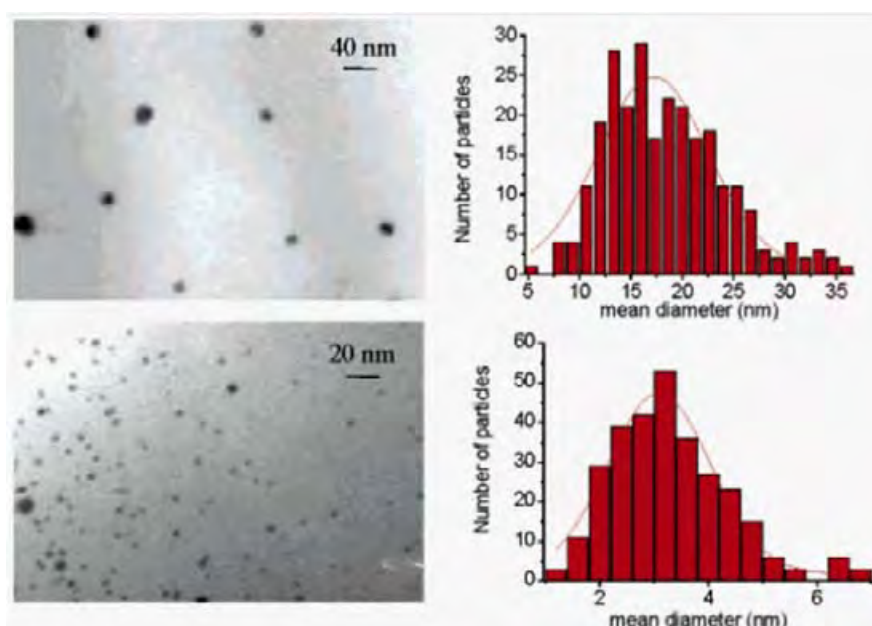


Figure II.28. TEM micrographs and corresponding histograms illustrating the particle size distribution of gold NPs embedded in composites formed in a polydomain (up) or monodomain (bottom) smectic phase [168].

Gascon et al. [168] have demonstrated that not only the liquid crystalline nature can have a strong influence on the nanoparticle size but also the local organization of a given mesophase. For this, liquid crystalline elastomer based on side chain polysiloxane (Table II.3) with the same chemical structure but different macroscopic organizations (polydomain and monodomain) were synthesized. Whereas in the smectic phase of a monodomain polymer, Au NPs of 3 nm were obtained, larger Au NPs of 50 nm were obtained when the

same experiment was realized in the isotropic state (see Figure II.28). The discrepancies observed might be related to the formation of NPs within the structure defects of the LC, polydomain samples presenting due to their intrinsic nature more defects than monodomain materials.

More recently D. Dasgupta et al. [169] have synthesized nanoporous smectic liquid crystalline polymer networks and used them as template for the photochemical synthesis of silver nanoparticles. They have shown that the diameter of the NPs is controlled by the length of the cross linking agent used during synthesis. Indeed this length allowed controlling the periodicity of the layered morphology and therefore of the *in situ* generated silver nanoparticles. Those materials have been used to fabricate patternable organic/inorganic hybrid materials.

A new strategy to improve a control over NP growth within the LC mesophase have been published by S. Saliba et al [170], [171]. This approach involves the *in situ* hydrolysis of dicyclohexylzinc, $[Zn(Cy_2)]$ leading to ZnO NPs with volatile cyclohexane as the unique side product. The use of LC compounds having an oligomeric or a polymeric structure that contain various amine and amide chemical functions favour interactions between the LC and $[Zn(Cy_2)]$ /ZnO NPs. Those interactions were evidenced both by experiments in solution and by solid state ^{13}C -NMR studies in LC state and limit disruption of the LC organization and increase the templating effect of the LC phase. Two different types of LCs which differ by their type of backbone were investigated (see Figure II.29).

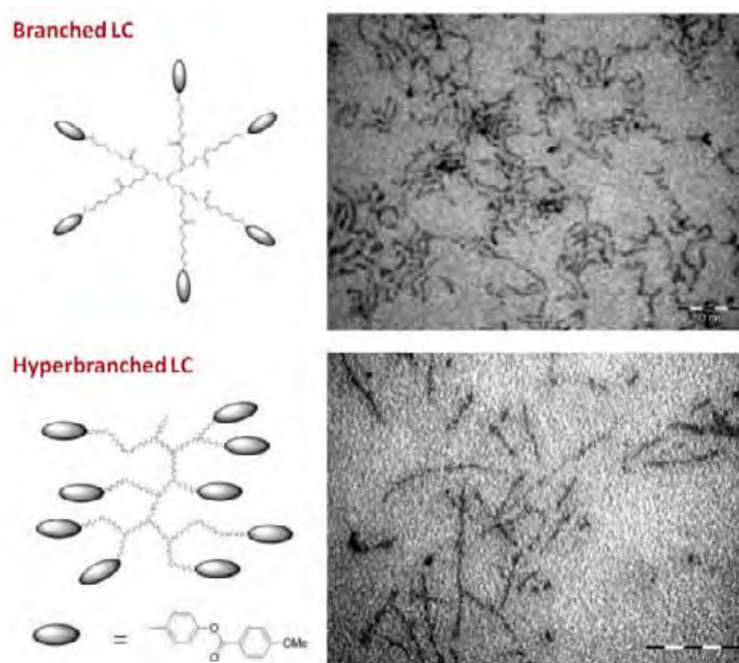


Figure II.29. TEM micrographs of ZnO NPs synthesized under various conditions: in branched LC at 30°C (scale: 200 nm) or in hyperbranched LC at 45°C (scale: 50 nm). Adapted from ref [170], [171].

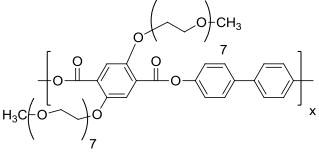
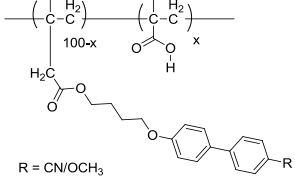
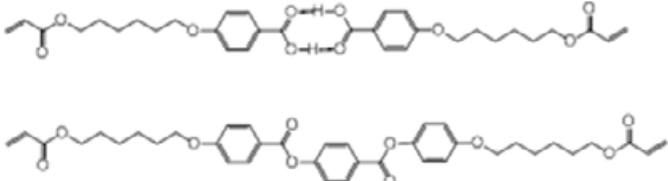
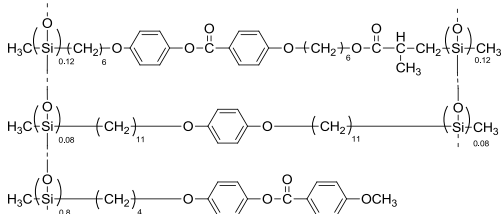
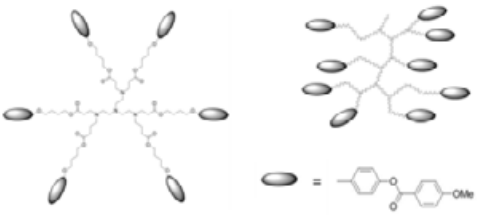
Both targeted LCs exhibited a mesophase (*i.e.* nematic phase) close to- or at ambient temperatures. In isotropic conditions, hydrolysis of the $[Zn(Cy)_2]$ precursor led to isotropic

NPs. At these given temperatures, growth control could be achieved: the average size of the NPs is around 5.4 ± 0.7 nm and 2.7 ± 0.3 nm, respectively.

When the experiments were performed in the nematic phase state of the LC compound (*i.e.* at lower temperatures), anisotropic ZnO structures, were obtained. As shown in Figure II.29 either nano-worm-like or nano-wires structures were grown in branched LC and hyperbranched LC. They have an average width of 2.5 ± 0.2 nm and 2.7 ± 0.4 nm, respectively. Polydispersed lengths vary from a few nanometers up to around 100 nm when the branched LC was used, while lengths from around 10 to 200 nm were obtained when the hyperbranched LC was used. Thus, a direct correlation between the structural characteristics of the LC and the morphology of the nanostructures was demonstrated. The new LC/NPs composites present, at the same time, LC properties and optical properties originating from ZnO. This new *in situ* strategy paves the way for new LC/NP composites of controllable and stable properties.

Therefore in order to tailor the NP morphology using a LC phase, different criteria should be fulfilled. Primarily, the chemical reaction leading to the NPs should not disrupt the LC organization. Thus, the LC molecules should not play the role of reactants (side products should be avoided as much as possible throughout the NP formation). Next in order, interactions between the LC molecules, the NP precursor and eventually the synthesized NPs, should favour the templating effect of the LC phase. Finally, the use of relatively high viscosity LCs should prevent a fast disruption of the organization during the NP formation.

Table II.3. Highlighted example of thermotropic LCs used for direct synthesis of NPs.

LC Type	NP type / Ref
	Au NPs (7-14 nm) [163]
	Ag NPs (5-30 nm) [164]
	Ag Nps (5 nm) [169]
	Au NPs (3-50 nm) [168]
	ZnO nanoworms nanowires [170], [171]

4. Conclusion:

NPs/LC hybrids have been the subject of many reports in the last few years. Such materials can be obtained either by *ex situ* or *in situ* strategies. The former is often the most appropriated strategy, when monodisperse NPs are needed for a chosen applications. Nevertheless it can necessitate tedious synthetic steps to render NPs compatible with a LC medium. In that context LC polymers can incorporate specific moieties in their structure that can render them suitable to interact with the preformed NPs and allow increasing colloidal stability within a LC medium. The mesophases obtained from such polymer can then be taken in good account to organize NPs within the LC structure in a precise and controlled fashion which is required when dealing with optical properties of those assemblies for instance. *In situ* strategy has also been used with such polymers. In that case the main issues concern the difficulties to perform chemistry in a LC medium without disrupting the LC order. Those difficulties have been circumvented either by using physical methods, by using LC as a reactant or by diffusion of reactants in a gas phase within the LC structure. Up to date most studies have focused on the use of lamellar and nematic mesophases obtained from such LC polymers. Therefore LC polymers that induces different mesophases (cubic, columnar, ...) could be materials of choice to induce specific growth mechanism and induce specific arrangement of NPs within those hybrids. In that context hyperbranched structures could be of special interest.

III. Objectives of the projects

The two main objectives of this thesis project were: 1) The investigation of the capability of dendritic based core-shell polymers to induce the formation of different systems: lyotropic aggregates, gel phases or liquid crystal polymers responsive to external stimuli. For this we have chosen to use 3 different dendritic polymers: dendrimer, hyperbranched and dendrigraft and also used covalent and no-covalent modification to obtain core-shell structures. These systems with interesting structural order could be used to generate nanohybrid materials.

2) The use of these self-assembled systems as soft-template to stabilize as well as to *in situ* synthesis of metal nanoparticles. We have chosen gold nanoparticles due to its optical properties. It could allow us to gain insight in the interaction between the soft-template and the nanoparticles themselves. The objective was not only the synthesis and stabilization of Au NPs within host structures but also to study the effect of Au NPs incorporation on the properties of the hybrid materials. For such a task, we envisaged using different strategies *in situ* approach or *ex situ* approach.

Throughout this project we will pursue the understanding of the nanomaterial's interaction with the polymer self-assembled structures. Several different systems will be investigated based on dendritic core-shell structures including (lyotropic aggregates, gels, liquid crystals).

For this purpose, polymeric core-shell structures were prepared by both covalent and non-covalent modification of dendritic polymers owing to three different families.

Amine terminated Dendrimer polyamidoamine (PAMAM) purchased from Aldrich, PAMAM dendrimers consist of alkyl-diamine core and tertiary amine branches and a lot of primary amine groups on the surface.

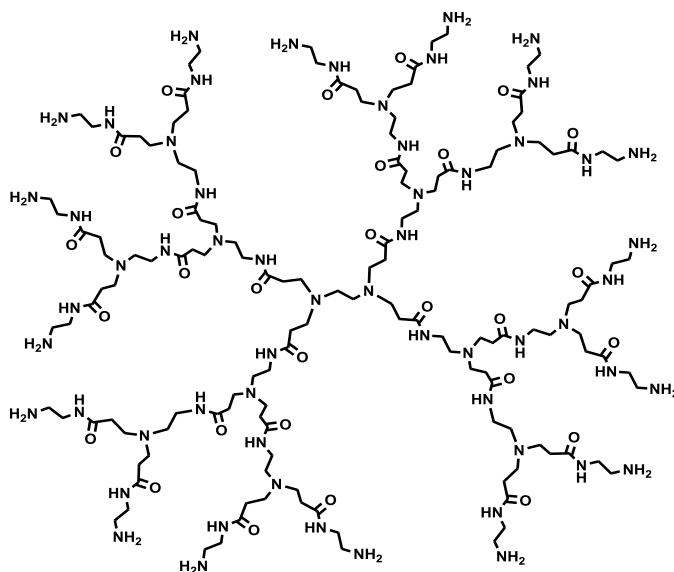


Figure III.1. Chemical structure of dendrimer polyamidoamine (PAMAM) generation 2

Hyperbranched polyamidoamine (HYPAM) with analogous structure to PAMAM dendrimer, which is synthesized in our laboratory, it contains of tertiary amine branches and primary amine groups on the surface. Their structure and synthesis is already published [146], [172] and will be discussed with details in a later state in this thesis.

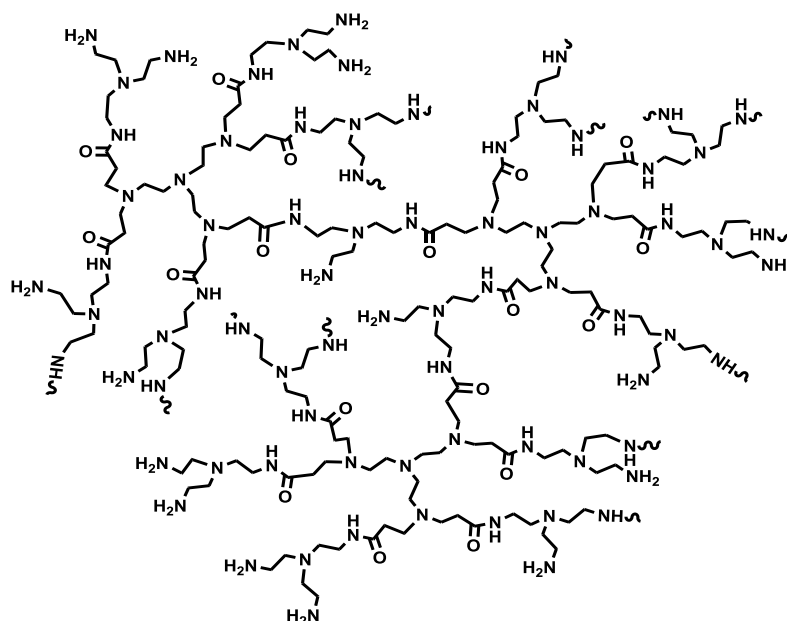


Figure III.2. Hyperbranched polyamidoamine (HYPAM)

Dendrigrraft polylysine (DGL) consisting of branched polylysines and numerous of amine (ammonium) groups are supplied by Colcom company.

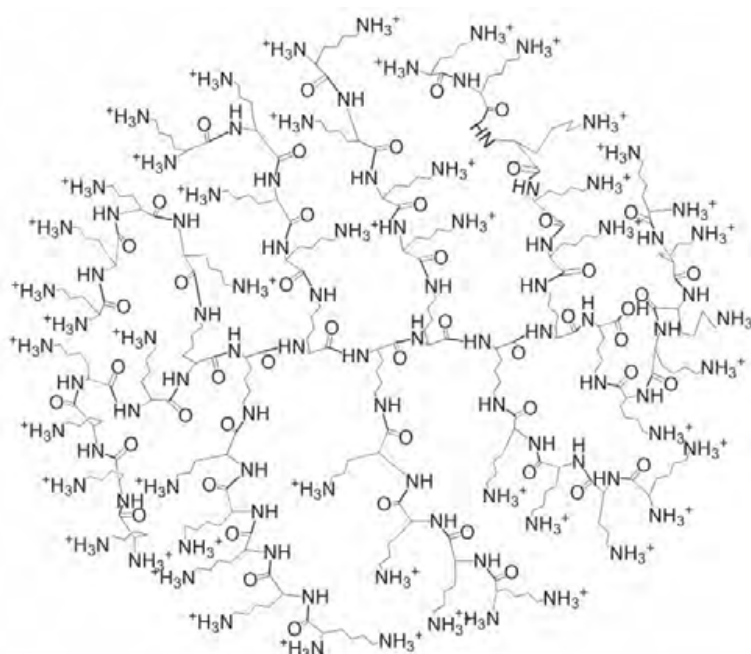


Figure III.3. Polylysine dendrigrraft (DGL) of generation 2

IV. References

1. Yan, D., Gao, C. & Frey, H. *Hyperbranched Polymers: Synthesis, Properties, and Applications*. (John Wiley & Sons, 2011).
2. Qiu, L. Y. & Bae, Y. H. *Polymer Architecture and Drug Delivery*. *Pharm. Res.* **23**, 1–30 (2006).
3. Keilitz, J. et al. Dendritic Polymers with a Core-Multishell Architecture: A Versatile Tool for the Stabilization of Nanoparticles. *Chem. Mater.* **20**, 2423–2425 (2008).
4. Kurniasih, I. N. et al. Synthesis and transport properties of new dendritic core-shell architectures based on hyperbranched polyglycerol with biphenyl-PEG shells. *New J. Chem.* **36**, 371–379 (2012).
5. Liu, Y. et al. Amphiphilic hyperbranched copolymers bearing a hyperbranched core and a dendritic shell as novel stabilizers rendering gold nanoparticles with an unprecedentedly long lifetime in the catalytic reduction of 4-nitrophenol. *J. Mater. Chem.* **22**, 21173–21182 (2012).
6. Jikei, M. & Kakimoto, M. Hyperbranched polymers: a promising new class of materials. *Prog. Polym. Sci.* **26**, 1233–1285 (2001).
7. Tomalia, D. A., Hedstrand, D. M. & Ferritto, M. S. Comb-burst dendrimer topology: new macromolecular architecture derived from dendritic grafting. *Macromolecules* **24**, 1435–1438 (1991).
8. Gauthier, M. & Moeller, M. Uniform highly branched polymers by anionic grafting: arborescent graft polymers. *Macromolecules* **24**, 4548–4553 (1991).
9. Teertstra, S. J. & Gauthier, M. Dendrigrft polymers: macromolecular engineering on a mesoscopic scale. *Prog. Polym. Sci.* **29**, 277–327 (2004).
10. Taton, D. et al. Controlled polymerizations as tools for the design of star-like and dendrimer-like polymers. *Polym. Int.* **55**, 1138–1145 (2006).
11. Kamigaito, M., Ando, T. & Sawamoto, M. Metal-Catalyzed Living Radical Polymerization. *Chem. Rev.* **101**, 3689–3746 (2001).
12. Tsarevsky, N. V. & Matyjaszewski, K. ‘Green’ Atom Transfer Radical Polymerization: From Process Design to Preparation of Well-Defined Environmentally Friendly Polymeric Materials. *Chem. Rev.* **107**, 2270–2299 (2007).
13. Abraham, S., Choi, J. H., Ha, C.-S. & Kim, I. Synthesis of star polymers via nitroxide mediated free-radical polymerization: A ‘core-first’ approach using resorcinarene-based alkoxyamine initiators. *J. Polym. Sci. Part Polym. Chem.* **45**, 5559–5572 (2007).
14. Stenzel-Rosenbaum, M., Davis, T. P., Chen, V. & Fane, A. G. Star-polymer synthesis via radical reversible addition-fragmentation chain-transfer polymerization. *J. Polym. Sci. Part Polym. Chem.* **39**, 2777–2783 (2001).
15. Angot, S., Murthy, K. S., Taton, D. & Gnanou, Y. Atom Transfer Radical Polymerization of Styrene Using a Novel Octafunctional Initiator: Synthesis of Well-Defined Polystyrene Stars. *Macromolecules* **31**, 7218–7225 (1998).
16. Gao, H. & Matyjaszewski, K. Synthesis of Star Polymers by A New ‘Core-First’ Method: Sequential Polymerization of Cross-Linker and Monomer. *Macromolecules* **41**, 1118–1125 (2008).

17. Zhang, X., Xia, J. & Matyjaszewski, K. End-Functional Poly(tert-butyl acrylate) Star Polymers by Controlled Radical Polymerization. *Macromolecules* **33**, 2340–2345 (2000).
18. Amamoto, Y., Higaki, Y., Matsuda, Y., Otsuka, H. & Takahara, A. Programmed Thermodynamic Formation and Structure Analysis of Star-like Nanogels with Core Cross-linked by Thermally Exchangeable Dynamic Covalent Bonds. *J. Am. Chem. Soc.* **129**, 13298–13304 (2007).
19. Gao, H., Min, K. & Matyjaszewski, K. Synthesis of 3-Arm Star Block Copolymers by Combination of ‘Core-First’ and ‘Coupling-Onto’ Methods Using ATRP and Click Reactions. *Macromol. Chem. Phys.* **208**, 1370–1378 (2007).
20. Kuckling, D. & Wycisk, A. Stimuli-responsive star polymers. *J. Polym. Sci. Part Polym. Chem.* **51**, 2980–2994 (2013).
21. Blencowe, A., Tan, J. F., Goh, T. K. & Qiao, G. G. Core crosslinked star polymers via controlled radical polymerization. *Polymer* **50**, 5–32 (2009).
22. Inoue, K. Functional dendrimers, hyperbranched and star polymers. *Prog. Polym. Sci.* **25**, 453–571 (2000).
23. Xia, X., Ye, Z., Morgan, S. & Lu, J. ‘Core-First’ Synthesis of Multiarm Star Polyethylenes with a Hyperbranched Core and Linear Arms via Ethylene Multifunctional ‘Living’ Polymerization with Hyperbranched Polyethylenes Encapsulating Multinuclear Covalently Tethered Pd-Diimine Catalysts. *Macromol. Wash. DC U. S.* **43**, 4889–4901 (2010).
24. Miura, Y. & Dote, H. Syntheses of 12-arm star polymers and star diblock copolymers by nitroxide-mediated radical polymerization using dendritic dodecafunctional macroinitiators. *J. Polym. Sci. Part Polym. Chem.* **43**, 3689–3700 (2005).
25. Popeney, C. S. et al. Tandem Coordination, Ring-Opening, Hyperbranched Polymerization for the Synthesis of Water-Soluble Core-Shell Unimolecular Transporters. *ACS Macro Lett.* **1**, 564–567 (2012).
26. Gauthier, M., Tichagwa, L., Downey, J. S. & Gao, S. Arborescent Graft Copolymers: Highly Branched Macromolecules with a Core-Shell Morphology. *Macromolecules* **29**, 519–527 (1996).
27. Yun, S. I., Cao, L., Kang, T.-B., Huh, M. & Gauthier, M. Morphology of Polystyrene Core-dPoly(ethylene oxide) Shell Arborescent Copolymer Micelles from Small-Angle Neutron Scattering Analysis. *J. Macromol. Sci. Part B Phys.* **50**, 2318–2333 (2011).
28. Schoemer, M. & Frey, H. Organobase-Catalyzed Synthesis of Multiarm Star Polylactide With Hyperbranched Poly(ethylene glycol) as the Core. *Macromol. Chem. Phys.* **212**, 2478–2486 (2011).
29. Liu, H. et al. Core-shell-type multiarm star polyethylenimine-block-poly(ϵ -caprolactone): Synthesis and guest encapsulation potential. *J. Polym. Sci. Part Polym. Chem.* **44**, 4165–4173 (2006).
30. Cao, P.-F. et al. Covalently stabilized vesicles derived from amphiphilic multiarm star polymers: Preparation, characterization, and their capability of hosting different polarity of guests. *J. Polym. Sci. Part Polym. Chem.* **50**, 227–236 (2012).
31. Zheng, Y. et al. Biodegradable Core-Shell Materials via RAFT and ROP: Characterization and Comparison of Hyperbranched and Microgel Particles. *Macromol. Wash. DC U. S.* **44**, 1347–1354 (2011).

32. Dong, Z., Liu, X., Liu, H. & Li, Y. Synthesis of Novel Star Polymers with Vinyl-Functionalized Hyperbranched Core via 'Arm-First' Strategy. *Macromol. Wash. DC U. S.* **43**, 7985–7992 (2010).
33. Appelhans, D. et al. Hyperbranched PEI with Various Oligosaccharide Architectures: Synthesis, Characterization, ATP Complexation, and Cellular Uptake Properties. *Biomacromolecules* **10**, 1114–1124 (2009).
34. Tripp, S., Appelhans, D., Striegler, C. & Voit, B. Oligosaccharide Shells as a Decisive Factor for Moderate and Strong Ionic Interactions of Dendritic Poly(ethylene imine) Scaffolds under Shear Forces. *Chem. - Eur. J.* **20**, 8314–8319 (2014).
35. Thuenemann, A. F., Bienert, R., Appelhans, D. & Voit, B. Core-Shell Structures of Oligosaccharide-Functionalized Hyperbranched Poly(ethylene imines). *Macromol. Chem. Phys.* **213**, 2362–2369 (2012).
36. Li, J., Li, J., Xu, S., Zhang, D. & Liu, D. Hydrophobic oligopeptide-based star-block copolymers as unimolecular nanocarriers for poorly water-soluble drugs. *Colloids Surf. B Biointerfaces* **110**, 183–190 (2013).
37. Jin, M., Liu, H., Pu, H. & Wan, D. Kinetic topology-selective encapsulation and mixture separation by a nanocapsule with hyperbranched polyethylenimine as core and polystyrene as shell. *J. Polym. Sci. Part B Polym. Phys.* **51**, 1273–1281 (2013).
38. Beckmann, R. & Beginn, U. Synthesis and characterization of new poly(ethyleneimine)-g-poly(methyl methacrylate) star-block copolymers with hyperbranched cationic core. *J. Polym. Sci. Part Polym. Chem.* **51**, 3700–3715 (2013).
39. Liu, Y. et al. Amphiphilic hyperbranched copolymers bearing a hyperbranched core and dendritic shell: synthesis, characterization and guest encapsulation performance. *Soft Matter* **8**, 8361–8369 (2012).
40. Kurniasih, I. N. et al. A bifunctional nanocarrier based on amphiphilic hyperbranched polyglycerol derivatives. *J. Mater. Chem. B Mater. Biol. Med.* **1**, 3569–3577 (2013).
41. Tian, W. et al. Biocompatible amphiphilic hyperbranched nanocapsules with a functional core: Synergistic encapsulation and asynchronous release properties towards multi-guest molecules. *RSC Adv.* **2**, 11976–11987 (2012).
42. Tian, W., Wei, X., Yang, G. & Fan, X. Synthesis of amphiphilic hyperbranched polymers for controlled release of double-guest molecules. *J. Controlled Release* **152**, e97–e98 (2011).
43. Ho, C. H. et al. Conventional and microwave-assisted synthesis of hyperbranched and highly branched polylysine towards amphiphilic core-shell nanocontainers for metal nanoparticles. *Polymer* **53**, 4623–4630 (2012).
44. Dong, Z. & Ye, Z. Synthesis of Hyperbranched Poly(phenylacetylene)s Containing Pendant Alkyne Groups by One-Pot Pd-Catalyzed Copolymerization of Phenylacetylene with Diynes. *Macromol. Wash. DC U. S.* **45**, 5020–5031 (2012).
45. Schueler, F., Kerscher, B., Beckert, F., Thomann, R. & Muelhaupt, R. Hyperbranched Polymeric Ionic Liquids with Onion-like Topology as Transporters and Compartmentalized Systems. *Angew. Chem. Int. Ed.* **52**, 455–458 (2013).
46. Yu, S. et al. Synthesis and Self-Assembly of Amphiphilic Aptamer-Functionalized Hyperbranched Multiarm Copolymers for Targeted Cancer Imaging. *Biomacromolecules* **15**, 1828–1836 (2014).

47. Zeng, D. et al. One-step synthesis of amphiphilic hyperbranched amylopectin derivatives, characterization and use as functional nanovehicles. *Carbohydr. Polym.* **98**, 905–913 (2013).
48. Qiu, F. et al. Control of the Optical Properties of a Star Copolymer with a Hyperbranched Conjugated Polymer Core and Poly(ethylene glycol) Arms by Self-Assembly. *Chem. – Eur. J.* **16**, 12710–12717 (2010).
49. Weng, Z., Zheng, Y., Tang, A. & Gao, C. Synthesis, Dye Encapsulation, and Highly Efficient Colouring Application of Amphiphilic Hyperbranched Polymers. *Aust. J. Chem.* **67**, 103–111 (2014).
50. Zhang, L., Hu, C., Fan, Y. & Wu, Y. Binary gene vectors based on hyperbranched poly(l-lactide-co-polyglycerol) and polyethylenimine for prolonged transgene expression via co-assembly with DNA into fiber core-shell triplexes. *J. Mater. Chem. B Mater. Biol. Med.* **1**, 6271–6282 (2013).
51. Xu, W. et al. Octreotide-functionalized and resveratrol-loaded unimolecular micelles for targeted neuroendocrine cancer therapy. *Nanoscale* **5**, 9924–9933 (2013).
52. Wang, D. et al. Supramolecular amphiphilic multiarm hyperbranched copolymer: synthesis, self-assembly and drug delivery applications. *Polym. Chem.* **4**, 85–94 (2013).
53. Han, J., Li, S., Tang, A. & Gao, C. Water-Soluble and Clickable Segmented Hyperbranched Polymers for Multifunctionalization and Novel Architecture Construction. *Macromol. Wash. DC U. S.* **45**, 4966–4977 (2012).
54. Prabakaran, M., Grailer, J. J., Pilla, S., Steeber, D. A. & Gong, S. Folate-conjugated amphiphilic hyperbranched block copolymers based on Boltorn H40, poly(L-lactide) and poly(ethylene glycol) for tumor-targeted drug delivery. *Biomaterials* **30**, 3009–3019 (2009).
55. Yoon, H., Dell, E. J., Freyer, J. L., Campos, L. M. & Jang, W.-D. Polymeric supramolecular assemblies based on multivalent ionic interactions for biomedical applications. *Polymer* **55**, 453–464 (2014).
56. Kokufuta, E., Ogawa, K., Doi, R., Kikuchi, R. & Farinato, R. S. Geometrical Characteristics of Polyelectrolyte Nanogel Particles and Their Polyelectrolyte Complexes Studied by Dynamic and Static Light Scattering†. *J. Phys. Chem. B* **111**, 8634–8640 (2007).
57. Nishiyama, N., Jang, W.-D. & Kataoka, K. Supramolecular nanocarriers integrated with dendrimers encapsulating photosensitizers for effective photodynamic therapy and photochemical gene delivery. *New J. Chem.* **31**, 1074–1082 (2007).
58. Sousa-Herves, A., Fernandez-Megia, E. & Riguera, R. Synthesis and supramolecular assembly of clicked anionic dendritic polymers into polyion complex micelles. *Chem. Commun.* 3136–3138 (2008). doi:10.1039/B805208E
59. Hoffman, A. S. et al. Really smart bioconjugates of smart polymers and receptor proteins. *J. Biomed. Mater. Res.* **52**, 577–586 (2000).
60. Cai, Y. & Liu, Y.-Y. Amphiphilic Unimolecular Nanoparticles Based on a Hyperbranched Polyacrylate Core and a PNIPAm Shell: Synthesis via ATRP and Properties. *Macromol. Chem. Phys.* **214**, 882–891 (2013).
61. Tian, W., Lv, X., Huang, L., Ali, N. & Kong, J. Multiresponsive Properties of Triple-Shell Architectures with Poly(N,N-diethylaminoethyl methacrylate), Poly(N-

- vinylcaprolactam), and Poly(N,N-dimethylaminoethyl methacrylate) as Building Blocks. *Macromol. Chem. Phys.* **213**, 2450–2463 (2012).
62. Luo, S. et al. Thermoresponsive unimolecular micelles with a hydrophobic dendritic core and a double hydrophilic block copolymer shell. *J. Colloid Interface Sci.* **353**, 76–82 (2011).
 63. Xu, J., Luo, S., Shi, W. & Liu, S. Two-Stage Collapse of Unimolecular Micelles with Double Thermoresponsive Coronas. *Langmuir* **22**, 989–997 (2006).
 64. Wan, D. & Pu, H. Synthesis of a thermoresponsive platinum nanocomposite using a three-layer onion-like polymer as template. *Mater. Lett.* **61**, 3404–3408 (2007).
 65. Lin, H.-H. & Cheng, Y.-L. In-Situ Thermoreversible Gelation of Block and Star Copolymers of Poly(ethylene glycol) and Poly(N-isopropylacrylamide) of Varying Architectures. *Macromolecules* **34**, 3710–3715 (2001).
 66. Schmalz, A., Schmalz, H. & Müller, A. H. E. Smart hydrogels based on responsive star-block copolymers. *Soft Matter* **8**, 9436–9445 (2012).
 67. Zhang, H. et al. Fabrication of thermo-responsive hydrogels from star-shaped copolymer with a biocompatible β -cyclodextrin core. *Polymer* **53**, 3719–3725 (2012).
 68. Ge, Z., Zhou, Y., Tong, Z. & Liu, S. Thermogelling of Double Hydrophilic Multiblock and Triblock Copolymers of N,N-Dimethylacrylamide and N-Isopropylacrylamide: Chain Architectural and Hofmeister Effects. *Langmuir* **27**, 1143–1151 (2011).
 69. Chen, Y., Shen, Z., Gehringer, L., Frey, H. & Stiriba, S. E. Supramolecular thermotropic liquid crystalline materials with nematic mesophase based on methylated hyperbranched polyethylenimine and mesogenic carboxylic acid. *Macromol. Rapid Commun.* **27**, 69–75 (2006).
 70. Marcos, M. et al. Photosensitive Ionic Nematic Liquid Crystalline Complexes Based on Dendrimers and Hyperbranched Polymers and a Cyanoazobenzene Carboxylic Acid. *Chem. Mater.* **20**, 5209–5217 (2008).
 71. Martín-Rapún, R. et al. Ionic Thermotropic Liquid Crystal Dendrimers. *J. Am. Chem. Soc.* **127**, 7397–7403 (2005).
 72. Canilho, N., Scholl, M., Klok, H.-A. & Mezzenga, R. Thermotropic Ionic Liquid Crystals via Self-Assembly of Cationic Hyperbranched Polypeptides and Anionic Surfactants. *Macromolecules* **40**, 8374–8383 (2007).
 73. Hernández-Ainsa, S., Barberá, J., Marcos, M. & Serrano, J. L. Nanoobjects coming from mesomorphic ionic PAMAM dendrimers. *Soft Matter* **7**, 2560–2568 (2011).
 74. Jeong, B., Kim, S. W. & Bae, Y. H. Thermosensitive sol–gel reversible hydrogels. *Adv. Drug Deliv. Rev.* **64**, **Supplement**, 154–162 (2012).
 75. Plummer, R., Hill, D. J. T. & Whittaker, A. K. Solution Properties of Star and Linear Poly(N-isopropylacrylamide). *Macromolecules* **39**, 8379–8388 (2006).
 76. Patrickios, C. S. & Georgiou, T. K. Covalent amphiphilic polymer networks. *Curr. Opin. Colloid Interface Sci.* **8**, 76–85 (2003).
 77. Tsitsilianis, C. Responsive reversible hydrogels from associative ‘smart’ macromolecules. *Soft Matter* **6**, 2372–2388 (2010).
 78. Tanaka, T. *Gels. Sci. Am.* **244**, 124–138 (1981).
 79. Jeong, B., Lee, D. S., Shon, J.-I., Bae, Y. H. & Kim, S. W. Thermoreversible gelation of poly(ethylene oxide) biodegradable polyester block copolymers. *J. Polym. Sci. Part Polym. Chem.* **37**, 751–760 (1999).
 80. Dierking, I. *Textures of liquid crystals.* (Wiley-VCH, 2013).

81. Takezoe, H. & Takanishi, Y. Bent-Core Liquid Crystals: Their Mysterious and Attractive World. *Jpn. J. Appl. Phys.* **45**, 597 (2006).
82. Hegmann, T., Qi, H. & Marx, V. M. Nanoparticles in Liquid Crystals: Synthesis, Self-Assembly, Defect Formation and Potential Applications. *J. Inorg. Organomet. Polym. Mater.* **17**, 483–508 (2007).
83. D. Demus, J. Goodby, G. W. Gray, H.-W. Spiess & V. Vill. *Handbook of Liquid Crystals: Fundamentals*. **1**, (Wiley-VCH Verlag GmbH & Co. KGaA).
84. Blumstein, A. *Liquid Crystalline Order in Polymers*. (Elsevier Inc., 1978).
85. Barberá, J., Marcos, M. & Serrano, J. L. Dendromesogens: Liquid Crystal Organizations versus Starburst Structures. *Chem. – Eur. J.* **5**, 1834–1840 (1999).
86. Lorenz, K., Holter, D., Stuhn, B., Mulhaupt, R. & Frey, H. A mesogen-functionalized carbosilane dendrimer: A dendritic liquid crystalline polymer. *Adv. Mater.* **8**, 414–& (1996).
87. Donnio, B. & Guillon, D. in *Supramolecular Polymers Polymeric Betains Oligomers* (eds. Donnio, B. et al.) **201**, 45–155 (Springer-Verlag Berlin, 2006).
88. Martin-Rapun, R. et al. Poly(propyleneimine) liquid crystal codendrimers bearing laterally and terminally attached promesogenic groups. *Chem. Mater.* **16**, 4969–4979 (2004).
89. Percec, V., Chu, P. & Kawasumi, M. Toward Willowlike Thermotropic Dendrimers. *Macromolecules* **27**, 4441–4453 (1994).
90. Percec, V. & Kawasumi, M. Liquid-Crystalline Polyethers Based on Conformational Isomerism .23. Synthesis and Characterization of a Thermotropic Nematic Liquid-Crystalline Dendrimeric Polymer. *Macromolecules* **25**, 3843–3850 (1992).
91. Bauer, S., Fischer, H. & Ringsdorf, H. Highly Branched Liquid-Crystalline Polymers with Chiral Terminal Groups. *Angew. Chem.-Int. Ed. Engl.* **32**, 1589–1592 (1993).
92. Sunder, A., Quincy, M. F., Mulhaupt, R. & Frey, H. Hyperbranched polyether polyols with liquid crystalline properties. *Angew. Chem.-Int. Ed.* **38**, 2928–2930 (1999).
93. Marcos, M., Martín-Rapún, R., Omenat, A. & Serrano, J. L. Highly congested liquid crystal structures: dendrimers, dendrons, dendronized and hyperbranched polymers. *Chem. Soc. Rev.* **36**, 1889–1901 (2007).
94. Bousquet, A. et al. pH responsive surfaces with nanoscale topography. *J. Polym. Sci. Part Polym. Chem.* **48**, 2982–2990 (2010).
95. Li, S., Tiwari, A., Ge, Y. & Fei, D. A pH-responsive, low crosslinked, molecularly imprinted insulin delivery system. *Adv. Mater. Lett.* **1**, 4–10 (2010).
96. Kang, S. I. & Bae, Y. H. pH-Induced solubility transition of sulfonamide-based polymers. *J. Controlled Release* **80**, 145–155 (2002).
97. Boyer, C., Whittaker, M. R., Chuah, K., Liu, J. & Davis, T. P. Modulation of the Surface Charge on Polymer-Stabilized Gold Nanoparticles by the Application of an External Stimulus. *Langmuir* **26**, 2721–2730 (2010).
98. Boylan, N. J. et al. Enhancement of airway gene transfer by DNA nanoparticles using a pH-responsive block copolymer of polyethylene glycol and poly-l-lysine. *Biomaterials* **33**, 2361–2371 (2012).
99. Yan, Y. et al. Poly(l-lysine)-based star-block copolymers as pH-responsive nanocarriers for anionic drugs. *Colloids Surf. B Biointerfaces* **95**, 137–143 (2012).
100. Kramer, M. et al. pH-responsive molecular nanocarriers based on dendritic core-shell architectures. *Angew. Chem. Int. Ed.* **41**, 4252–4256 (2002).

101. Xu, S., Luo, Y. & Haag, R. Water-soluble pH-responsive dendritic core-shell nanocarriers for polar dyes based on poly(ethylene imine). *Macromol. Biosci.* **7**, 968–974 (2007).
102. Sunder, A., Hanselmann, R., Frey, H. & Müllhaupt, R. Controlled Synthesis of Hyperbranched Polyglycerols by Ring-Opening Multibranching Polymerization. *Macromolecules* **32**, 4240–4246 (1999).
103. Nowag, S. et al. Biocompatible, hyperbranched nanocarriers for the transport and release of copper ions. *J. Mater. Chem. B Mater. Biol. Med.* **2**, 3915–3918 (2014).
104. Yan, Y. et al. A poly(L-lysine)-based hydrophilic star block co-polymer as a protein nanocarrier with facile encapsulation and pH-responsive release. *Acta Biomater.* **8**, 2113–2120 (2012).
105. Huang, H. et al. Poly(l-glutamic acid)-based star-block copolymers as pH-responsive nanocarriers for cationic drugs. *Eur. Polym. J.* **48**, 696–704 (2012).
106. Yan, Y., Liao, L. & Liu, D. Poly(L-glutamic acid)-based star-block copolymers as pH-responsive release systems. *J. Controlled Release* **152**, e60–e61 (2011).
107. Wan, D., Jin, M., Pu, H. & Wang, G. Charge selective encapsulation by polymeric micelles with cationic, anionic, or zwitterionic cores. *J. Polym. Sci. Part Polym. Chem.* **50**, 1342–1350 (2012).
108. Wan, D., Ohta, S., Kakuchi, T. & Satoh, T. A hydrophilic unimolecular nanocapsule with cyclodextrin moieties in the core: chemically triggered on-demand release and pH-response. *Soft Matter* **7**, 6422–6425 (2011).
109. Calderon, M. et al. Development of efficient acid cleavable multifunctional prodrugs derived from dendritic polyglycerol with a poly(ethylene glycol) shell. *J. Controlled Release* **151**, 295–301 (2011).
110. Jiang, G. & Ren, J. Preparation of a multiarm star polymer as encapsulation and release carrier for guest molecules. *Des. Monomers Polym.* **13**, 427–436 (2010).
111. Zhu, L. et al. Construction and Application of a pH-Sensitive Nanoreactor via a Double-Hydrophilic Multiarm Hyperbranched Polymer. *Langmuir* **26**, 8875–8881 (2010).
112. Liang, Y., Wan, D., Cai, X., Jin, M. & Pu, H. Unimolecular micelle derived from hyperbranched polyethylenimine with well-defined hybrid shell of poly(ethylene oxide) and polystyrene: A versatile nanocapsule. *J. Polym. Sci. Part Polym. Chem.* **48**, 681–691 (2010).
113. Xu, S., Kraemer, M. & Haag, R. pH-responsive dendritic core-shell architectures as amphiphilic nanocarriers for polar drugs. *J. Drug Target.* **14**, 367–374 (2006).
114. Pang, Y. et al. Bioreducible unimolecular micelles based on amphiphilic multiarm hyperbranched copolymers for triggered drug release. *Sci. China Chem.* **53**, 2497–2508 (2010).
115. You, Y.-Z., Hong, C.-Y. & Pan, C.-Y. Facile One-Pot Approach for Preparing Dually Responsive Core-Shell Nanostructure. *Macromol. Wash. DC U. S.* **42**, 573–575 (2009).
116. Wang, D., Yu, Z.-Q., Hong, C.-Y. & You, Y.-Z. Strong fluorescence emission from PEGylated hyperbranched poly(amido amine). *Eur. Polym. J.* **49**, 4189–4194 (2013).
117. Sahiner, N. Soft and flexible hydrogel templates of different sizes and various functionalities for metal nanoparticle preparation and their use in catalysis. *Prog. Polym. Sci.* **38**, 1329–1356 (2013).

118. Bisoyi, H. K. & Kumar, S. Liquid-crystal nanoscience: an emerging avenue of soft self-assembly. *Chem. Soc. Rev.* **40**, 306 (2011).
119. Hu, X., Zhou, L. & Gao, C. Hyperbranched polymers meet colloid nanocrystals: a promising avenue to multifunctional, robust nanohybrids. *Colloid Polym. Sci.* **289**, 1299–1320 (2011).
120. Hayat, M. A. *Colloidal gold: principles, methods, and applications*. (Academic Press, 1989).
121. Jain, P. K., Huang, X., El-Sayed, I. H. & El-Sayed, M. A. Noble metals on the nanoscale: optical and photothermal properties and some applications in imaging, sensing, biology, and medicine. *Acc. Chem. Res.* **41**, 1578–1586 (2008).
122. Yasun, E. et al. Cancer cell sensing and therapy using affinity tag-conjugated gold nanorods. *Interface Focus* **3**, (2013).
123. Baptista, P., Conde, J., Rosa, J. & Baptista, P. Gold-Nanobeacons as a theranostic system for the detection and inhibition of specific genes. *Protoc. Exch.* (2013). doi:10.1038/protex.2013.088
124. Mody, V. V., Siwale, R., Singh, A. & Mody, H. R. Introduction to metallic nanoparticles. *J. Pharm. Bioallied Sci.* **2**, 282–289 (2010).
125. Daniel, M.-C. & Astruc, D. Gold Nanoparticles: Assembly, Supramolecular Chemistry, Quantum-Size-Related Properties, and Applications toward Biology, Catalysis, and Nanotechnology. *Chem. Rev.* **104**, 293–346 (2004).
126. Turkevich, J., Stevenson, P. C. & Hillier, J. A study of the nucleation and growth processes in the synthesis of colloidal gold. *Discuss. Faraday Soc.* **11**, 55–75 (1951).
127. Brust, M., Walker, M., Bethell, D., Schiffrin, D. J. & Whyman, R. Synthesis of thiol-derivatised gold nanoparticles in a two-phase Liquid–Liquid system. *J. Chem. Soc. Chem. Commun.* 801–802 (1994). doi:10.1039/C39940000801
128. Alshammari, A. Influence of Single Use and Combination of Reductants on the Size, Morphology and Growth Steps of Gold Nanoparticles in Colloidal Mixture. *Open J. Phys. Chem.* **02**, 252–261 (2012).
129. Sistach, S. et al. Bolaamphiphile Surfactants as Nanoparticle Stabilizers: Application to Reversible Aggregation of Gold Nanoparticles. *Chem. Mater.* **20**, 1221–1223 (2008).
130. Pérignon, N. et al. Hyperbranched Polymers Analogous to PAMAM Dendrimers for the Formation and Stabilization of Gold Nanoparticles. *Macromolecules* **40**, 3034–3041 (2007).
131. Beija, M., Marty, J.-D. & Destarac, M. RAFT/MADIX polymers for the preparation of polymer/inorganic nanohybrids. *Prog. Polym. Sci.* **36**, 845–886 (2011).
132. Gomez, S. et al. Gold nanoparticles from self-assembled gold(I) amine precursors. *Chem. Commun.* 1945–1946 (2000). doi:10.1039/B005327I
133. Jana, N. R., Gearheart, L. & Murphy, C. J. Seeding Growth for Size Control of 5–40 nm Diameter Gold Nanoparticles. *Langmuir* **17**, 6782–6786 (2001).
134. Zheng, J.-N. et al. Popcorn-like PtAu nanoparticles supported on reduced graphene oxide: Facile synthesis and catalytic applications. *J. Mater. Chem. A* **2**, 8386–8395 (2014).
135. Moukarzel, W., Fitremann, J. & Marty, J.-D. Seed-less amino-sugar mediated synthesis of gold nanostars. *Nanoscale* **3**, 3285–3290 (2011).

136. Lemonier, S. Préparation et caractérisation de nanoparticules d'or. Stabilisation par des polysiloxanes et dépôt contrôlé sur des surfaces chargées. (Université Paul Sabatier, 2013).
137. Dey, P., Blakey, I., Thurecht, K. J. & Fredericks, P. M. Hyperbranched Polymer-Gold Nanoparticle Assemblies: Role of Polymer Architecture in Hybrid Assembly Formation and SERS Activity. *Langmuir* **30**, 2249–2258 (2014).
138. Zill, A. et al. Clickable polyglycerol hyperbranched polymers and their application to gold nanoparticles and acid-labile nanocarriers. *Chem. Commun. Camb. U. K.* **47**, 1279–1281 (2011).
139. Shen, Y. et al. Gold nanoparticles coated with a thermosensitive hyperbranched polyelectrolyte: towards smart temperature and pH nanosensors. *Angew. Chem. Int. Ed.* **47**, 2227–2230 (2008).
140. Shi, Y. et al. In situ preparation of Au or Ag nanoparticles in the presence of hyperbranched poly(amidoamine)s with hydrophobic end-groups as nanoreactors and reductants. *Polym. Compos.* **34**, 526–530 (2013).
141. Li, H., Cooper-White, J. J. & Kim, I. Facile and controllable incorporation of gold nanoparticles within one-dimensional self-assemblies of hyperbranched polymers. *Soft Matter* **9**, 5270–5276 (2013).
142. Sekowski, S. et al. Synthesis and characterisation of hybrid materials based on gold nanoparticles and HBP hyperbranched polyesters: Preparation of 'volcano-rings' nanostructures. *Colloids Surf. Physicochem. Eng. Asp.* **417**, 170–178 (2013).
143. Zhang, Z. & Shou, C. Synthesis of gold nanoparticles in hyperbranched polyol dispersions. *J. Appl. Polym. Sci.* **122**, 2849–2854 (2011).
144. Hu, N., Yin, J.-Y., Tang, Q. & Chen, Y. Comparative study of amphiphilic hyperbranched and linear polymer stabilized organo-soluble gold nanoparticles as efficient recyclable catalysts in the biphasic reduction of 4-nitrophenol. *J. Polym. Sci. Part Polym. Chem.* **49**, 3826–3834 (2011).
145. Jiang, G., Sun, X., Wang, Y. & Ding, M. Synthesis and fluorescence properties of hyperbranched poly(amidoamine)s with high density tertiary nitrogen. *Polym. Chem.* **1**, 1644–1649 (2010).
146. Perignon, N. et al. Hyperbranched Polymers Analogous to PAMAM Dendrimers for the Formation and Stabilization of Gold Nanoparticles. *Macromol. Wash. DC U. S.* **40**, 3034–3041 (2007).
147. Liu, X.-Y., Cheng, F., Liu, Y., Liu, H.-J. & Chen, Y. Preparation and characterization of novel thermoresponsive gold nanoparticles and their responsive catalysis properties. *J. Mater. Chem.* **20**, 360–368 (2009).
148. Liu, X.-Y. et al. Thermoresponsive gold nanoparticles with adjustable lower critical solution temperature as colorimetric sensors for temperature, pH and salt concentration. *J. Mater. Chem.* **20**, 278–284 (2009).
149. Wang, X. et al. Effective gel for gold nanoparticle formation, support and metal oxide templating. *Chem. Commun.* 3060–3062 (2007). doi:10.1039/B704825D
150. Vemula, P. K. & John, G. Smart amphiphiles: hydro/organogelators for in situ reduction of gold. *Chem. Commun.* 2218–2220 (2006). doi:10.1039/B518289A
151. Faoucher, E. et al. In situ preparation of network forming gold nanoparticles in agarose hydrogels. *Chem. Commun.* 6661–6663 (2009). doi:10.1039/B915787E

152. Murali Mohan, Y., Lee, K., Premkumar, T. & Geckeler, K. E. Hydrogel networks as nanoreactors: A novel approach to silver nanoparticles for antibacterial applications. *Polymer* **48**, 158–164 (2007).
153. Kazimierska, E. A. & Ciszowska, M. Thermoresponsive Poly-N-isopropylacrylamide Gels Modified with Colloidal Gold Nanoparticles for Electroanalytical Applications. 1. Preparation and Characterization. *Electroanalysis* **17**, 1384–1395 (2005).
154. Pong, F. Y., Lee, M., Bell, J. R. & Flynn, N. T. Thermoresponsive Behavior of Poly(N-Isopropylacrylamide) Hydrogels Containing Gold Nanostructures. *Langmuir* **22**, 3851–3857 (2006).
155. Saliba, S., Mingotaud, C., Kahn, M. L. & Marty, J.-D. Liquid crystalline thermotropic and lyotropic nanohybrids. *Nanoscale* **5**, 6641–6661 (2013).
156. Shandryuk, G. A. et al. Effect of H-Bonded Liquid Crystal Polymers on CdSe Quantum Dot Alignment within Nanocomposite. *Macromolecules* **41**, 2178–2185 (2008).
157. Ezhov, A. A. et al. Liquid-Crystalline Polymer Composites with CdS Nanorods: Structure and Optical Properties. *Langmuir* **27**, 13353–13360 (2011).
158. Vasilets, V. N. et al. Immobilization of quantum dots of cadmium selenide on the matrix of a graft liquid-crystalline polymer. *Polym. Sci. Ser. A* **53**, 521–526 (2011).
159. Li, F., Chen, W. & Chen, Y. Mesogen induced self-assembly for hybrid bulk heterojunction solar cells based on a liquid crystal D–A copolymer and ZnO nanocrystals. *J. Mater. Chem.* **22**, 6259–6266 (2012).
160. Shi, Y., Li, F., Tan, L. & Chen, Y. Hybrid Bulk Heterojunction Solar Cells Based on the Cooperative Interaction of Liquid Crystals within Quantum Dots and Diblock Copolymers. *ACS Appl. Mater. Interfaces* **5**, 11692–11702 (2013).
161. Zadoina, L. et al. In situ synthesis of cobalt nanoparticles in functionalized liquid crystalline polymers. *J. Mater. Chem.* **21**, 6988–6994 (2011).
162. Domracheva, N. E., Pyataev, A. V., Manapov, R. A. & Gruzdev, M. S. Magnetic Resonance and Mössbauer Studies of Superparamagnetic γ -Fe₂O₃ Nanoparticles Encapsulated into Liquid-Crystalline Poly(propylene imine) Dendrimers. *ChemPhysChem* **12**, 3009–3019 (2011).
163. Lee, J.-W. & Jin, J.-I. Formation of gold nanoparticles within a liquid crystalline polymeric matrix. *J. Nanosci. Nanotechnol.* **3**, 219–221 (2003).
164. Barmatov, E. B., Pebalk, D. A. & Barmatova, M. V. Influence of Silver Nanoparticles on the Phase Behavior of Side-Chain Liquid Crystalline Polymers. *Langmuir* **20**, 10868–10871 (2004).
165. Taubert, A. CuCl Nanoplatelets from an Ionic Liquid-Crystal Precursor. *Angew. Chem. Int. Ed.* **43**, 5380–5382 (2004).
166. Dobbs, W., Suisse, J.-M., Douce, L. & Welter, R. Electrodeposition of Silver Particles and Gold Nanoparticles from Ionic Liquid-Crystal Precursors. *Angew. Chem. Int. Ed.* **45**, 4179–4182 (2006).
167. Mallia, V. A., Vemula, P. K., John, G., Kumar, A. & Ajayan, P. M. In Situ Synthesis and Assembly of Gold Nanoparticles Embedded in Glass-Forming Liquid Crystals. *Angew. Chem. Int. Ed.* **46**, 3269–3274 (2007).
168. Gascon, I., Marty, J.-D., Gharsa, T. & Mingotaud, C. Formation of Gold Nanoparticles in a Side-Chain Liquid Crystalline Network: Influence of the Structure and Macroscopic Order of the Material. *Chem Mater* **17**, 5228–5230 (2005).

169. Dasgupta, D. et al. Patterned Silver Nanoparticles embedded in a Nanoporous Smectic Liquid Crystalline Polymer Network. *J. Am. Chem. Soc.* **135**, 10922–10925 (2013).
170. Saliba, S., Coppel, Y., Mingotaud, C., Marty, J.-D. & Kahn, M. L. ZnO/Liquid Crystalline Nanohybrids: From Properties in Solution to Anisotropic Growth. *Chem. – Eur. J.* **18**, 8084–8091 (2012).
171. Saliba, S. et al. Thermotropic Liquid Crystals as Templates for Anisotropic Growth of Nanoparticles. *Angew. Chem. Int. Ed.* **50**, 12032–12035 (2011).
172. Perignon, N., Mingotaud, A.-F., Marty, J.-D., Rico-Lattes, I. & Mingotaud, C. Formation and Stabilization in Water of Metal Nanoparticles by a Hyperbranched Polymer Chemically Analogous to PAMAM Dendrimers. *Chem. Mater.* **16**, 4856–4858 (2004).

Chapter 2

**Thermoresponsive Hyperbranched
Polymers:**

**Synthesis, Characterization and
applications for the Synthesis of Gold
Nanostructures**

CONTENTS

I. INTRODUCTION	97
II. SYNTHESIS AND CHARACTERIZATION OF THE HYPERBRANCHED POLYMERS CONSISTING OF THE PNIPAM SHELL AND HYPERBRANCHED POLYAMIDOAMINE CORE ...	98
A. HYPERBRANCHED POLY(AMIDOAMINE)	98
1. <i>Synthesis</i>	98
2. <i>Characterization</i>	99
a. NMR	99
b. Quantification of number primary amine groups	99
c. Determination of average molecular weights	102
d. SANS measurements	103
B. HYPERBRANCHED CORE-SHELL POLYMERS	104
1. <i>Synthesis by CDI activated coupling</i>	104
2. <i>Characterization of core-shell polymers</i>	105
a. Evaluation of grafting efficiency	105
i) SEC	105
ii) NMR	107
iii) FT-IR	110
iv) Glass transition temperature of bulk polymers	111
b. Evaluation of grafting ratios	112
i) Determination from FT-IR	112
ii) Determination from DSC	114
III. PROPERTIES OF AQUEOUS SOLUTIONS OF HYPERBRANCHED POLYMERS	116
1. <i>Behavior in diluted solution</i>	116
2. <i>Thermoresponsive properties</i>	118
IV. STABILIZATION AND <i>IN SITU</i> SYNTHESIS OF GOLD NANOCOMPOSITES	123
A. <i>EX SITU</i> SYNTHESIS AND STABILIZATION OF GOLD NANOPARTICLES	124
1. <i>Preformed Au NPs</i>	124
2. <i>Stabilization of Au NPs by PNIPAM based hyperbranched polymer</i>	125
a. Synthesis of Au NPs nanocomposite	125
b. Salt adding effect	127
c. Thermoresponsive properties	130
B. <i>IN SITU</i> SYNTHESIS OF GOLD NANOPARTICLES	135
1. <i>In situ synthesis of Au NPs by using NaBH₄ as reductant</i>	135
2. <i>Architecture effect on the size of formed Au NPs</i>	135
V. CONCLUSIONS	138
VI. REFERENCES	138

I. Introduction

Stimuli-responsive materials have benefited from significant advances in polymer science which open the way on the implementation of new smart materials such as organic/inorganic stimuli-responsive nanohybrids. The latter adopt some characteristics from the components that compose it such as thermoresponsiveness of the polymer part and physical, mechanical properties from the organic part. Synergistic effects can also create properties not present in any of the parts.

When a thermoresponsive polymer is physically or chemically attached to the surface of a gold NP, not only a steric stability is acquired for the NPs, but also the properties of the NPs can be controlled to some extent in response to any change in temperature [1], [2]. Hence, coating of Au NPs using different families of polymers have been extensively described in literature as we have shown in chapter 1. Among them poly(N-isopropylacrylamide) (PNIPAM) is by far the most commonly described but other families such as polyvinylcaprolactame [1], poly(oligo(ethylene glycol) methacrylate) [3], have also been used. Those nanohybrids can be obtained either by a “grafting from” or a “grafting to” approach, or by direct growth of the NPs within polymer [4].

Hyperbranched polymers and their derivatives show huge capacity to encapsulate and stabilize metal nanoparticles due to their unique topologies. Up to date, ends groups modified hyperbranched polymers were used for the synthesis of nanohybrids, but dendritic core-shell structures seem to be rarely exploited for this purpose.

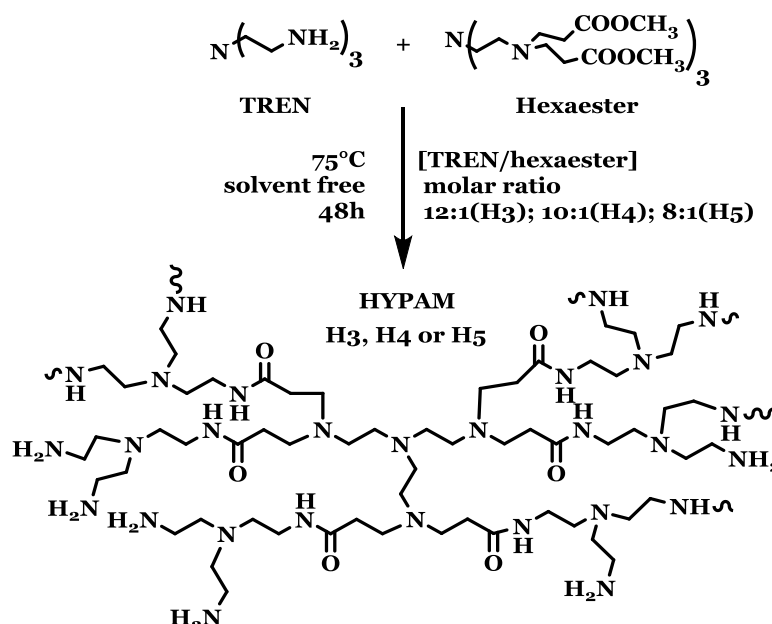
In this chapter we aim at understanding the effect of macromolecular architecture, i.e. average molecular weight of the core and molar mass of the grafting moiety, on the properties of those nanohybrids. For this purpose, the synthesis and characterization of a new family of dendritic polymers comprising a hyperbranched polyamidoamine core and a PNIPAM shell is described. This allowed assessing the key macromolecular parameters that will control i) the growth mechanism of *in situ* synthesized gold NPs, ii) the colloidal stability and iii) the thermoresponsive properties of the obtained nanohybrids.

II. Synthesis and characterization of the hyperbranched polymers consisting of the PNIPAM shell and hyperbranched polyamidoamine core

A. Hyperbranched poly(amidoamine)

1. Synthesis

The synthesis of the hyperbranched poly(amidoamine) polymers (HYPAM) is outlined in Scheme II.1. HYPAM cores with a structure similar to the one of PAMAM dendrimers were synthesized following a previously published procedure adapted from Dvornic et al [5]. The hexaester, tris(2-di(methylacrylate)aminoethyl)amine was first synthesized by Michael addition of tris(2-aminoethyl)amine and methyl acrylate. Its formation was monitored by ^1H NMR spectroscopy through the disappearance of proton signals corresponding to ethylene groups. Simple evaporation of solvent was performed to obtain final product (yield >95%). Then one step polycondensation reaction between tris(2-aminoethyl)amine (TREN) and the hexaester tris(2-di(methylacrylate)aminoethyl)amine led to hyperbranched structures in large quantities. Molar weights of the polymers were easily adjusted by changing the ratio between the reactants. TREN on hexaester molar ratios close to 12:1, 10:1, or 8:1 led to polymers with molecular weight close to those of PAMAM of the third, fourth, and fifth generation were therefore noted H3, H4 or H5 respectively. The main drawback of this synthesis is however, the formation of polymers with broad molecular weight distributions.



Scheme II.1. Synthesis of hyperbranched poly(amidoamine)

2. Characterization

a. NMR

The hyperbranched polymers were firstly analyzed by ^1H NMR spectroscopy. A typical spectrum for hyperbranched H4 polymer was given in Figure II.1. Two-dimension NMR (COSY, HSQC, HMBC) experiments were also performed in order to obtain the attribution of the peaks (Figure II.2.). Complete assignation is reported in the experimental section.

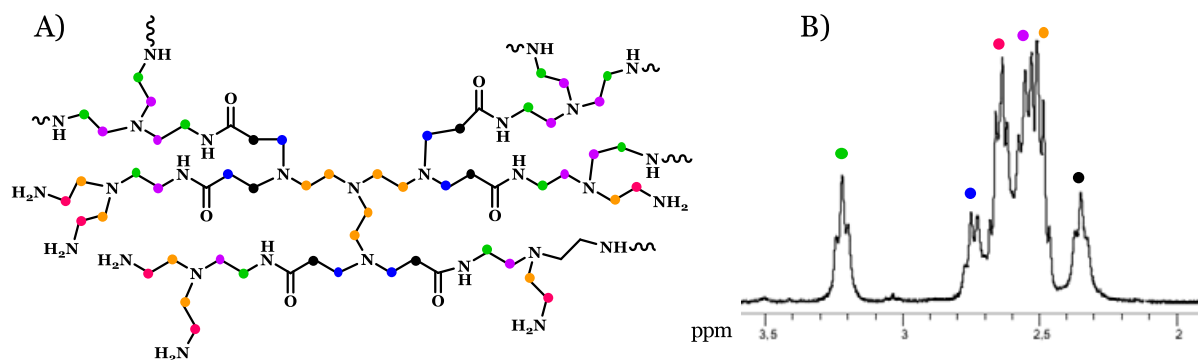


Figure II.1. A) Representative chemical structure of HYPAM, B) ^1H NMR spectrum of H4 in D_2O

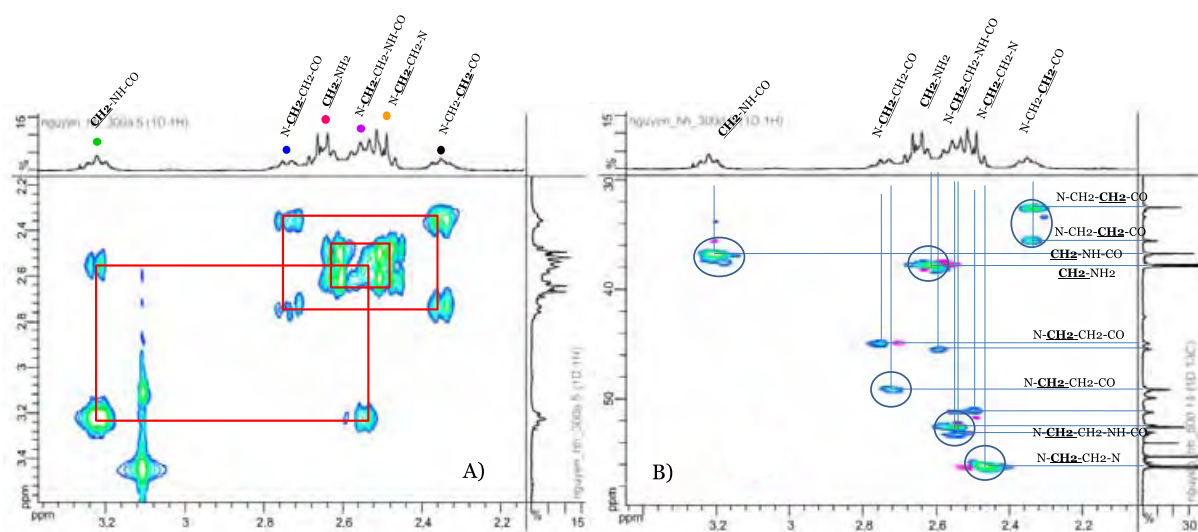


Figure II.2. A) COSY-NMR of H4 (300 MHz, D_2O , 308K) and B) HSQC-NMR of H4 (300 MHz, D_2O , 308K)

b. Quantification of number primary amine groups

In order to compare the structure of the HYPAM hyperbranched polymers with the one of PAMAM dendrimers, titration of the amine groups for the polymers was carried out by quantitative ^{13}C NMR using Tetramethylammonium hydroxide pentahydrate ($\text{Me}_4\text{NOH} \cdot 5\text{H}_2\text{O}$) as an internal standard (IS). A typical spectrum is reported in Figure II.3 with attributions of carbon atoms.

The quantity of primary amine groups was obtained by comparison of the CH₂-NH₂ peak at 37.47 ppm to the Me₄NOH peak at 55.82 ppm (enlargement Figure II.3.B) The quantity of primary amine (in mmol.g⁻¹ of polymer) is then calculated using the Equation II.1 and reported in Table II.1.

$$n_{\text{NH}_2} = \frac{\frac{m_{\text{IS}}}{181.23} \times 4}{m_{\text{Polymer}} \frac{I_{\text{IS}}}{I_{\text{NH}_2}}} \quad (\text{mol. g}^{-1})$$

Equation II.1. Quantification of number primary amine group of HYPAM, IS: Internal standard, I_{IS}: Intensity of CH₃ group of internal standard, I_{NH₂} : Intensity of carbon atom in alpha of NH₂ group of the polymer, m_{IS}: weight of internal standard; m_{polymer}: weight of polymer in grams; 181.23 g.mol⁻¹ : molar mass of Me₄NOH . 5H₂O.

The quantity of tertiary amine and amide groups were calculated in the same manner by comparison of the integration of CO-NH signal at 174 ppm and the summary of carbon signals of tertiary amine groups (56, 50, 51.4, 52,5 and 49.3 ppm) to the Me₄NOH peak at 55.82 ppm. (Figure II.3.A)

For PAMAM₄, this method gave a value of 3.8 mmol primary amine per gram, which is relatively close to the theoretical one (4.5 mmol per gram). Table II.3 shows that the quantity of primary amine groups was found slightly higher for the other polymers used in this study. Comparing HYPAM and PAMAM polymers at more or less constant molecular weight (i.e, H₄ with PAMAM₄, etc...), the number of primary and tertiary amines was close regardless of the structure (see Table II.2). The largest difference between those two types of polymers was the quantity of amide groups within the polymer: by construction, these values are largely reduced in the hyperbranched structure compared to dendrimers.

Table II.1. Number of primary amine of polymers

Sample	Primary amines [mmol.g ⁻¹]	Sample	Primary amines [mmol.g ⁻¹]
H3	5.0	PAMAM ₃	4.6 ^a
H4	6.2	PAMAM ₄	(3.8) 4.5 ^a
H5	4.2	PAMAM ₅	4.4 ^a

^a Values obtained from molecular structure

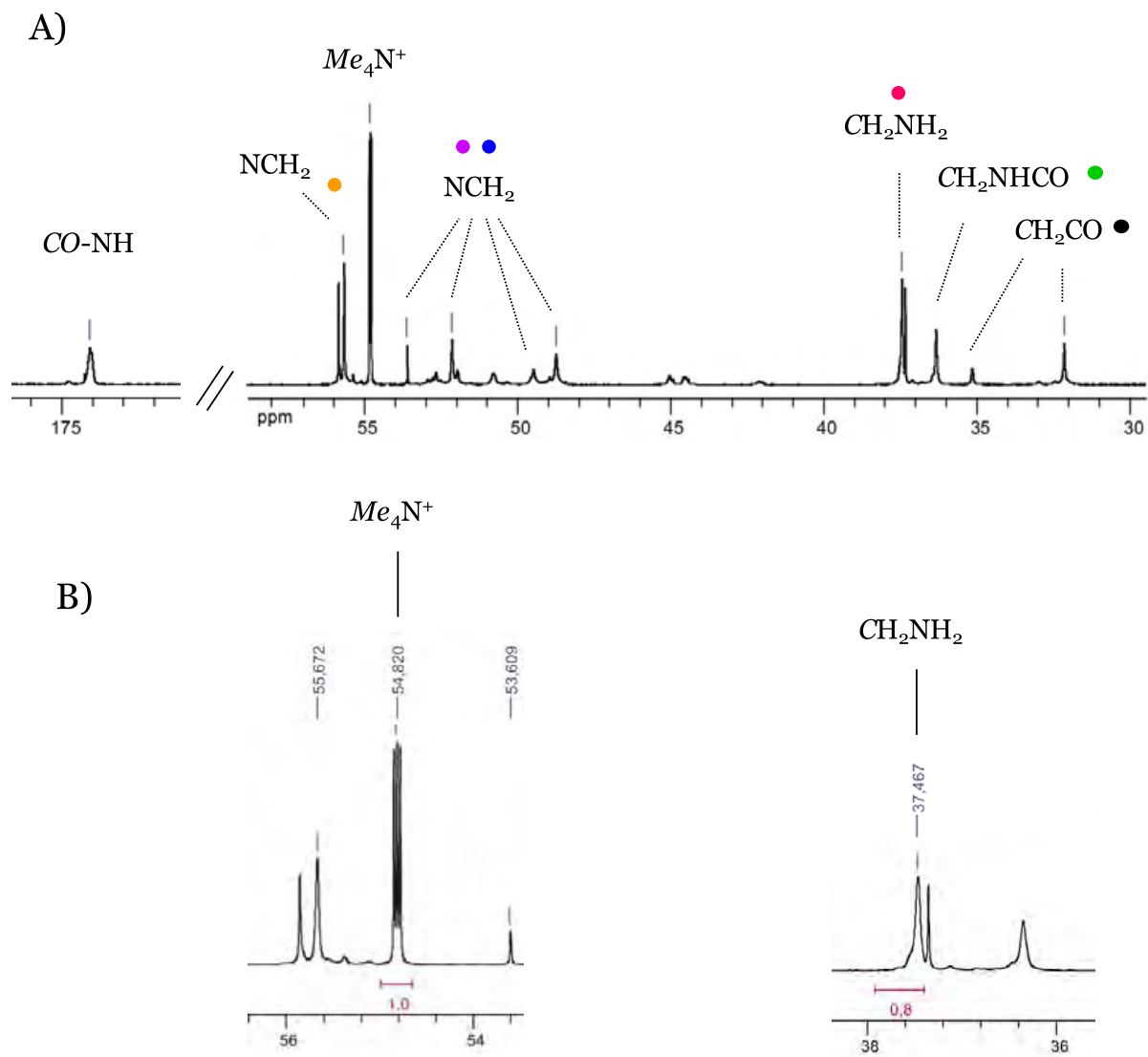


Figure II.3. A) ^{13}C NMR quantitative spectrum of H4 (500 MHz, D_2O , 308K) A) enlargements.

Table II.2. Comparison of chemical structures between H4 and PAMAM

Sample	Primary amines (mmol.g^{-1})	Tertiary amines (mmol.g^{-1})	Amide groups (mmol.g^{-1})
H4*	6.2	5.1	3.4
PAMAM4*	3.8	3.9	7.1
PAMAM4**	4.5	4.4	8.7

* Values obtained from quantitative ^{13}C NMR experiments. ** Values obtained from molecular structure.

c. **Determination of average molecular weights**

The average molecular weights of the hyperbranched polymers were evaluated by size exclusion chromatography (SEC) in carbonate buffer at pH 10 (Na_2CO_3 0.1M and NaHCO_3 0.1M) equipped with refractive index and light scattering detectors. A typical chromatogram is presented in Figure II.4. Calculated weight average molar weights and polydispersity indexes are summarized in Table II.3 and compared to the one obtained from the well defined PAMAM dendritic polymers. Weight Average Molar weights of the three cores H3, H4, H5 were evaluated at 5200, 13000 and 27000 $\text{g}\cdot\text{mol}^{-1}$ respectively, these values are very close to the ones of PAMAM 3, 4 and 5 dendrimers. The refractive index increments for PAMAM dendrimers were measured in the same eluent at ambient temperature and was found equal to $\text{dn}/\text{dc} = 0.175$ ($\text{mL}\cdot\text{g}^{-1}$). The values for the hyperbranched polyamides were assumed to be identical. Considering the fact that these polymers have been observed to trap some solvent, even after prolonged drying under vacuum, the accuracy for the molecular weight measurement is estimated around 20%.

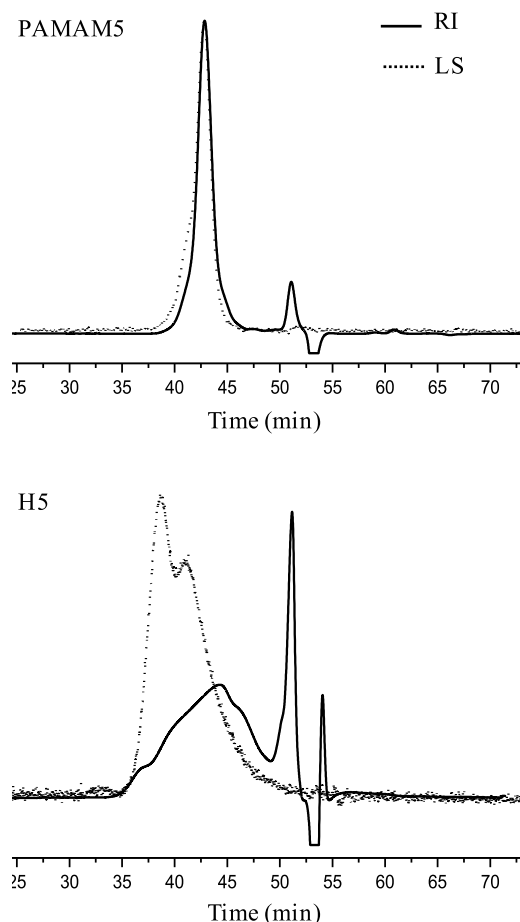


Figure II.4. SEC chromatograms of PAMAM5 (top) and H5 (bottom) in carbonate buffer at pH10: 5-10 mg/mL polymer concentration, flow rate, 1 mL \cdot min $^{-1}$, refractive index (RI, solid line) and light scattering (LS, dot line) detectors signals.

Table II.3: Characteristics of Polymer Samples: Weight Average Molar weight (\overline{M}_w), Polydispersity index (PDI) and Primary Amine Content

Sample	Triamine/hexaester ratio	\overline{M}_w^a	PDI ^a	R_g [nm] ^b
H3	12	5200	1.4	1.4
PAMAM ₃	-	6900	n.d.	n.d.
H4	10	13000	2.0	2.7
PAMAM ₄	-	14000	1.1	n.d.
H5	8	27000	2.3	3.2
PAMAM ₅	-	28000	1.1	

^a Molecular weight and dispersity index determined by LS-SEC. ^b Values obtained from SANS fits. Abbreviations: n.d.: not determined.

d. **SANS measurements**

Moreover, small-angle neutron scattering (SANS) measurements were carried out to quantitatively analyze the size and conformation of the H3, H4 and H5 cores in D₂O solution at 20°C. Figure II.5 shows the scattering vector q dependence of the measured neutron scattering intensity $I(q)$ for H3, H4 and H5 solutions in D₂O (1wt %). The scattering intensity reached a plateau at low q which demonstrates that entities with defined molar mass are present. These traces can be fitted using the Guinier model which provides an estimate of the gyration radius (R_g) of these hyperbranched polymers. As expected, the R_g values increase with the polymer generation i.e. 1.4, 2.7, and 3.2 nm for H3, H4 and H5 respectively. Further structural information is obtained from the dependence of the radius of gyration on the weight average molecular mass (Figure II.5, inset). The double-logarithmic plot of R_g vs M_w show a linear dependence which proves the fractal behavior of the HPs (Figure II.5, inset), with a power law, $R_g = 0.0878 M_w^{0.356}$. The slope of this linear plot is 0.356 and thus is very close to 1/3, which is usually found for spheres. This indicates H3, H4 and H5 hyperbranched polymers are collapsed in compact spherical objects, as already observed in others hyperbranched polymers [6]. The sizes are similar of those of theoretical radius of PAMAM (1.8 nm, 2.25 nm and 2.7 nm for generation 3, 4 and 5 respectively) which is in accordance with unimolecular objects.

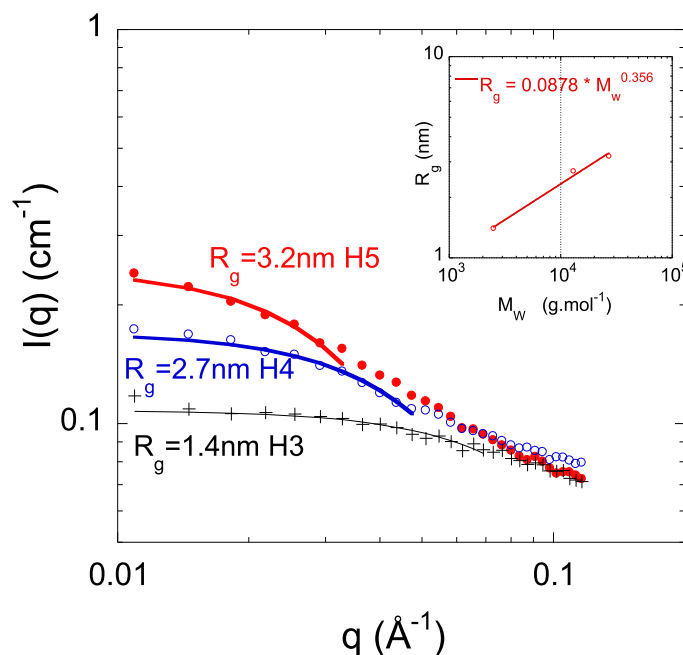


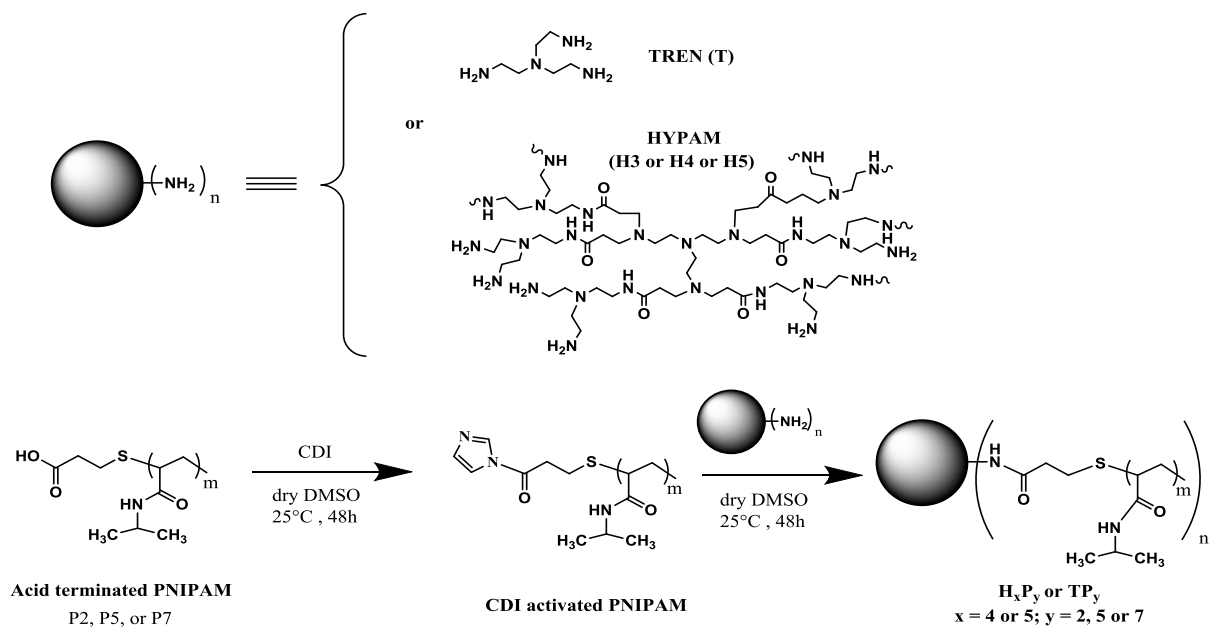
Figure II.5. Scattering intensity $I(q)$ vs scattering vector q for the hyperbranched hypam (H3, H4 and H5) in D_2O (1wt %). Lines are best fits obtained from Guinier law from which radii of gyration R_g of polymers are deduced. In the inset, the double-logarithmic plot of R_g versus the weight average molecular weight (determined by SEC) of hyperbranched polymers.

B. Hyperbranched core-shell polymers

1. Synthesis by CDI activated coupling

Poly(*N*-isopropyl acrylamide) (PNIPAM) with three different molar weights \overline{M}_w of 2000, 5000 or 7000 $g.mol^{-1}$ (P2, P5, P7) were grafted to the amino-terminated cores (TREN, H4, H5) chains by an amide coupling reaction as shown in Scheme II.2.

First, carboxylic acid terminated PNIPAM is reacted with 1,1'-carbonyldiimidazole (CDI) in dried DMSO to form carbonyldiimidazolide-terminated PNIPAMs. Then activated PNIPAMs were reacted with the amino-terminated HYPAM cores to form the core-shell architectures. The obtained compounds, noted TP2, 5 or 7 and HxP2, 5 or 7 with $x = 4$ or 5, were purified by dialysis and analyzed to evaluate grafting efficiency of this reaction.



Scheme II.2. Synthesis of core-shell polymers based on hyperbranched polymer HYPAM or three-branched molecular TREN.

2. Characterization of core-shell polymers

a. Evaluation of grafting efficiency

i) SEC

The successful grafting of PNIPAM chains onto branched core was first evidenced by size exclusion chromatography in DMF as eluant with 1 g/L LiCl. For example, Figure II.6 showed SEC traces for P2, TP2, H4P2 and H5P2.

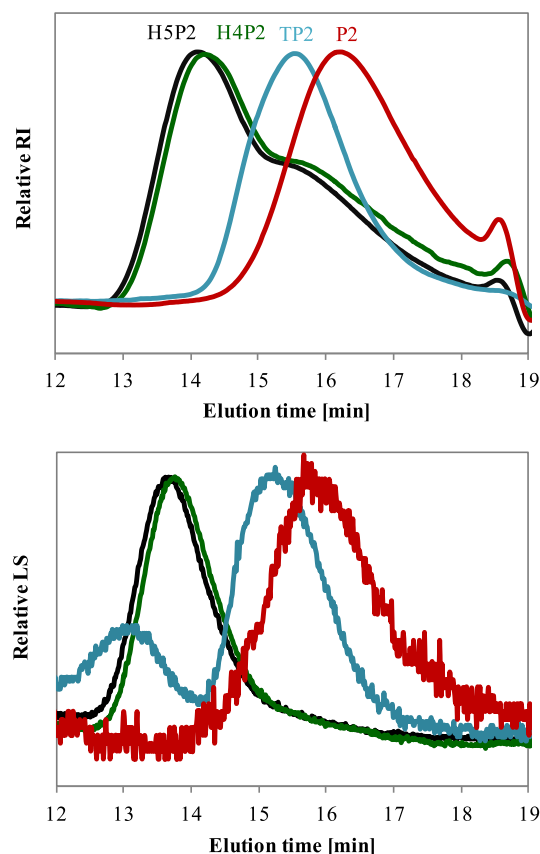


Figure II.6. Superimposition of normalized SEC chromatograms (Refractive index I (top) and Light scattering (bottom) detection in DMF with 1 g/L LiCl) of P2, TP2, H4P2 and H5P2.

Grafting of P2 to the hyperbranched core (TREN or HYPAM) led as expected to shortened elution times. Whereas the first two polymers present rather thin peaks, hyperbranched based polymers present larger elution profile, as expected from the large dispersity of the pristine HYPAM polymers used as a core. The use of light scattering detector together with a refractometric one, provides an evaluation of the molecular weight of the polymers and of the polydispersity (PDI). In DMF, the experimental molecular weight values were M_w P2: 2800 g/mol (PDI=1.2); TP2: 5600 g/mol (PDI=1.3); H4P2: 30600 g/mol (PDI: 1.9), H5P2: 31200 g/mol (PDI=2.0). Nevertheless, due to the hyperbranched nature of the polymers those values could not be determined accurately. Moreover, for wide distributions, the difference of sensitivity of light scattering between high and low molecular masses leads to an underestimated polydispersity index [7]. Lastly, these polymers (as well as PAMAM dendrimers) have been observed to trap solvent molecules even after prolonged drying. Thus, the measured molecular weights should be considered only as indicative values. Therefore in Table II.4 were also given obtained experimental values (M_w and PDI).

Table II.4. Macromolecular characteristics of PNIPAM chains and core-shell polymers

Compounds	M_w SEC (PDI)	$M_{n,theo}$ (g/mol)	Wt. % PNIPAM _{theo}	Number of PNIPAM chains	T_g (°C)
P2	2800 (1.2)	2000	100%	/	112.3
P5	4300(2.1)	5000	100%	/	130.1
P7	7900(2.2)	7000	100%	/	133.3
TP2	5600 (1.3)	5300	97%	2.6	119.1
TP5	10100(2.1)	13000	99%	2.6	130.7
TP7	15400(2.1)	17000	99%	2.4	136.4
H4P2	30600(1.8)	56000	88%	24.7	122.6
H4P5	41000(2.0)	135000	95%	25.7	130.2
H4P7	51200(1.7)	192000	97%	26.5	135.0
H5P2	31200(2.3)	73000	84%	30.6	85.8
H5P5	35000(2.0)	182000	94%	34.1	127.6
H5P7	35000(2.0)	253000	95%	34.5	138.7

ii) NMR

The amide coupling between TREN or HYPAM cores and the carboxylic acid terminated Poly(N-isopropyl acrylamide) was evidenced by ^1H NMR experiments as illustrated in Figure II.7 and Figure II.8. An additional peak at 3.23 ppm assigned to proton in α position of the forming amide groups was clearly identified on ^1H NMR of TP2 (Figure II.7). In the case of hyperbranched cores, the proton in α position of the amide groups coming from coupling reaction coincide with the one that is already present in the structure of the core (noted d in Figure II.8).

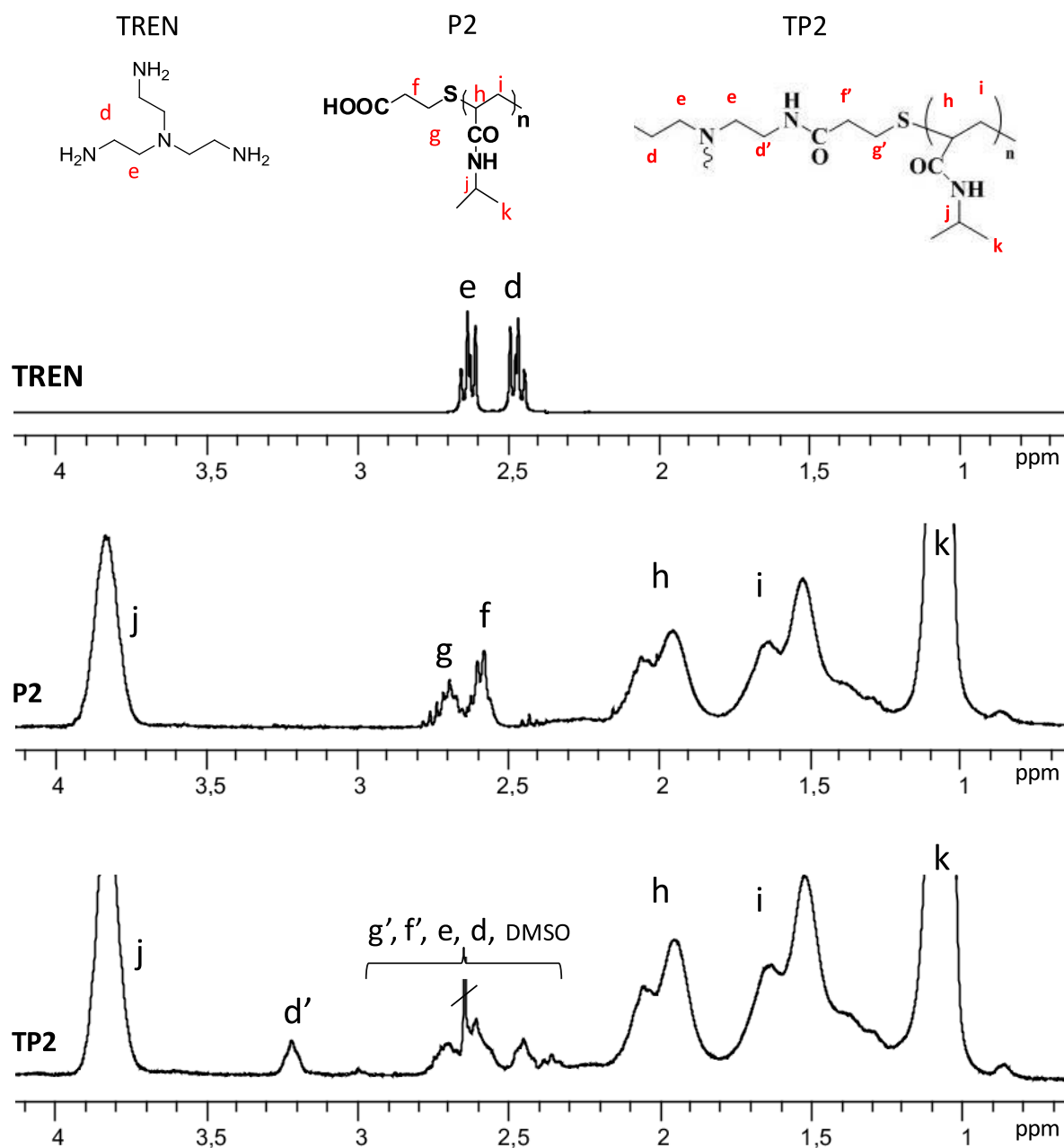


Figure II.7. $^1\text{H-NMR}$ spectra for TREN, P2, and TP2 in D_2O .

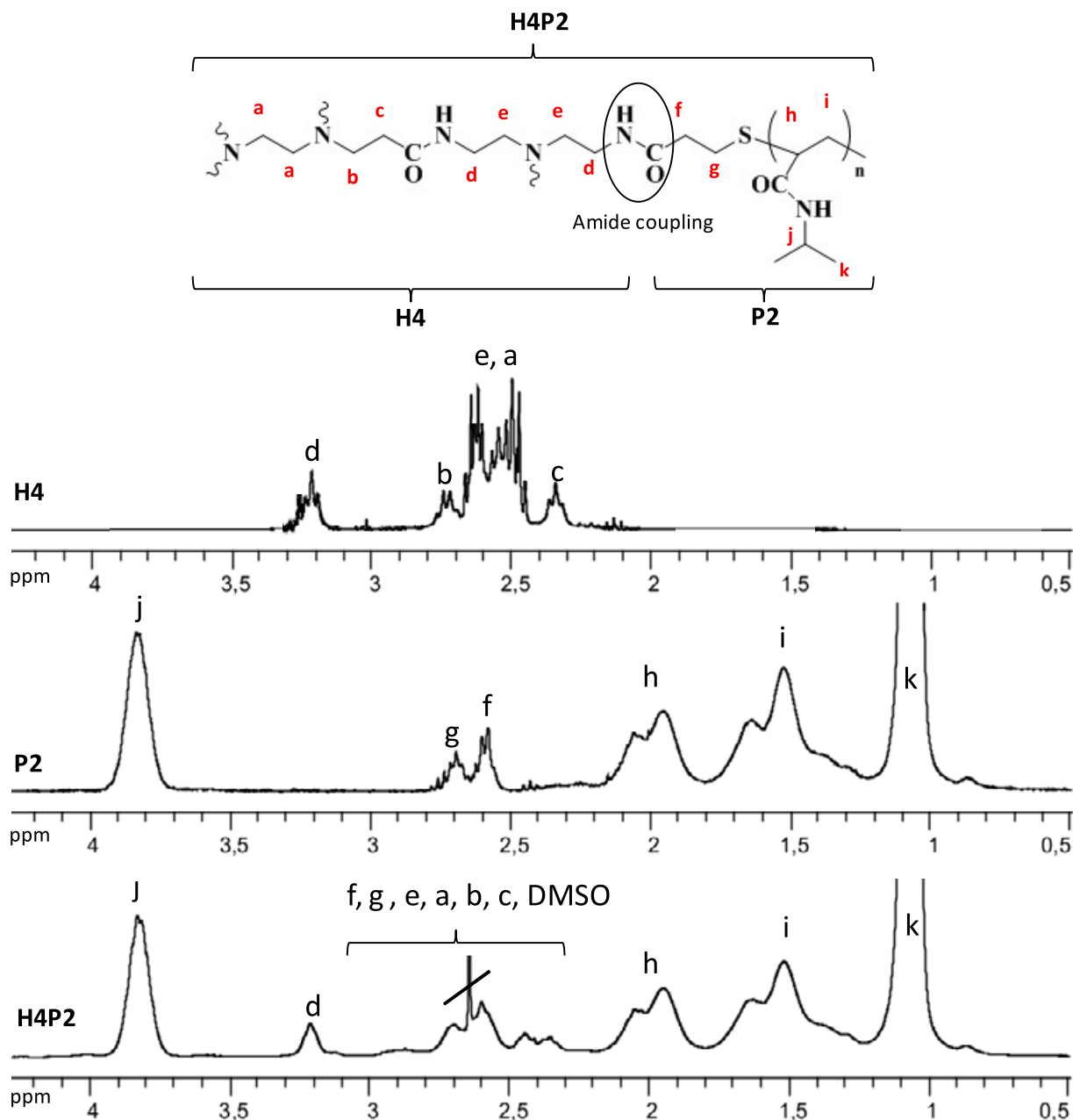


Figure II.8. ^1H -NMR spectra for H4, P2, and H4P2 in D_2O .

Moreover, successful grafting of PNIPAM chains was further evidenced by pulsed gradient spin-echo (PGSE) NMR spectroscopy (Figure II.9) allows to determine a self-diffusion coefficient, D , for grafted polymer lower than for the corresponding PNIPAM homopolymer: thus in the case of H4P5 $d = 0.4 \cdot 10^{-10} \text{ m}^2/\text{s}$ whereas it is twice lower in the case of P5 ($d = 0.8 \cdot 10^{-10} \text{ m}^2/\text{s}$).

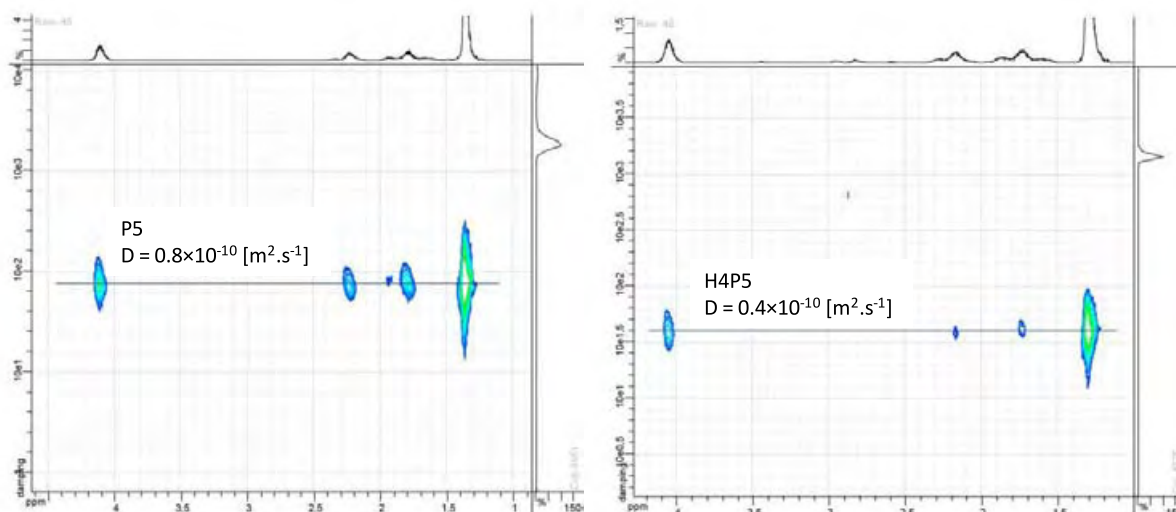


Figure II.9. PGSE-NMR spectra of P5 and H4P5 core-shell polymer after grafting P5 chains on H4 core in D_2O at 298K with evaluated diffusion coefficients.

iii) FT-IR

The amide coupling between TREN or HYPAM cores and the carboxylic acid terminated Poly(N-isopropyl acrylamide) was further evidenced by ATR-FTIR experiments on dialyzed samples as illustrated in Figure II.10. In ATR-FTIR the disappearance of C=O asymmetric stretching band of carboxylic function at 1712 cm^{-1} corresponding to carboxylic acid terminated poly(N-isopropylacrylamide) was accompanied with the appearance of a new absorbance band at 2934 cm^{-1} characteristic of methyl moieties.

In figure II.10 amide I and amide II bands are attributed to the stretching motion of the C=O groups and the bending motion of the N-H coupled to C-N stretching.

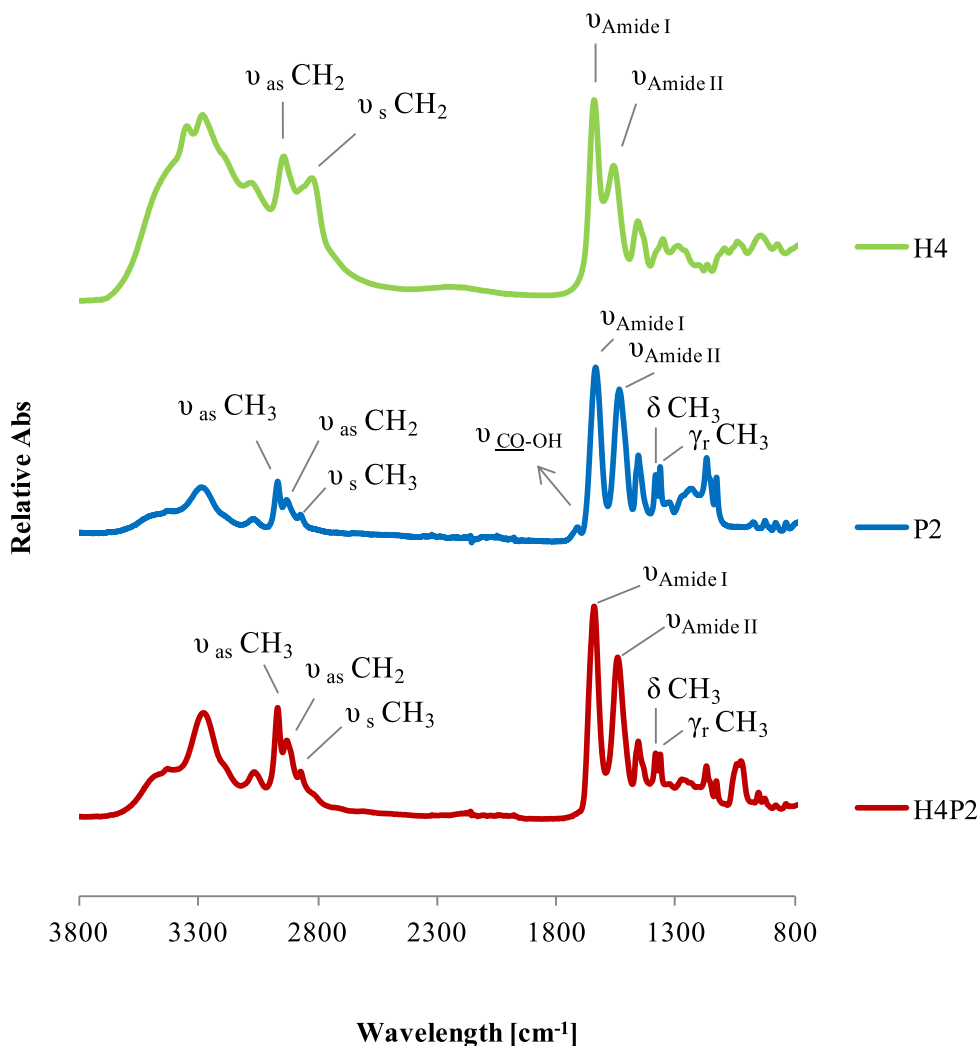


Figure II.10. ATR-FTIR spectra of H4, P2 and H4P2

iv) Glass transition temperature of bulk polymers

Differential scanning calorimetry (DSC) analyses were performed on all crude polymers (Figure II.11). A glass transition temperature (T_g) was evidenced for all polymers as reported in Figure II.11. This one arises from PNIPAM polymer. As expected shorter PNIPAM chains led to a significant decrease of T_g value whatever the core of the considered polymer.

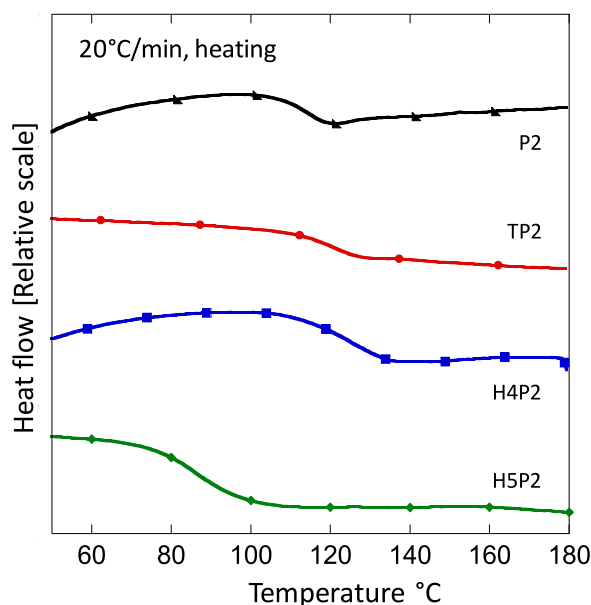


Figure II.11. DSC thermograms recorded at 20°C/min on heating of solid state of P2, TP2, H4P2 and H4P2.

Along with this first transition temperature, a second one is barely visible around -20°C arising from HYPAM core. Indeed this one is only clearly seen in the case of HYPAM core (Figure II.12).

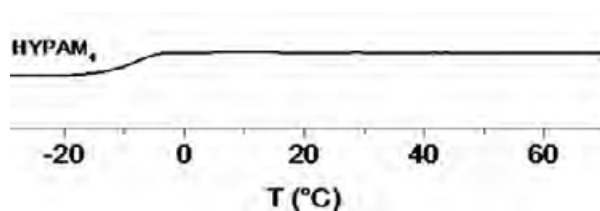


Figure II.12. Thermogram of H4 recorded with a heating rate of 20°C/min .

b. *Evaluation of grafting ratios*

i) Determination from FT-IR

Grafting ratios were determined by using a calibration curve established from mechanical homogeneous mixtures of HYPAM and PNIPAM at different ratio (while PNIPAM is kept constant). The homogenized mixtures of HYPAM or TREN core and PNIPAM chain were prepared according to 1:1; 1:0.8; 1:0.6 and 1:0.33 [NH₂]:[COOH] molar ratio corresponding to 100%, 80%, 60%, 33.3% grafting ratios. The homogeneous solutions were then freeze-dried and the obtained solids were analyzed by ATR-FTIR (Ex. for H4 and P7 see Figure II.13). The ratio between the intensity of the band at 1386 cm⁻¹ (characteristic for the C-H deformation of CH₃ group for the PNIPAM chain) and the one at 1641 cm⁻¹ (stretching vibration of C=O group, amide I) was measured for each mechanical mixture. The calibration curve obtained for the physical mixture of H4 and P7 is given in Figure II.13. A

calibration was 100% grafting degree means that all the NH₂ groups of the core were anchored by PNIPAM chains.

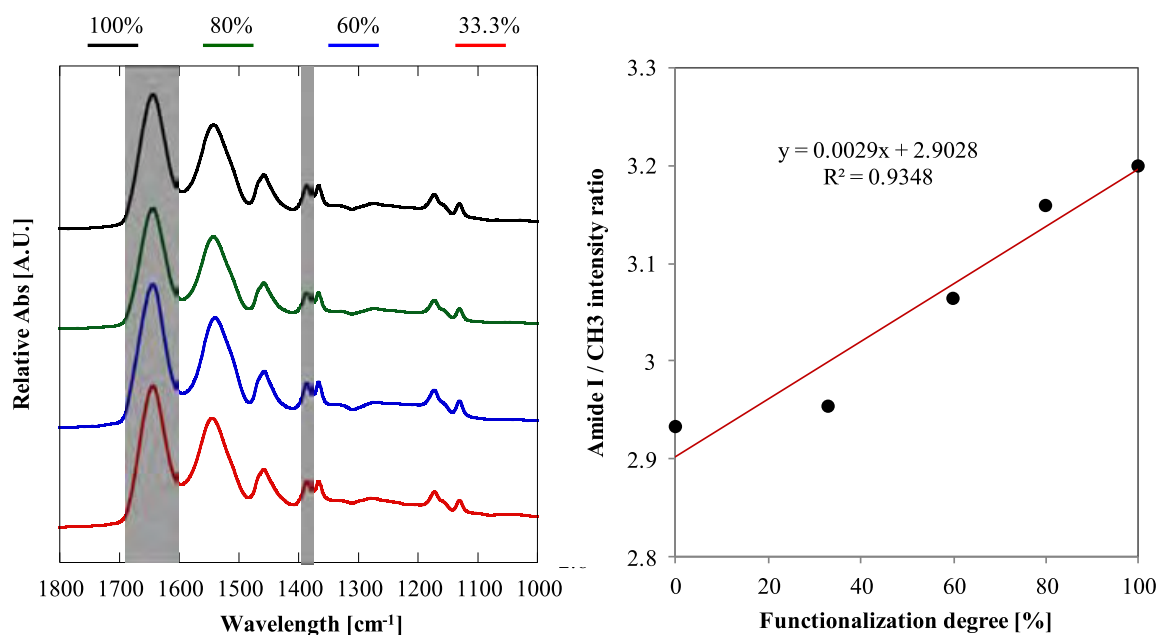


Figure II.13. On the left: FT-IR spectra of physical mixtures of H4 and P7 with 100, 80, 60, 33.3% grafting ratio. On the right: Calibration curve: ratio between intensity of band amide I at 1641 cm⁻¹ and band CH₃ deformation at 1386 cm⁻¹ as a function of grafting ratio of mechanical mixture of H4 and P7.

The intensity ratio between amide I band and CH₃ deformation band was then measured for the grafted polymer. Grafting ratios for core-shell structure was then evaluated thanks to the calibration curves. The grafting ratio values determined by this method were reported in Table II.5.

Table II.5. Determination of grafting ratio by NMR, FTIR and DSC methods

Compounds	¹ H NMR	FTIR	DSC
TP2	90.4	86%	87%
TP5	92.6	87%	89%
TP7	91.3	81%	83%
H4P2	n.d.	61%	49%
H4P5	n.d.	64%	72%
H4P7	n.d.	66%	71%
H5P2	n.d.	62%	51%
H5P5	n.d.	69%	73%
H5P7	n.d.	70%	79%

ii) Determination from DSC

Taken in account that grafted polymer solutions exhibit a cloud point which arises from dehydration of PNIPAM shells, the grafting ratios were also evaluated from DSC experiments using 0.5 wt.% polymer solutions. For this, the variation of enthalpy registered for a given polymer was compared to the variation of enthalpy measured for pure PNIPAM at the same concentration, assuming that grafting does not modify significantly energy involved during the dehydration process (Example for P7, TP7 and H4P7 see Figure II.14). Then PNIPAM weight content in the core shell structures was calculated from this. Grafting ratios (r) were then deduced from Equation II.2.

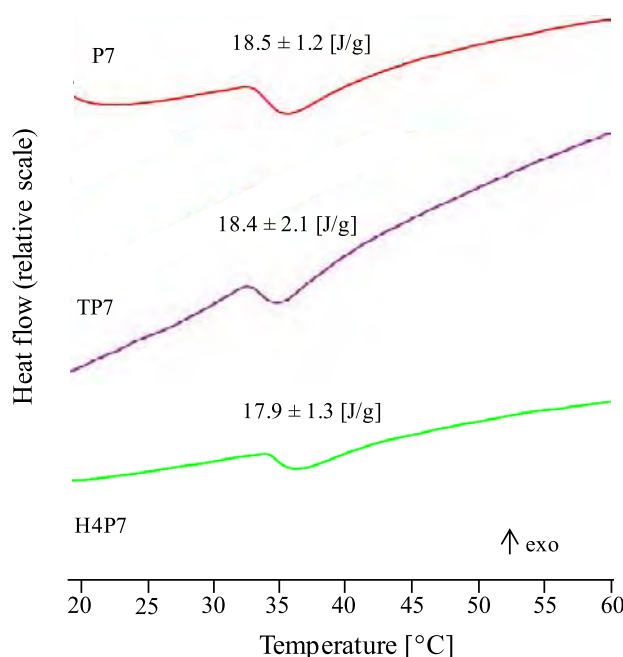


Figure II.14. DSC thermograms of 0.5 wt.% aqueous solutions of P7, TP7, H4P7, heating rate: $2^{\circ}\text{C}\cdot\text{min}^{-1}$.

$$r [\%] = \frac{wt_{P_x} \%}{(1 - wt_{P_x} \%) \times n_{NH_2} \times M_{P_x}} \times 100$$

Equation II.2. Grafting ratio r [%], weight content of PNIPAM shells determined from enthalpy variations: $wt_{P_x} \%$, amount of primary amines of the core $n_{NH_2} [mol \cdot g^{-1}]$, molar weight of the PNIPAM shells M_{P_x} .

All obtained results are summarized in Table II.5. Both degree of polymerization estimated by those two techniques were in good agreement and were found in the 60-80 % ranges which is a usual value found for this kind of materials. The only discrepancy observed was for H4P2 and H5P2 where DSC experiments led to an under estimate of degree of grafted

polymer chains. This may arise from slow dehydration phenomenon observed for those structures.

From molecular weight of the core and estimated grafting ratios, average molecular weight are calculated and given in Table II.3. Those values should be more accurate than the one evaluated from SEC analysis.

III. Properties of aqueous solutions of hyperbranched polymers

1. Behavior in diluted solution

At 25°C, since water is a good solvent for the hyperbranched polymers, the grafted polymers are easily dissolved in water for low concentration. As depicted in Table III.1, all polymers present an average hydrodynamic diameter ($\langle D_h \rangle$) around 10 nm suggesting the presence of unimolecular object. As expected, for a given core (TREN, H4 or H5), D_h tend to slightly increase by increasing the molar mass of the PNIPAM moiety grafted.

Table III.1. Hydrodynamic diameters (in number distribution) of polymers in 0.1 wt.% solution at 25°C.

Compounds	DLS, $\langle D_h \rangle$ (nm)	Compounds	DLS, $\langle D_h \rangle$ (nm)
<i>P2</i>	6±1	<i>H4P2</i>	10±1
<i>P5</i>	7±1	<i>H4P5</i>	13±2
<i>P7</i>	7±1	<i>H4P7</i>	8±1
<i>TP2</i>	6±1	<i>H5P2</i>	7±1
<i>TP5</i>	7±2	<i>H5P5</i>	12±1
<i>TP7</i>	8±1	<i>H5P7</i>	12±1

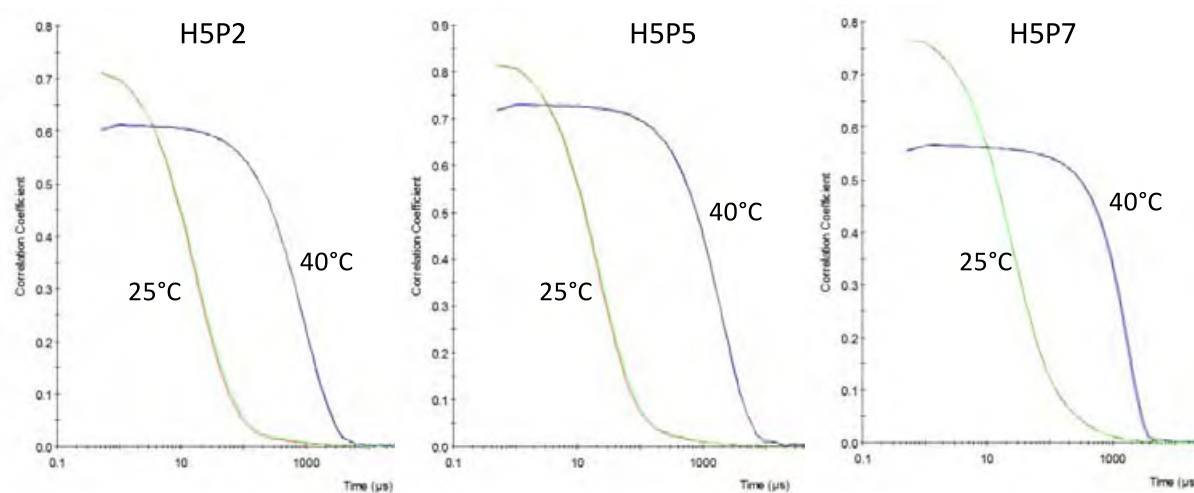


Figure III.1. Correlograms of H5P2, H5P5 and H5P7 polymer solutions at 25°C and 40°C. [polymer]=0.1%

The behavior of those polymers was further analyzed by SANS measurements which is presented in Figure III.2. Scattering of hyperbranched core-shell structures are much larger than the ones of the cores (compare Figure II.5 and Figure III.2). At room temperature, all the curves reveal large fluctuations at large distances (low q upturn) and small fluctuations that have been characterized by a simple correlation length ξ deduced from fits at large q . These correlation lengths, listed in Table II.3, are slightly larger than the structure of cores as expected after branching PNIPAM chains: ξ values are normally increasing with the molecular weight of PNIPAM branches.

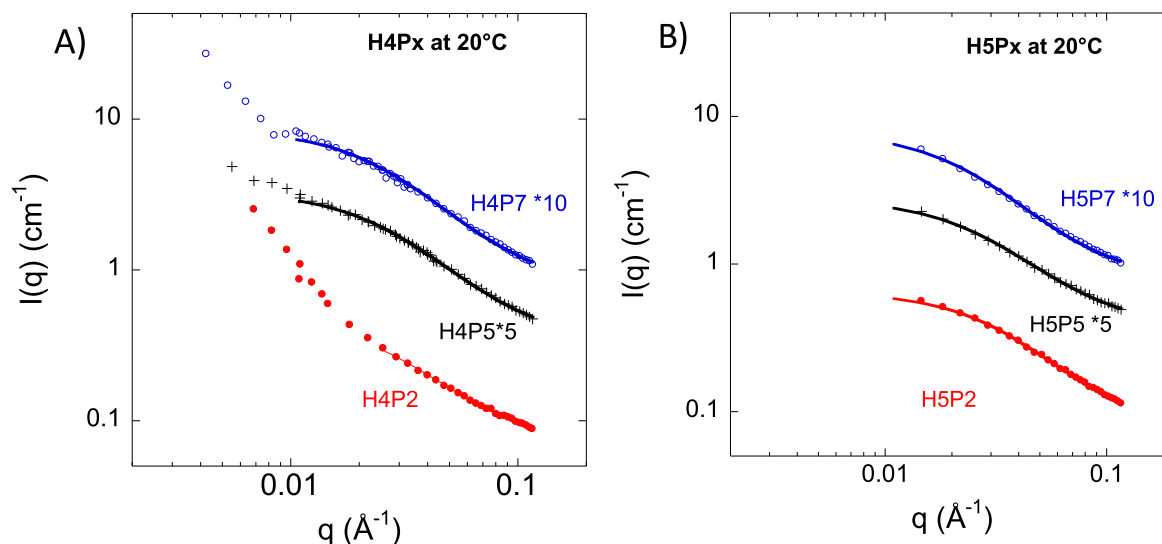


Figure III.2. $I(q)$ vs q of A) H4 grafted polymers: H4P2, H4P5, H4P7; B) H5 grafted polymers: H5P2, H5P5 and H5P7. $T = 20^\circ\text{C}$, $[\text{polymer}] = 1 \text{ wt. } \%$.

Table III.2. Correlation length deduced from fit of SANS curves obtained at 20°C on PNIPAM-based hyperbranched structures

Cores\Shells	Correlation length ξ (nm)		
	P2	P5	P7
H4	3	3.7	3.9
H5	3.1	3.7	4.3

TEM images of dried aqueous solutions show regular monodisperse spherical nanoobjects (Figure III.3) with diameters larger than the one obtained from scattering experiments. Therefore, as already observed in the case of PNIPAM, those polymers tend to aggregate when dried probably due the tendency of PNIPAM to form nanogels structures at high concentration through hydrogen bonds between amide functionalities in solution. This tendency will be taken into account to allow the formation of gels in a latter chapter.

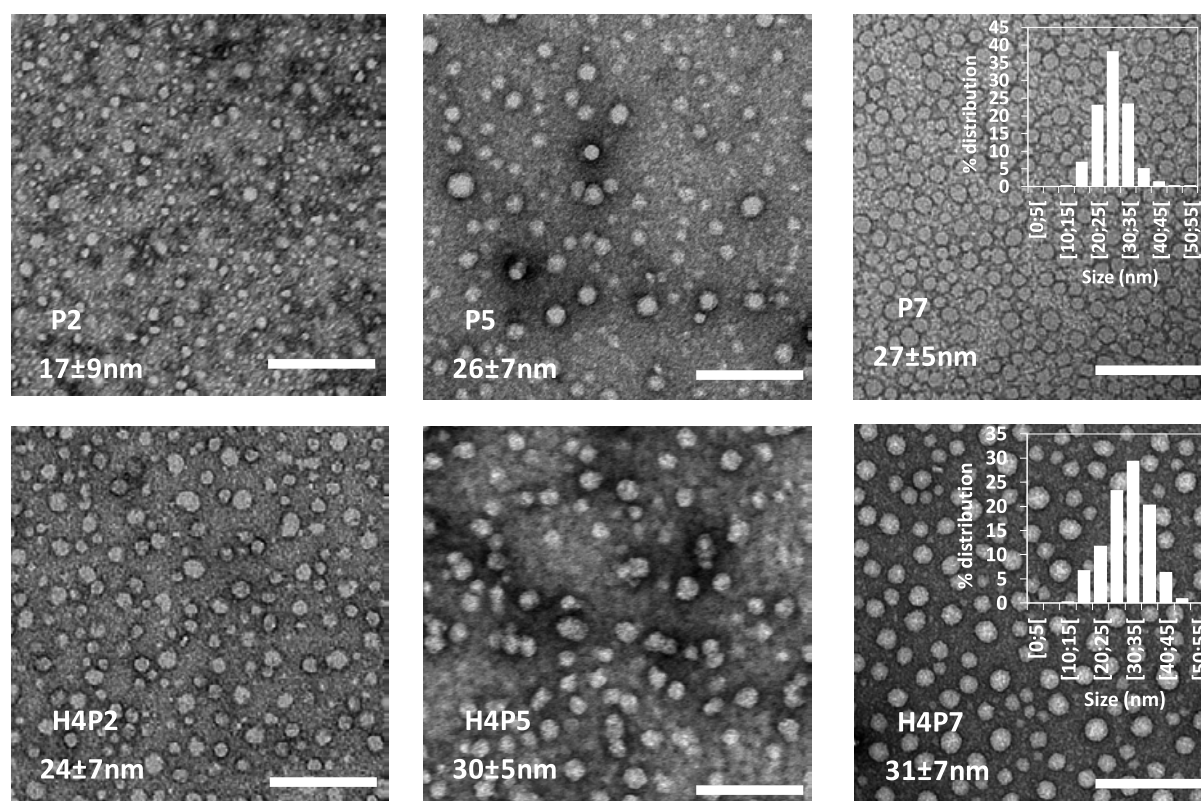


Figure III.3. TEM micrographs of P2, P5, P7 and H4P2, H4P5, H4P7 0.1 wt.% solution samples stained with uranyl acetate at 25°C, bare scale: 200 nm.

2. Thermoresponsive properties

When solutions of those hyperbranched structures were heated, a transition temperature occurred that corresponds to the transition between the hydrated and dehydrated form of PNIPAM polymer. This phenomenon is clearly evidenced by turbidimetry measurements and scattering measurements as depicted in Figure III.4.

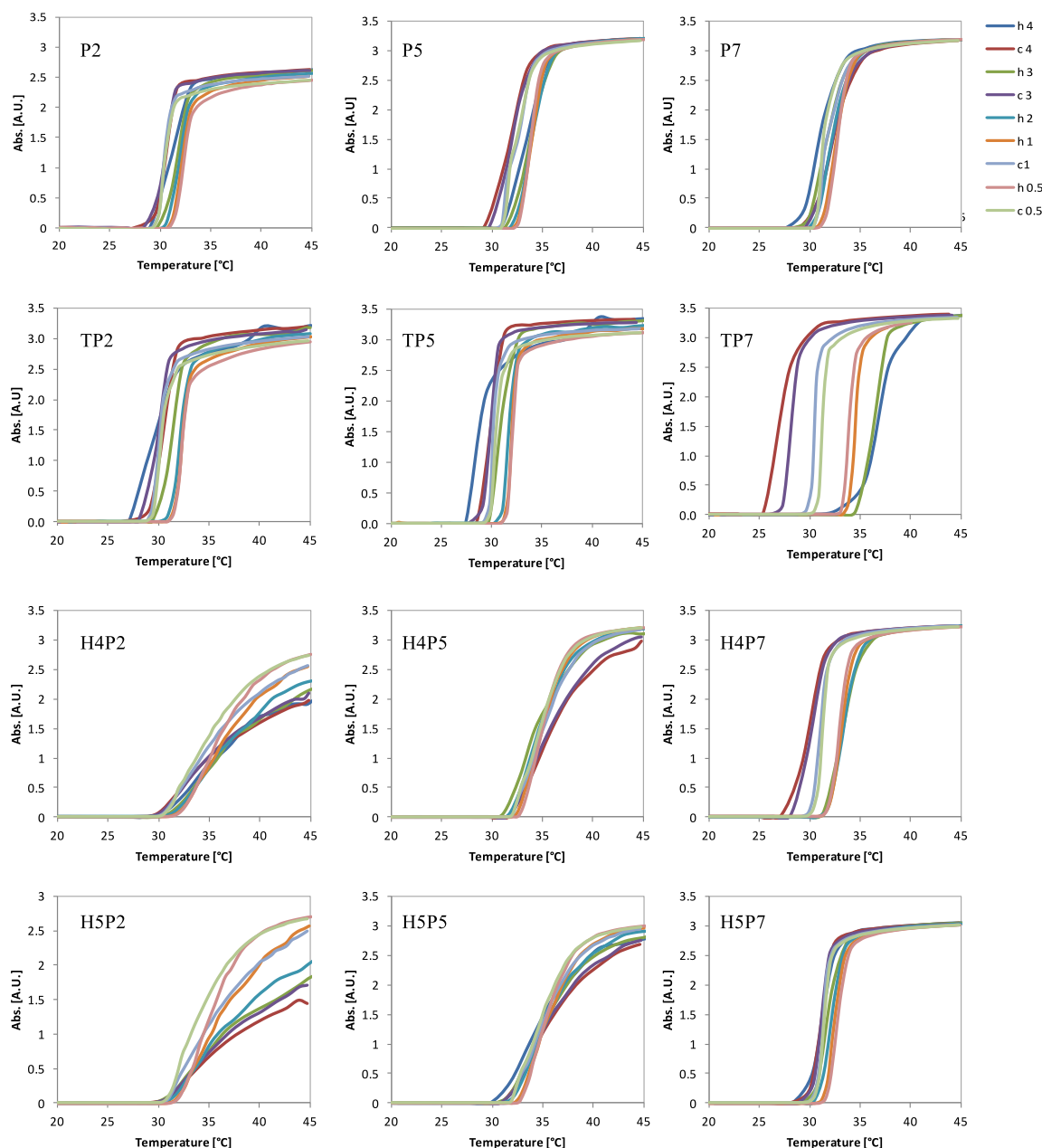


Figure III.4. Evolution of absorbance measured at 500 nm vs temperature for 0.1 wt. % aqueous solution of PNIPAM and grafted polymers during heating (h) and cooling (c) from 20 to 45°C for 4 different heating/cooling rate, i.e. 4, 3, 2, 1, 0.5°C.min⁻¹.

A hysteresis between the heating process and the cooling process could be observed for all solutions, which was accentuated for higher heating/cooling rates (Figure III.4). Cloud point temperatures (T_c) values were obtained from inflexion point extrapolated at 0°C/min heating rate were reported in table III-2. This phenomenon can be explained by the fact that the swelling of the compact aggregates formed at higher temperatures is relatively difficult because of the interchain entanglement.

Table III.3. Thermoresponsive properties

Compounds	T _c [°C]			ΔH [J/g]
	DLS ^a	UV ^b	DSC ^c	DSC ^d
P2	33	30.9	32.1	20.5 ± 2.1
P5	34	32.3	32.7	19.0 ± 1.1
P7	32.5	31.2	33.4	18.5 ± 1.2
TP2	32.5	31.1	33.9	20.0 ± 0.9
TP5	34	31.3	34.1	18.8 ± 1.5
TP7	31.5	32.9	33.0	18.4 ± 2.1
H4P2	32	35.2	33.3	18.5 ± 0.6
H4P5	33.5	36.1	34.0	18.2 ± 1.1
H4P7	30.4	32.2	33.4	17.9 ± 2.0
H5P2	30.9	34.9	33.8	18.0 ± 0.8
H5P5	33	35.8	34.4	17.9 ± 1.2
H5P7	31.5	31.9	33.6	17.8 ± 1.3

^a DLS measurements were carried out on heating 20 to 45 °C, [polymer] = 0.1%, T_c values were taken at inflexion points; ^b UV measurement were carried out with 5 heating-cooling cycles from 20 to 45°C at 4, 3, 2, 1, 0.5°C.min⁻¹, T_c values were taken at inflexion points and extrapolated to zero speed, ^c DSC measurements were carried out with 4 heating-cooling cycles at different rates; 10, 5, 2 and 1 °C.min⁻¹, transition temperatures were taken at the top of the DSC peaks, and extrapolated to zero speed. ^d The variation of enthalpy was average of 6 values.

T_c values were also determined by DSC experiments by extrapolating values at the peak maximum to 0 °C/min. Those values are reported in Table II.2 as well as the corresponding associated variation of enthalpy. Cloud point temperatures were all found around 33.0 ± 1 °C which is close to cloud point values of free PNIPAM. Therefore grafting of PNIPAM to the HYPAM does not significantly modified characteristics temperatures observed. Above T_c, diffusion experiments evidenced the formation of very large aggregates with a hydrodynamic diameter above 300 nm (Figure III.5.B).

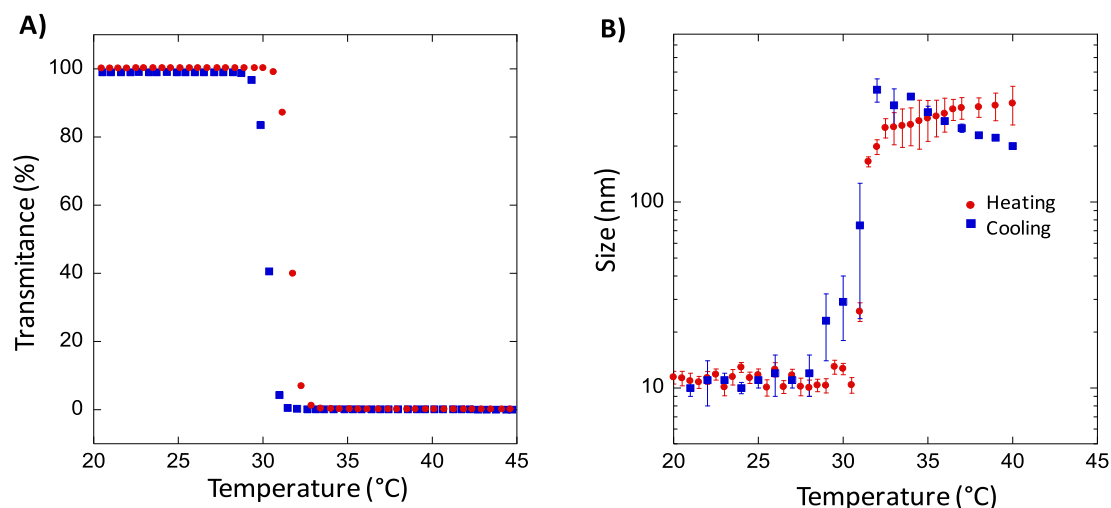


Figure III.5. (A) Turbidimetry measurements (heating and cooling rate equal to 1°C/min); (B) DLS measurements of H5P7 solution at 0.1wt. % in water.

As shown on TEM images (Figure III.6), those aggregates seem to have no defined morphology or size. Neutron scattering experiments confirmed the formation of such large aggregates (Figure III.7).

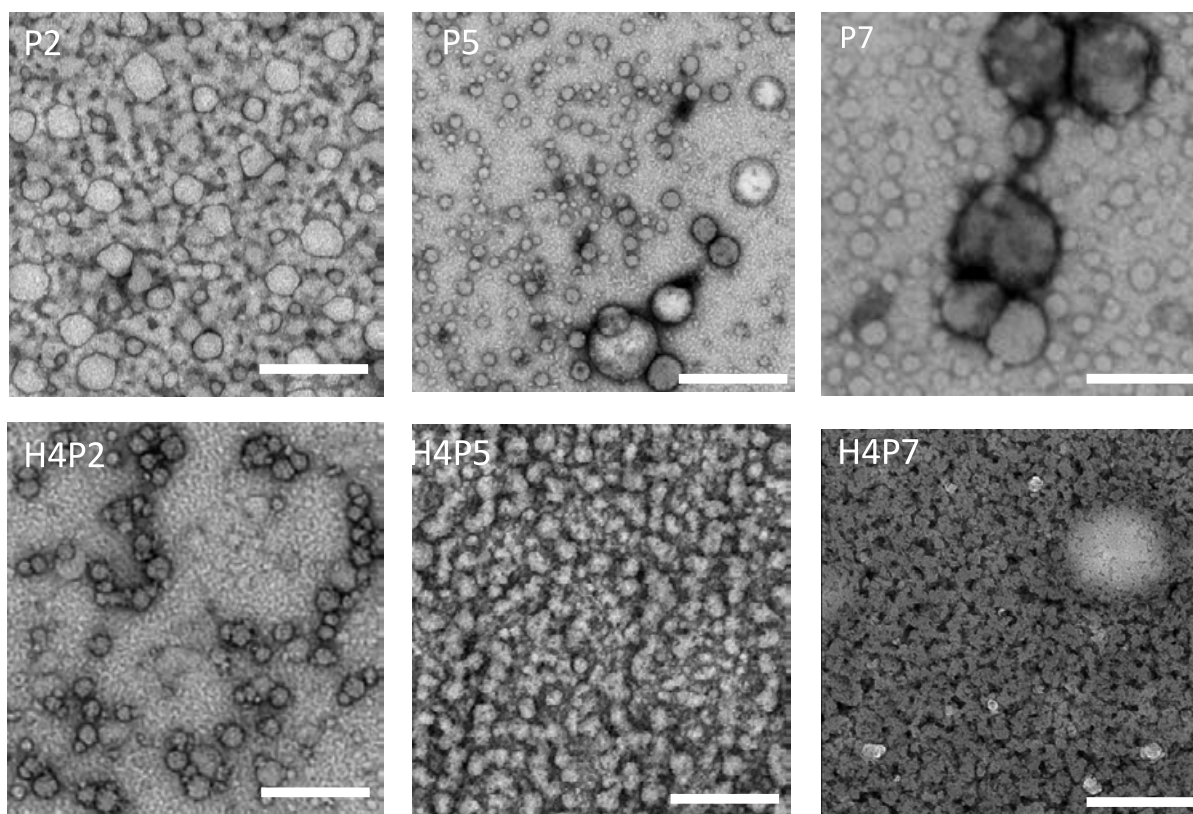


Figure III.6. TEM micrographs of P2, P5, P7 and H4P2, H4P5, H4P7 0.1 wt.% solution samples stained with uranyl acetate at 40°C, scale bare: 200 nm

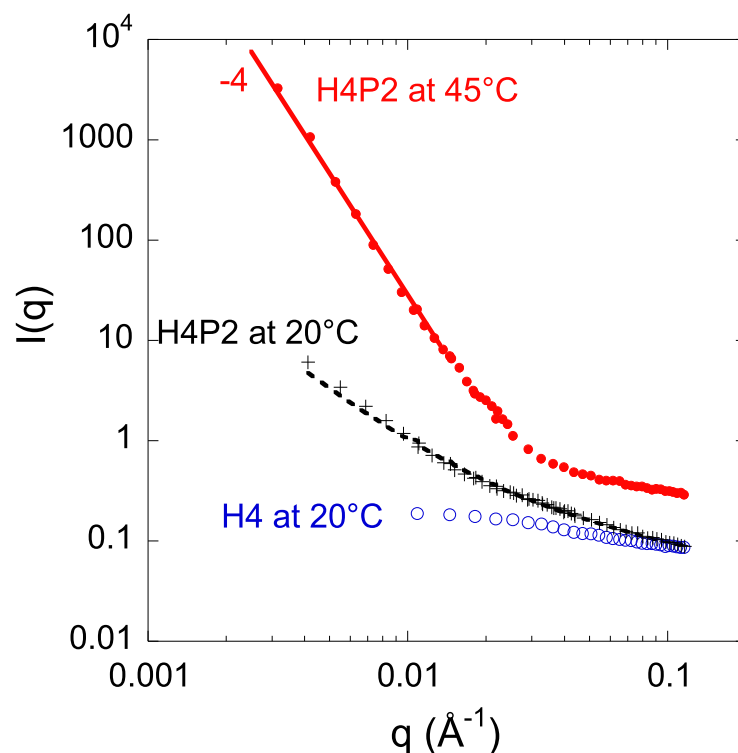


Figure III.7. H4 and H4P2 at 20°C and 45°C. Dotted line on the curve at 20°C is the best fit to a fractal aggregate model.

Neutron scattering experiments confirmed the formation of such large aggregates. Indeed, above the cloud point of PNIPAM, huge increasing of the SANS intensities are observed on all the samples (see Figure III.7 for H4P2). The characteristic Porod's law (slope -4) observed at low q and the huge signal measured are indicating the presence of very large scale fluctuations, well above 25 nm ($1/q_{\min}$) with sharp interfaces with the solvent. No specific size can be deduced from these curves due to the limited q small q values reached by SANS experiments.

The kinetics of hydration/dehydration phenomena was then studied. This effect was evaluated for each polymer from the transmission profile by evaluating the variation of temperature needed to decrease down to 10% of transmitted signal (Figure III.5.A, Figure III.4). All results were reported in Figure III.8. Whereas the grafting of PNIPAM onto TREN does not modify significantly the speed rate of this phenomenon comparatively to the ungrafted PNIPAM, its grafting on HYPAM core induced a slower process: ΔT is thus increased from 2°C for P2 and TP2 to 7°C for HxP2. Interestingly, increasing the size of PNIPAM chain length for a given core tends to accelerate this rate. Thus, ΔT decreased from 7°C to 2°C for H5Px when increasing PNIPAM chain length from 2000 up to 7000 g/mol. Therefore, hyperbranched structure seemed to slow down the hydration/dehydration process only when small chains of PNIPAM were grafted onto them. This may originate from more heterogeneous surroundings of PNIPAM for such small polymer chains that hinder the modifications of conformation induced by the transition process.

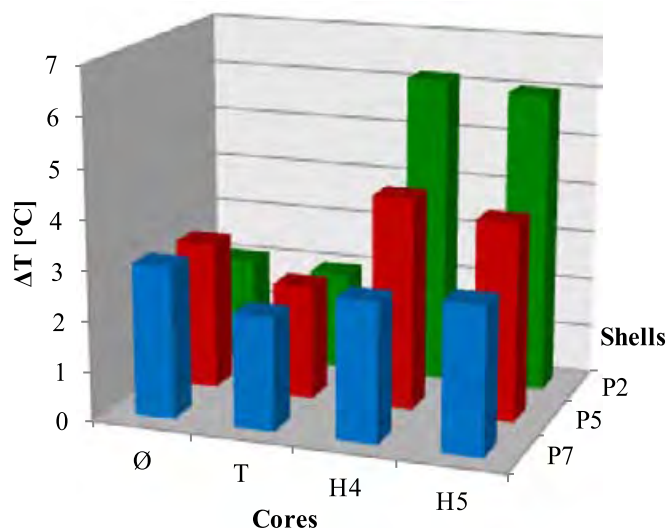
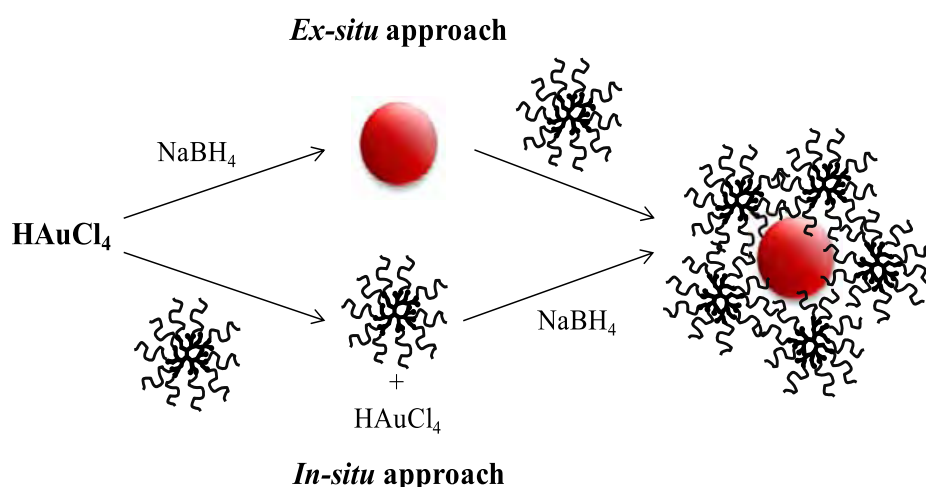


Figure III.8. Variation of temperature needed to reach 10% of transmission when considering the variation of transmission measured by UV spectroscopy at 500 nm ($[\text{polymer}] = 0.1 \text{ wt\%}$ in water, heating rate = $1^\circ\text{C}/\text{min}$).

IV. Stabilization and *in situ* synthesis of gold nanocomposites

In order to understand the macromolecular parameters that will play a critical role on the properties of gold nanohybrids obtained from them, two different strategies of synthesis have been used (Scheme IV.1). For the *ex situ* strategy, Au NPs were synthesized separately and subsequently mixed with the polymer by using a grafting from approach. Through this, a direct comparison of the stabilization and thermoresponsive properties of different families of polymer is made possible. In addition, this also prevents any chemical modification of the polymers that could occur during NPs formation. Moreover to evaluate the effect of macromolecular parameters on the growth of gold NPs an *in situ* strategy has also been used.



Scheme IV.1. Stabilization of *in situ* and *ex situ* formed nanoparticles in HxPy solutions.

A. *Ex situ* synthesis and stabilization of gold nanoparticles

1. Preformed Au NPs

For the first *ex situ* method, preformed Au NPs synthesized by a method allowing the use of small amount of stabilizing agent is preferred. Indeed, getting rid of these stabilizing agents will require tedious step of purification after ligand exchange with the hyperbranched structures to obtain purified nanohybrids. For this a synthetic protocol using a direct reduction of HAuCl_4 by NaBH_4 was selected [8]. Whereas no additional stabilizing agent was added, experimental conditions such as pH and gold precursor concentration have to be chosen carefully to obtain well-controlled Au NPs with good stabilization properties. First, the pH value of the HAuCl_4 needs to be adjusted around 8.0 before addition of NaBH_4 solution: in such conditions HAuCl_4 was present mainly as $\text{Au}(\text{OH})_4^-$ in solution whose reduction favored the formation of Au NPs as single colloids [9]. In addition, gold concentration need to be kept below $5 \times 10^{-4} \text{ mol} \cdot \text{L}^{-1}$ to avoid further aggregation of Au NPs (Figure IV.1).

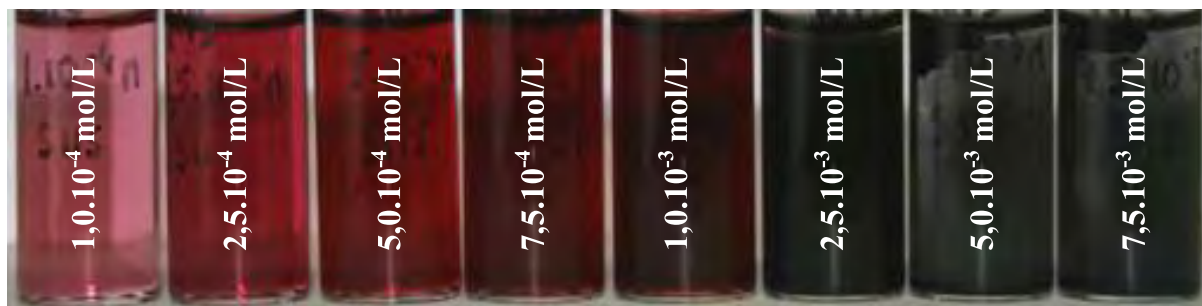


Figure IV.1. Au NPs solution formed at different $[\text{HAuCl}_4]$ concentrations 10 minutes after reductant adding. $[\text{HAuCl}_4]/[\text{NaBH}_4] = 1/1$

The NPs dispersions obtained by this procedure exhibited a broad absorption band around 516 nm, resulting in a pink-red color of the dispersions. TEM measurements showed isolated Au NPs with an average diameter of approximately $5 \pm 2 \text{ nm}$ (Figure IV.2). In addition, their hydrodynamic radius measured by DLS was found at $7.3 \pm 0.7 \text{ nm}$, so they are present mainly as single colloid in aqueous solutions. Those NPs are negatively charged (due to the presence of chloride, hydroxide and borate derivatives ions at the surface of the NPs) with a zeta potential around $-30 \pm 2 \text{ mV}$. Moreover, these Au NPs are stable in water with no significant change of optical properties over a month period (Figure IV.2).

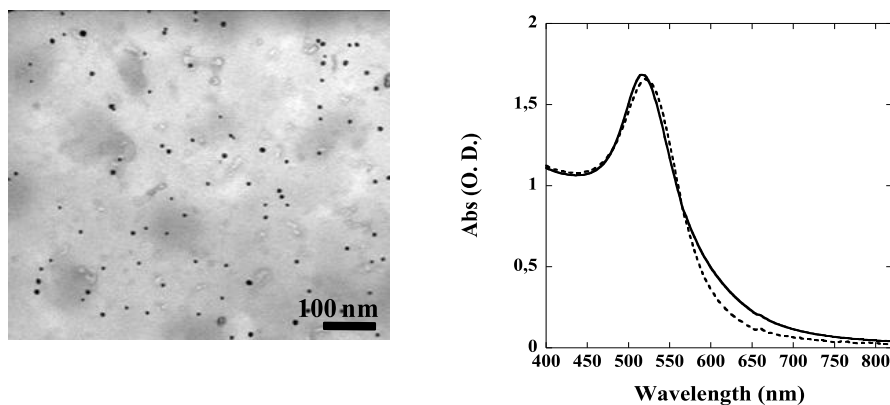


Figure IV.2. TEM image (left) and UV-vis spectra (right) of colloidal dispersions of Au NPs synthesized by reduction of HAuCl_4 solutions ($5 \times 10^{-4} \text{ mol} \cdot \text{L}^{-1}$) with one equivalent of NaBH_4 obtained after 1 hour (solid line) and 1 month (dash line). The Au NPs sizes obtained by this method vary from 5 to 10 nm. In our cases we obtain 5 ± 1 nm NPs.

Those Au NPs are sensitive to any increase of the ionic strength or change in pH, inducing charge neutralization and then aggregation. Thus, increasing ionic strength of the Au NPs dispersion modified the color of the solution from red to purple. This corresponded to a large change of the UV-visible spectrum of the solution: the surface plasmon band (SPB) of the NPs initially at 520 nm (associated to well-dispersed Au NPs) decreased strongly and was accompanied by an increase in absorbance at higher wavelength (suggesting aggregated Au NPs).

2. Stabilization of Au NPs by PNIPAM based hyperbranched polymer

a. *Synthesis of Au NPs nanocomposite*

The effect of the polymer concentration and the macromolecular architecture on the stability of the hybrids was subsequently studied by monitoring the surface plasmon band (Figure IV.3). For this an adequate amount of polymer solution was added to Au NPs solutions to reach the final desired polymer concentration (from 1×10^{-6} to 5×10^{-2} wt.%).

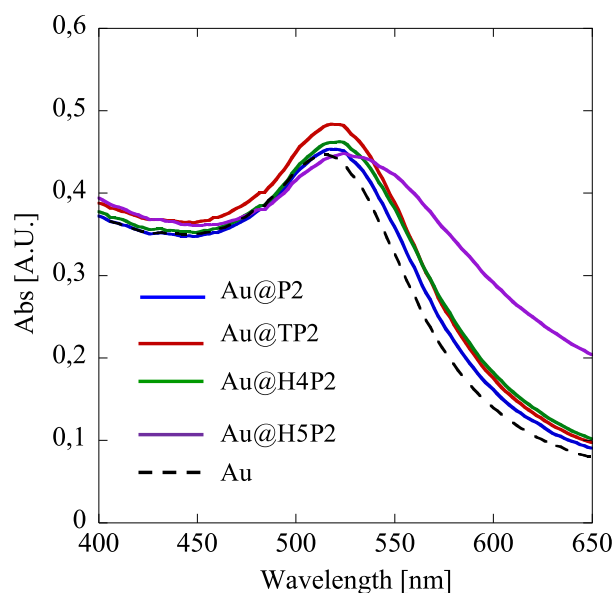


Figure IV.3. UV Spectrum of colloid solution of polymers coated Au NPs (solid line) and Au NPs without polymers (dash line). $[\text{Au NPs}] = 2.5 \times 10^{-4} \text{ mol} \cdot \text{L}^{-1}$ and $[\text{polymer}] = 0.05 \text{ wt.}\%$.

When the polymer was introduced in the medium, the plasmon band shifted from 518 nm for bare particles to 522 nm up to 527 nm depending on the polymer nature and on the polymer concentration. This bathochromic shift of the maximum wavelength is consistent with the change of the dielectric constant around the particles and demonstrates the efficiency of polymers to interact with the surface of Au NPs. This shift is observed for polymer concentration above $10^{-4} \text{ wt.}\%$ (Figure IV.4). The polymer/gold hybrids resulting from the addition of the different polymers were stable over several weeks. The role of the polymer is of course predominant for NPs stability and we then decided to challenge it against the addition of sodium chloride salt which is known to induce gold NPs aggregation.

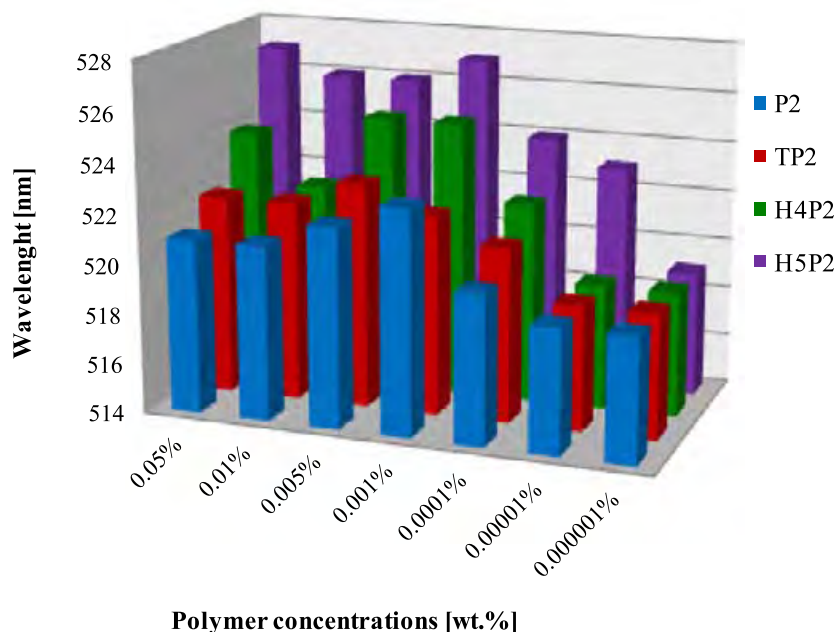


Figure IV.4. λ_{\max} value of UV spectra of Au NPs coated P2, TP2, H4P2 and H5P2, [Au NPs]= 2.5×10^{-4} mol·L⁻¹ and [polymer]=0.05 wt.% to 10^{-6} wt.%

b. *Salt adding effect*

Two different mechanisms are assumed to append when salts are introduced in the medium. In the case of bare Au NPs, the surface charges are shielded thus promoting their immediate aggregation. For polymer-coated-particles, a salting-out effect takes place, increasing the hydrophobic interactions between the polymer chains, which also leads to aggregation. In the present experiments, when poorly stabilized particles were in presence of NaCl 1 mol·L⁻¹, the solution turned immediately blue with a SPB shift up to 565 nm for bare NPs (Figure IV.5). With this approach we clearly got access to the minimal polymer concentration needed to efficiently stabilize the hybrids.

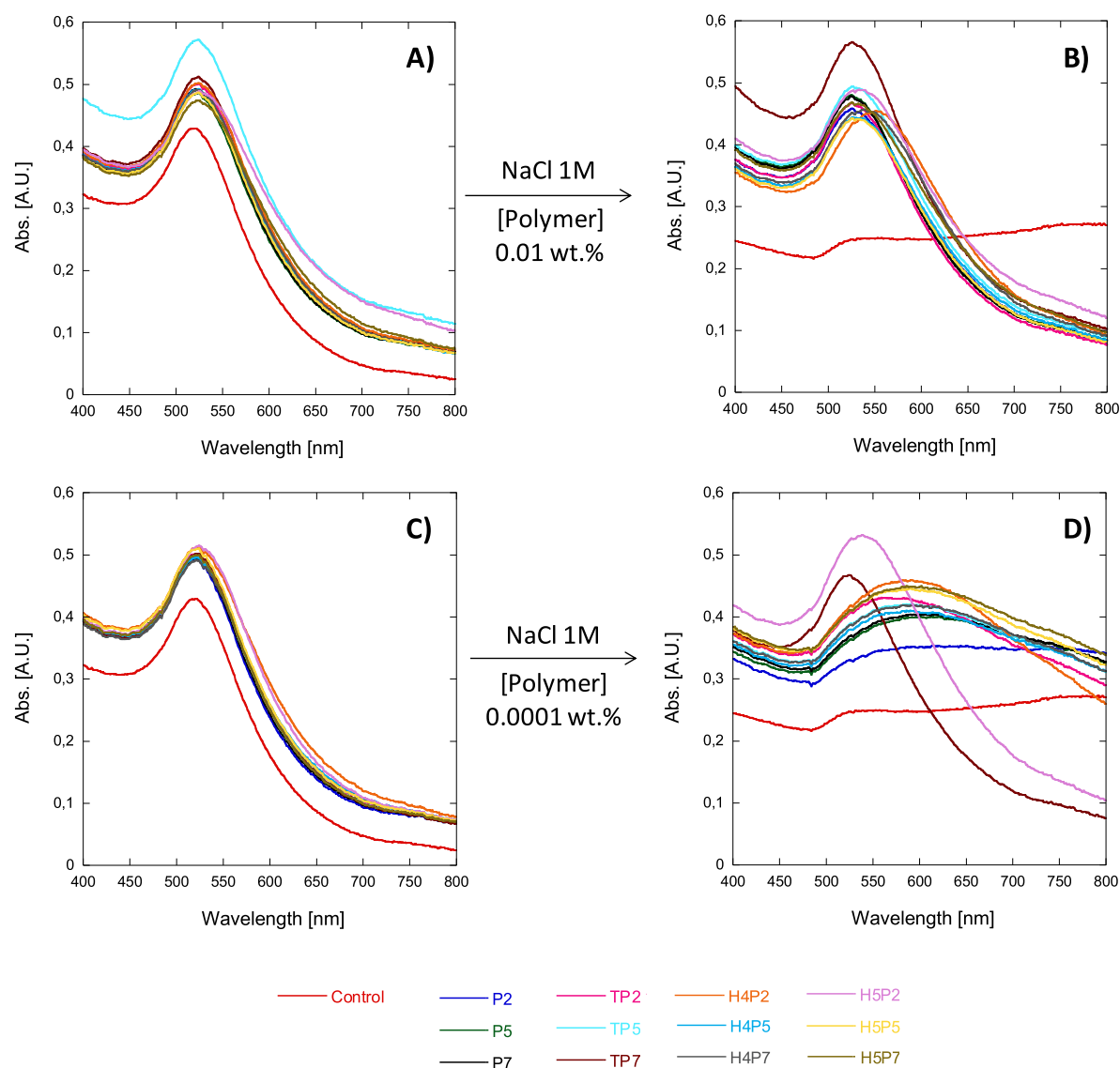


Figure IV.5. UV-spectra of polymer/gold hybrids ([Polymer]=0.01 wt. %) A) before addition of NaCl B) after addition of NaCl. UV-spectra of polymer/gold hybrid at [Polymer]=0.0001 wt. % C) before addition of NaCl, D) after addition of NaCl. In all cases [NaCl]_{final}=1M.

As evidenced on the 96-well plates experiments (Figure IV.6), depending on the nature of the polymer, this minimum varies between 10^{-4} to 0.5×10^{-1} wt.%. Linear PNIPAM structures were found to be the less efficient to stabilize NPs: only P5 and P7 at 0.05 wt.% were able to successfully stabilize Au NPs. Linear PNIPAM polymers terminated by a carboxylate moiety conferred to the NPs a lower stability in comparison with thio or thioester end groups. This results are consistent with previous report were it was found that PNIPAM needed to be end terminated by suitable anchoring group (such as thiol or thioester) to be able to interact properly with the surface of Au NPs [10]. Other branched structures require only concentration down to 10^{-4} wt% to avoid aggregation. Among them, TREN based structures (TP2, TP5 and TP7) proved to be the most effective. Indeed for HYPAM based structures an aggregation phenomenon is still observed for a concentration up to 0.5×10^{-2} wt.%. Lastly the effect of PNIPAM chain length appeared to be less important on stabilization

properties as less significant differences were observed when comparing polymer with the same hyperbranched core bearing P2, P5 or P7. It is to be noticed that in the case of H4P7 and H5P7 a strong tendency to aggregation was observed (more pronounced in the case of H5P7). This could be ascribed to some difficulties of this polymer of high molecular mass to interact efficiently with the NPs surface probably due to their specific conformation in solution. Therefore these experiments tends to demonstrate in order to gain high colloidal stability that i) a branched structure is more efficient than the corresponding linear one, ii) an optimal size of the branched structures is required to be able to interact in an optimal way with the NPs surface.

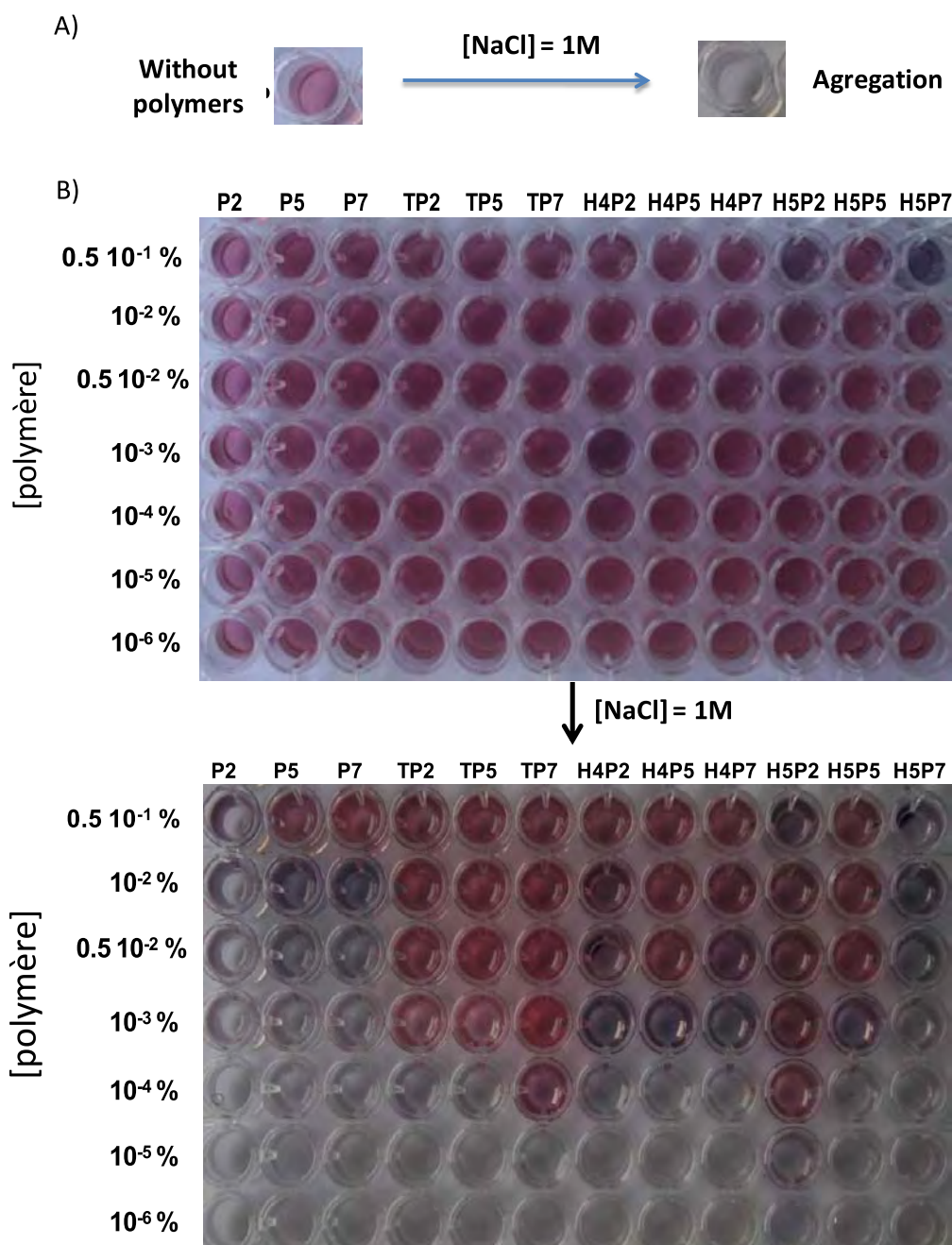


Figure IV.6. Stabilization of preformed Au NPs without polymers (A) or by HxPy polymer aqueous solution at different concentration (from 1×10^{-6} to 5×10^{-1} wt.%) before and after addition of NaCl (final concentration of NaCl is 1 mol.L^{-1} , $[\text{Au}]_0$ is fixed at $2.5 \times 10^{-4} \text{ mol.L}^{-1}$).

Largest structure obtained through the use of large core (H4 or H5) or of a longer PNIPAM chain will lead to less efficient stabilizing agent. By assuming a perfect reduction of the gold salt and a NPs size of 5 nm, the minimum density of adsorbed polymer to obtain good stabilization properties can be calculated from the minimal polymer concentration. Values obtained were in the range of 3.10^4 ng/cm². This high value suggested that a large excess of polymer is needed to obtain good stabilization properties in chosen conditions. Indeed, TEM images obtained after negative staining of dispersions of PNIPAM-coated Au NPs confirmed the formation of a thick layer of PNIPAM around NPs (Figure IV.7) [10]. On TEM images the hybrid Au/polymer particles clearly showed to have a core-shell morphology, the dark cores corresponding to the electron-dense Au atom embedded into a more or less circular brighter polymer shell. The overall sizes of those composites were 8.5 ± 2.6 nm. Numerous free polymer globules were also present in the case of copolymer coated NPs when polymer concentration used is far beyond the capacity of Au NPs surfaces to interact with polymer.

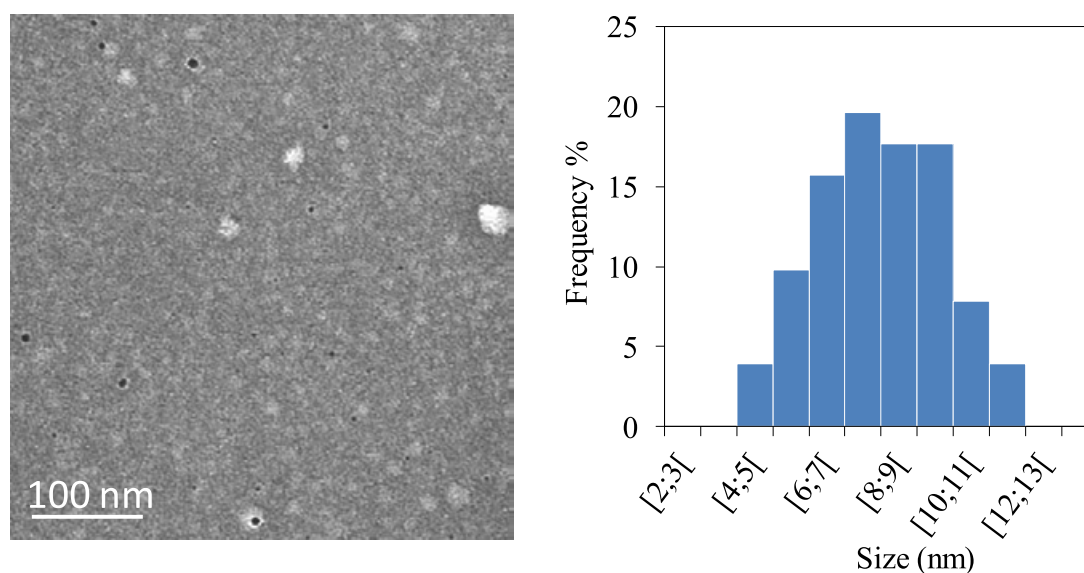


Figure IV.7. TEM image and corresponding size histogram of H4P5@Au object. [Au NPs]= 2.5×10^{-4} mol·L⁻¹ and [polymer]= 0.1 wt.%.

c. *Thermoresponsive properties*

When polymer concentrations were above 10⁻² wt%, no significant variation of the cloud point temperature of the nanohybrid solution was observed comparatively to pristine polymer. Indeed most of the polymer remains free in solution and thus does not interact with the surface of the NPs. Keeping the Au NPs solution above T_c for several hours results in the formation of a red precipitate that could be redispersed rapidly by cooling the solution below T_c. UV-vis measurements showed no change in their spectroscopic properties after several heating-cooling cycles (Figure IV.8) and so confirmed the complete reversible nature of the transition at T_c.

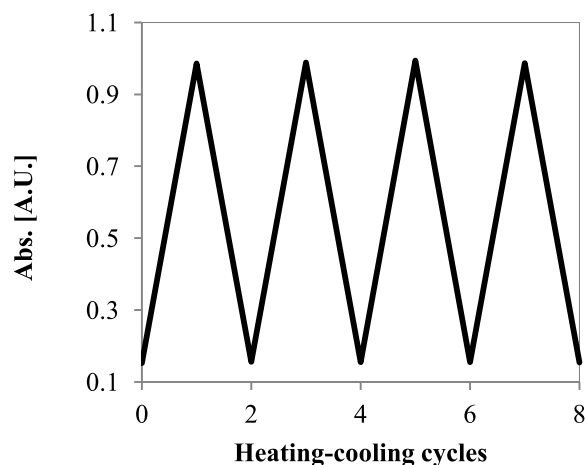


Figure IV.8. Evolution of relative absorbance measured at 650 nm for gold nanohybrids during heating/cooling cycles between 25 to 45 °C. [Au NPs]= 2.5×10^{-4} mol·L⁻¹ and [H4P7]=0.05 wt.%.

In order to assess the effect of macromolecular architecture on the thermoresponsive properties the changes in the surface plasmon band of Au NPs as a function of temperature was followed as shown in Figure IV.9Figure IV.10Figure IV.11. This enables to get rid of the excess of PNIPAM based polymer that could not interfere on the plasmonic properties of those nanohybrids. The influence of turbidity of the solution on the value of absorbance was removed by first subtracting the absorbance at 400 nm. Curves were then normalized so that the absorbances vary from 1 to 0. Indeed, the surface plasmon band of Au NPs was sensitive to many factors including the refractive index in the surroundings of the NPs. As expected whereas, no modification in absorption spectrum occurs for pristine gold NPs (i.e. in absence of thermoresponsive coating polymer, see Figure IV.9), significant changes were observed for NPs coated with thermoresponsive polymers (Figure IV.10 and Figure IV.11). The collapse of PNIPAM at LCST due to the dehydration of the polymer chains usually induced a significant decrease of I_{\max} and a slight modification of λ_{\max} [7].

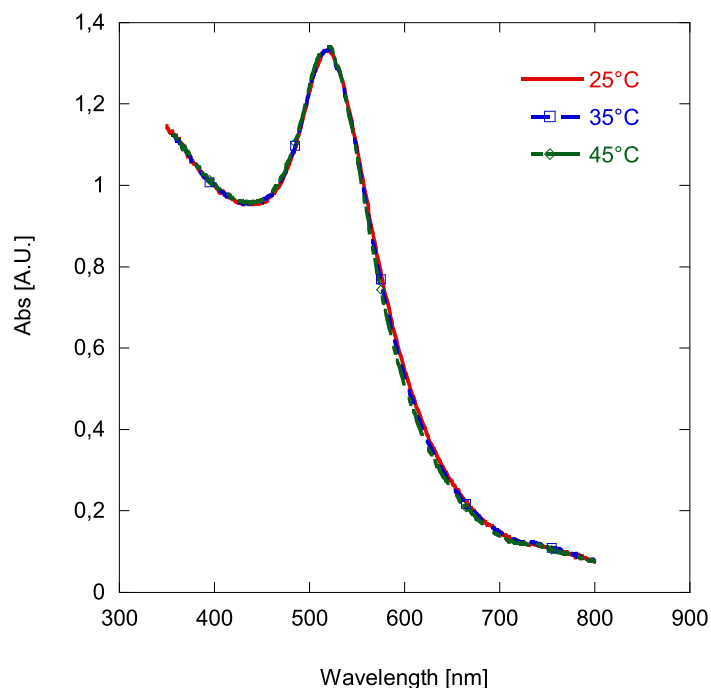


Figure IV.9. Absorption spectra of Au NPs colloid solution (without polymer coating) with increasing temperature. $[\text{Au NPs}] = 2.5 \times 10^{-4} \text{ mol} \cdot \text{L}^{-1}$ and $[\text{polymer}] = 0 \text{ wt.}\%$.

Whereas this effect was clearly observed in the case of Au@P2 (Figure IV.10), amplitude of those modifications increased significantly in the case of Au@TP2 and Au@H4P2 (Figure IV.10 B and C). Such discrepancies could not be ascribed to an aggregation phenomenon of nanohybrids induced by the increase of temperature: indeed TEM images obtained from sample deposited above T_c showed well dispersed individual NPs with corona that does not differ significantly from the one observed below T_c (Figure IV.10). In addition, these changes in the surface plasmon band were observed to be reversible as the temperature was lowered back to 25°C upon several heating-cooling cycles (Figure IV.8). Therefore, such differences may be mainly ascribed from the molecular architecture of the polymer in direct interaction with the surface of the NPs. Hyperbranched structures allowed to obtain more densely packed inner layer around the NPs surface. This induces both higher sensitivity to dehydration phenomenon and higher efficiency as stabilizing agent of metallic NPs as demonstrated above.

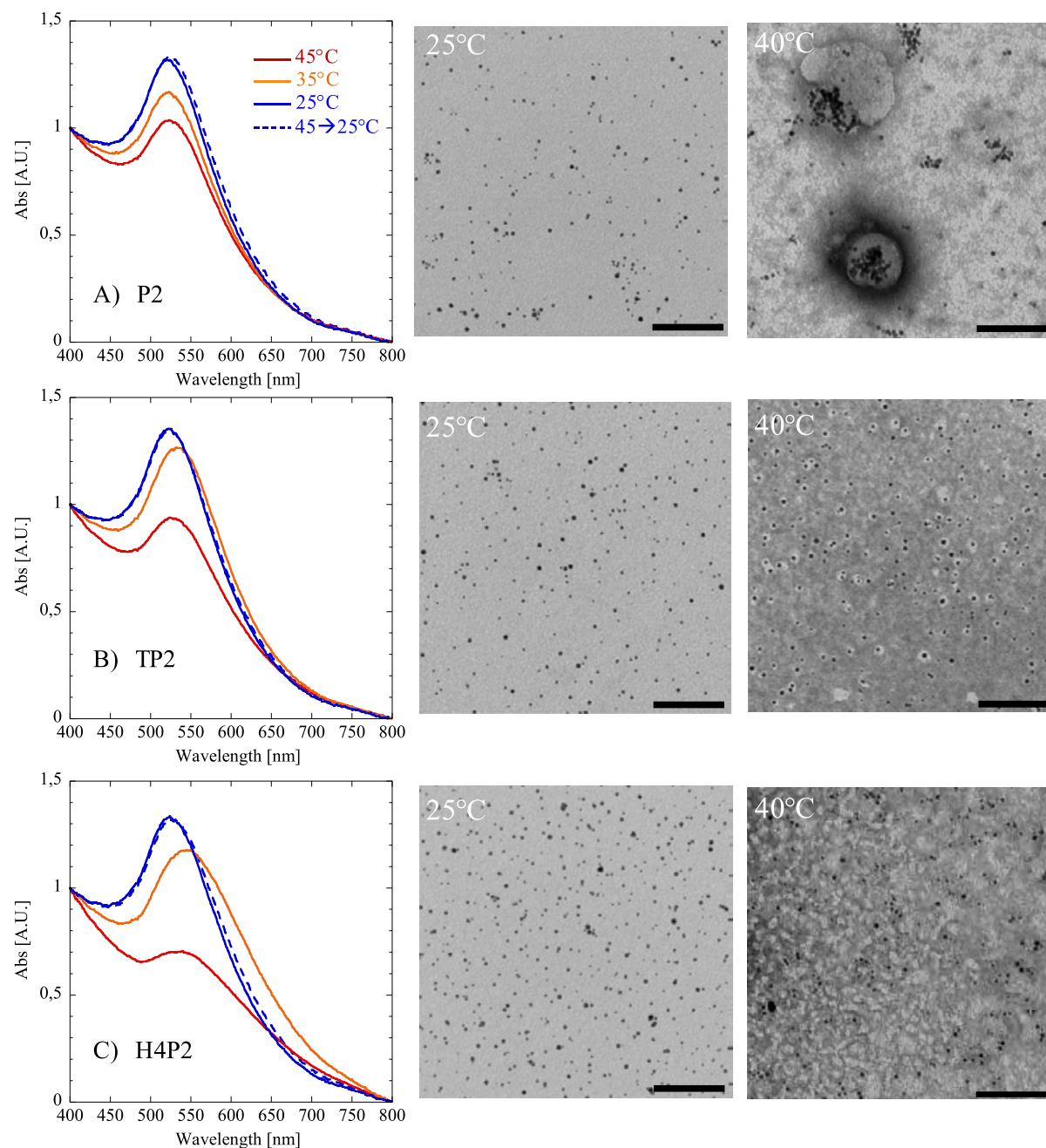


Figure IV.10. Changes in absorption spectra of Au@P2, Au@TP2 and Au@H4P2 with increasing temperature and corresponding TEM images. The absorbance at 400 nm was subtracted from the spectra, then normalized at 800 nm to remove scattering contribution and multiplied by a factor in a way that absorbance vary from 0 to 1. $[\text{Au NPs}] = 2.5 \times 10^{-4} \text{ mol} \cdot \text{L}^{-1}$ and $[\text{polymer}] = 0.05 \text{ wt.}\%$.

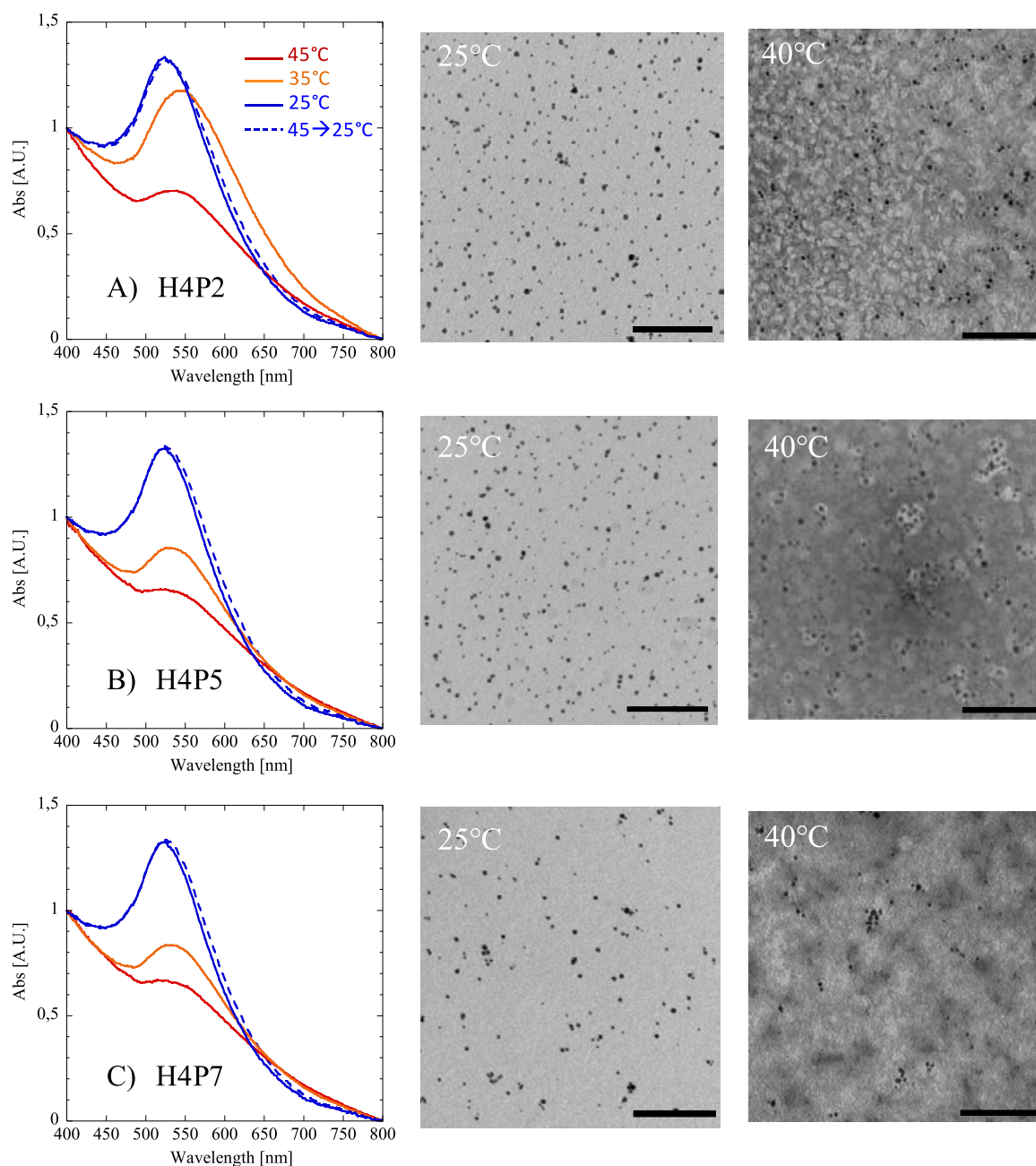


Figure IV.11. Changes in absorption spectra of Au@H4P2, Au@H4P5 and Au@H4P7 with increasing temperature and corresponding TEM images. The absorbance at 400 nm was subtracted from the spectra, then normalized at 800 nm to remove scattering contribution and multiplied by a factor in a way that absorbance vary from 0 to 1. $[Au\ NPs]=2.5\times 10^{-4}\ \text{mol}\cdot\text{L}^{-1}$ and $[\text{polymer}]=0.05\ \text{wt.}\%$.

B. *In situ* synthesis of gold nanoparticles

1. *In situ* synthesis of Au NPs by using NaBH₄ as reductant

The last and more striking evidence of the effects of molecular architecture was given by the controlled growth of particles in the presence of polymer. For those experiments, polymer concentration of 0.01 wt.% was chosen because an efficient stabilization is provided in such conditions. The formation of NPs was followed by UV-Vis measurements and transmission electron microscopy (TEM). After reduction, the color of the final solution, which is related to the SPB wavelength and was obtained in few minutes, varied from red to light orange depending on the polymer used (Figure IV.12.A). This clearly evidences the formation of gold nanoparticles of different sizes. TEM images of the so-obtained hybrid NPs confirmed that the macromolecular structure had a strong influence on the final size and polydispersity of particles (Figure IV.12.B).

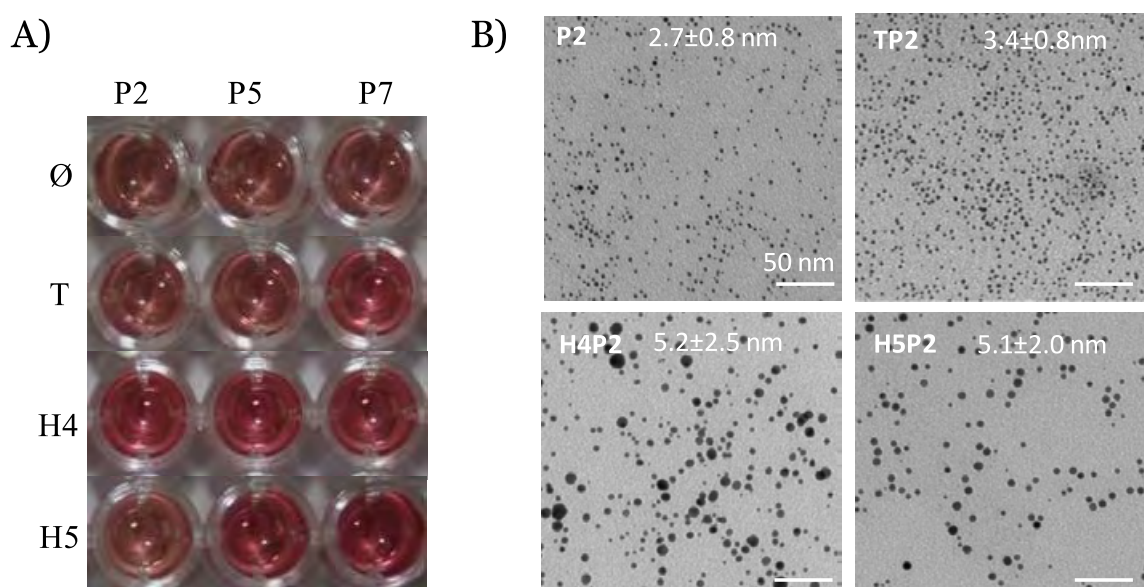


Figure IV.12. A) *In situ* synthesized Au NPs in HxPy polymer aqueous solutions using NaBH₄ as reductant, [Au]/[NaBH₄] = 1, [Au] = 2.5×10⁻⁴ mol·L⁻¹, [polymer] = 0.01wt. %, B) TEM images of *in situ* synthesized Au NPs. [Au NPs]=2.5×10⁻⁴ mol·L⁻¹ and [polymer]=0.01 wt.%

2. Architecture effect on the size of formed Au NPs

A summary of the results obtained is presented in Figure IV.13. As described above in the absence of polymer, NPs with an average diameter of 5 ± 2 nm were obtained. Addition of polymer strongly modified this average size suggesting that they play a critical role on nucleation-growth process.

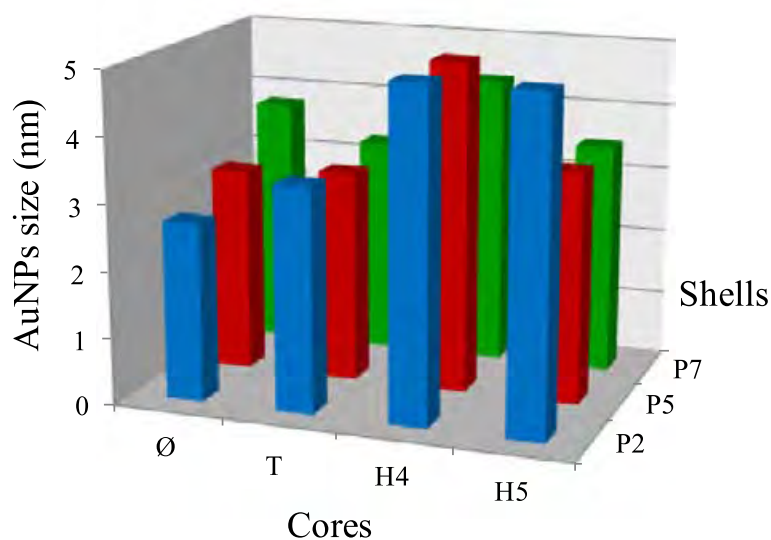


Figure IV.13. *In situ* synthesized AuNP sizes measured from TEM images. $[\text{Au NPs}] = 2.5 \times 10^{-4} \text{ mol} \cdot \text{L}^{-1}$ and $[\text{polymer}] = 0.01 \text{ wt.}\%$.

In the case of linear PNIPAM, the mean sizes of particles were 2.7 ± 0.8 , 3.1 ± 0.8 and $3.8 \pm 1.2 \text{ nm}$ for P2, P5 and P7 respectively. Thus increasing macromolecule length tends to increase the average size of the obtained NPs. This trend was confirmed when PNIPAM moiety was grafted on branched core. For a given PNIPAM chain length, increasing the size of the core, i.e. increasing the final macromolecular masses, induces an increase of gold NPs size: hence in the case of P2, the size of NPs increase to 3.4 ± 0.8 , 5.2 ± 2.5 and $5.1 \pm 2.0 \text{ nm}$ respectively for TP2, H4P2 and H5P2. Similar trends were observed for other PNIPAM chain length. Moreover in the case of branched structures a slower kinetics of formation of NPs is evidenced as slight changes of color occurs with time within the first hours. This difference in size can be correlated to different level of interaction during NPs growth mechanism. Small polymers seem to interact strongly with NPs surface as they can diffuse and rearrange more quickly onto these surface at the early stage of the NPs growth. For larger polymers, such interaction is less efficient during the growing step as NPs presented size similar to the one of the control experiment (i.e. without stabilizing agent). Nevertheless, as demonstrated in the previous part, hyperbranched structures can interact efficiently with Au NPs as they act as better stabilizing agent once the colloidal solutions are obtained. Even if those large structures interact probably more slowly with NPs surface preventing them to be a good growth control agent, their specific structure enables them to hinder more efficiently the NPs surface and thus to avoid aggregation.

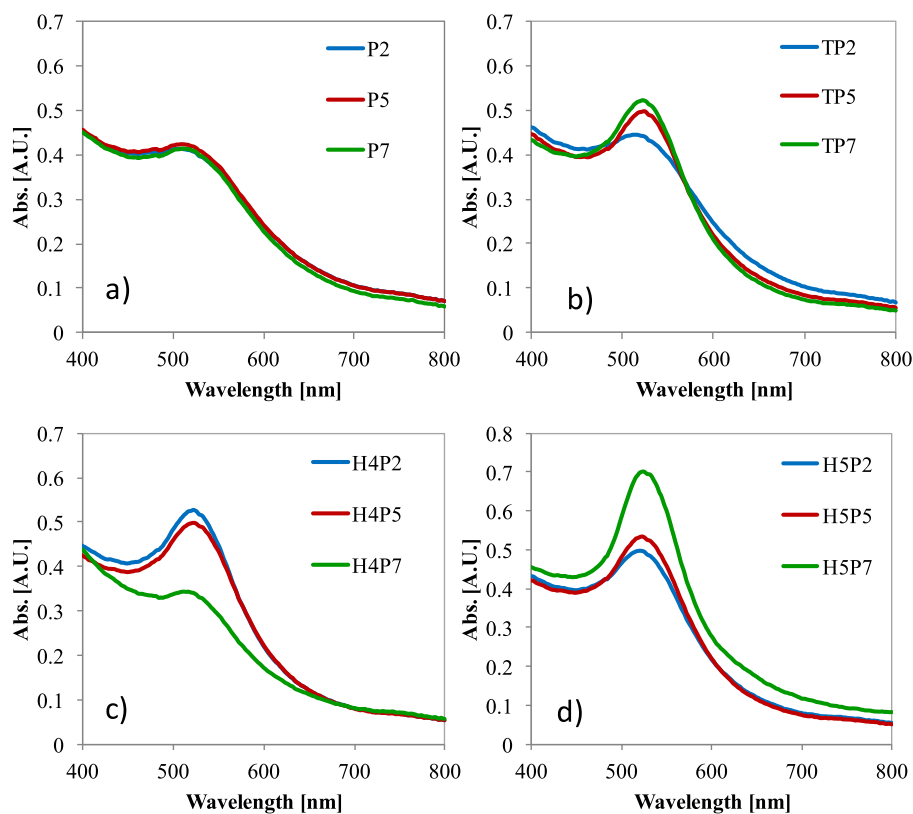


Figure IV.14. UV spectra of *in situ* synthesized Au NPs in polymer solution a) P_x, b) TP_x, c) H4P_x, d) H5P_x, x= 2, 5 or 7. [Au NPs]= 2.5×10^{-4} mol·L⁻¹ and [polymer]= 0.01 wt.%

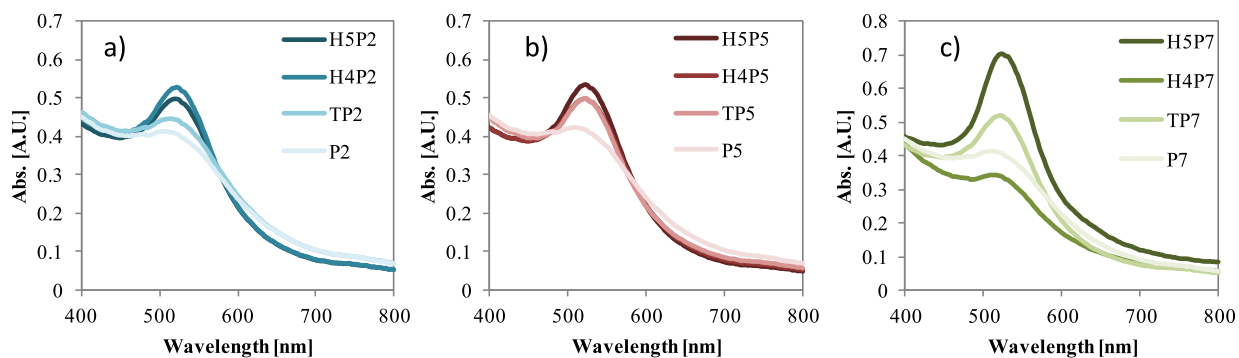


Figure IV.15. UV spectra of *in situ* synthesized Au NPs in polymer solution a) P₂ and P₂ grafted polymers, b) P₅ and P₅ grafted polymers, c) P₇ and P₇ grafted polymers. [Au NPs]= 2.5×10^{-4} mol·L⁻¹ and [polymer]= 0.01 wt.%

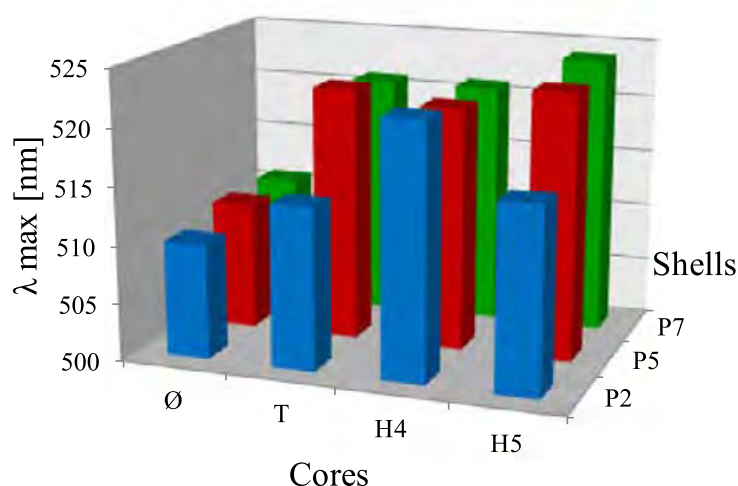


Figure IV.16. λ_{\max} value of UV spectra of polymer coated Au NPs, $[\text{Au NPs}] = 2.5 \times 10^{-4} \text{ mol} \cdot \text{L}^{-1}$ and $[\text{polymer}] = 0.01 \text{ wt.}\%$

V. Conclusions

PNIPAM-based hyperbranched structures were prepared from different branched core and their properties were studied in aqueous solutions. Those experiments permit to assess a relationship between macromolecular architecture and thermoresponsiveness of those polymers. These polymers were then employed as stabilizers of Au NPs dispersions by either *a posteriori* adsorption on Au NPs or *in situ* formation. Both approaches were successful for stabilization and reversibility of the thermoresponsive precipitation process was demonstrated. In *in situ* approach, we showed that, macromolecular architectures greatly influence the growth mechanism of NPs formed and smaller linear polymers allow a better control on NPs growth. In *ex situ* approach, macromolecular architectures also have an impact on the colloidal stability of the obtained nanohybrids : branched structures proved to be better stabilizing agent. Moreover, for this purpose, TREN based structures were found to be more efficient than highly branched structures HYPAM. These strategies should be easily applied to other type of metal NPs, and should lead to useful “smart” materials for a range of applications including drug-delivery devices and catalyst.

VI. References

1. Beija, M., Marty, J.-D. & Destarac, M. Thermoresponsive poly(N-vinyl caprolactam)-coated gold nanoparticles: sharp reversible response and easy tunability. *Chem. Commun.* **47**, 2826–2828 (2011).
2. Beija, M. et al. Control of the catalytic properties and directed assembly on surfaces of MADIX/RAFT polymer-coated gold nanoparticles by tuning polymeric shell charge. *J. Mater. Chem.* **20**, 9433–9442 (2010).

3. Lutz, J.-F., Akdemir, Ö. & Hoth, A. Point by Point Comparison of Two Thermosensitive Polymers Exhibiting a Similar LCST: Is the Age of Poly(NIPAM) Over? *J. Am. Chem. Soc.* 128, 13046–13047 (2006).
4. Beija, M., Marty, J.-D. & Destarac, M. RAFT/MADIX polymers for the preparation of polymer/inorganic nanohybrids. *Prog. Polym. Sci.* 36, 845–886 (2011).
5. Dvornic, P. R., Hu, J., Meier, D. J., Nowak, R. M. & Parham. Hyperbranched Polyureas, Polyurethanes, Polyamidoamines, Polyamides and Polyesters. 01611113 A1: US, 2012
6. Garamus, V. M. et al. Hyperbranched Polymers: Structure of Hyperbranched Polyglycerol and Amphiphilic Poly(glycerol ester)s in Dilute Aqueous and Nonaqueous Solution. *Macromolecules* 37, 8394–8399 (2004).
7. Sistach, S. et al. Thermoresponsive Amphiphilic Diblock Copolymers Synthesized by MADIX/RAFT: Properties in Aqueous Solutions and Use for the Preparation and Stabilization of Gold Nanoparticles. *Chem. Mater.* 22, 3712–3724 (2010).
8. Sistach, S. et al. Bolaamphiphile Surfactants as Nanoparticle Stabilizers: Application to Reversible Aggregation of Gold Nanoparticles. *Chem. Mater.* 20, 1221–1223 (2008).
9. Moreau, F., Bond, G. C. & Taylor, A. O. Gold on titania catalysts for the oxidation of carbon monoxide: control of pH during preparation with various gold contents. *J. Catal.* 231, 105–114 (2005).
10. Glaria, A., Beija, M., Bordes, R., Destarac, M. & Marty, J.-D. Understanding the Role of ω -End Groups and Molecular Weight in the Interaction of PNIPAM with Gold Surfaces. *Chem. Mater.* 25, 1868–1876 (2013).

Chapter 3

**Hydrogel-nanocomposites based on
thermogels of hyperbranched
polyamidoamine and
Poly(N-isopropylacrylamide) core-shell
polymers**

CONTENTS

I.	INTRODUCTION.....	145
II.	SYNTHESIS AND CHARACTERIZATION OF THERMOGELS OF HYPERBRANCHED POLYAMIDOAMINE AND POLY(N-ISOPROPYLACRYLAMIDE) CORE-SHELL POLYMERS....	147
A.	SYNTHESIS OF THE THERMORESPONSIVE HYDROGELS	147
1.	<i>Synthesis of polymers.....</i>	147
2.	<i>Synthesis of thermoresponsive hydrogels</i>	148
B.	CHARACTERIZATION OF THE HYDROGELS.....	148
1.	<i>Sol-gel transition</i>	148
2.	<i>Structure of the gels by cryo-SEM.....</i>	150
3.	<i>Rheological measurements</i>	151
4.	<i>UV following of thermoreversibility</i>	152
III.	IN SITU SYNTHESIS OF GOLD NANOPARTICLES IN THE GELS	153
A.	IN SITU SYNTHESIS OF AUNPS.....	153
B.	EFFECT OF AUNPS ON THE PROPERTIES OF THE HYBRID GELS	154
1.	<i>Structure of the gels.....</i>	154
2.	<i>Sol-gel transition</i>	155
a.	DSC.....	155
b.	Rheological measurements.....	157
3.	<i>Gel strength</i>	158
4.	<i>UV following of thermoreversibility</i>	159
IV.	CONCLUSIONS	159
V.	REFERENCES.....	160

I. Introduction

Response to external stimuli is central to how biological systems work, especially at the cellular level, with subsequent changes in properties and function from the molecular to the macroscopic level. The observations of the various systems where such processes occur allow designing hydrogels capable of responding to stimuli (i.e. temperature, pH, light...) in a controllable and predictable fashion. In response to this external stimuli, these hydrogels have the ability to change drastically their properties (i.e. dimensions, structures, interactions, viscosity,...) and therefore have been applied as biomaterials, drug delivery systems or as nanoreactors.[1], [2] In most case, their formation involved the use of polymer which are physically or chemically crosslinked. This has been described earlier in literature review chapter.

Of special interest are thermo responsive hydrogels: a small temperature changes around a critical value induce the collapse or expansion of polymer chains as a response to the new adjustments of the interactions between the polymeric chains and the aqueous media. When the phase diagrams of polymer solutions appear as monophasic below a specific temperature and biphasic above it exhibit a lower critical solution temperature (LCST). Different families of polymer exhibiting such a property, have been described in literature like poly(N- isopropylacrylamide) (i.e. PNIPAM), polyvinylcaprolactame,[3] poly(oligo(ethylene glycol) methacrylate),[4] poly(methyl vinyl ether),[5] poly(N-acryloyl-N'-propyl piperazine).[6] Among them, PNIPAM which presents a LCST around 32 °C in aqueous solutions have been by far the most common used for the formation of hydrogel.[7]–[13] In the transition regime, water becomes a poor solvent as polymer water H-bonds are disrupted and PNIPAM undergoes conformational changes including both intrachain “coil-to-globule” transitions and interchain self-association. Those PNIPAM based hydrogels have been used for the formation of hybrid materials with tunable optical or catalytical properties, of nanovectors for drug delivery or of smart hydrogels with striking mechanical properties. [2], [14]

Depending on the preparation method and applications expected hydrogels with bulk, micro and nano dimensions have been described in literature. Whatever their overall dimensions are, properties of those hydrogels depend also strongly on their internal structure. Therefore intensive efforts have been made to gain control over it at a nanoscale level. Finely tuning this structure allow getting access to materials with improved responsiveness in term of kinetics, change of dimension, etc ...[2]

In the previous chapter we studied the diluted solutions of different PNIPAM based core-shell polymers. Herein we interest in the gel states of these polymers. We aim first to understand how the internal structure of PNIPAM based hydrogels can be modified by playing with the molecular architecture of the polymer. For this purpose we chose to compare the behavior of linear polymer of PNIPAM with the one of three branched structure and the hyperbranched one. We chose a family derived from PNIPAM with an average molar mass equal to 7000 g.mol⁻¹ for this study namely PNIPAM 7000 g.mol⁻¹ (P7), TREN grafted PNIPAM (TP7) and Hyperbranched polyamidoamine grafted PNIPAM (H4P7). We study the transition rates and rheological behavior of such hydrogels. Moreover those materials can act

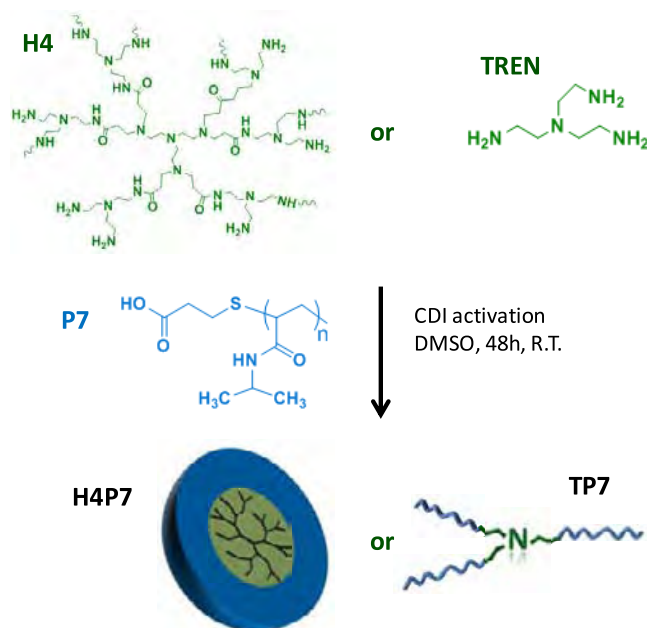
as reactor to mediate the formation of gold nanoparticles (NPs). Their effects on the internal structure and on the properties of the gels were evaluated.

II. Synthesis and characterization of thermogels of hyperbranched polyamidoamine and Poly(N-isopropylacrylamide) core-shell polymers

A. Synthesis of the thermoresponsive hydrogels

1. Synthesis of polymers

The synthesis and characterization of polymers which were used in this study was described in details in chapter 3. The PNIPAM 7000 g.mol⁻¹ grafted polymer family was chosen for the study of gelation transition. As described in chapter 3, at diluted concentration, the thermoresponsive properties of those polymers were affected by branching degree and the core nature. Nevertheless, all transition temperatures values remain in the same range (between 31 and 33°C). Synthesis scheme is reported in Scheme II.1, main characteristics of P7, TP7 and H4P7 polymers were given in Table II.1



Scheme II.1. Synthesis of TREN and HYPAM-based hyperbranched polymers with a PNIPAM thermoresponsive shell.

Table II.1. Characterization of P7, TP7 and H4P7 polymers

Compounds	\overline{M}_n^a [g/mol]	Grafting ratio [%] by IR / by DSC
P7	7000	-
TP7	17000	81 / 83
H4P7	192000	66 / 71

^a estimated by synthesis method

2. Synthesis of thermoresponsive hydrogels

Solutions of the different PNIPAM based polymers were studied at different concentration ranging from 0.5% to 20%. The polymer solutions were placed at 40°C for 10 minutes and simple tube inversion experiment revealed the concentration from which sol-gel transformation can take place (Figure II.1). Below the transition temperatures, aqueous solutions of P7, TP7 and H4P7 look like free flowing liquids whatever the concentration. As the solutions are heated above the transition temperature, the solutions became rapidly white and turbid. The formation of gel was only observed for the highest concentration of polymer used (i.e. 20%wt) in the case of P7: in this case the solution became gel-like structure and was not flowable by tube inversion experiment. For the two other polymers, gel formation occurred at lower concentration (15%). In all cases, those gelation concentrations were found well above entanglement concentration which can be evaluated around 3 %wt in the case of P7.[15] Therefore this allows to discard the effect of molar mass upon gelation properties. To confirm this, PNIPAM with a molar mass similar to the one of TP7 was studied (ie : 20000 g.mol⁻¹): as expected its behavior in solution is similar to the one of P7, gelation only occurs at 20 wt%. In the following, in order to compare the effects of molar mass, substitution level and architecture on the thermogel formation only the highest concentration (i.e. 20%wt) will be considered.

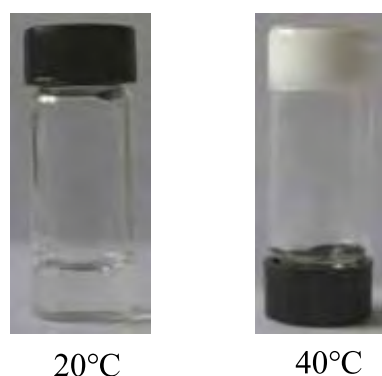


Figure II.1. Tube inversion experiment: 20 wt.% of H4P7 solution at 20 and 40°C.

B. Characterization of the hydrogels

To understand how the internal structure of PNIPAM hydrogel can be modified by playing with the molecular architecture of the polymer we performed different experiments to characterize the sol-gel transition, the strength as well as the structure of the formed gels.

1. Sol-gel transition

Cloud point temperatures (T_c) and related enthalpy variations for 20 % wt. aqueous solutions of P7, TP7 and H4P7 were evaluated by using DSC measurements. DSC thermograms were recorded at heating and cooling process in a range of temperature 20°C to 45 °C, at the rate of 1°C.min⁻¹. Typical thermogram of 20%wt. solution of H4P7 is shown in Figure II.2. We investigate at the temperature changing rate of 1°C.min⁻¹ to avoid syneresis effects at lower heating/cooling rate and hence gain accurate comparison between polymers. T_c values for all samples were taken at the top of the peak of the transition and were reported

in Table II.2. The associated enthalpy variation normalized on PNIPAM content are given in the same table.

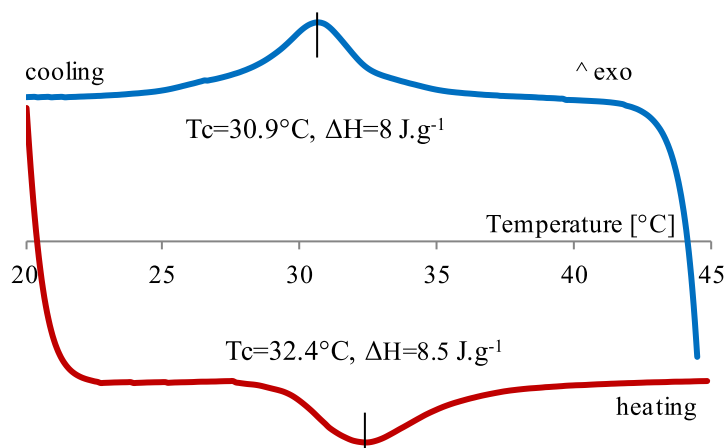


Figure II.2. DSC thermogram for 20 wt.% solution of H4P7 recorded at 1°C.min⁻¹ on heating (red line) and cooling (blue line).

Table II.2. DSC characteristics of the hydrogels

Compounds	DSC					
	T _c (°C) on ^a			ΔH [J/g] ^b		
	heating	cooling	ΔT	heating	cooling	Δ(ΔH)
P7	29.3	28.7	0.6	30.9	2.4	28.5
TP7	31	28.8	2.2	14.6	3.6	11
H4P7	32.4	30.9	1.5	8.5	8.0	0.5

^ameasurements of temperature transitions at heating or cooling rate of 1°C/min for polymer solution at 20 wt.%. ^b normalized on PNIPAM content

Obviously, there are differences between the curves on heating and on cooling. There is hysteresis on cooling process revealed in a shift of the transitions to lower temperatures. This phenomenon is more remarkable for branched polymers TP7 ($\Delta T = 2.2^\circ\text{C}$) and H4P7 ($\Delta T = 1.5^\circ\text{C}$) than the linear P7 ($\Delta T = 0.6^\circ\text{C}$). This can be explained firstly by looking at the molecular shape of the molecules. They are all macromolecular molecules but difference architectures. For macromolecular molecules, the probability that the molecules are oriented the way they need to be in order to build a phase of a certain order is much lower than in the case of a small flexible molecule. Due to this fact it takes more time and therefore cooling to lower temperatures than in the heating curve, where molecular ordering is broken up. On the other hands, syneresis phenomenon is more pronounced for hydrogels of PNIPAM or other polymers where intramolecular and intermolecular $\text{NH} \cdots \text{O}=\text{C}$ hydrogen bonding interactions occur upon heating process above cloud point temperature. These additional interactions hinder the rehydration of PNIPAM on cooling process leading to the observed hysteresis [16].

P7 is linear polymer while TP7 has three branched and H4P7 is composed of a highly

polydisperse hyperbranched core and a lot of P7 chains. We suggest that the linear molecule are oriented in a less entangled way than branched polymers when building a gel phase hence the difference in transition temperature on heating and on cooling (hysteresis) is more remarkable for branched polymers.

Considering the heating process, first observation shows that T_c slightly increased with the degree of branching from 29.3 to 32.4°C (Figure II.3.left, Table II.2). As already observed in the case of block copolymer, this might result from the incorporation of some hydrophilic content (TREN and HYPAM core) within the polymer.[17] Interestingly associated enthalpy variation normalized on PNIPAM content showed a strong decreased when the degree of branching increased (Figure II.3.right). As such a decrease is not observed in dilute conditions, this tends to demonstrate a clear difference between the different polymers concerning the polymer/polymer and polymer/solvent interactions in gel solution that strongly modified the dehydration process for the hydrogels.

If we measured the difference on the variation of enthalpy issued from heating or cooling processes (Figure II.3 right, Table II.2), we clearly see that this difference is more pronounced compared with hyperbranched structures TP7 and H4P7. This can be resulted from a marked syneresis effect on P7 sample or from kinetics effects.

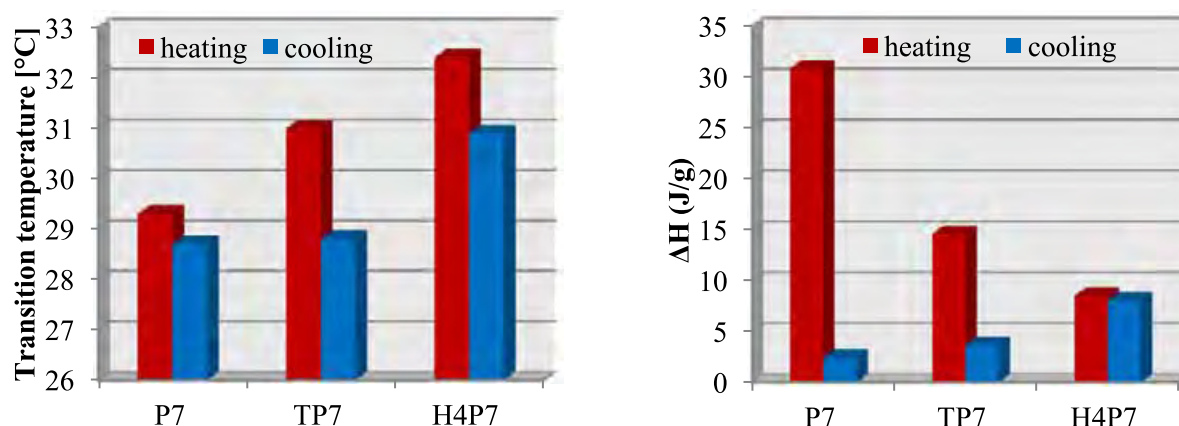


Figure II.3. Transition temperatures on heating and cooling at 1°C/min of polymer gel P7, TP7, H4P7 at 20wt% (left). Energies involved in sol-gel transition on heating and cooling at 1°C/min of polymer gel P7, TP7, H4P7 at 20wt% (right).

2. Structure of the gels by cryo-SEM

To get an insight in the network structure of the hydrogels, freeze-dried samples were analyzed by scanning electron microscopy (SEM, Figure II.4). Microstructures of the three freeze-dried hydrogels show honeycomb-like structure with nearly dense cell walls. Nevertheless, their average size differs strongly decreasing from 2.8 μm down to 1.4 μm and 0.5 μm for P7, TP7 and H4P7 respectively (Table II.3). Moreover, as depicted in Figure II.4 some dendritic structures appear in the case of the TP7 intermediate branched structure. Therefore a clear relationship between molecular architecture and microstructures is evidenced. This result is in agree with the suggestion made in the former subsection.

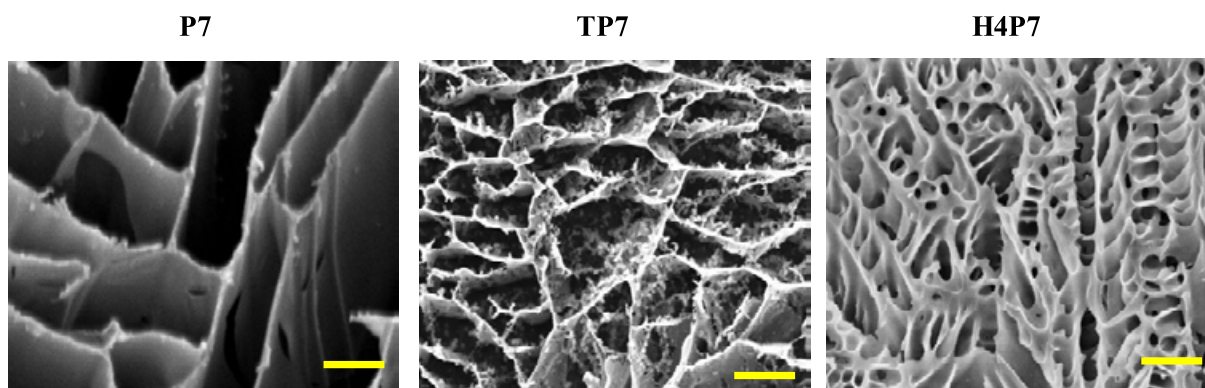


Figure II.4. Images obtained from cryo-SEM of gel structure at 40°C of P7, TP7, H4P7, bare scale: 2 μ m.

Table II.3. Gel pore sizes measured from SEM images.

Compounds	Gel pore sizes [μ m]
P7	2.8 ± 0.9
TP7	1.4 ± 0.5
H4P7	0.5 ± 0.3

3. Rheological measurements

To get further insight on the consequence of such modifications at a macroscopic level during sol-gel transition we studied the mechanical properties of these different gels. Rheological measurements provided a quantitative characterization of the mechanical changes during sol-gel transition.

The elastic modulus G' and the viscous modulus G'' were monitored from 25 to 40°C, heating at 1°C/min, at 1Hz and an oscillatory stress amplitude at 1 Pa. Figure II.5 shows the variation of G' and G'' with temperature for P7, TP7 and H4P7 solutions at 20 wt% in water.

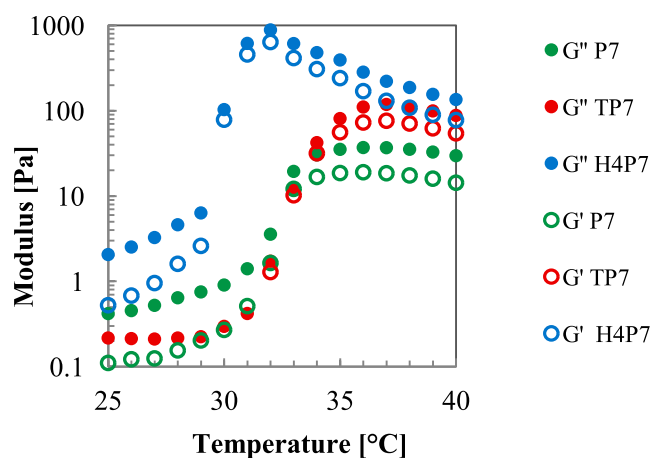


Figure II.5. Temperature-dependent storage and loss moduli of P7 (green), TP7 (red), H4P7 (blue) in 20wt% solution on heating and cooling at 1°C/min.

First observation shows that P7 and TP7 display a quite similar behavior, both showing a sol-gel transition at the PNIPAM transition at 32.5°C. The introduction of the TREN core tends to increase a bit the stiffness of the gel, illustrated by the change of G' from 20 Pa in P7 to 80 Pa in TP7. A more important change is displayed by the hyperbranched polymer H4P7, for which the transition temperature decrease from 32.5 to 30°C and a maximal elastic modulus G' is observed at 1000 Pa. A good correlation is observed between this increasing G' modulus and the density of entanglements in the gels, as can be seen on the SEM images.

4. UV following of thermoreversibility

The thermoreversibility of these hydrogels was studied by monitoring the transition to the liquid state. For this, the turbidity of gels, preformed at 40°C and then placed at 25°C, was recorded as a function of time by following the transmittance at 720 nm (Figure II.6). This wavelength was chosen in order to have suitable comparison with the nanocomposite gels (see next section). Branched structures required a longer time to return back to the initial clear hydrated system (8 min, 11 min and 22 min respectively for P7, TP7 and H4P7) (Figure II.6.right). Both the rheological and the transition rate results correlate with the density of entanglements (of cells) observed by cryo-SEM: gels become stiffer and with slower sol-gel transition as the branching degree increases.

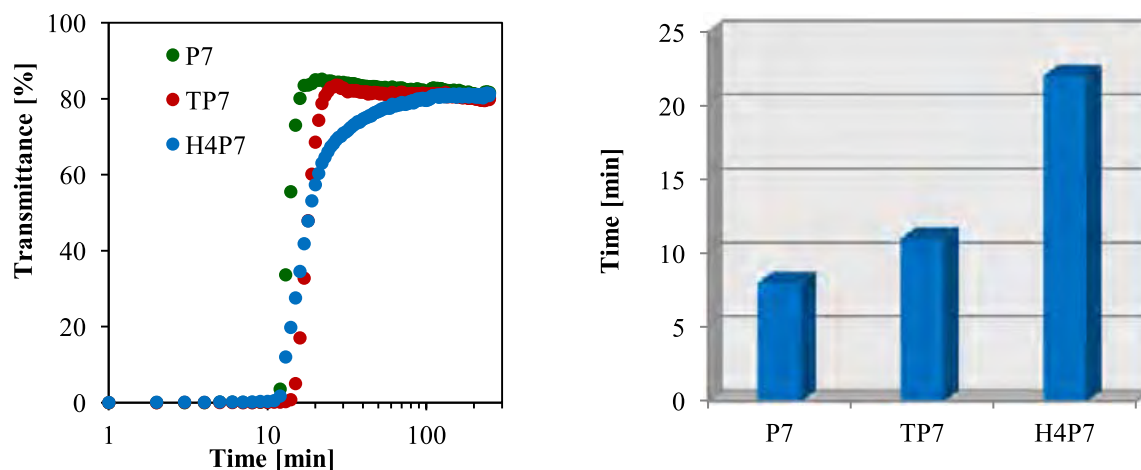


Figure II.6. Time-dependent turbidity of gels of TP7 at 20wt%, preformed at 40°C, and placed at 25°C. Time necessary for the 40°C preformed gels placed at 25°C to return to 90% of their maximum transmittance (right).

III. *In situ* synthesis of gold nanoparticles in the gels

A. *In situ* synthesis of AuNPs

These hydrogels can act as nanoreactor to mediate the *in situ* formation of nanoparticles. Hyperbranched structures based on polyamidoamine compounds (PAMAM or HYPAM) have demonstrated their ability to interact in solution with AuCl_4^- ions to mediate the synthesis of gold NPs. [18], [19] This interaction was taken into account to obtain homogeneous solution of gold ions within the hydrogels prior to reduction to gold NPs. The high viscosity of gel medium discards the possibility of using fast reducing agent as sodium borohydride. Therefore glucosamine was chosen to act as a slow reducing agent. It is mixed to the hydrogel below T_c then temperature is subsequently increased to reach the gel state.[20]

Successful reduction was first evidenced by a change of color of the solutions from yellow to red due to the characteristic plasmon band of Au NPs (Figure III.1)

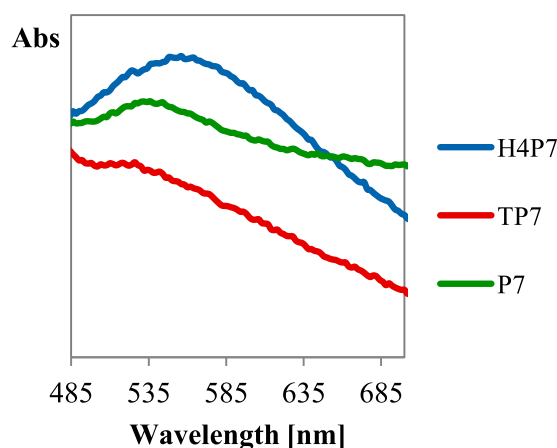


Figure III.1. UV spectrum of Au NPs formed in gel structures of P7, TP7, H4P7 at 20wt%.

It is noted that we have also investigated the ability of these hydrogels to stabilize preformed Au NPs. In this case, preformed Au NPs colloids were introduced in concentrated polymer solutions in order to have the final concentration of polymer around 20 wt.%. It is observed that Au NPs were precipitated giving a black color in the bottom of the test tube. Preformed Au NPs cannot well disperse in concentrated solution to give homogeneous nanocomposites.

In order to investigate sizes and shapes of *in situ* formed Au NPs, the nanocomposites were cooled to ambient temperature, diluted 10 times with water and hence deposited on TEM grids. TEM images evidenced the formation of such particles whose sizes decreased with the level of branching: thus P7 led to the formation of NPs with an average diameter of 13.7 ± 5.5 nm, whereas TP7 and H4P7 induced the formation of NPs with an average diameter of 10.5 ± 2.4 nm and 5.9 ± 2.1 nm respectively (Figure III.2). Explanation for this can be the affinity between AuCl_4^- and the hyperbranched core and hence the better interaction of gold precursor and the gel phase resulted in small AuNPs of 6 nm. The same reduction performed in the fluid state only, below T_c , led to the formation of slightly brown

solutions corresponding to Au NPs with characteristic sizes below 5 nm. The smaller size than the one observed within hydrogel is a good evidence of the effect of gel structure during the growth of gold nanoparticles.

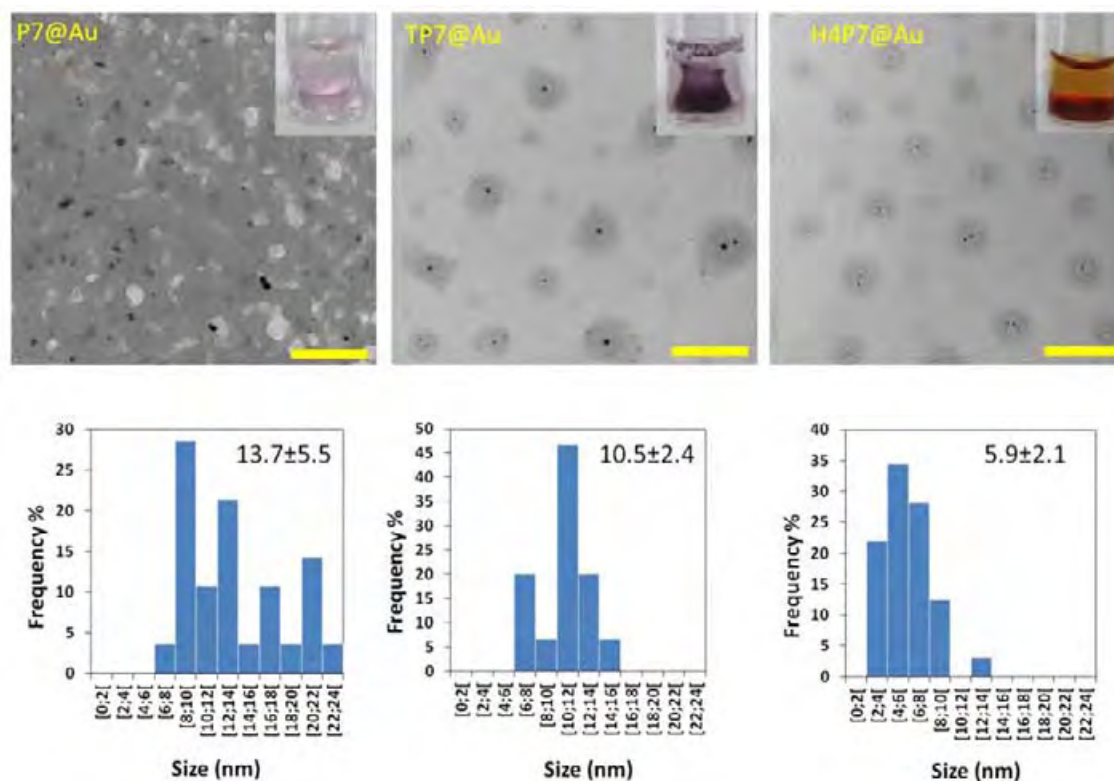


Figure III.2. TEM images of gold nanoparticles formed in gel structures of P7, TP7, H4P7 at 20wt%, with corresponding size distribution.

In return, the introduction of the gold nanoparticles in the structure affects different features of the gel which will be discussed in the next section.

B. Effect of AuNPs on the properties of the hybrid gels

1. Structure of the gels

The presence of Au NPs within the gel structure induces strong modifications of microstructures observed by SEM (Figure III.3) when compared to the free Au NPs hydrogels. Hence, P7@Au gel switched from a compartmented gel structure to a filamentous-like structure. For TP7 and H4P7, the average pore size decreased from 1.4 to 0.6 and from 0.5 to 0.1 μm respectively (Table III.1). The increase is quite low for TP7, and much stronger for H4P7, which shows a much more pronounced increase in density of the network. In the case of P7@Au, the moduli increased also a bit despite the transition to the filamentous structure. Inset in Figure III.3 shows the homogeneous inclusion of gold NPs within the gels.

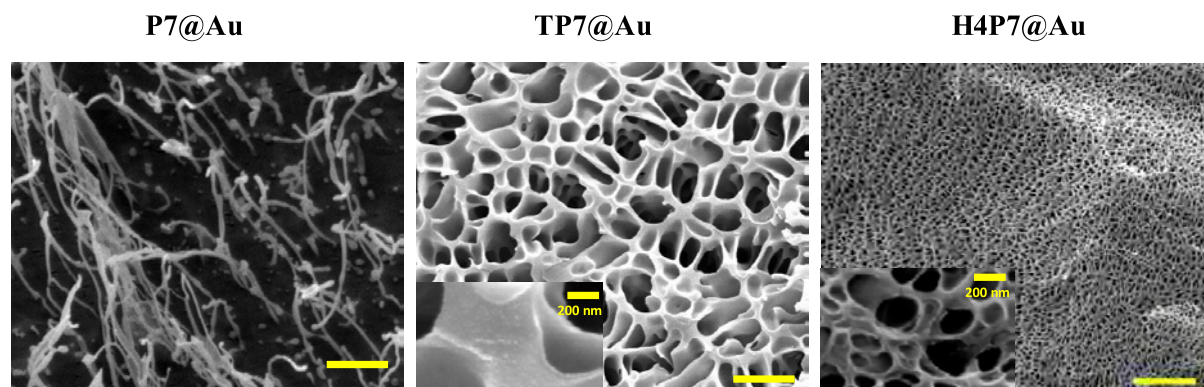


Figure III.3. Images obtained from cryo-SEM of gel structure at 40°C gels with *in situ* synthesized gold nanoparticles. Bare scale: 2 μ m, zoom scale: 200nm.

Table III.1. TEM and SEM result for the hydrogels and corresponding nanocomposites

Compounds	SEM	TEM
	Gel pore sizes [μ m]	AuNPs Diameter [nm]
P7	2.8 ± 0.9	-
TP7	1.4 ± 0.5	-
H4P7	0.5 ± 0.3	-
P7@Au	n.d.	13.7 ± 5.5
TP7@Au	0.6 ± 0.4	10.5 ± 2.4
H4P7@Au	0.11 ± 0.08	5.9 ± 2.1

2. Sol-gel transition

a. DSC

The nanocomposites sol-gel transition was firstly studied by DSC. The same experiment condition performed in the case of gel without NPs was applied for the nanocomposite ones (heating and cooling rate: 1°C/min), thermograms were shown in Figure III.4. Figure III.5 shows transition temperature as well as energies involved on heating and cooling processes of Au embedded gels. First observation shows a similar trend than the one observed for the gels without NPs: branched structures display higher transition temperatures. Nevertheless, the incorporation of Au NPs within the gel doesn't affect greatly the sol-gel transition temperatures. However, as shown in Table III.2, the variation of enthalpies involved in these transitions decreased when Au NPs were inserted in the gel structures (except for H4P7 when compared to free Au NPs hydrogels).

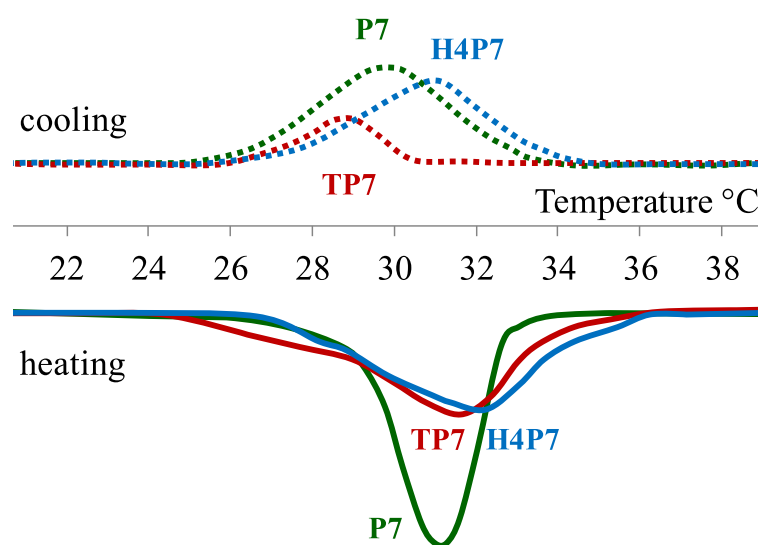


Figure III.4. DSC thermograms for Au embedded P7, TP7 and H4P7 gels recorded at $1^{\circ}\text{C}\cdot\text{min}^{-1}$ on heating (dashed line) and cooling (plain line). [polymer] = 20 wt.%

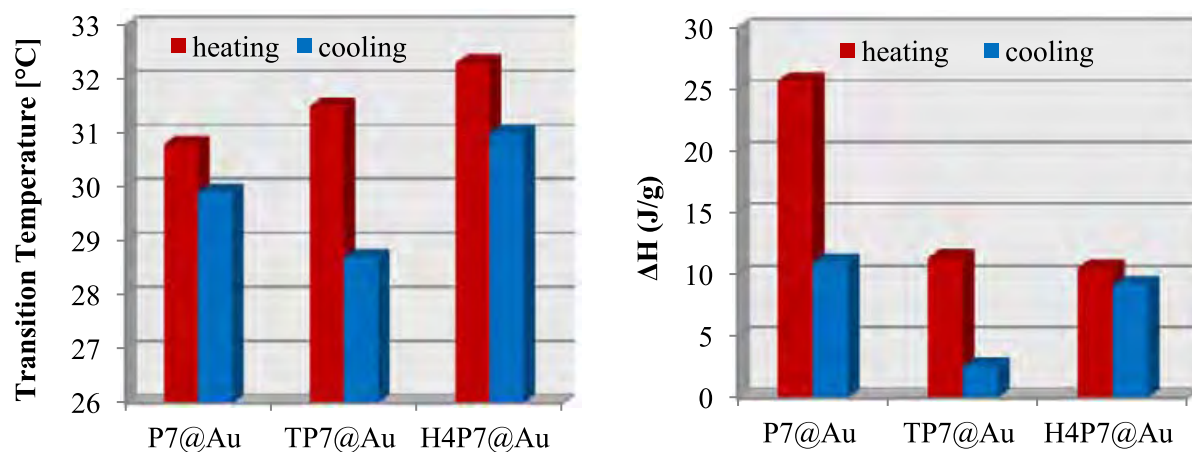


Figure III.5. Transition temperatures on heating and cooling at $1^{\circ}\text{C}/\text{min}$ of polymer gels P7, TP7, H4P7 at 20wt% with *in situ* synthesized gold nanoparticles (left). Energies involved in sol-gel transition on heating and cooling at $1^{\circ}\text{C}/\text{min}$ of polymer gel P7, TP7, H4P7 at 20wt% with *in situ* synthesized Au NPs (right).

Table III.2. DSC results of the hydrogels and corresponding nanocomposites

Compounds	DSC (1°C/min, [polymer] = 20wt. %)					
	ΔH [J/g]			T_c (°C)		
	heating	cooling	$\Delta(\Delta H)$	heating	cooling	ΔT
P7	30.9	2.4	28.5	29.3	28.7	0.6
TP7	14.6	3.6	11	31	28.8	2.2
H4P7	8.5	8.0	0.5	32.4	30.9	1.5
P7@Au	25.7	11	14.7	30.8	29.9	0.9
TP7@Au	11.4	2.6	8.8	31.5	28.7	2.8
H4P7@Au	10.6	9.2	1.4	32.3	31.0	1.3

b. *Rheological measurements*

Sol-gel transitions temperatures of these polymer-nanoparticles composites, extracted either from DSC or rheological measurements are found very similar from both techniques (Table III.2, Figure III.6). More pronounced differences have been previously observed from the two techniques for hydrogels without embedded NPs. These differences can reach up to 2.7°C (nearly 3°C) in the case of P7, both on heating or cooling cycles. A more efficient heat transfer thanks to the inclusion of NPs might be responsible for that lower discrepancy between the two techniques. Nevertheless, a strong hysteresis between heating and cooling transition (especially for TP7@Au) was still observed that depend once again on the microstructures of the considered hydrogels.

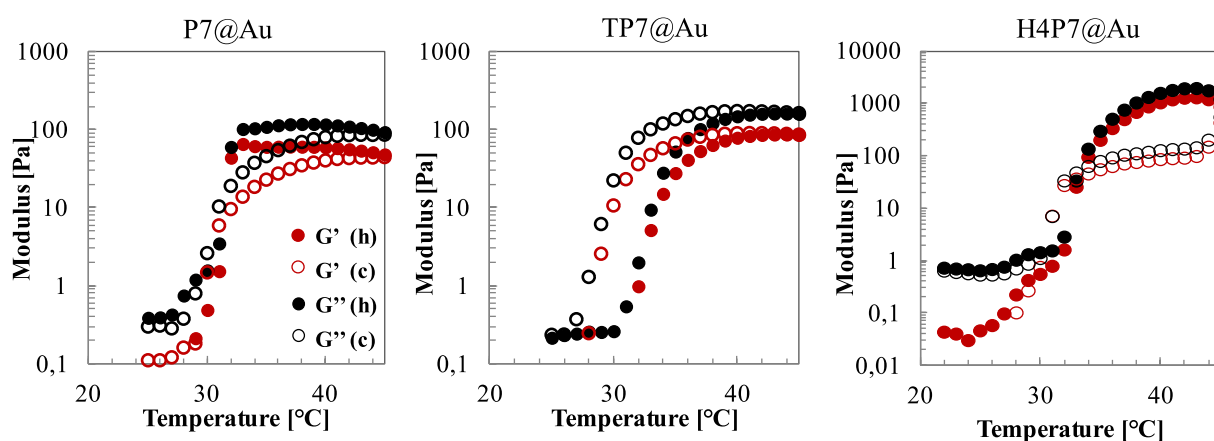


Figure III.6. Temperature- dependent storage and loss moduli of P7@Au (left), TP7@Au (middle), H4P7@Au (right) in 20wt% solution on heating (h) and cooling (c) at 1°C/min.

3. Gel strength

Gel strengths of hybrid gels were evaluated by rheological measurements. Higher moduli were observed for TP7@Au and H4P7@Au compared to the corresponding gels (Table III.2). This observation is consistent with SEM experiments. The increase is quite low for TP7, and much stronger for H4P7 (Figure III.6), which shows a much more pronounced increase in density of the network. From SEM images of P7@Au, showing a kind of filamentous deconstruction of the gel, we would expect a moduli decrease upon nanoparticles addition what is not the case, since the moduli increased also a bit. In all cases NPs acts as crosslinking agent and improved the stiffness of the gels as already observed in literature.[21], [22]

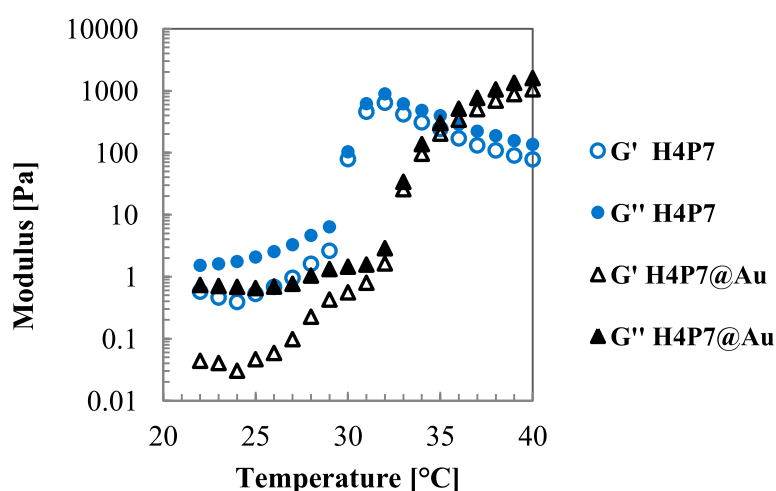


Figure III.7. Temperature-dependent storage and loss moduli of P7@Au (left), TP7@Au (middle), H4P7@Au (right) in 20wt% solution on heating and cooling at 1°C/min.

Table III.3. Rheology results of the hydrogels and corresponding nanocomposites

Compounds	Rheology (1°C/min, [polymer] = 20wt. %)			
	G' [Pa] 40°C on heating	G'' [Pa] 40°C heating	Tc (°C)	
			heating	cooling
P7	14	30	32	31
TP7	54	88	33	31
H4P7	78	135	30	29
P7@Au	60	117	31	31
TP7@Au	79	150	33	29
H4P7@Au	1050	1595	33	31

4. UV following of thermoreversibility

The thermoreversibility of the hybrid hydrogels was studied by monitoring the transition to the liquid state. For this, the turbidity of gels, preformed at 40°C and then placed at 25°C, was recorded as a function of time by following the transmittance at 720 nm (Figure III.8). This wavelength was chosen in order to avoid absorbance of Au NPs embedded in the hydrogels. Comparing to the gels without NPs, this experiment shows a noticeable difference in rehydration process (Figure III.8). The gels@Au took more time to return to the solution state. This result is in good correlation with conclusion from rheological and cryo-SEM results. NPs can act as cross linking agent and thus improved the stiffness of the gels and modified its responsiveness to temperature as already observed in literature.[21], [22]

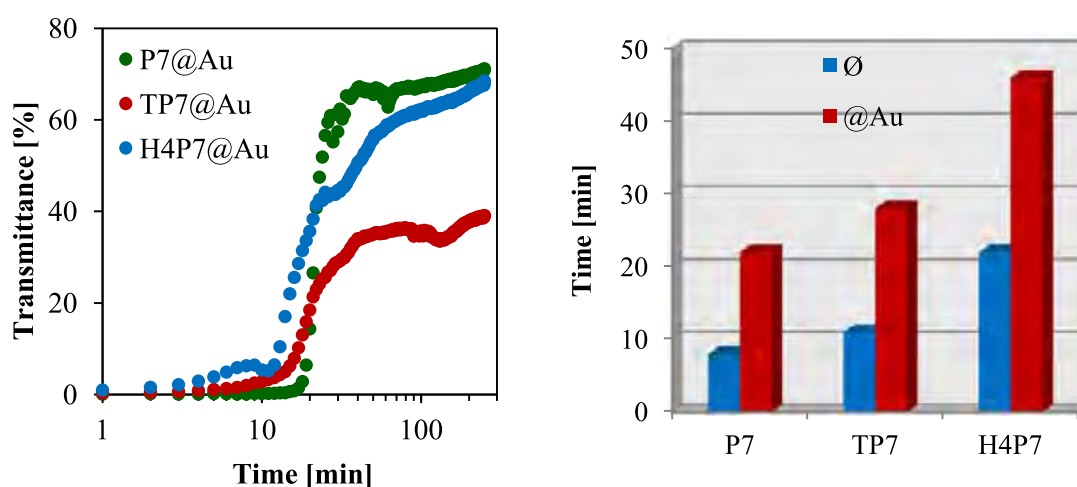


Figure III.8. Time-dependent turbidity at 25°C of 40°C preformed gels of TP7 at 20wt% with and without *in-situ* synthesized gold nanoparticles (left). Necessary time for the 40°C preformed gels (blue) and corresponding nanocomposites (red) to get to 90% of maximum transmittance value at 25°C (right).

IV. Conclusions

Thermoresponsive hydrogels have been successfully synthesized from core-shell hyperbranched polymers and PNIPAM. The molecular architecture of the polymer modulates the microscopic structure of hydrogel and therefore its thermoresponsive and rheological properties. These hydrogels were utilized for the *in situ* synthesis of well-defined gold nanoparticles. The presence of AuNPs within the gels acted as crosslinking points and improved its gelation properties. Those effects should be modulated by controlling the size/amount of AuNPs within the hydrogel.

Interestingly, the observation by TEM of nanocomposites obtained from hydrogels structures, led to the observation of some fractal structure as presented in Figure IV.1. Those structures were obtained from the deposits of a 5 time diluted solution of hydrogel (i.e. 4 wt.%) on a TEM grid. The observed structures may result from gel formation and instability

phenomenon occurring during the drying process on TEM grids and was only observed in presence of gold nanoparticles. More investigations to understand the driving forces responsible of such observation are under way.

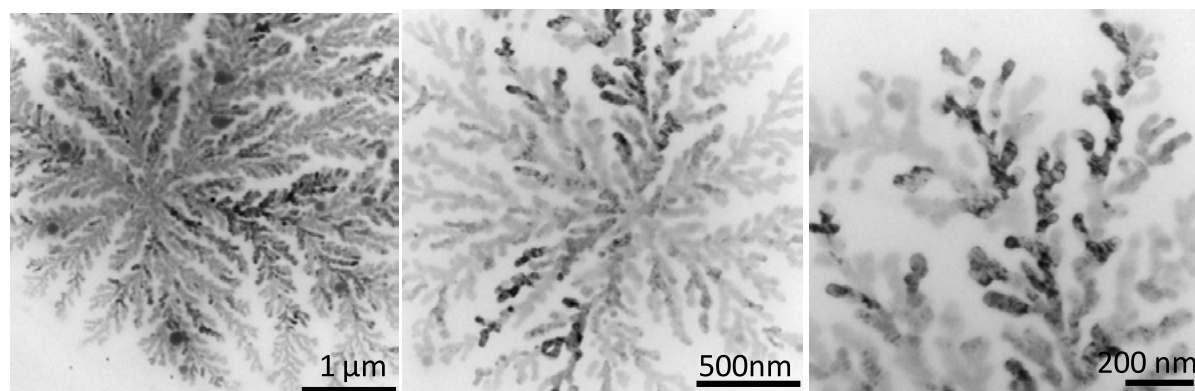


Figure IV.1. Images for TP7@Au after diluted 5 times in water and deposited on TEM grid.

V. References

1. Kawamura, A. & Miyata, T. in *Intelligent Stimuli-Responsive Materials* (ed. Li, Q.) 335–362 (John Wiley & Sons, Inc., 2013).
2. Sahiner, N. Soft and flexible hydrogel templates of different sizes and various functionalities for metal nanoparticle preparation and their use in catalysis. *Prog. Polym. Sci.* **38**, 1329–1356 (2013).
3. Beija, M., Marty, J.-D. & Destarac, M. Thermoresponsive poly(N-vinyl caprolactam)-coated gold nanoparticles: sharp reversible response and easy tunability. *Chem. Commun.* **47**, 2826–2828 (2011).
4. Lutz, J.-F., Akdemir, Ö. & Hoth, A. Point by Point Comparison of Two Thermosensitive Polymers Exhibiting a Similar LCST: Is the Age of Poly(NIPAM) Over? *J. Am. Chem. Soc.* **128**, 13046–13047 (2006).
5. Verdonck, B., Goethals, E. J. & Du Prez, F. E. Block Copolymers of Methyl Vinyl Ether and Isobutyl Vinyl Ether With Thermo-Adjustable Amphiphilic Properties. *Macromol. Chem. Phys.* **204**, 2090–2098 (2003).
6. Gan, L. H., Gan, Y. Y. & Deen, G. R. Poly(N-acryloyl-N'-propylpiperazine): A New Stimuli-Responsive Polymer. *Macromolecules* **33**, 7893–7897 (2000).
7. Hu, L. *et al.* Poly (N-isopropylacrylamide) microgel-based assemblies. *J. Polym. Sci. Part Polym. Chem.* **51**, 3004–3020 (2013).
8. Snowden, M. J., Chowdhry, B. Z., Vincent, B. & Morris, G. E. Colloidal copolymer microgels of N-isopropylacrylamide and acrylic acid: pH, ionic strength and temperature effects. *J. Chem. Soc. Faraday Trans.* **92**, 5013–5016 (1996).
9. Wu, X., Pelton, R. H., Hamielec, A. E., Woods, D. R. & McPhee, W. The kinetics of poly(N-isopropylacrylamide) microgel latex formation. *Colloid Polym. Sci.* **272**, 467–477 (1994).

10. Morris, G. E., Vincent, B. & Snowden, M. J. Adsorption of Lead Ions onto N-Isopropylacrylamide and Acrylic Acid Copolymer Microgels. *J. Colloid Interface Sci.* **190**, 198–205 (1997).
11. Dai, Z. & Ngai, T. Microgel particles: The structure-property relationships and their biomedical applications. *J. Polym. Sci. Part Polym. Chem.* **51**, 2995–3003 (2013).
12. Saunders, B. R. & Vincent, B. Microgel particles as model colloids: theory, properties and applications. *Adv. Colloid Interface Sci.* **80**, 1–25 (1999).
13. Gan, D. & Lyon, L. A. Tunable Swelling Kinetics in Core–Shell Hydrogel Nanoparticles. *J. Am. Chem. Soc.* **123**, 7511–7517 (2001).
14. Xia, L.-W. *et al.* Nano-structured smart hydrogels with rapid response and high elasticity. *Nat. Commun.* **4**, (2013).
15. Füllbrandt, M., Klitzing, R. von & Schönhals, A. Probing the phase transition of aqueous solutions of linear low molecular weight poly(N-isopropylacrylamide) by dielectric spectroscopy. *Soft Matter* **8**, 12116–12123 (2012).
16. Hocine, S., Li, M-H. Thermoresponsive self-assembled polymer colloids in water. *Soft Matter* **9**, 5839–5861 (2013).
17. Beija, M., Marty, J.-D. & Destarac, M. RAFT/MADIX polymers for the preparation of polymer/inorganic nanohybrids. *Prog. Polym. Sci.* **36**, 845–886 (2011).
18. Perignon, N. *et al.* Hyperbranched Polymers Analogous to PAMAM Dendrimers for the Formation and Stabilization of Gold Nanoparticles. *Macromol. Wash. DC U. S.* **40**, 3034–3041 (2007).
19. Zhao, M. & Crooks, R. M. Intradendrimer Exchange of Metal Nanoparticles. *Chem. Mater.* **11**, 3379–3385 (1999).
20. Moukarzel, W., Fitremann, J. & Marty, J.-D. Seed-less amino-sugar mediated synthesis of gold nanostars. *Nanoscale* **3**, 3285–3290 (2011).
21. Kar, T., Dutta, S. & Das, P. K. pH-Triggered conversion of soft nanocomposites: in situ synthesized AuNP-hydrogel to AuNP-organogel. *Soft Matter* **6**, 4777–4787 (2010).
22. Appel, E. A. & Scherman, O. A. Gluing gels: A nanoparticle solution. *Nat. Mater.* **13**, 231–232 (2014).

Chapter 4

**Mesomorphic Ionic Hyperbranched
Polymers:**

**Effect of Structural Parameters on Liquid-
Crystalline Properties and on the
Formation of Gold Nanohybrids**

CONTENTS

I. INTRODUCTION	167
II. SYNTHESIS AND CHARACTERIZATION OF THE HYPERBRANCHED-DODECYL SULFATE COMPLEXES	169
A. HYPERBRANCHED POLY(AMIDOAMINE).....	169
B. MESOMORPHIC IONIC HYPERBRANCHED POLYMERS.....	169
1. <i>Synthesis</i>	169
2. <i>Characterization of the interaction between the core and the shell</i>	170
a) Interaction between the core and the shells by FT-IR.....	170
b) Interaction between the core and the shells by ¹ H NMR and 1D NOE experiment.....	171
3. <i>Quantification of functionalization degree</i>	172
4. <i>Behavior in solution and formation of aggregates</i>	174
a) Behavior in solution.....	174
b) Formation of aggregates.....	178
III. THERMAL AND MESOMORPHIC PROPERTIES	180
A. STUDY OF THERMAL PROPERTIES BY DSC AND POM.....	180
1. <i>Experimental conditions of DSC measurements</i>	180
2. <i>Phase transitions</i>	181
B. PHASE IDENTIFICATION OF HYPAM-DS100	183
1. <i>POM-SAXS-DSC studies for H4-DS100</i>	183
2. <i>FT-IR</i>	186
3. <i>Conclusion</i>	187
C. EFFECT OF STRUCTURAL PARAMETERS.....	187
1. <i>Effect of the core molar mass</i>	187
2. <i>Hydrophilic/hydrophobic composition balance</i>	191
3. <i>Effect of the nature of the core: Dendrimer vs hyperbranched core</i>	192
D. CONCLUSIONS	193
IV. IN SITU FORMATION OF GOLD NPS	194
A. SYNTHESIS OF AUNPS IN LC MATRIX.....	194
1. <i>Interaction between HAuCl₄ and the core HYPAM</i>	194
2. <i>Synthesis process</i>	195
B. MESOMORPHIC PROPERTIES OF HYBRID MATERIALS OF H4-DS100@AUNPS	196
C. MORPHOLOGY OF THE <i>IN SITU</i> SYNTHESIZED AUNPS WITHIN MESOPHASES OF H4-DS100	199
D. THE EFFECT OF MOLECULAR ARCHITECTURE ON THE FORMATION OF GOLD NPS.....	201
V. CONCLUSIONS	204
VI. REFERENCES	205

I. Introduction

In recent years, tremendous research efforts to develop nanoscale organic/inorganic building blocks with well controlled morphology and to define efficient self-assembly protocols to get access to functional materials have been described in literature. In this context, intimate mixtures of liquid crystals (lyotropic or thermotropic) and nanoparticles have aroused great interest in the scientific community.[1-3] If most described studies involved the mixing of preformed nanoparticles (NPs) within liquid crystals, literature reveals particularly interesting attempts in synthesizing NPs within mesophases of liquid crystals.[2, 4] For instance, ZnSe nanomaterials have been synthesized in lyotropic systems based on amphiphilic triblock copolymers. Depending on the liquid crystalline state, quantum dots, nanodisks or even nanowires could be obtained.[5, 6] Nanoporous materials (generally silica) have also been fabricated via true liquid crystal templating.[7] Whereas the large majority of such research employs lyotropic liquid crystals, very few publications deal with the elaboration of nanomaterials within thermotropic ones.[8-15] Indeed, the development of an in situ procedure to generate NPs within a thermotropic liquid crystalline (LC) medium has proved to be quite a challenging task mainly due to diffusion hindrance of reactants in such medium. Most studies involve the in situ reduction of metal precursors via oxidation of the LC medium in order to obtain the desired NPs. For instance, the formation of CuCl nanostructures inside a mixture of an ionic liquid and a derivative of ascorbic acid has been reported.[13, 14] This resulted in the formation of CuCl nanoplatelets with a relatively uniform thickness of about 220 nm and in-plane sizes of 5-50 nm. Glass-forming liquid crystalline materials acting as a reducing agent were also used to obtain gold NPs whose size and shape depended on both the amount of precursor content and the LC state.[10] Isotropic NPs of gold or silver have also been synthesized by heating LC materials doped with the corresponding metal salts.[9] In other cases, sputtering[15] or electrodeposition[8] techniques were used to form NPs in thermotropic systems. Recently, we reported the use of a thermotropic liquid crystal branched and hyperbranched polymers obtained from the grafting of LC moiety on a branched core for such a purpose.[11, 12] To avoid disruption of the liquid crystalline mesophase during NPs formation, this approach involves the in situ hydrolysis of dicyclohexylzinc, [Zn(Cy₂)] leading to ZnO NPs with volatile cyclohexane as the only side product.[16] We demonstrated a direct correlation between the structural characteristics of the LC, the type of organization implicated during NPs synthesis and the morphology of the nanostructures obtained. Whereas in isotropic conditions only isotropic NPs were obtained, experiments performed in the nematic phase state of the LC compound led to the formation of anisotropic ZnO structures.[11, 12] Thus, nano-worm-like or nano-wire structures were grown in branched .[11] and hyperbranched liquid crystals.[10]

Mesomorphic dendritic polymers appear thus as good candidates for the synthesis of nanohybrids. Moreover, interactions of the organic structure with metal precursor appear as a key parameter to control their morphology. In this context, the use of LC branched polymer exhibiting an ionic part could be of special interest to study the effect of the mesophase nature on the NPs growth. Indeed, these ionic structures will facilitate interactions with ionic metal precursor and thus will insure the homogeneity of hybrid materials. In the past few years, LC dendritic structures made of components interacting by means of ionic interactions have attracted great interest: they do not necessitate tedious synthetic procedures like

dendritic structures obtained by means of covalent bonds between a dendritic core and a LC group. In addition, the nature of the external functional group can be easily tuned. This strategy has been well described in the case of amine-terminated dendritic structures complexed with different carboxylic acids exhibiting or not LC properties. [17-30] Ionic LC dendrimers based on polyethyleneimine (PEI), [25, 29, 30] poly(propylene imine) (PPI) [18, 20-22, 24, 26-28] and poly(amidoamine) (PAMAM) [17, 19, 23, 25] dendrimers have been especially studied. They exhibited mesophases of different nature depending mainly on the generation and chemical nature of the hyperbranched core and on the structure of the alkyl chain of the carboxylic acid (number of alkyl chain per acid or introduction of fluorinated moieties). Smectic A or square and hexagonal columnar mesophases were thus observed. These specific mesomorphic organizations could induce specific diffusion phenomena that could be taken into account to modulate NPs growth mechanism. If most of those studies focused on the use of well-defined dendrimers cores, ionic LC hyperbranched structures have not been thoroughly studied. [25, 31, 32]

In this chapter, in a first part, the synthesis of a new family of thermotropic dendritic polymers comprising a hyperbranched polyamidoamine core HYPAM [33, 34] and a dodecylsulfate-based shell based on non-covalent concept is described. The liquid crystalline properties of these core-shell architectures are thoroughly investigated by means of polarizing optical microscopy (POM), differential scanning calorimetry (DSC), and small-angle X-ray scattering (SAXS). The relationship between the structural characteristics of the polymers (size of the hyperbranched core, hyperbranched or dendritic nature of the core, substitution ratio) and the mesomorphic properties were closely investigated. Organizations as large aggregates in aqueous solutions of those polymers obtained from dilution of mesomorphic structures were also evidenced. In a second part, we highlighted how those thermotropic structures comprising ionic counterpart can be taken in account to interact in a homogeneous way with ionic salts. Interestingly, diffusion of dihydrogene inside those mesomorphic structures allowed the *in situ* formation of gold NPs within the liquid-crystalline phase. The effect of polymer structure and organization on the morphology of gold nanoparticles is then evaluated.

II. Synthesis and characterization of the hyperbranched-dodecyl sulfate complexes

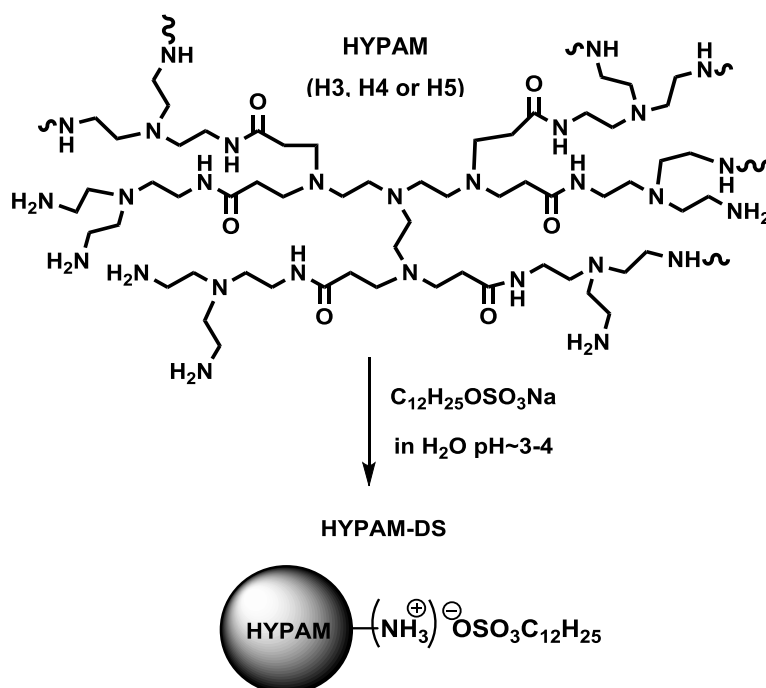
A. Hyperbranched poly(amidoamine)

Synthesis and characterization of hyperbranched polyamidoamine were already presented in chapter 2 will not be repeated here.

B. Mesomorphic Ionic Hyperbranched Polymers

1. Synthesis

Amino-terminated HYPAMs cores were mixed with dodecylsulfate (DS) moieties leading to the formation of HYPAM-DS complexes (Scheme II.1). For this, a dilute aqueous solution of sodium dodecylsulfate (SDS) was added to an aqueous solution of HYPAM at pH 3-4 adapting a procedure used by Canilho et al.[32] The complex was obtained as a precipitate and the excess of sodium chloride salt was removed by washing with water. The small excess of non-interacting DS ligands, evidenced by the presence of thin peaks in ^1H NMR in DMSO- D_8 , was removed by dissolution of the precipitate in DMSO followed by reprecipitation in acidic water.



Scheme II.1. Synthesis of ionic complex HYPAM and Dodecyl Sulfate

Hyperbranched polyamidoamines (H3, H4, H5) and TREN (tree branched molecule) were used for the synthesis of the complexes. In order to study the effect of the hydrophobic/hydrophilic composition balance on the LC properties of the complexes, the

proportion of DS in the complexes was also varied from 50, 75, 90, to 100% molar ratio with reference to the primary amine groups of the core. Those complexes were called Hx-DSy or TREN-DSy. In this expression, x refers to the generation of the core; y refers to the grafting ratio (in molar percents).

2. Characterization of the interaction between the core and the shell

The characterization of the interaction between the core and the shell as well as the quantification of the functionalization degree was then studied by FT-IR and $^1\text{H-NMR}$.

a) *Interaction between the core and the shells by FT-IR*

ATR-FTIR spectroscopy was used to confirm the interactions between HYPAM and DS moieties. This is illustrated on the FTIR spectrum of hyperbranched polyamidoamine H4 with a 100% grafting ratio of primary amine in Figure II.1 and at 25°C.

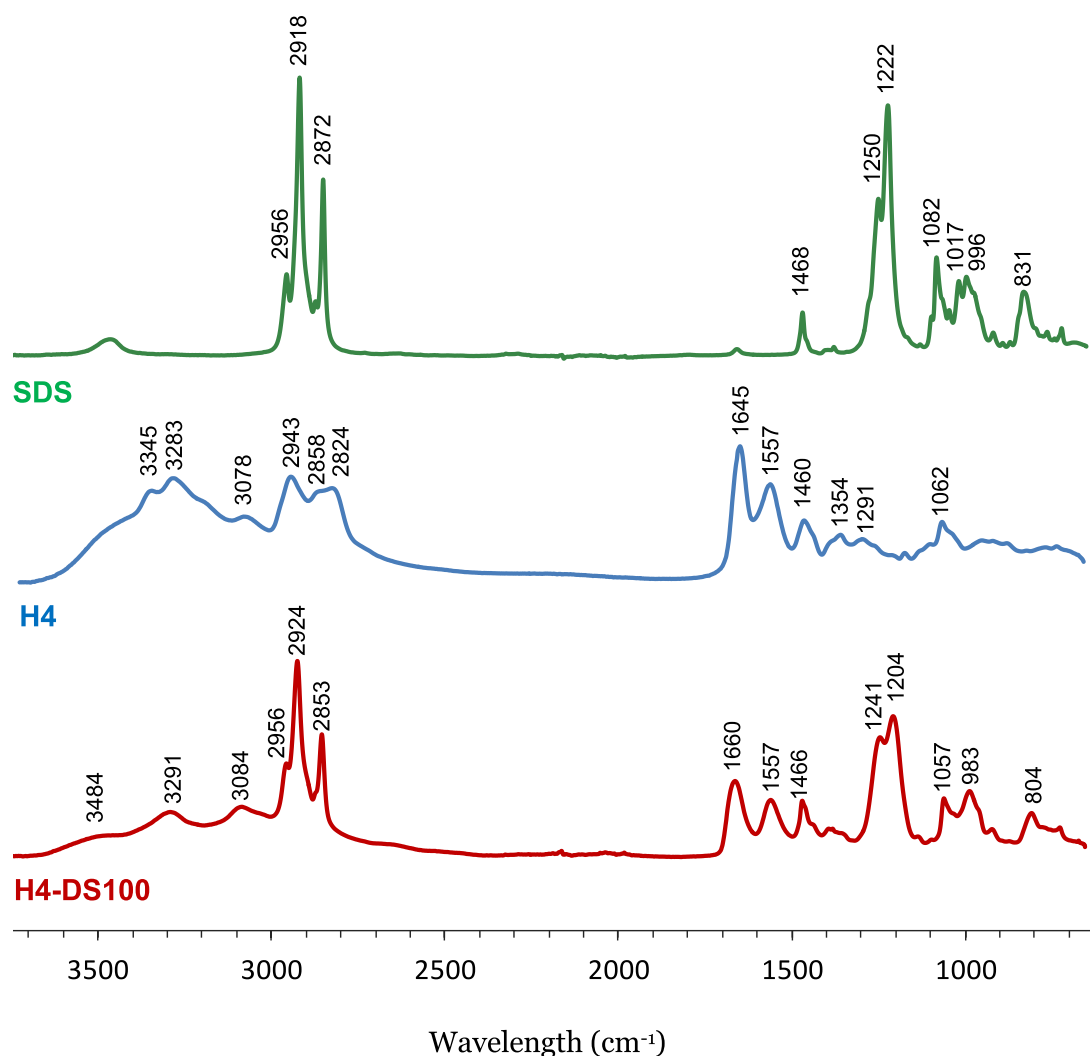


Figure II.1. ATR-FTIR spectra of SDS, H4, and H4-DS100.

The formation of the ionic complex was confirmed by the shift of the two S=O asymmetric stretching bands of sulfate group from 1250 cm⁻¹ and 1222 cm⁻¹ to 1241 cm⁻¹ and

1204 cm^{-1} respectively. In addition, the decrease in frequency of the symmetric S=O stretching band, from 1082 cm^{-1} to 1057 cm^{-1} can be interpreted as a change of counterion.[38] The vibration bands of amide I of HYPAM at 1645 cm^{-1} are also shifted to 1660 cm^{-1} in the complex.

b) *Interaction between the core and the shells by ^1H NMR and 1D NOE experiment*

As the complex was fully soluble in THF and CHCl_3 , while neither HYPAM nor SDS is soluble in these two solvents, is in favor of complex formation. The existence of interactions between HYPAM and DS moieties was further evidenced by NMR techniques. A broadening of the signals corresponding to DS was observed on the ^1H NMR spectrum of H4-DS100 in CDCl_3 (Figure II.2 a). This was expected for DS in strong interaction with a macromolecule.

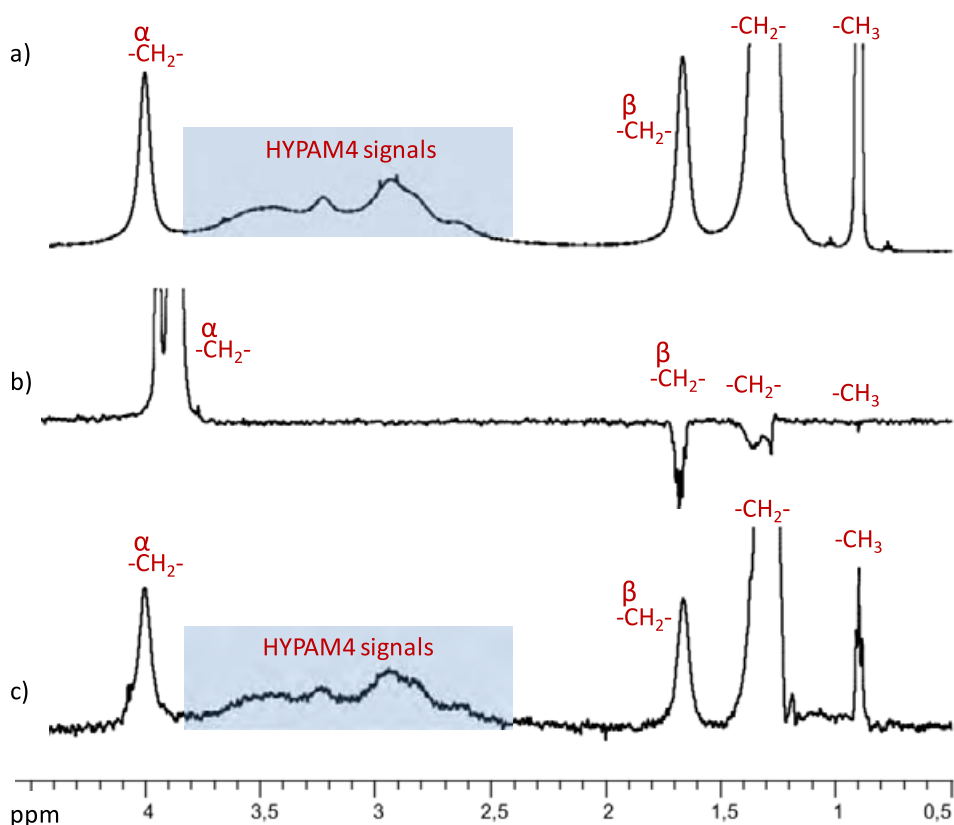


Figure II.2. a) ^1H NMR spectrum of H4-DS100 in CHCl_3 ; b) and c) Selective 1D ^1H NOESY experiment with dodecyl sulphuric acid and H4-DS100 respectively in CDCl_3 after selective excitation of methylene group in α position of sulfate function (NOE mixing time : 800 ms).

To confirm this, a 1D NOE NMR experiment was performed by selectively irradiating the methylene protons in the α position of the sulfate function of DS (Figure II.3). A negative NOE effect was observed on both protons of the HYPAM core and the DS hydrophobic chain (Figure II.2 c). A control experiment was performed on acidified SDS (Figure II.2 b) (as mentioned before, SDS is not soluble in CHCl_3). In this case, a positive NOE effect on the

vicinal protons was observed. This confirmed the strong interaction of HYPAM with DS. Indeed, macromolecules like HYPAM exhibit negative NOE effect with a fast build-up rate, while low-molecular weight DS has positive NOE signals with a slow build-up rate. When DS binds to HYPAM, it gains motional correction time of the macromolecules, thus developing a negative NOE in the bound state. This negative intramolecular trNOE signals of DS indicates that those chains are in interaction with HYPAM core. This was confirmed by the presence of negative trNOE signals for the protons characteristic of the HYPAM core. The long mixing times used here (800 ms) generate pseudo-cross-peaks attributed to spin diffusion and magnetization transfer and thus explain the appearance of such an effect for all protons of the core. From both FTIR results in bulk and NMR experiments in solution an interaction may be assumed between HYPAM and DS chains. Those interactions likely arise from ionic interactions between sulfate group and protonated amine groups of the HYPAM hyperbranched core.[32]

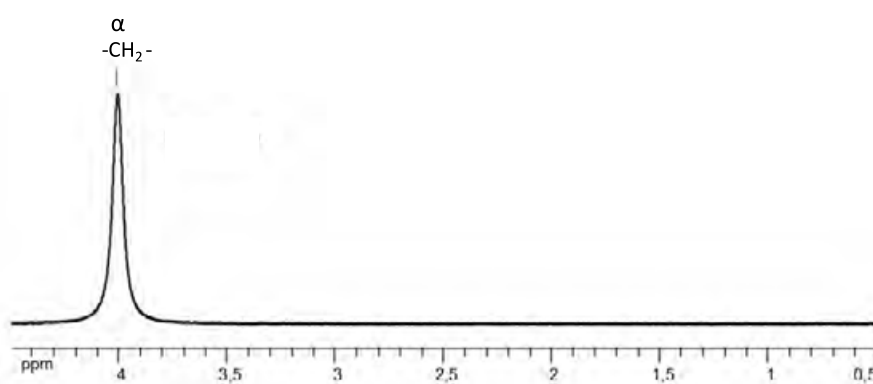


Figure II.3. 1D ¹H NOESY experiment with H4-DS100 in CDCl₃: selective excitation of methylene group in α position of sulfate function (NOE mixing time : 800 ms).

3. Quantification of functionalization degree

In order to study the influence of structural parameters on the mesomorphic behavior, different level of functionalization of amine groups of H4 by DS were studied. For this, four different molar ratios of primary amine/sulfate groups were used: 1:1, 1:0.90, 1:0.75 and 1:0.5 leading to the formation of H4-DS100, H4-DS90, H4-DS75 and H4-DS50 respectively. ATR-FTIR spectroscopy was used to quantify the HYPAM/DS proportions. Indeed, this molar ratio is proportional to the ratio of the intensity of the amide I band (1660 cm⁻¹) to the intensity of the sulfate stretching bands (1204 cm⁻¹). A calibration curve was obtained by measuring this ratio on spectra of the simple mixtures (without interaction) of HYPAM and SDS, for which the molar ratio of primary amine groups of HYPAM and SDS was varied from 1:1 to 1:0.5 (Figure II.4). Results are reported in Table II.1.

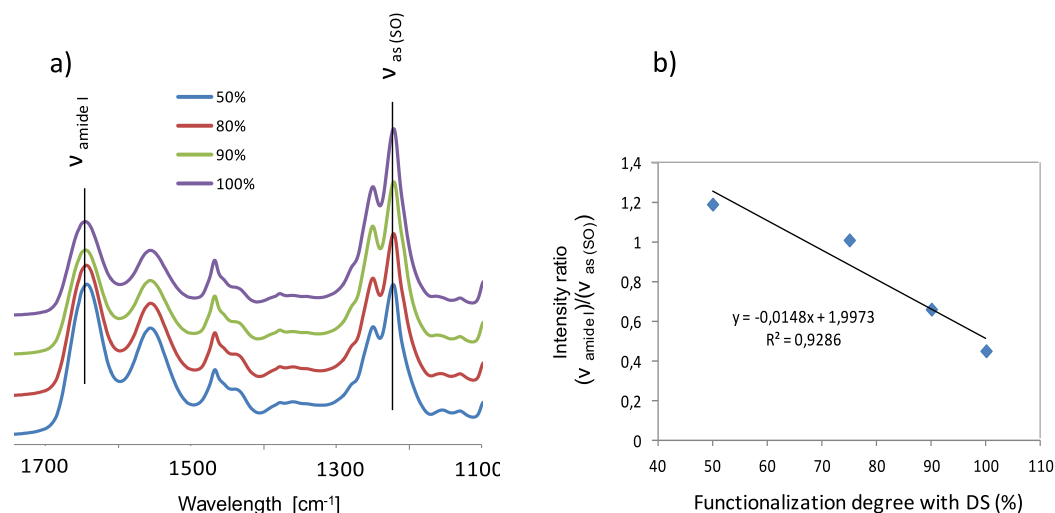


Figure II.4. Quantification of functionalization degree by indirect FT-IR method. a) spectra of physical mixtures of H4 and DS; b) calibration curve.

Table II.1. Quantification of functionalization degree by indirect FT-IR method

Compounds	DS/NH ₂ molar ratio [%]
H ₃ -DS ₁₀₀	100 ^b
H ₄ -DS ₁₀₀	97 ^a
H ₅ -DS ₁₀₀	100 ^b
PAMAM ₄ -DS ₁₀₀	99 ^a
PAMAM ₅ -DS ₁₀₀	100 ^b
H ₄ -DS ₅₀	51 ^a
H ₄ -DS ₇₅	82 ^a
H ₄ -DS ₉₀	95 ^a
PAMAM ₄ -DS ₉₀	89 ^a
PAMAM ₅ -DS ₉₀	90 ^b

^a estimated from FT-IR measurements (standard deviation ± 2), ^b estimated from experimental conditions.

A good agreement with theoretical expected values was observed for all studied compounds. Complexes obtained with hyperbranched HYPAM of different molar masses (H₃ or H₅) or with the corresponding perfectly defined PAMAM dendrimers were also synthesized with two targeted degree of functionalization: 90 and 100% (Table II.1) with also a good agreement with theoretical values.

4. Behavior in solution and formation of aggregates

a) *Behavior in solution*

Due to their hydrophobic shell, the studied complexes were not soluble in water and were only soluble in a very limited range of solvent (THF, chloroform, DMSO but not alkanes). As expected, the nature of solvent can dramatically affect the strength of interactions between the core and the shell. To characterize this effect and the aggregation phenomenon, we performed NMR and DLS studies in those solvents. Depending on the nature of solvent and its dissociative properties, these complexes presented different kinetics of dissociation as demonstrated by ^1H NMR. Hence, whereas in THF-d8 HYPAM the core is barely visible around 3 ppm, both peaks from HYPAM and DS appear as large peaks in CDCl_3 or DMSO-d6 (Figure II.5) suggesting a different exchange mechanism in each case. NOE transfer experiments demonstrated the interactions of DS ligands with HYPAM in CDCl_3 . Nevertheless, based on DOSY experiments, a faster exchange mechanism may be assumed in the case of DMSO.

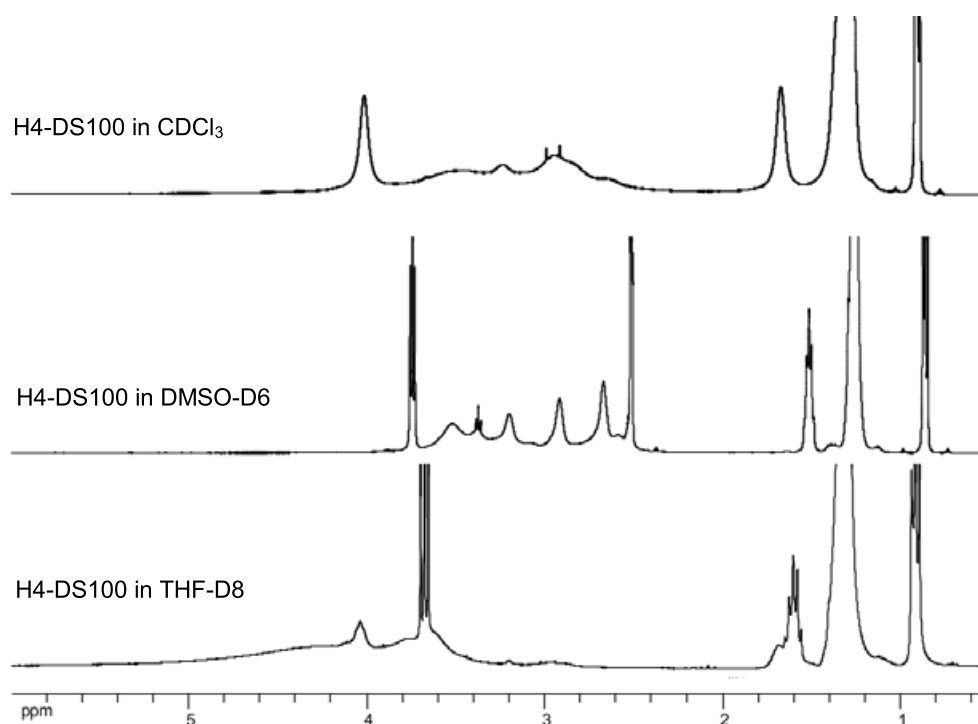


Figure II.5. ^1H NMR spectra of H4-DS100 in CDCl_3 , DMSO-d6 and THF-d8 (500 MHz)

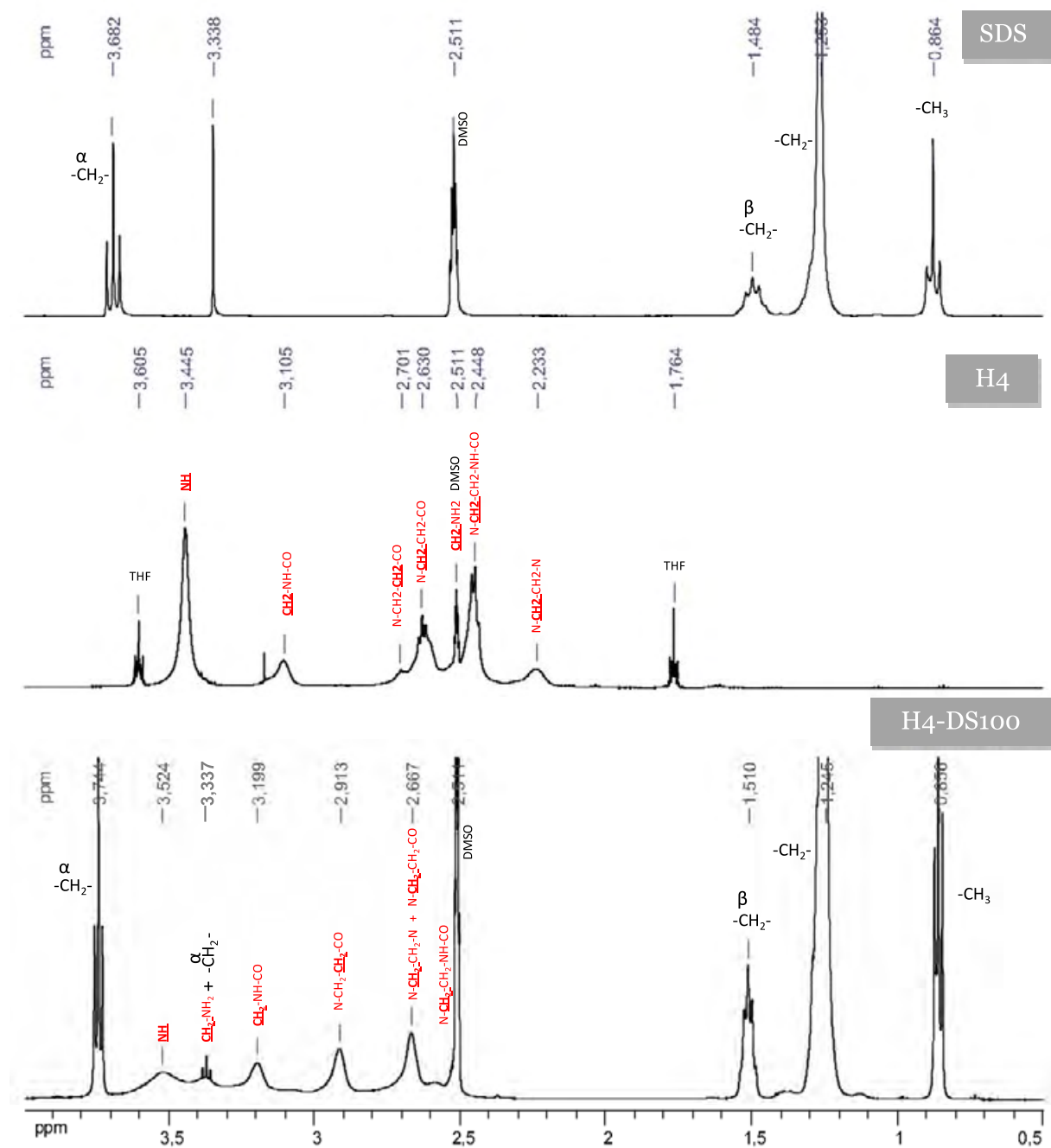


Figure II.6. ^1H NMR spectra of SDS, H4 and H4-DS100 (500 MHz, DMSO- d_6 , 308K)

The attribution of the peaks was carried out by one-dimensional ^1H and ^{13}C NMR and two-dimensional ^1H - ^1H COSY, ^1H - ^{13}C HSQC experiments (Figures II.6-7-8-9). A greater shift of the proton signal at 2.51 ppm to 3.37 ppm corresponding to the protonation of the primary amine in CH_2NH_2 group was observed. The shift from 2.24 ppm to 2.66 ppm of the signal of the methylene in the α position of tertiary amines ($\text{NCH}_2\text{CH}_2\text{NH}_2$) revealed that tertiary amines were also protonated. The chemical shifts for the other protons are weakly modified in H4 and in its corresponding complexes.

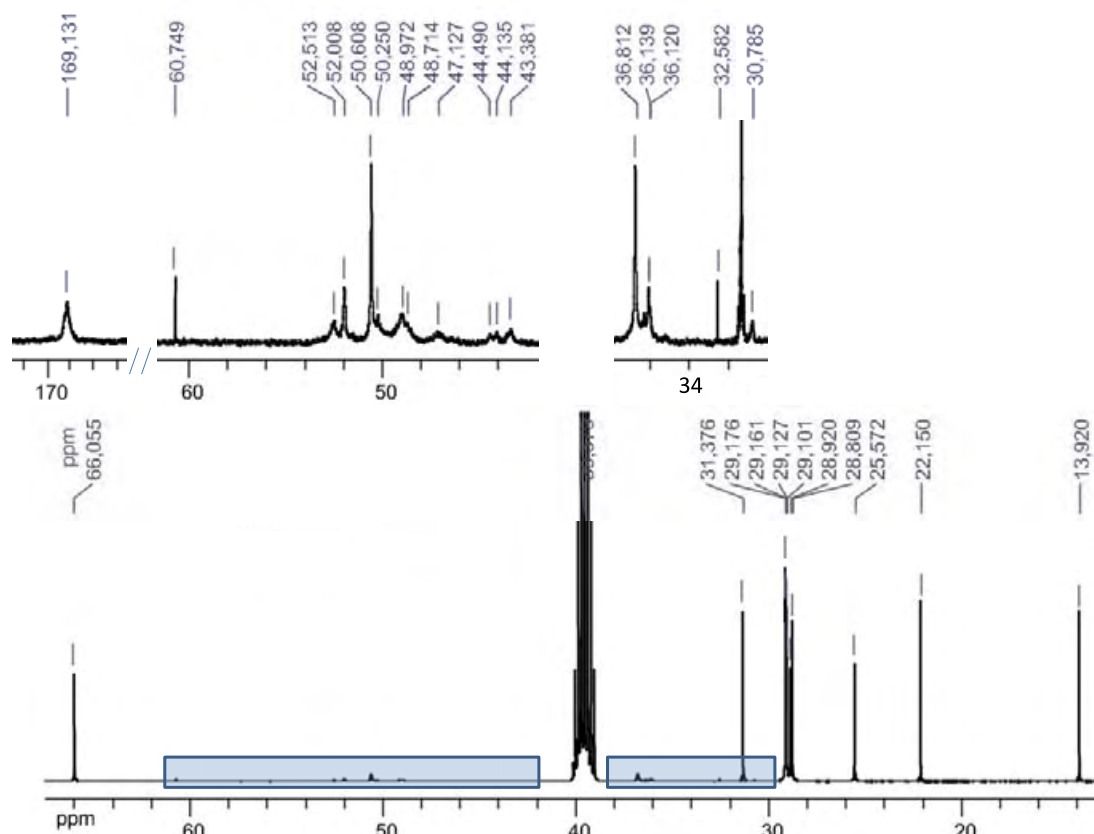


Figure II.7. ^{13}C NMR spectrum of H4-DS100 (500 MHz, DMSO- d_6 , 308K)

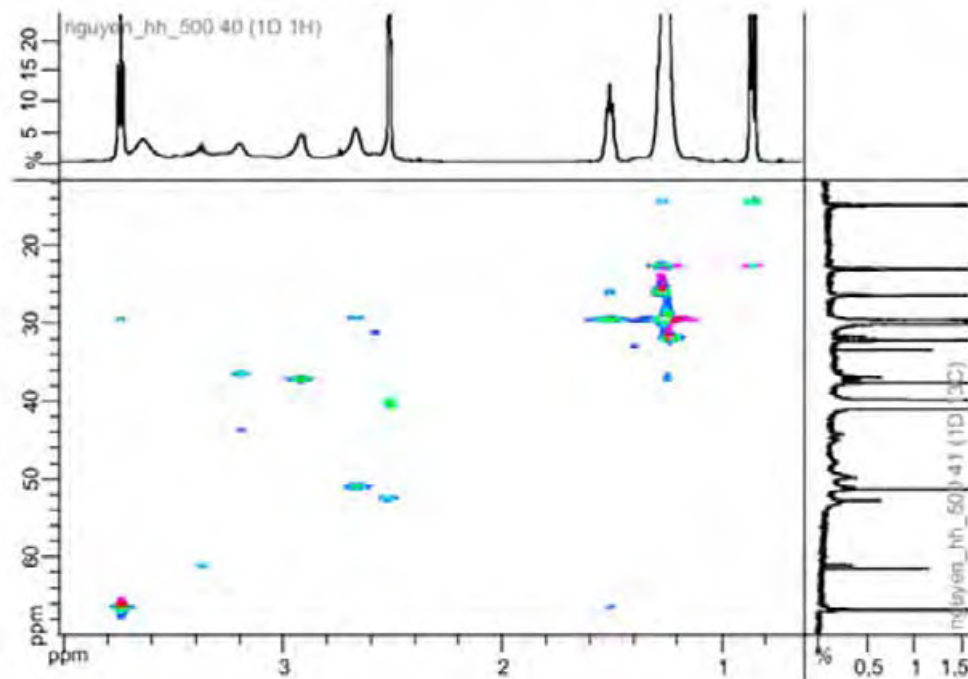


Figure II.8. HSQC-NMR spectrum of H4-DS100 (500 MHz, DMSO- d_6 , 308K)

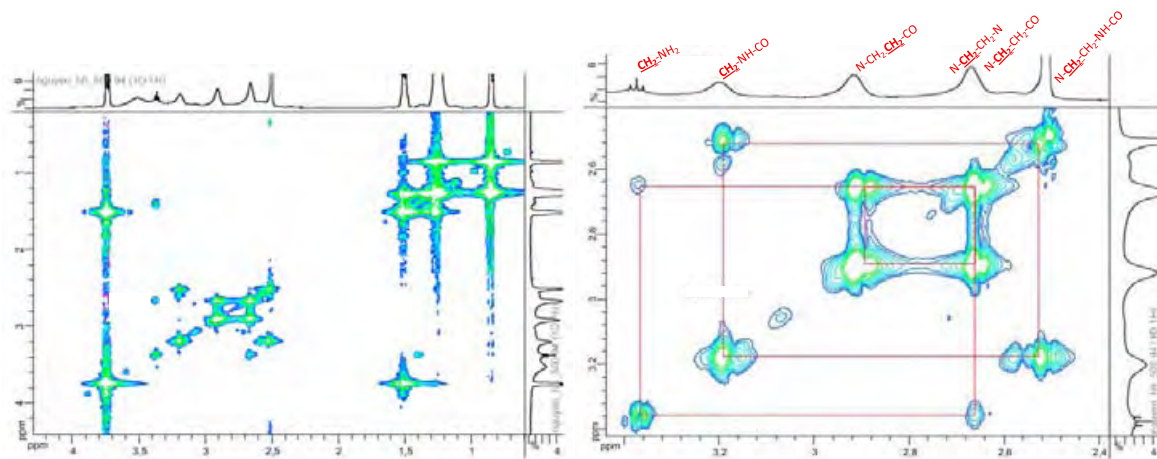


Figure II.9. COSY-NMR spectrum of H4-DS100 (500 MHz, DMSO-d₆, 308K)

In addition, self-diffusion coefficients of H₄, H₄-DS100 and SDS were evaluated in DMSO solution at 308 K using the Pulsed-Gradient Spin-Echo (PGSE) NMR technique (Figure II.10).

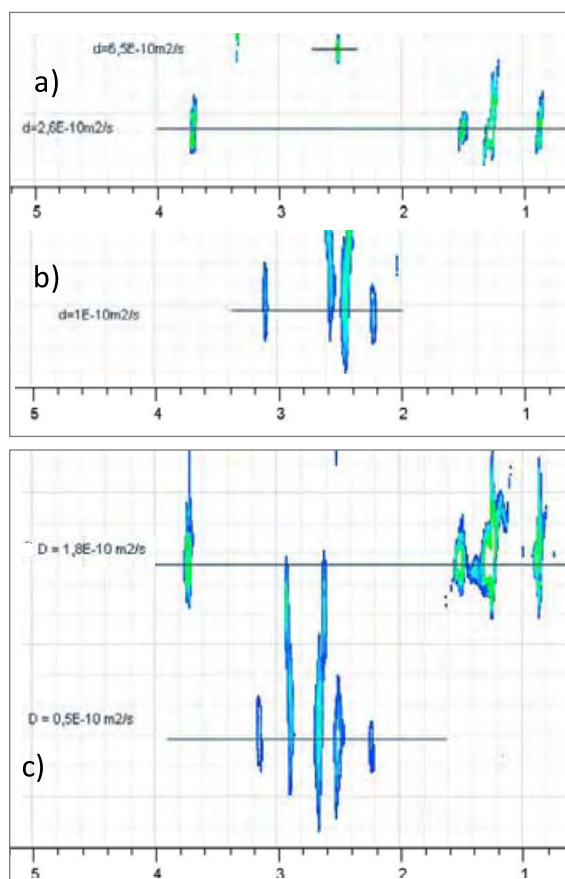


Figure II.10. PGSE-NMR spectra of SDS (a) H₄ (b) and H₄DS100 (c) in DMSO at 308K with evaluated diffusion coefficients

The obtained results are summarized in Table II.2. Due to the large difference of hydrodynamic volume, H4 and SDS species exhibit a great difference in diffusion coefficients (10^{-10} and $2.6 \cdot 10^{-10} \text{ m}^2 \cdot \text{s}^{-1}$ respectively). In the case of H4-DS100 complex, two diffusion peaks were observed with smaller diffusion constants than for DS and H4 taken separately. This confirmed the formation of a complex with fast exchange mechanism in DMSO with respect to the time scale of diffusion ($d_{20}=120\text{ms}$). Indeed only one diffusion coefficient was observed when PGSE NMR analysis was performed in THF-d8 which is a less dissociative solvent. From these values, the hydrodynamic radius (R_h) of the different components was calculated by means of the Stokes-Einstein equation. Both values were reported in Table II.2.

Table II.2. Self-diffusion coefficients and hydrodynamic radius (R_h) of SDS, H4 and H4-DS100 obtained by PGSE NMR and DLS.

<i>Compounds</i>	<i>Diffusion coefficient ($\text{m}^2 \cdot \text{s}^{-1}$)</i>	<i>R_h (nm) PGSE NMR</i>
<i>SDS^a</i>	<i>$2.6 \cdot 10^{-10}$</i>	<i>0.5</i>
<i>H4^a</i>	<i>$1 \cdot 10^{-10}$</i>	<i>1.4</i>
<i>H4-DS100^a</i>	<i>$0.5 \cdot 10^{-10}$ $1.8 \cdot 10^{-10}$</i>	<i>n.d.^d</i>
<i>H4-DS100^b</i>	<i>$1.1 \cdot 10^{-10}$</i>	<i>4.3</i>
<i>DMSO^c</i>	<i>$6.5 \cdot 10^{-10}$</i>	

a measured in DMSO (0.1 wt% polymer solution); b measured in THF (0.1 wt% polymer solution); c measured in DMSO or THF; d Ionic complex cannot be isolated in DMSO, thus R_h were not calculated in this solvent

b) **Formation of aggregates**

The amphiphilic structures of those ionic complexes may lead to the formation of structured aggregates in solution. Hence, JL Serrano and coll. have previously observed the formation of spherical aggregates from hyperbranched mesomorphic structures favored by the pristine liquid crystalline organization.^[23] To prepare aggregates, H4-DS100 was dissolved in a good solvent DMSO at a concentration of 0.5 wt%. As shown above, by NMR measurements, H4-DS complexes are soluble in those conditions and a rearrangement of ligand is still possible while preserving ionic interactions. Milli-Q water, which was a poor solvent, was then added very slowly ($\sim 10 \mu\text{L} \cdot \text{min}^{-1}$) to the complex solution in DMSO (1.5 mL) with slight shaking (final volume water content around 25%). The nature of the formed aggregates was examined by transmission electron microscopy (TEM) with negative staining. Those objects with approximately spherical shape around 200nm of diameter were obtained as shown in Figure II.11. As described in literature, these structures may arise from a lamellar organization where hydrophobic aliphatic chains are wrapped by the hydrophilic dendrimer core forming well-packed layers in which all the alkyl chains are oriented parallel to each other.

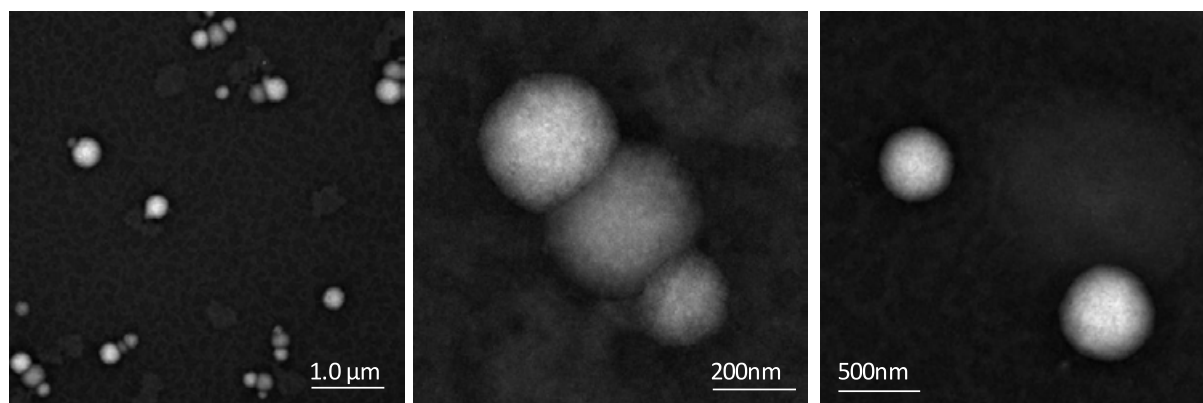


Figure II.11. Representative TEM images of H4-DS100 samples stained with uranyl acetate of nanoobjects obtained in DMSO/water 3/1 v/v solution.

III. Thermal and mesomorphic properties

As discussed in the previous section, the dendritic ionic complexes can form spherical aggregates in solutions. In this section we investigated the self-assembly of this ionic complex in absence of solvent, in other words, their liquid crystal properties. The mesomorphic behaviour of the dendritic complexes was studied by Differential Scanning Calorimetry (DSC), Polarizing Optical Microscopy (POM) and Small Angle X-ray Scattering (SAXS) experiments.

A. Study of thermal properties by DSC and POM

1. Experimental conditions of DSC measurements

The thermograms for each HYPAM and each PNIPAM complexes were recorded on heating and cooling rates of 10, 5 and 2°C/min. Typical thermograms obtained on heating and cooling at 10°C/min are given in Figure III.1. The thermogram in heating mode exhibits two endothermic transitions. The first one at T_1 is associated with a high variation of enthalpy and the second one at T_2 is less energetic transition.

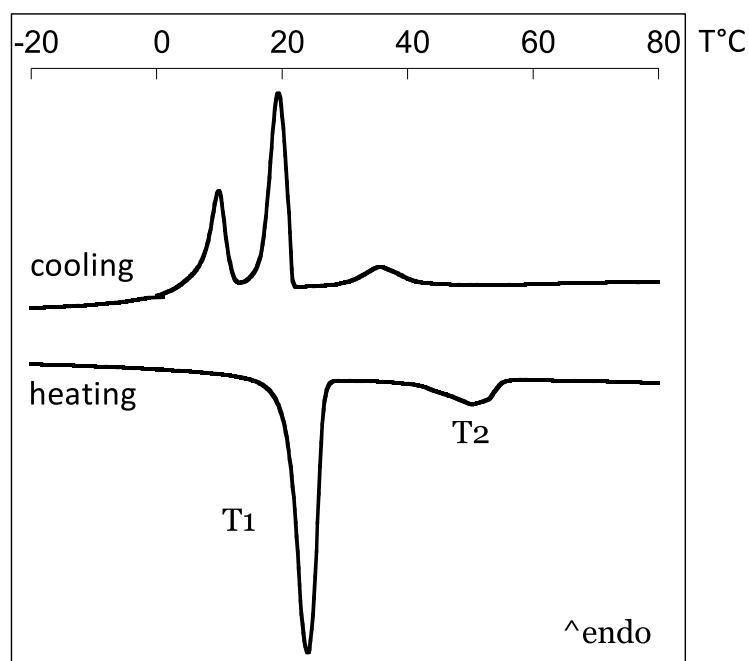


Figure III.1. DSC thermogram recorded for H4-DS100 at heating and cooling rate of 10°C/min

Obviously, there are differences between the curves on heating and on cooling. On cooling process, there is a shift of the transitions to lower temperatures. This can be explained firstly by looking at the molecular shape of the molecules. The compound is a macromolecule which is composed of a highly polydisperse hyperbranched core and dodecylsulfate shell. So the probability that the molecules are oriented the way they need to be in order to build a phase of a certain order is much lower than in the case of a small

flexible molecule. Due to this fact it takes more time and therefore cooling to lower temperatures than in the heating curve, where molecular ordering is broken up. In another words, the metastable state of the materials on cooling process resulted in a different thermal history compare to the heating process.

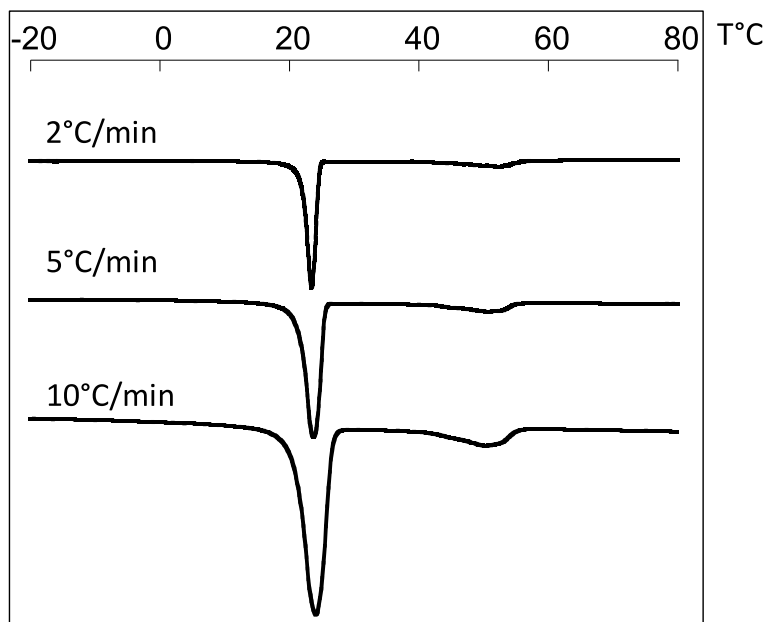


Figure III.2. DSC thermograms recorded for H4-DS100 at heating rate of 10°C/min, 5°C/min and 2°C/min.

Besides, these differences can also resulted from the different heating and cooling rates, especially at high heating and cooling rate. In order to avoid these problems and gain accurate results, we perform the measurement at three rates (2, 5, 10°C/min) and extrapolate the transition temperature to zero speed (Figure III.2). All transition temperatures and associated enthalpies are summarized in Table III.1.

2. Phase transitions

For almost all complexes, glass transition temperature is barely or not visible. This may be ascribed to the high level of ordered structure of those complexes. This ordered structure is responsible of a first transition peak (at T_1) associated with a high variation of enthalpy and arises from the association of hydrophobic fatty chains.[32] Additionally, for most of the dendritic structures, a second but less energetic transition is visible in the thermograms (T_2). (see Table III.1 and Figure III. 1-2-7-10-11)

Birefringent and different textures were observed by POM below T_1 and between T_1 and T_2 after which the material starts losing its birefringence suggesting the existence of two different liquid crystalline organizations of the studied materials (Figure III.3-4-8-9). While no pre-mesogenic moiety is present in the polymer complexes, LC properties arise from a molecular segregation phenomenon between hydrophobic chains and the hydrophilic or ionic part of the complexes.[23] This segregation necessitates a hydrophilic core of sufficient molar mass: thus ionic complexes between tris(2-aminoethyl)amine and DS does not exhibit mesomorphic properties (Figure III.7). The nature of the mesophases below T_1 and between

T_1 and T_2 were further identified by SAXS

Table III.1. Thermal characteristics of the different complexes determined by DSC measurements (values extrapolated to 0°C/min heating rate).

<i>Compounds</i>	<i>LC</i>		<i>LC</i>		<i>I</i>
	T_1 [°C]	(ΔH_1) [J/g]	T_2 [°C]	(ΔH_2) [J/g]	
<i>H3-DS100</i>	• 28.3	(17)	• 50.3	(0.6)	•
<i>H4-DS100</i>	• 23.5	(26)	• 48.8	(3.8)	•
<i>H5-DS100</i>	• 23.5	(20)	• 50.9	(4.0)	•
<i>PAMAM4-DS100</i>	• 24.0	(28)	• 47.2	(1.9)	•
<i>PAMAM5-DS100</i>	• 25.8	(24)	• 50.2	(2.3)	•
<i>H4-DS50</i>	-	-	-	-	-
<i>H4-DS75</i>	• 45.1	(15)	• 65.6	(1.3)	•
<i>H4-DS90</i>	• 23.3	(22)	• 52.5	(3.9)	•
<i>PAMAM4-DS90</i>	• 24.2	(24)	• 50.5	(2.8)	•
<i>PAMAM5-DS90</i>	• 24.5	(28)	• 48.7	(1.9)	•

B. Phase identification of HYPAM-DS100

1. POM-SAXS-DSC studies for H4-DS100

Hence, H4-DS100 displayed two transition temperatures at $T=23.5\text{ }^{\circ}\text{C}$ and $48.8\text{ }^{\circ}\text{C}$ with an associated variation of enthalpy of 26 J/g and 3.8 J/g respectively (Figure III.3 and Table III.1). By POM observation, characteristic textures of columnar (below T_1) and lamellar mesophases (between T_1 and T_2) were identified.

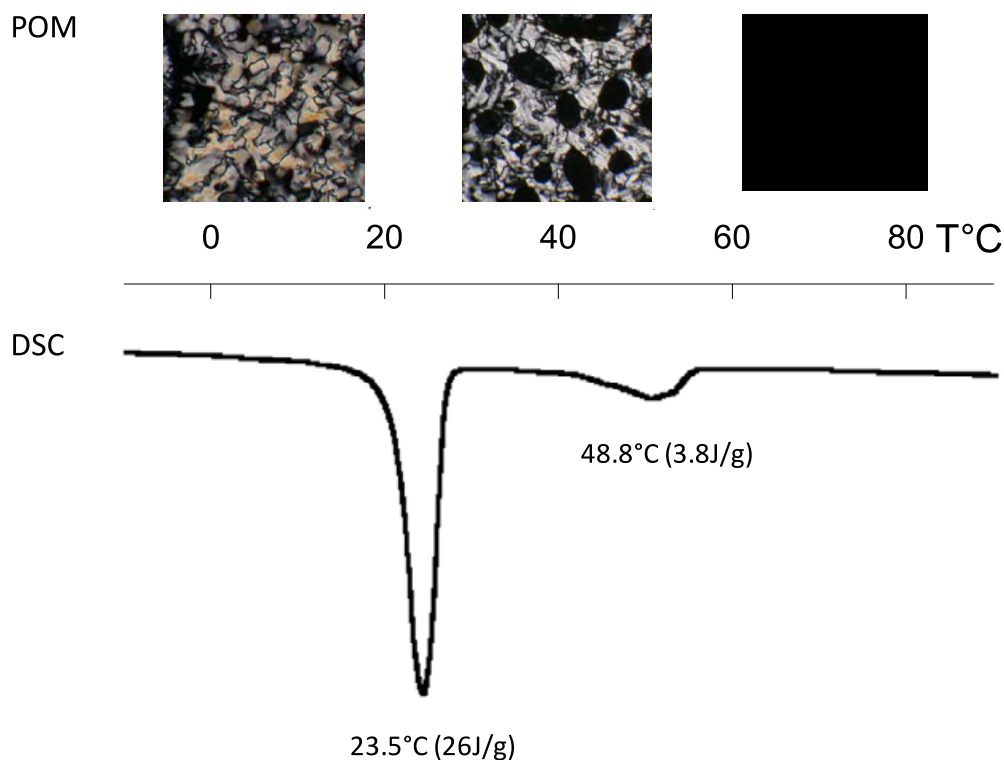


Figure III.3. POM images for H4-DS100 at $20\text{ }^{\circ}\text{C}$, $40\text{ }^{\circ}\text{C}$ and $65\text{ }^{\circ}\text{C}$ (top); DSC thermogram recorded for H4-DS100 at heating rate of $10\text{ }^{\circ}\text{C}/\text{min}$ (bottom).

The nature of these mesophases was clearly confirmed by SAXS measurements (Figure III.4). At temperatures lower than the first transition peak (i.e. $20\text{ }^{\circ}\text{C}$), peaks at 1.45 and 1.80 nm^{-1} appeared on the radial averaged diffraction intensity profile extracted from the 2D SAXS diffraction pattern (Figure III.4 a). Those peaks could be ascribed to a rectangular columnar mesophase with C_{2mm} planar space group (Col_r, C_{2mm}) and with lattice constants $a = 7.0\text{ nm}$ and $b = 5.3\text{ nm}$ (see Figure III.4 a). The formation of such mesophase was previously observed by J.L. Serrano et al. for PAMAM derivative dendrimers.[23, 39] An arrangement for which the molecules are located at the centre and at the corners of the unit cell in such a way that the hydrocarbon chains segregate in layers could be proposed for this structure (Scheme III.1).

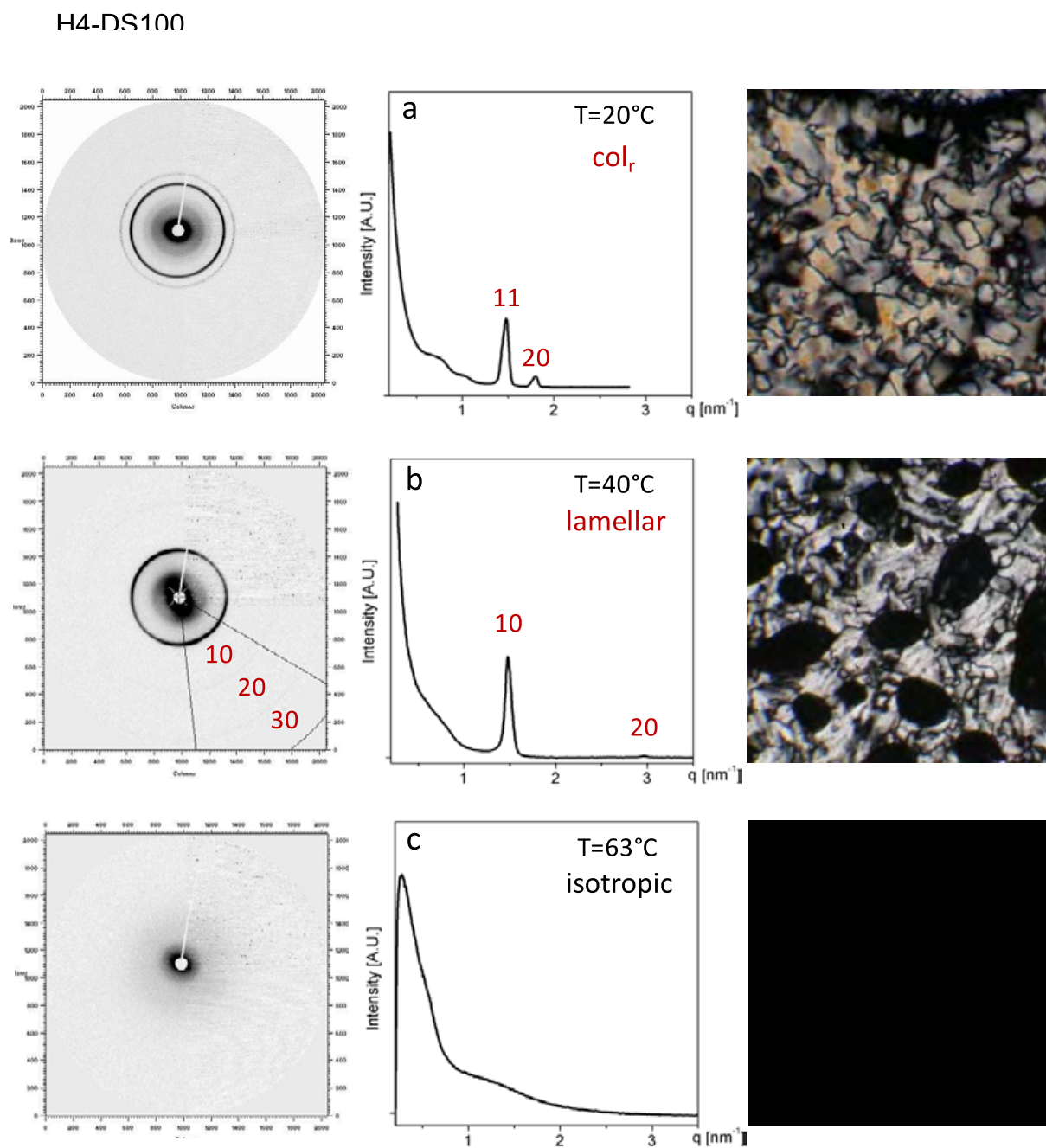
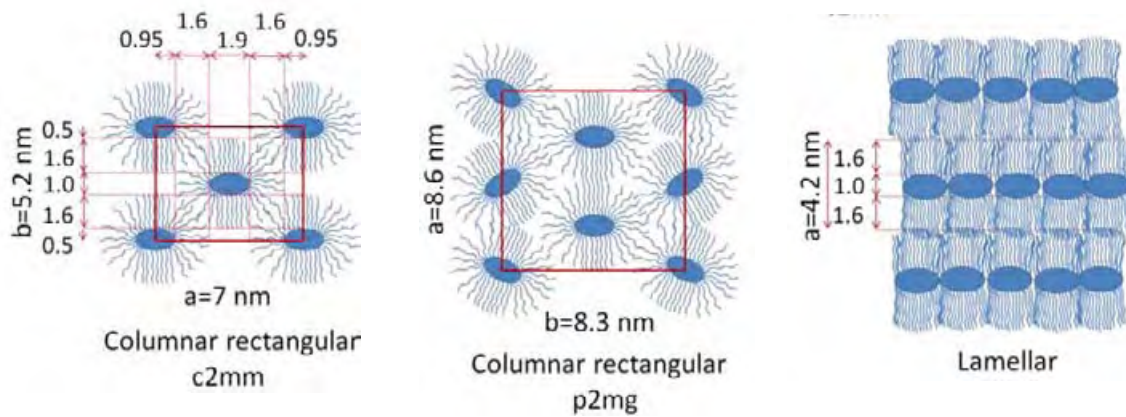


Figure III.4. Diffraction intensity profiles extracted from SAXS diffraction pattern for H4-DS100 at 20°C (Col_r), 40°C (Lamellar) and 63°C (Isotropic) and corresponding POM images.



Scheme III.1. Schematic models of the rectangular columnar Colr,p2mg, Colr,c2mm and lamellar mesophases.

By roughly estimating the contour length of fully stretched C12 alkyl tails to 1.6 nm and assuming no interdigitated alkyl chain configuration, an asymmetric domain size of $1 \times 1.9 \text{ nm}^2$ can be estimated for hyperbranched domains. This value is in good agreement with both the expected and the observed values in literature.[23, 39] At the transition to the lamellar mesophase, the correlation along the columnar axis is lost due to the melting of crystalline structures leading to the disruption of the two-dimensional rectangular positional ordering. This was confirmed by SAXS measurements by the displacement of a sharp peaks in the wide angle region ($q=14\text{-}16 \text{ nm}^{-1}$ i.e. 4.2 \AA) characteristics of the crystallinity of the surfactants domains at the first transition temperature (see Figure III.5) towards low q regions at high temperature (i.e. toward a less organized system).[32]

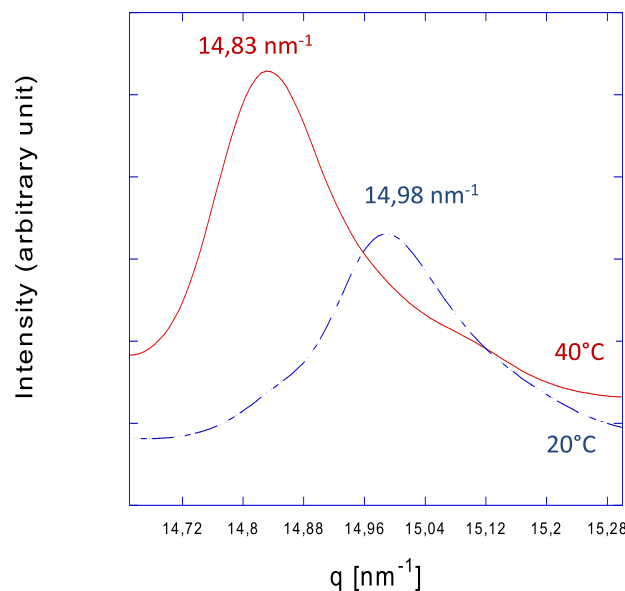


Figure III.5. Diffraction intensity profile extracted from diffraction pattern in the wide angle region for H4-DS100 at 20°C (Colr) and 40°C (Lamellar) showing the shift of the surfactants domains at the first transition temperature towards low q regions at higher temperature i.e. to less organized domains

Between the two transitions peaks, SAXS diffraction pattern showing three peaks $q_1:q_2:q_3$ (at 1.49, 2.98 and 4.47 nm^{-1}), spaced as 1:2:3 (Figure III.4 b), confirmed the lamellar nature of the liquid crystalline organization. The lattice parameter of the lamellar phase 4.2 nm corresponding to the width of hyperbranched and alkyl tails domains. Hence, a minimum width of 1.0 nm can be estimated for hyperbranched domains. Above T_c , both birefringence in POM and reflections of the LC in SAXS disappeared as expected for an isotropic phase (Figure III.4 c).

Mesomorphic properties of H4-DS100 are summarized in Table III-2.

Table III.2. Layer spacing and rectangular lattice constants determined by SAXS for the compounds at the indicated temperature

<i>Compounds</i>	<i>T °C</i>	<i>Mesophase</i>	<i>Lattice parameters (nm)</i>
<i>H4-DS100</i>	<i>20</i>	<i>Col_r, c2mm</i>	<i>a=7.0, b=5.3</i>
	<i>40</i>	<i>lamellar</i>	<i>a=4.2</i>
	<i>63</i>	<i>Isotropic</i>	

2. FT-IR

FT-IR allowed confirming previous results concerning the loss of crystalline order of DS chains at the first transition temperature T_1 . Indeed, the CH_2 asymmetric and symmetric stretching vibrational frequencies can be used to describe the conformation of SDS molecules. The intensity of the signal relative to the CH_2 asymmetric stretching band was analyzed as a function of temperature (Figure III.6).

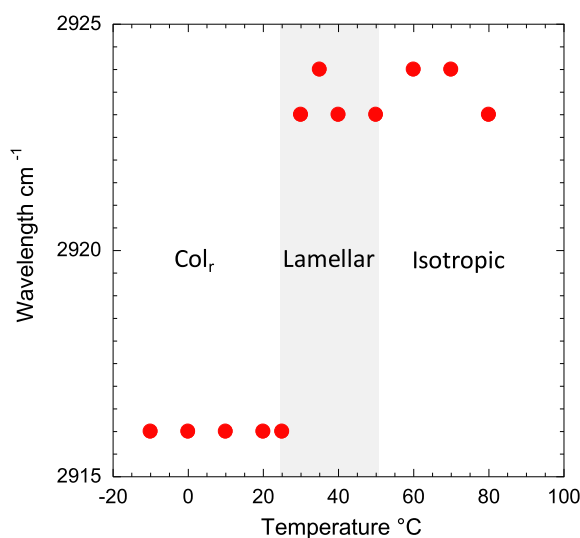


Figure III.6. Thermal evolution of CH_2 asymmetric stretching band of H4-DS100 followed FT-IR.

Interestingly, a significant jump was observed around 23°C, i.e. at the first transition temperature from columnar to lamellar mesophase. This suggests a strong change in SDS

conformation at this transition temperature.[40] Furthermore, the separation between $\nu_{as}(\text{SO}_2)$ bands was an indication of the conformational structure of the surfactant.[41] Values from 27 to 29 cm^{-1} were characteristic of the SDS crystalline conformation (all-*trans* conformation), from 39 to 48 cm^{-1} of SDS bulk and from 32 to 33 cm^{-1} of SDS liquid crystals.[41] At 25°C, the band separation in our study is 28 cm^{-1} for crystalline SDS and for mechanical mixtures of HYPAM and SDS. This gap increases to 37 cm^{-1} for the complex. This also reflects a more disordered conformation in the lamellar phase than in the crystalline state. In addition, below T_1 the CH_2 asymmetric stretching band appears at 2917 cm^{-1} suggesting an ordered hydrocarbon chain in all-*trans* CH_2 configuration. The band shifts to a higher frequency at 25°C (2924 cm^{-1}) meaning that the number of all-*trans* conformers decreases and the number of gauche conformers of alkyl chain increases. This same value was found by Sperline for SDS molecules in a liquid crystal phase.[42] Additional information about alkyl chain conformation is also obtained at the CH_2 scissoring mode, $\alpha(\text{CH}_2)$. A frequency around 1466 cm^{-1} and a band broadening is an indication of partially ordered conformation, which is associated with a less organized structure of SDS.

3. Conclusion

Lamellar and columnar phases of H4-DS100 were clearly evidenced by different techniques: SAXS, DSC, POM and FT-IR.

C. Effect of structural parameters.

The effects of molar mass, substitution level and architecture on the observed mesomorphic properties were hence systematically studied.

1. Effect of the core molar mass

Changing the molar mass of hyperbranched core poorly affects mesomorphous properties, as already reported in the literature.[23] As discussed in section III.A.2 LC properties arise from a molecular segregation phenomenon between hydrophobic chains and the hydrophilic or ionic part of the complexes. This segregation necessitates a hydrophilic core of sufficient molar mass: thus ionic complexes between tris(2-aminoethyl)amine and DS does not exhibit mesomorphic properties (Figure III.7).

Interestingly, rectangular columnar mesophases were also identified below T_1 for H3-DS100 (see figure III.8) and H5-DS100 (see figures III.9 and Table III.3). Nevertheless, in both cases a more complex 2D diffraction pattern suggested a mixture of a rectangular columnar mesophase with C_{2mm} planar space group (Col_r, C_{2mm}) and $P2mg$ planar space group ($\text{Col}_r, P2mg$). Above the first transition temperature, a lamellar structure with structural parameter $a = 4.2$ nm was also identified. Once again, additional peaks depending on the thermal history of studied sample suggested partial ordering remaining within the lamellar structure. As shown in Table III. 3, lattice parameters were also not significantly modified by molar mass suggesting the predominant role of DS in the formation of such organized structures.

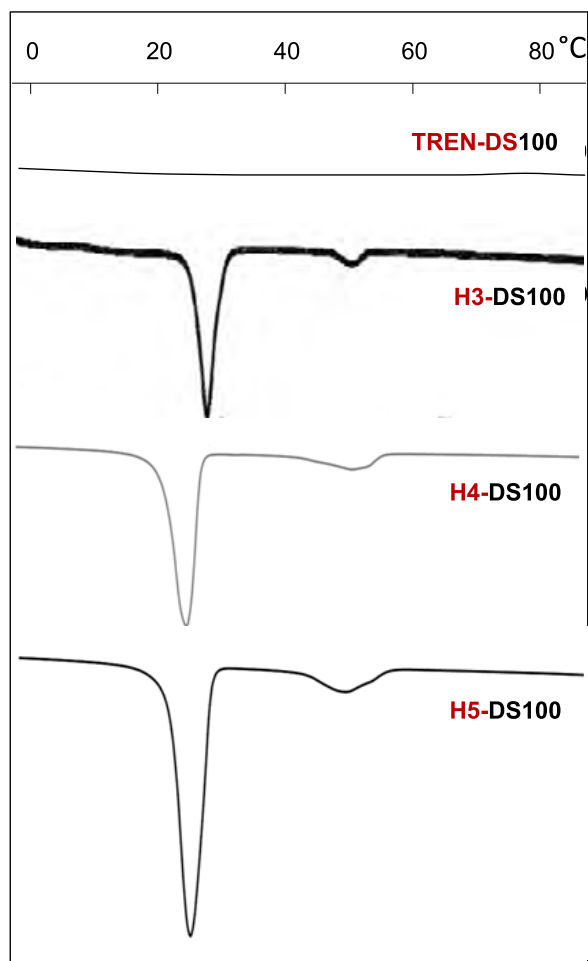


Figure III.7. DSC thermograms recorded (heating rate of 10°C/min) for TREN-DS100, H3-DS100, H4-DS100 and H5-DS100

H3-DS100

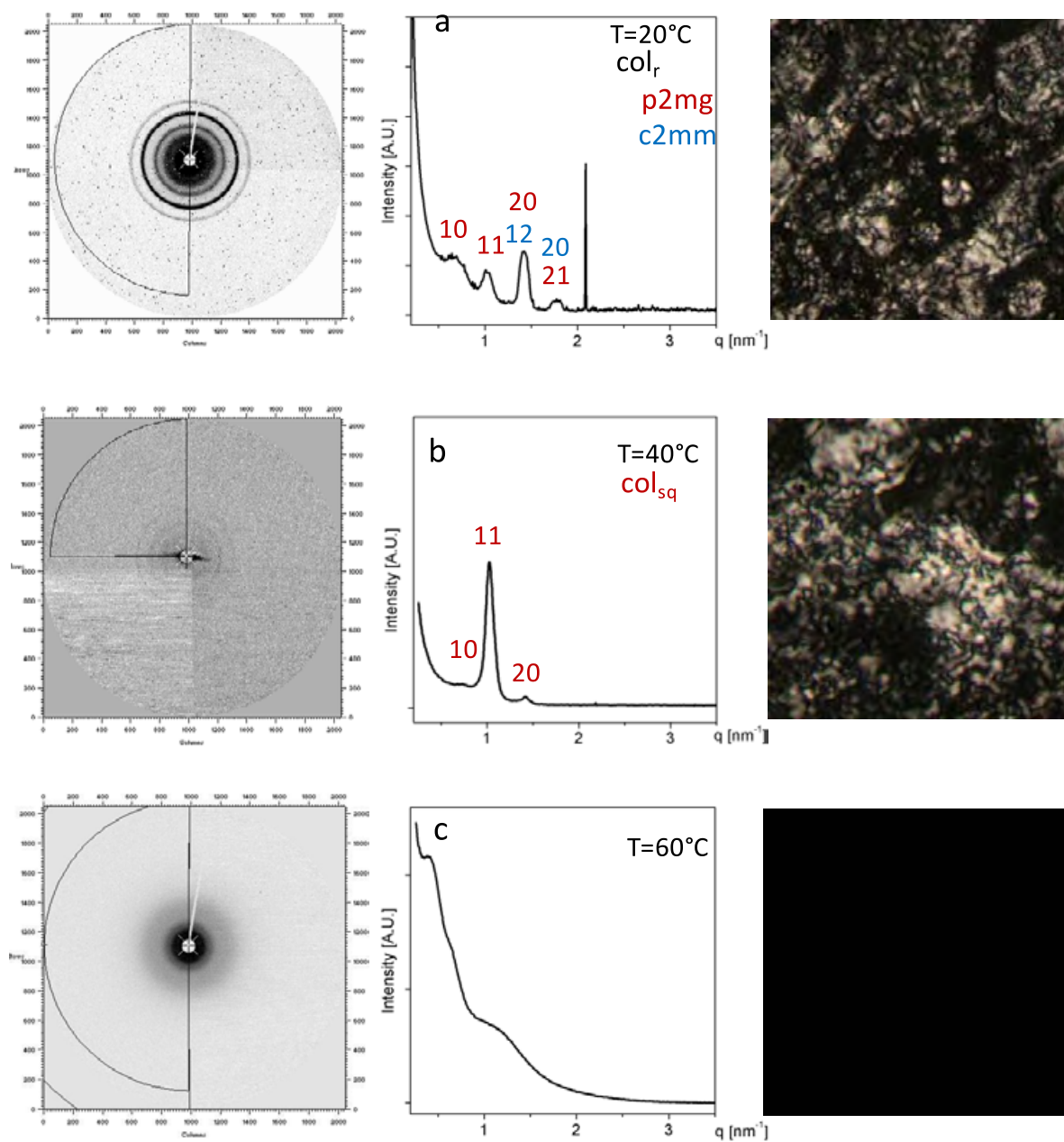


Figure III.8 Diffraction intensity profiles extracted from SAXS diffraction pattern for H3-DS100 at 20°C (Colsq), 40°C (Lamellar) and 63°C (Isotrope) and corresponding POM images.

H5-DS100

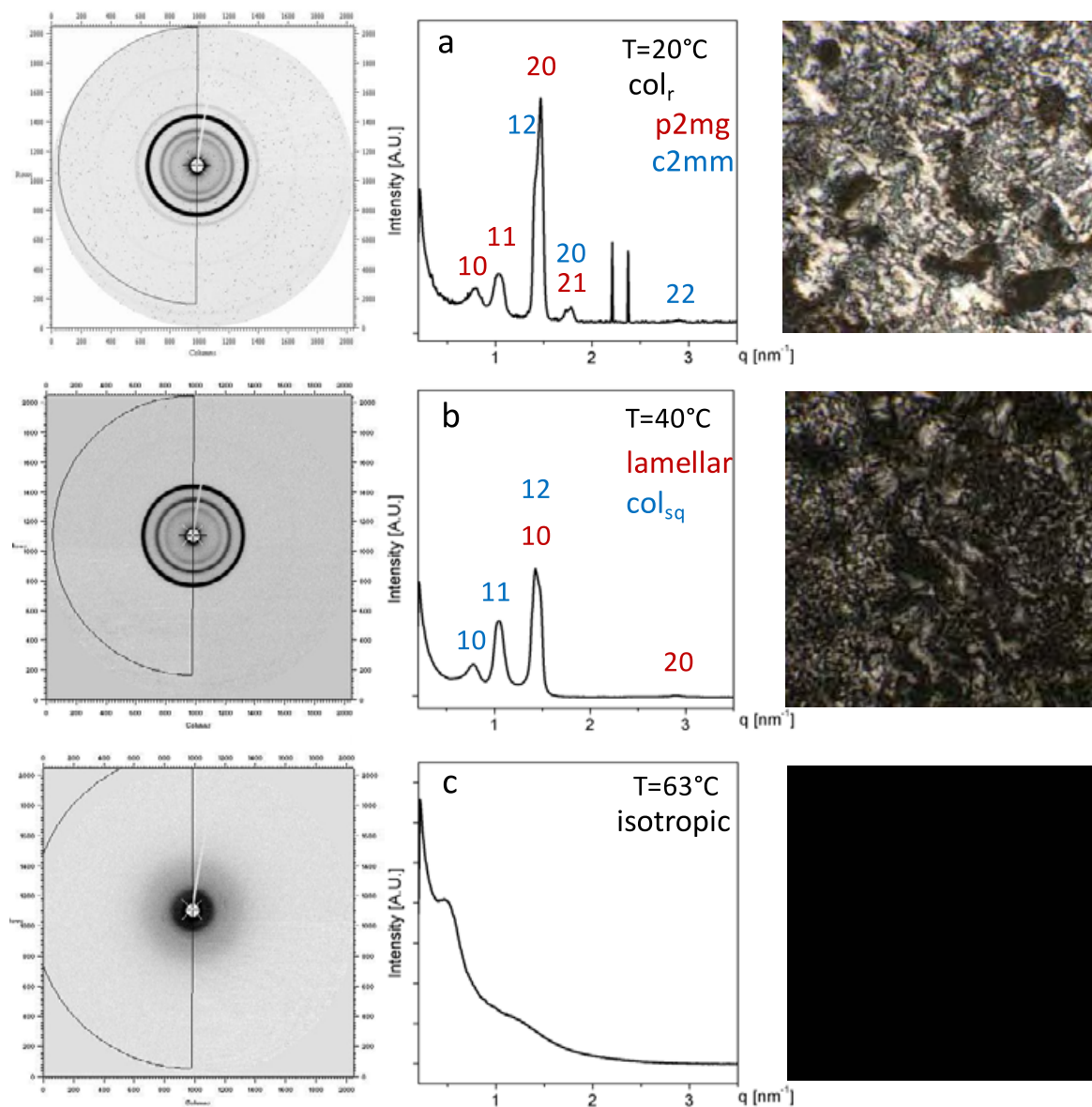


Figure III.9. Diffraction intensity profiles extracted from SAXS diffraction pattern for H5-DS100 at 20°C (Col_r), 40°C (Lamellar) and 63°C (Isotropic) and corresponding POM images.

Table III.3. Layer spacing and rectangular lattice constants determined by SAXS for the compounds at the indicated temperature

<i>Compounds</i>	<i>T °C</i>	<i>Mesophase</i>	<i>Lattice parameters (nm)</i>
<i>H3-DS100</i>	<i>20</i>	<i>Col_r p2mg</i>	<i>a=8.6, b=8.3</i>
		<i>Col_r c2mm</i>	<i>a=7.0, b=5.3</i>
	<i>40</i>	<i>Col_{sq}</i>	<i>a=8.6</i>
		<i>Lamellar</i>	<i>a=4.2</i>
<i>63</i>	<i>Isotropic</i>		
<i>H4-DS100</i>	<i>20</i>	<i>Col_r c2mm</i>	<i>a=7.0, b=5.3</i>
	<i>40</i>	<i>lamellar</i>	<i>a=4.2</i>
	<i>63</i>	<i>Isotropic</i>	
<i>H5-DS100</i>	<i>20</i>	<i>Col_r p2mg</i>	<i>a=8.6, b=8.3</i>
		<i>Col_r c2mm</i>	<i>a=7.0, b=5.3</i>
	<i>40</i>	<i>Col_{sq}</i>	<i>a=8.6</i>
		<i>Lamellar</i>	<i>a=4.2</i>
	<i>63</i>	<i>Isotropic</i>	

2. Hydrophilic/hydrophobic composition balance

Mesomorphic properties are more dramatically affected by changing the level of functionalization of amine terminal function as depicted in Figure III.10. Hence, T₁ and T₂ values increased from 23.5 to 45.1 °C and 48.8 to 65.6 °C respectively by decreasing the functionalization level from 97% to 82% (H4-DS100 and H4-DS75). As expected from the lower content of alkyl chain, the associated variation of enthalpy decreased accordingly. Interestingly, no mesomorphic behavior was observed when this level was decreased to 51% (H4-DS50).

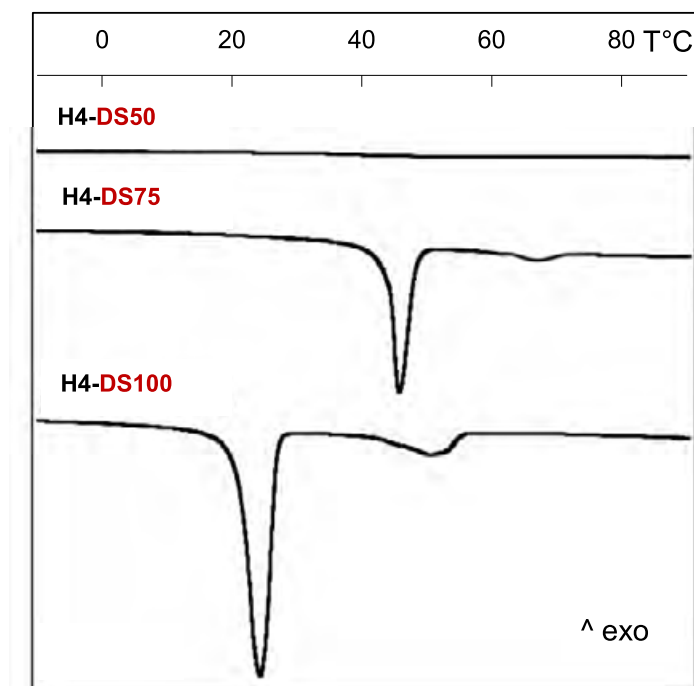


Figure III.10. DSC thermograms recorded (heating rate of 10°C/min) for H4-DS at 50%, 75%, 100% functionalization degree.

3. Effect of the nature of the core: Dendrimer vs hyperbranched core

Lastly, a comparison of the mesomorphism of dendrimer based complexes and their hyperbranched counterpart with similar molar masses allows demonstrating the effect of the dendritic architecture on the phase behavior. While transition temperatures were not significantly affected by this parameter (see Table III.1 for the comparison of H4-DS100 with PAMAM4-DS100), the widths of the peaks corresponding to clearing temperature were shown to be significantly larger in the case of hyperbranched polymer. This effect is clearly seen in Figure III.11 and may be ascribed to the larger dispersity of molar masses inherent for hyperbranched structures. It is noted that ionic complexes based on dendrigraft of polylysine (DGL) did not show liquid crystal properties. One assumption to explain this is the different in the rigidity of the cores. Moreover, the chemical structure of DGL is not the same compared to the one of HYPAM and PAMAM: The amine groups are not only at the polymer periphery but also in the interior linear branches of DGL.

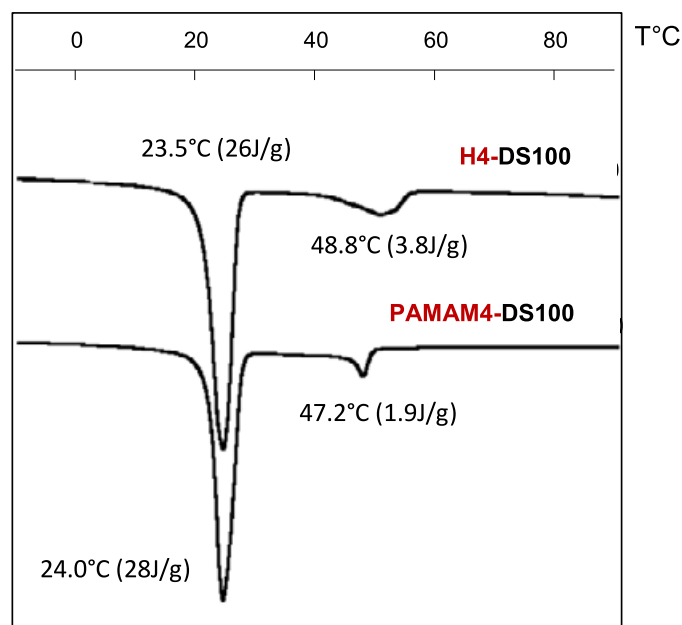


Figure III.11. DSC thermograms recorded (heating rate of 10°C/min) for H4-DS100 and PAMAM4-DS100.

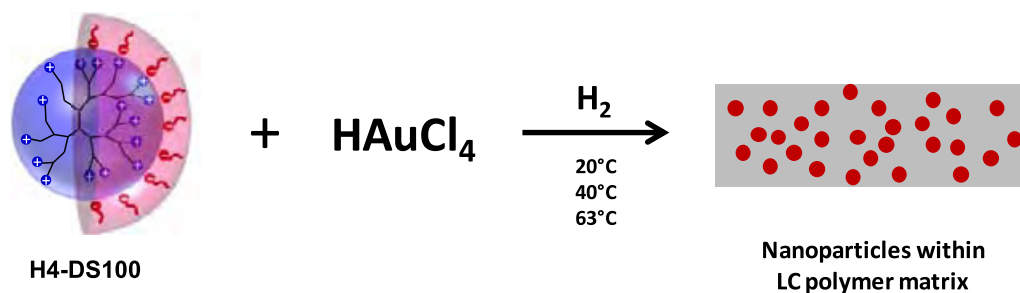
D. Conclusions

In conclusion, whereas LC properties of ionic complexes were not dependent on the molar mass of the hyperbranched functional cores, they significantly depended on the level of functionalization of the amine groups and to a lesser extent to the dendritic architecture. Interestingly, those structures presented a lamellar phase that could be taken into account either to control the growth of NPs within liquid crystalline phase. This will be described in the next section.

IV. *In situ* formation of gold NPs

The ability of those mesomorphic ionic complexes to act as templates for the formation of gold nanoparticles was then evaluated. As stated above, the development of an *in situ* procedure to generate NPs within a LC medium has proved to be quite a challenging task. [4] This is mainly due to two main factors. The first one is related to the difficulties to obtain a homogeneous medium from the mixture of LC and NPs precursor. We previously pointed out the importance of such interactions to control the growth mechanism of ZnO NPs. [11, 12] In that context, the use of thermotropic structures comprising the ionic counterpart facilitating interactions with the ionic metal precursor can ensure the homogeneity of hybrid materials before the formation of NPs. The second one is related to diffusion hindrance of reactants that induce the formation of NPs in such medium. Concerning this point, most studies involved the *in situ* reduction of metal precursor *via* oxidation of the LC medium in order to obtain the desired NPs. [9, 13, 14] In other cases, sputtering or electrodeposition techniques were used. [8, 15] Here a flux of dihydrogen will be used to ensure the reduction of gold precursor at the chosen temperature without disturbing the mesomorphic order. So our purpose was to evaluate if such ionic LC polymer (1) could lead to the formation of a homogeneous medium prior to the formation of NPs and (2) could allow synthesizing well defined hybrid materials made of monodisperse NPs. The effect of polymer structure and organization on the morphology of gold nanoparticles will also be evaluated.

In this section, we will present the synthesis process of gold NPs within polymeric LC medium. And then the characterization of the nanohybrid materials as well as the morphology of the formed AuNPs will be discussed.



Scheme IV.1. *In situ* synthesis of gold NPs within polymeric liquid crystalline phases.

A. Synthesis of AuNPs in LC matrix

1. Interaction between HAuCl₄ and the core HYPAM

Interactions between HAuCl₄ and HYPAM were evidenced by ¹H NMR experiments in D₂O solution: the addition of HAuCl₄ to a neutral polymer induced a shift of chemical shifts only for protons of primary and tertiary amines (an upfield shift of NCH₂CH₂NH₂ and a downfield shift of CH₂NH₂) (Figure VI.1). Thus, metal ions can be coordinated to the outer primary as well as tertiary polymer amine groups.

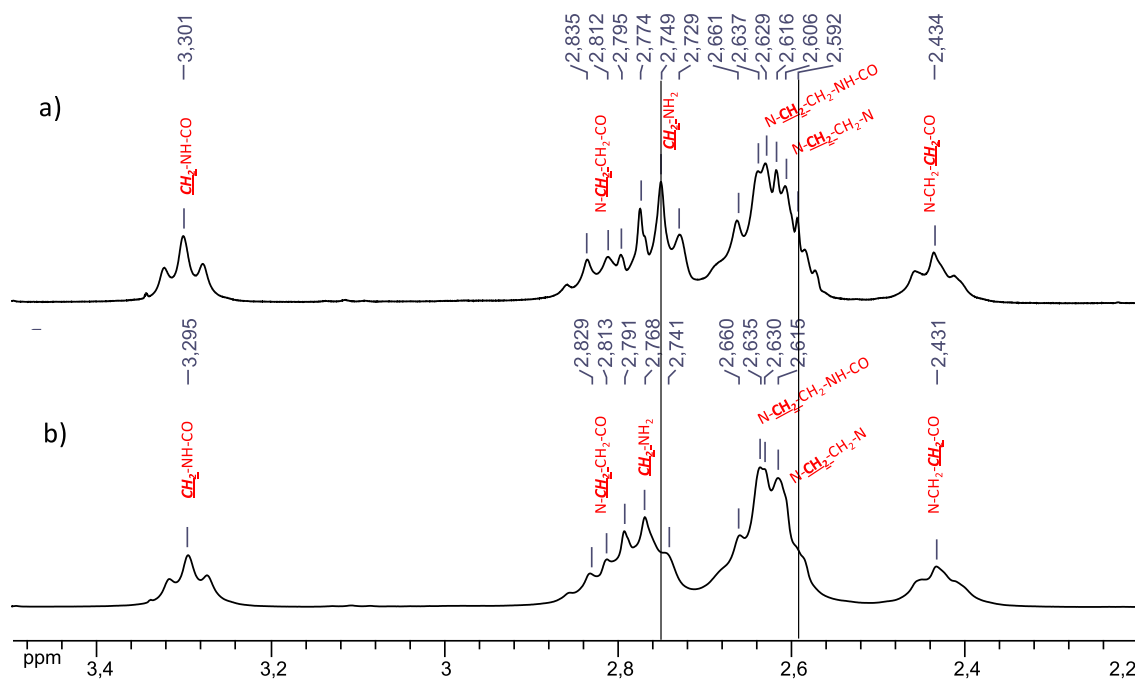


Figure IV.1. ^1H NMR spectra of a) H4 and b) H4-HAuCl₄ in D₂O (300 MHz).

2. Synthesis process

Gold NPs synthesis was performed either in the columnar phase (20 °C), lamellar phase (30 or 40°C) or in the isotropic state (50 and 65°C) to evaluate the effect of liquid crystalline organization on the NPs growth process. At each temperature a homogeneous mixture of ionic complexes and gold precursor was obtained by mechanical crushing the two components (see experimental section). In all cases, the molar ratio of [Au]/[HYPAM-DS] is adjusted to be equal to 120:1.

First attempts to obtain NPs by *in situ* reduction of HAuCl₄.H₂O *via* direct oxidation of the LC medium due to the presence of amine function [36, 37] led to the formation of polydisperse gold NPs (Figure IV.2). The kinetic of their formation was also found to be very slow: several hours were necessary to fulfill complete NPs formation as stated by measurement of absorbance of the growing NPs.

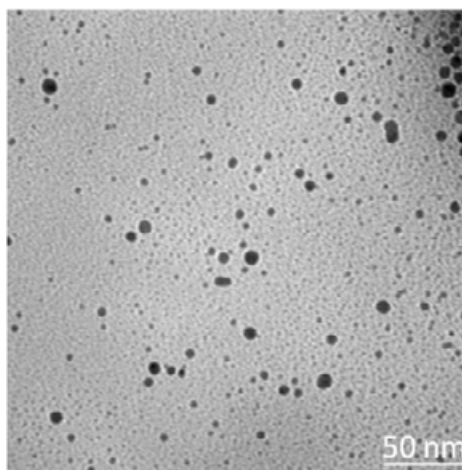


Figure IV.2. TEM micrograph of AuNPs synthesized in H5-DS100 at 65°C without using reducing agent H₂.

Decreasing the dispersity of gold NPs was mandatory in order to assess precisely the effect of LC organization on gold NPs formation. For this purpose, reduction of the bulk systems was achieved by using a flux of dihydrogen. Reduction occurred in a few seconds as stated by the slight change color of the hybrid materials. The formation of gold nanoparticles was first brought out by UV measurements by the appearance at 540 nm of a characteristic band corresponding to a surface plasmon resonance absorption band. (Figure IV.3).

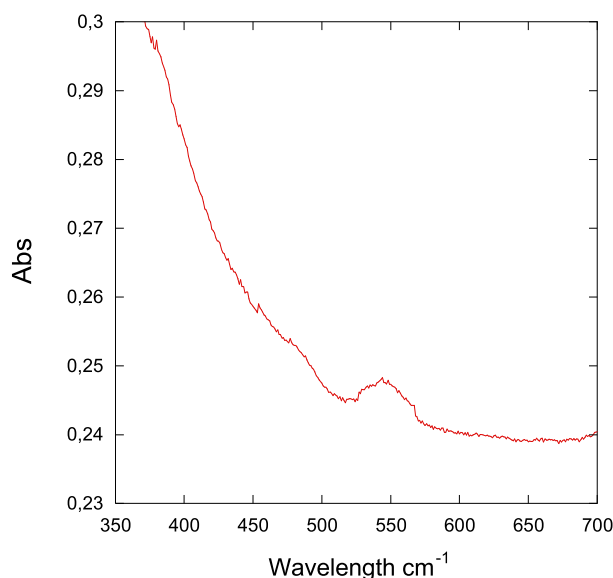


Figure IV.3. UV-reflection spectrum of AuNPs formed in lamellar phase of H4-DS100.

B. Mesomorphic properties of hybrid materials of H4-DS100@AuNPs

The liquid crystalline properties of these hybrid materials were studied by DSC, SAXS and POM techniques. For the hybrid materials H4-DS100@AuNPs synthesized at 30°C, the first transition temperature corresponding to the transition from the columnar to the lamellar mesophase disappeared and only the second transition corresponding to the

clearing temperature at 49.2°C remained. This value as well as the associated enthalpic variation is not significantly different from the one of pristine polymer (48.8°C) (Figure IV.4). Thus while preserving LC properties over a similar temperature range, AuNPs strongly disturbed the organisation of hyperbranched polymer preventing the formation of the highly organized columnar mesophase. This results in the appearance of a glass transition temperature at 3.3 °C.

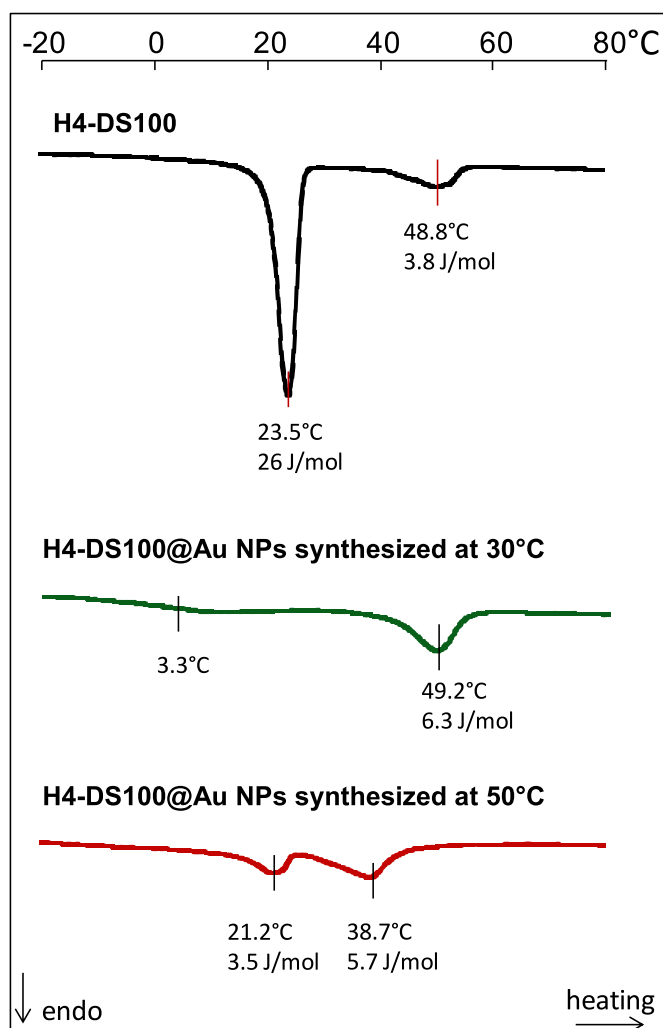


Figure IV.4. DSC thermograms recorded (heating rate of 10°C/min) for H4-DS100 (black line), H4-DS100 with AuNps synthesized at 30°C and 50°C (green and red line respectively).

A strong birefringence, with a texture characteristic of a lamellar mesophase was observed up to the clearing temperature. SAXS experiments performed at 20°C and 60°C support well this assumption (see Figure IV.5) with almost complete disappearance of signals arising from columnar mesophase at 20°C. Disappearance of columnar mesophase may occur during NPs formation explaining the similar NPs size obtained regardless of the nature of the pristine LC phase. For the hybrid material synthesized at 50°C, as can be seen on the thermogram, clearing temperature decrease to 40°C (see Figure IV.4).

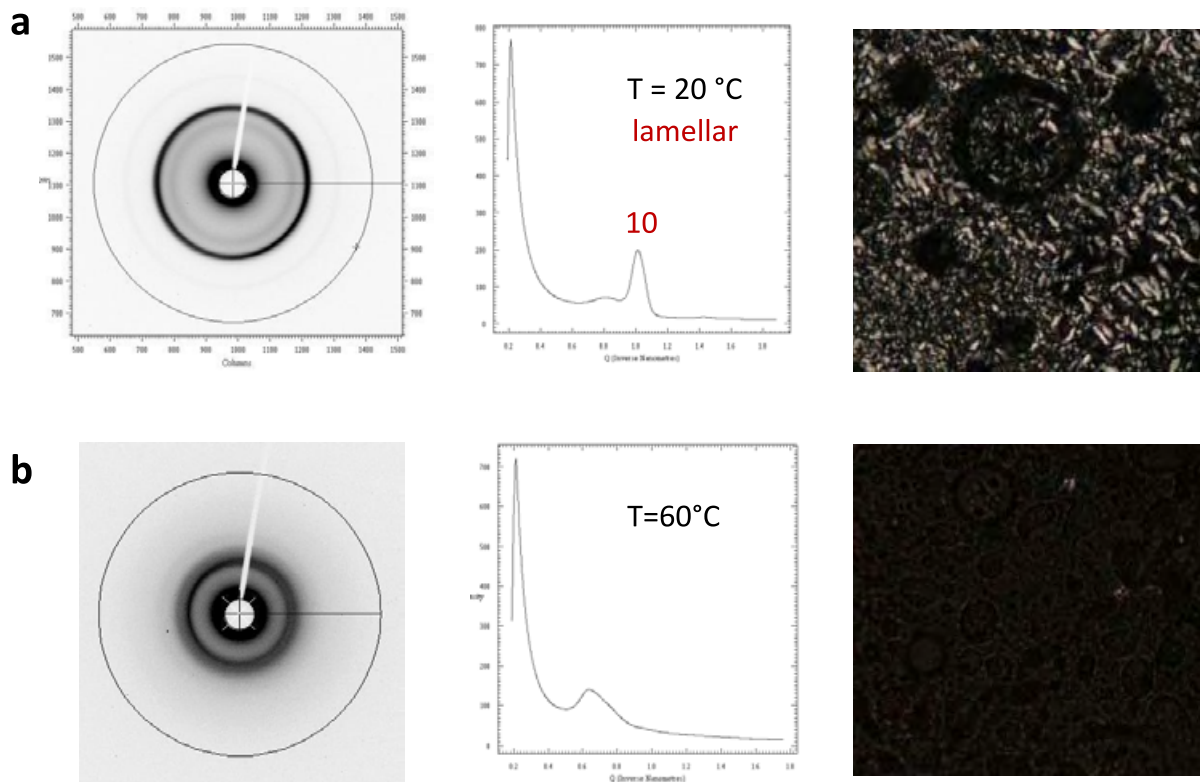


Figure IV.5. H4-DS100@AuNPs synthesized at 30°C: diffraction intensity profiles extracted from SAXS diffraction pattern and corresponding POM images a) at 20°C (LC lamellar state) and b) at 60 °C (isotropic state).

C. Morphology of the *in situ* synthesized AuNPs within mesophases of H4-DS100

Figure IV.6 and IV.7 depicted TEM results obtained for Au NPs growth within H4-DS100 at five different temperatures.

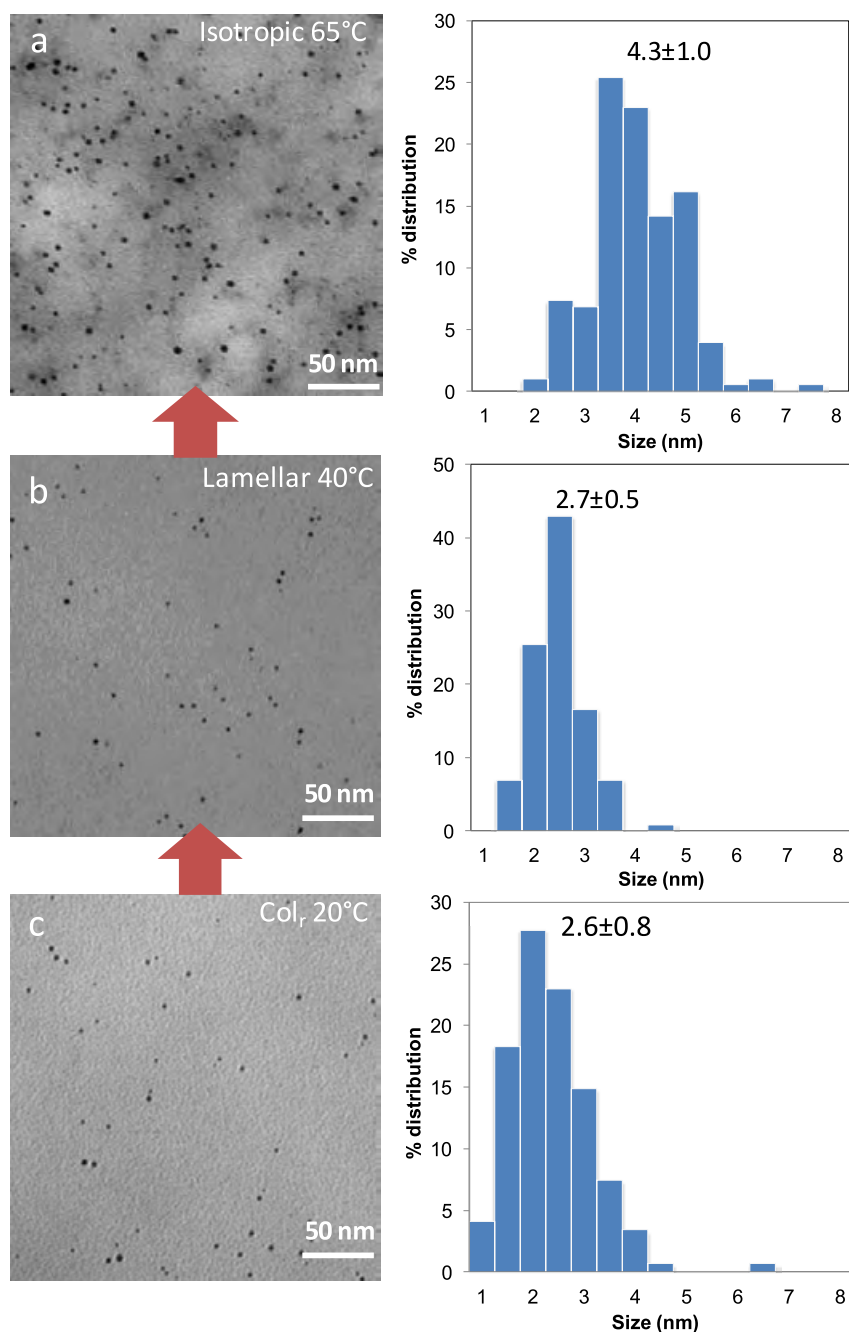


Figure IV.6. TEM micrographs of AuNPs synthesized either a) in isotropic conditions at 65°C or b) in a lamellar liquid crystalline state at 40°C or c) in a rectangular columnar state at 20°C, with corresponding size distributions.

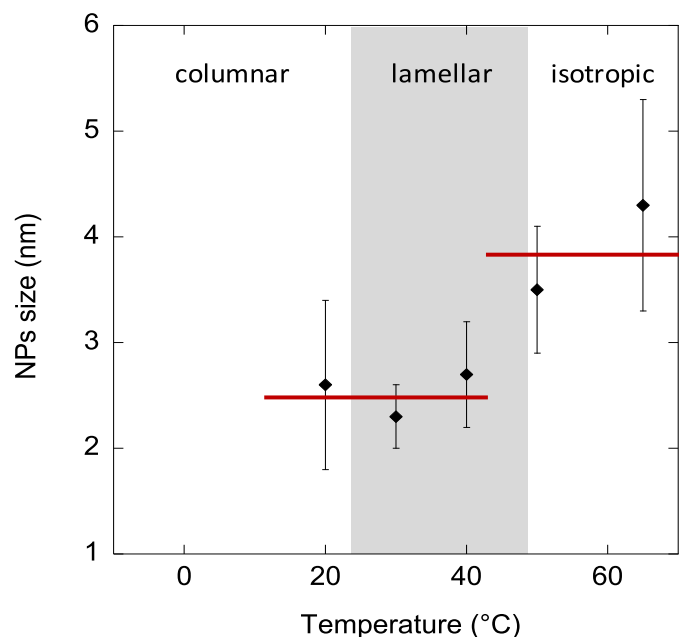


Figure IV.7. Effect on gold nanoparticle size of the temperature used during NPs synthesis. Liquid crystalline range corresponds to the one of mesomorphic polymer H4-DS100 before addition of salt and reduction.

A rather uniform distribution of particles throughout the sample was obtained either in the isotropic or in the LC states. This confirms the homogeneous character of the mixture prior to the reduction process. Interestingly, the obtained particles were smaller with a narrower distribution when growth of the particles occurred in the LC phases rather than in the isotropic state. Hence NPs size of 2.6 ± 0.8 , 2.3 ± 0.3 and 2.7 ± 0.5 nm were obtained at 20, 30 and 40°C respectively. At 50°C corresponding to the liquid crystalline to isotropic transition a slight but significant increase of NPs size at 3.5 ± 0.8 was observed. This increase in the isotropic state was further confirmed at 65°C for which NPs size of 4.3 ± 1.0 nm were found. Hence, as no difference in size was observed between 20 and 40°C, the effect of temperature could not alone explain the effect observed on NPs size. In addition an effect of the macromolecular organization should participate to this effect. To understand these results, we can assume that the main factor controlling the formation of gold particles is the diffusion of gold ions through the sample. Through electrostatic interactions between ammonium groups and the anionic gold salt, a preferential distribution of gold precursor within the ionic part of the complexes could be expected before reduction. The formation of gold NPs within LC structure may hence favour the formation of smaller Au NPs due to a better controlling diffusion of ionic species through hydrophilic regions of the lamellar phase. Formation of those NPs in the isotropic state facilitated diffusion of gold ions in all directions and thus increased the size of nanoparticles.

Nevertheless, NPs obtained either in the columnar or the lamellar phase presented similar sizes. To understand this, we go back to the mesomorphic behaviour of the synthesized bulk H4-DS/Au hybrids. The formation of the AuNPs disturbed the organization of the LC medium without destroying its LC structure. For the hybrid materials synthesized

at 30°C, the final phase at 20°C and 40°C corresponding to previous lamellar and columnar phase become similar explaining the fact of similar size of obtained NPs.

As expected, larger NPs obtained in isotropic conditions disturbed more strongly mesomorphic organization: thus, as can be seen on the thermogram, clearing temperature decrease to 40°C for the nanohybrids synthesized at 50°C (see Figure IV.4).

D. The effect of molecular architecture on the formation of gold NPs

To further analyze the effect of molecular architecture on the formation of gold NPs, the same set of experiments was performed with H3-DS100 and H5-DS100. As shown in Figure IV.8, similar results than the previous ones were obtained regardless of the molar mass of the hyperbranched structure.

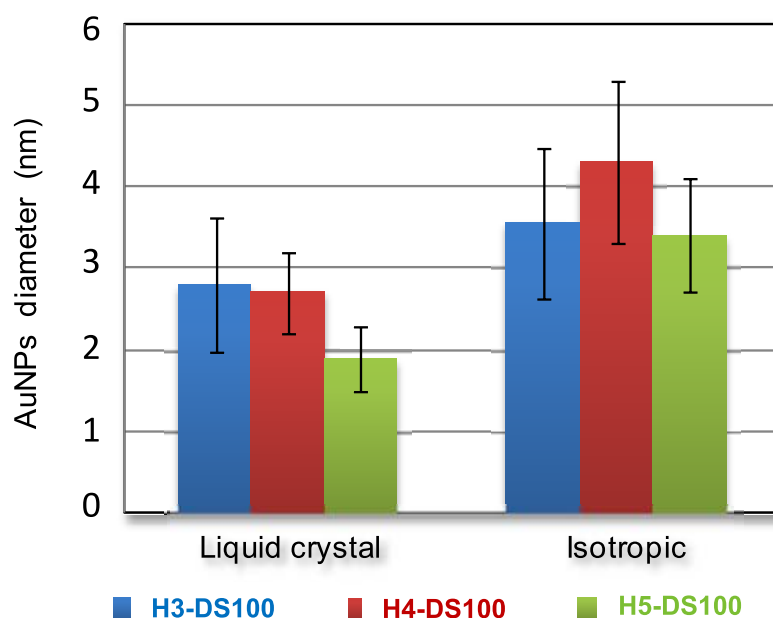


Figure IV.8. Histograms depicting the effect a) of the molar mass of the hyperbranched complex and b) of the polymer organization (lamellar or isotropic) on the Au NPs mean diameter.

It has to be noted that a small but significant decrease of AuNPs size was obtained when increasing the molar mass of the complex (see also Figure IV.9 and IV.10). This better control may be related to an increase of viscosity of the liquid crystalline phase. Such an effect has already been described to be a key parameter in previous studies leading in some cases to the formation of anisotropic structures.[11, 12]

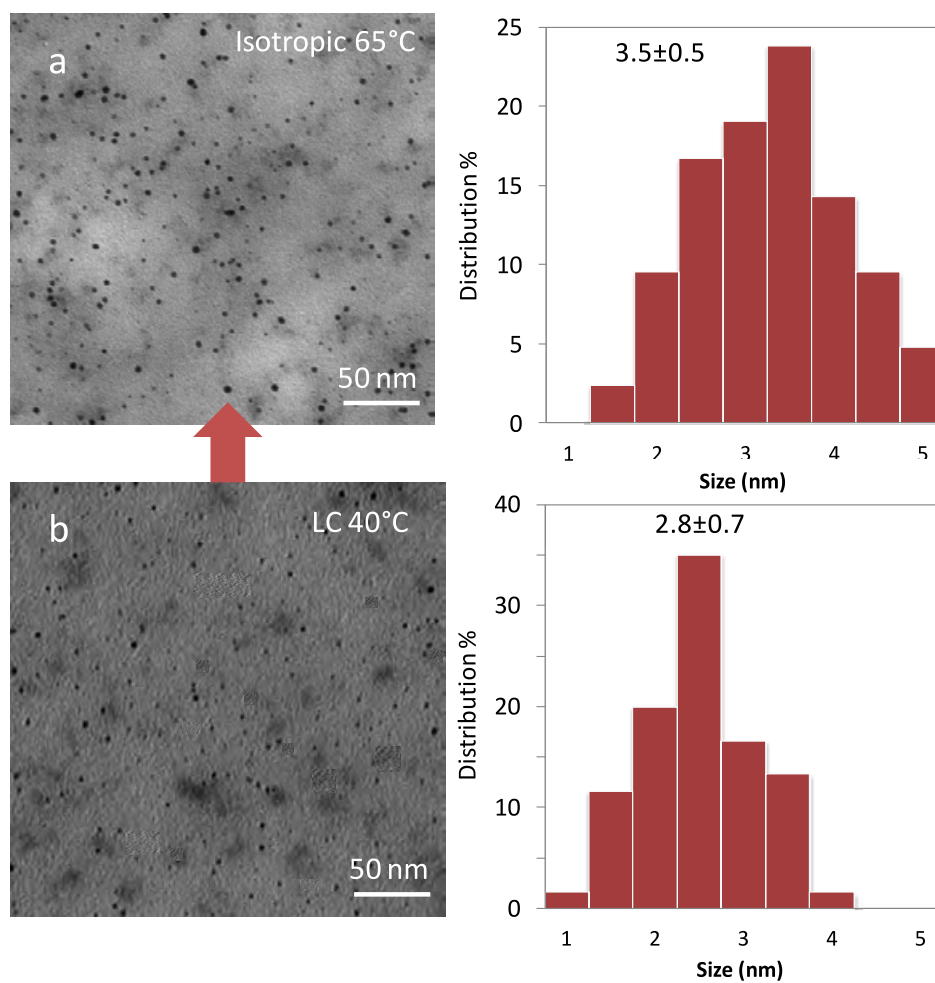


Figure IV.9. TEM micrographs of AuNPs synthesized in H₃-DS100 phase either (a) in isotropic condition at 65°C or (b) in a lamellar liquid crystalline state at 40°C with corresponding size distribution.

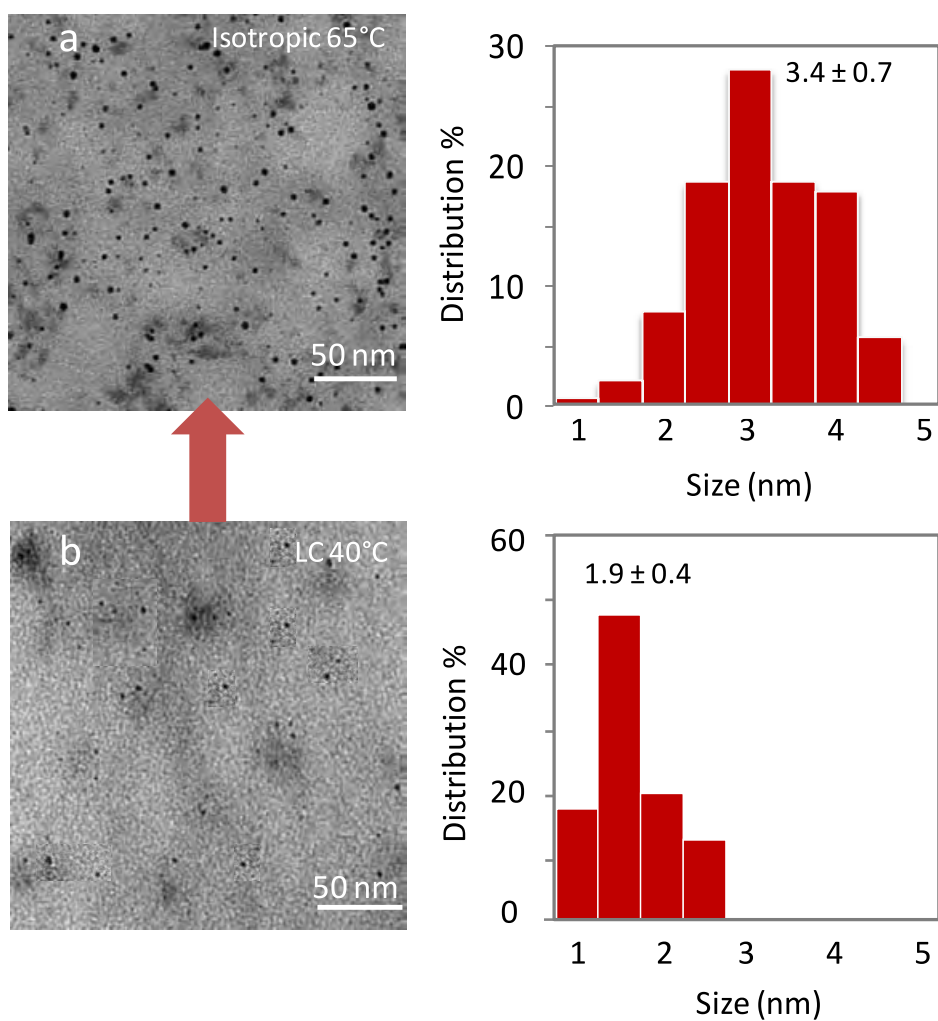


Figure IV.10. TEM micrographs of AuNPs synthesized in H5-DS100 phase either (a) in isotropic condition at 65°C or (b) in a lamellar liquid crystalline state at 40°C with corresponding size.

V. Conclusions

Branched thermotropic liquid crystals were successfully obtained from the ionic interactions between hyperbranched polyamidoamine and dodecylsulfate. These complexes present columnar rectangular and lamellar thermotropic mesophases as demonstrated by polarizing optical microscopy, differential scanning calorimetry, and small-angle X-ray scattering. The relationships between the structural characteristics of the polymers (size of the hyperbranched core, hyperbranched or dendritic nature of the core, substitution ratio) and the mesomorphic properties were studied. The liquid crystalline phase was then used for the *in situ* formation of gold nanoparticles. The templating effect of the liquid crystal mesophase resulted in the formation of isotropic nanoparticles, the size of which was dictated by the local organization of the mesophase and by the molar mass of the hyperbranched complex. The presence of NPs induced strong changes in local organization of the LCs polymer, nevertheless the obtained hybrid materials remained liquid crystalline. To conclude, we believe that such ionic complexes allowing strong interactions with inorganic materials precursors present promising opportunities for the formation of homogeneous hybrid materials within thermotropic structures. Further studies will also aim at taking advantage of the specific mesomorphic properties of such structures to obtain a further control on NPs growth and more precisely anisotropic growth.

VI. References

1. Bisoyi, H.K. and S. Kumar, Liquid-crystal nanoscience: an emerging avenue of soft self-assembly. *Chemical Society Reviews*, 2011. **40**(1): p. 306-319.
2. Hegmann, T., H. Qi, and V.M. Marx, Nanoparticles in liquid crystals: Synthesis, self-assembly, defect formation and potential applications. *Journal of Inorganic and Organometallic Polymers and Materials*, 2007. **17**(3): p. 483-508.
3. Nealon, G.L., et al., Liquid-crystalline nanoparticles: Hybrid design and mesophase structures. *Beilstein Journal of Organic Chemistry*, 2012. **8**: p. 349-370.
4. Saliba, S., et al., Liquid crystalline thermotropic and lyotropic nanohybrids. *Nanoscale*, 2013. **5**(15): p. 6641-6661.
5. Karanikolos, G.N., et al., Templated synthesis of ZnSe nanostructures using lyotropic liquid crystals. *Nanotechnology*, 2005. **16**(10): p. 2372-2380.
6. Karanikolos, G.N., P. Alexandridis, and T.J. Mountziaris, Growth of ZnSe and CdSe nanostructures in self-assembled block copolymer-stabilized templates. *Materials Science and Engineering B-Advanced Functional Solid-State Materials*, 2008. **152**(1-3): p. 66-71.
7. Groenewolt, M., M. Antonietti, and S. Polarz, Mixed micellar phases of nonmiscible surfactants: Mesoporous silica with bimodal pore size distribution via the nanocasting process. *Langmuir*, 2004. **20**(18): p. 7811-7819.
8. Dobbs, W., et al., Electrodeposition of Silver Particles and Gold Nanoparticles from Ionic Liquid-Crystal Precursors. *Angewandte Chemie International Edition*, 2006. **45**(25): p. 4179-4182.
9. Gascon, I., et al., Formation of Gold Nanoparticles in a Side-Chain Liquid Crystalline Network: Influence of the Structure and Macroscopic Order of the Material. *Chemistry of Materials*, 2005. **17**(21): p. 5228-5230.
10. Mallia, V.A., et al., In situ synthesis and assembly of gold nanoparticles embedded in glass-forming liquid crystals. *Angewandte Chemie-International Edition*, 2007. **46**(18): p. 3269-3274.
11. Saliba, S., et al., Thermotropic Liquid Crystals as Templates for Anisotropic Growth of Nanoparticles. *Angewandte Chemie-International Edition*, 2011. **50**(50): p. 12032-12035.
12. Saliba, S., et al., ZnO/Liquid Crystalline Nanohybrids: From Properties in Solution to Anisotropic Growth. *Chemistry-a European Journal*, 2012. **18**(26): p. 8084-8091.
13. Taubert, A., CuCl Nanoplatelets from an Ionic Liquid-Crystal Precursor. *Angewandte Chemie International Edition*, 2004. **43**(40): p. 5380-5382.
14. Taubert, A., P. Steiner, and A. Manton, Ionic liquid crystal precursors for inorganic particles: Phase diagram and thermal properties of a CuCl nanoplatelet precursor. *Journal of Physical Chemistry B*, 2005. **109**(32): p. 15542-15547.
15. Yoshida, H., et al., Nanoparticle-Dispersed Liquid Crystals Fabricated by Sputter Doping. *Advanced Materials*, 2010. **22**(5): p. 622-626.

16. Saliba, S., et al., Facile direct synthesis of ZnO nanoparticles within lyotropic liquid crystals: towards organized hybrid materials. *Journal of Materials Chemistry*, 2011. **21**(45): p. 18191-18194.
17. Chechik, V., M.Q. Zhao, and R.M. Crooks, Self-assembled inverted micelles prepared from a dendrimer template: Phase transfer of encapsulated guests. *Journal of the American Chemical Society*, 1999. **121**(20): p. 4910-4911.
18. Cook, A.G., U. Baumeister, and C. Tschierske, Supramolecular dendrimers: Unusual mesophases of ionic liquid crystals derived from protonation of DAB dendrimers with facial amphiphilic carboxylic acids. *Journal of Materials Chemistry*, 2005. **15**(17): p. 1708-1721.
19. Faul, C.F.J., et al., Solid-state nanostructure of PAMAM dendrimer-fluorosurfactant complexes and nanoparticles synthesis within the ionic subphase. *Colloids and Surfaces a-Physicochemical and Engineering Aspects*, 2003. **212**(2-3): p. 115-121.
20. Fitie, C.F.C., et al., Nanostructured materials through orthogonal self-assembly in a columnar liquid crystal. *Chemistry of Materials*, 2008. **20**(6): p. 2394-2404.
21. Hernandez-Ainsa, S., et al., Effect of the Phobic Segregation between Fluorinated and Perhydrogenated Chains on the Supramolecular Organization in Ionic Aromatic Dendrimers. *Chemistry of Materials*, 2010. **22**(16): p. 4762-4768.
22. Hernandez-Ainsa, S., et al., Influence of the Poly(propylene imine) Generation in the LC Properties of Ionic Codendrimers Bearing Fluorinated and Perhydrogenated Chains. *Journal of Polymer Science Part a-Polymer Chemistry*, 2011. **49**(1): p. 278-285.
23. Hernandez-Ainsa, S., et al., Nanoobjects coming from mesomorphic ionic PAMAM dendrimers. *Soft Matter*, 2011. **7**(6): p. 2560-2568.
24. Hernandez-Ainsa, S., et al., Philic and Phobic Segregation in Liquid-Crystal Ionic Dendrimers: An Enthalpy-Entropy Competition. *Angewandte Chemie-International Edition*, 2010. **49**(11): p. 1990-1994.
25. Marcos, M., et al., Photosensitive Ionic Nematic Liquid Crystalline Complexes Based on Dendrimers and Hyperbranched Polymers and a Cyanoazobenzene Carboxylic Acid. *Chemistry of Materials*, 2008. **20**(16): p. 5209-5217.
26. Marcos, M., et al., Ionic liquid crystal dendrimers with mono-, di- and trisubstituted benzoic acids. *Chemistry of Materials*, 2006. **18**(5): p. 1206-1212.
27. Martin-Rapun, R., et al., Ionic thermotropic liquid crystal dendrimers. *Journal of the American Chemical Society*, 2005. **127**(20): p. 7397-7403.
28. Martin-Rapun, R., et al., Liquid crystalline semifluorinated ionic dendrimers. *Liquid Crystals*, 2007. **34**(3): p. 395-400.
29. Ujiie, S., et al., Ionic liquid crystalline systems with branched or hyperbranched polymers. *Kobunshi Ronbunshu*, 2000. **57**(12): p. 797-802.
30. Ujiie, S., Y. Yano, and A. Mori, Liquid-crystalline branched polymers having ionic moieties. *Molecular Crystals and Liquid Crystals*, 2004. **411**: p. 1525-1531.
31. Bastardo, L.A., et al., The structures of complexes between polyethylene imine and sodium dodecyl sulfate in D₂O: A scattering study. *Journal of Physical Chemistry B*, 2005. **109**(1): p. 167-174.

32. Canilho, N., et al., Thermotropic ionic liquid crystals via self-assembly of cationic hyperbranched polypeptides and anionic surfactants. *Macromolecules*, 2007. **40**(23): p. 8374-8383.
33. Marty, J.D., et al., Hyperbranched polyamidoamine as stabilizer for catalytically active nanoparticles in water. *Journal of Colloid and Interface Science*, 2008. **326**(1): p. 51-54.
34. Saliba, S., et al., Hyperbranched Polymers for the Formation and Stabilization of ZnO Nanoparticles. *Chemistry of Materials*, 2010. **22**(23): p. 6301-6309.
35. Dvornic, P.R., et al., Hyperbranched Polyureas, Polyurethanes, Polyamidoamines, Polyamides and Polyesters. 2002.
36. Perignon, N., et al., Hyperbranched polymers analogous to PAMAM dendrimers for the formation and stabilization of gold nanoparticles. *Macromolecules*, 2007. **40**(9): p. 3034-3041.
37. Perignon, N., et al., Formation and stabilization in water of metal nanoparticles by a hyperbranched polymer chemically analogous to PAMAM dendrimers. *Chemistry of Materials*, 2004. **16**(24): p. 4856-+.
38. Scheuing, D.R. and J.G. Weers, A fourier-transform infrared spectroscopic study of dodecyltrimethylammonium chloride sodium dodecyl-sulfate surfactant mixtures. *Langmuir*, 1990. **6**(3): p. 665-671.
39. Rueff, J.M., et al., Lamellar to columnar mesophase evolution in a series of PAMAM liquid-crystalline codendrimers. *Macromolecules*, 2003. **36**(22): p. 8368-8375.
40. Palaprat, G., et al., Study of hydrogen bonding in liquid crystalline solvent by Fourier transform infrared spectroscopy. *Journal of Physical Chemistry A*, 2006. **110**(47): p. 12887-12890.
41. Viana, R.B., A.B.F. da Silva, and A.S. Pimentel, Infrared Spectroscopy of Anionic, Cationic, and Zwitterionic Surfactants. *Advances in Physical Chemistry*, 2012. **2012**: p. 14.
42. Sperline, R.P., Infrared spectroscopic study of the crystalline phases of sodium dodecyl sulfate. *Langmuir*, 1997. **13**(14): p. 3715-3726.

Chapter 5

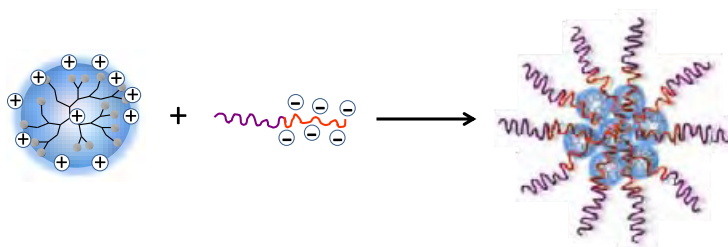
**Polyion Complexes based on Dendritic
Polymers**

CONTENTS

I. INTRODUCTION	213
II. FORMATION OF PICS BASED ON DENDRITIC ELECTROLYTES	214
A. ASSOCIATION OF HYPERBRANCHED POLYAMIDOAMIDE POLYMERS AND POLY(ETHYLENE OXIDE)- <i>B</i> - POLY(ACRYLIC ACID) COPOLYMERS PEO6-PAA6.5	214
1. <i>Characterization of formed PICS</i>	214
2. <i>Stability of formed PICS</i>	218
B. INFLUENCE OF THE STRUCTURAL PARAMETERS	220
1. <i>Change of hyperbranched electrolytes</i>	220
2. <i>Change of composition of block copolymers</i>	222
C. PICS BASED ON DENDRIGRAFT POLYLYSINE	223
D. PICS BASED ON PAMAM DENDRIMERS	224
E. CONCLUSION	225
III. THERMORESPONSIVE PICS	225
A. THERMORESPONSIVE PICS BASED ON HYPERBRANCHED POLYAMIDOAMINE H4	226
1. <i>Formation and stabilization of PICS</i>	226
2. <i>Thermoresponsive properties</i>	227
B. THERMORESPONSIVE PICS BASED ON DENDRIGRAFT POLYLYSINE DGL3	230
1. <i>Formation and stabilization of PICS</i>	230
2. <i>Stability of PICS colloidal solution</i>	230
3. <i>Thermoresponsive properties</i>	232
IV. CONCLUSION	236
V. REFERENCES	236

I. Introduction

As shown in the literature review chapter, charged ionic groups on the periphery of a dendritic polymers allow its stable incorporation into a polyion complex (PIC) micelle with a core-shell structure [1], through oppositely-charged electrostatic interactions as schematically shown in Scheme I.1. Addition of salts (i.e. modification of ionic strength), changing of pH, concentration or opposite charge ratio and morphology of the polyelectrolytes all influence the assembly [2].



Scheme I.1. Illustration of the formation of dendritic PICs

As introduced in the literature reviews, whereas a great number of polymeric micelle systems have been prepared using block copolymers, very few examples have been reported about dendritic polymer based PICs [3] [4]. The objective of this work is to develop different PIC systems using different kinds of cationic dendritic polymers including hyperbranched, dendrigraft and dendrimer. The conjugate anionic part was composed of double hydrophilic block copolymers. Polyacrylic acid (PAA) was chosen to interact with the cationic cores. PAA was then copolymerized either with (i) poly(ethylene glycol) PEO which is known to confer a high stability of micellar aggregates, or (ii) a thermoresponsive PNIPAM block. In all cases, we studied the parameters influencing the formation and the stability of dendritic PICs.

In the first part, a model system, namely hyperbranched polyamidoamide H₄ and a poly(ethylene oxide)-*b*-poly(acrylic acid) block copolymers (PEO₆-PAA_{6.5}) was chosen to determine the most suitable mixing charge ratio of both polymers to obtain PICs but also, the effect of salt addition, pH modification and the dilution. Then, the effect of macromolecular composition, size and nature of the branched core and the structure of the block copolymers (size of the hydrophilic and anionic blocks) were evaluated.

In the second part, we will present the study of thermoresponsive PICs containing dendritic electrolytes and PNIPAM based block copolymer. Besides the stability of PICs against the change of ionic strength, pH or dilution, the thermo-responsiveness of the PICs will be analyzed.

II. Formation of PICs based on dendritic electrolytes

A. Association of hyperbranched polyamidoamide polymers and poly(ethylene oxide)-*b*-poly(acrylic acid) copolymers PEO6-PAA6.5

Like PAMAM dendrimers, HYPAM have an outer shell of primary amines with a pKa value around 9 and internal, tertiary amine moieties with pKa values between 3 and 6 [5]. In neutral pH solution, the amine group is protonated and change into ammonium form ($\text{NH}_2 \rightarrow \text{NH}_3^+$). Concerning poly(ethylene oxide)-*b*-poly(acrylic acid) block copolymers, when the pH of the solution exceeds the pKa of the poly(acrylic acid) ($\text{pKa}=4.2$), the carboxyl group of the PAA block become deprotonated ($\text{COOH} \rightarrow \text{COO}^-$). Multi-ionic interactions between the carboxylate groups COO^- of the PAA block with the outer ammonium layer (NH_3^+) of the hyperbranched polymer lead to formation of PIC structures while hydrophilic block PEO provide solubility of the assembly.

Firstly, we will present the formation and stability of PICs obtained from hyperbranched polyamidoamine H4 and poly(ethylene oxide) of 6000 g/mol and poly(acrylic acid) of 6500 g/mol (PEO6-PAA6.5). This complex is noted H4@PEO6-PAA6.5.

1. Characterization of formed PICs

a) *Optimization of $[\text{COO}^-/\text{NH}_3^+]$ molar ratio for the formation of PICs*

In order to investigate the formation of PICs in function of opposite charge ratio, the $[\text{COO}^-/\text{NH}_3^+]$ molar ratio were varied from 0/1 to 1/1 by increasing the quantity of PEO6-PAA6.5 while keeping the concentration of hyperbranched polymers at 0.1 wt.% in the final mixture constant. PICs formation was carried out by slowly adding block copolymer PEO6-PAA6.5 solution to hyperbranched polymer solution using syringe pump in order to gain reproducibility. Prior addition, pH of the two solutions was adjusted at 7.

The evolution of the formation of PICs in function of different charge ratio was monitored by DLS measurements (size, zeta potential). Figure II.1 and Figure II.2 give the size intensity distributions and corresponding correlograms for H4@PEO6-PAA6.5 obtained for different charge ratio.

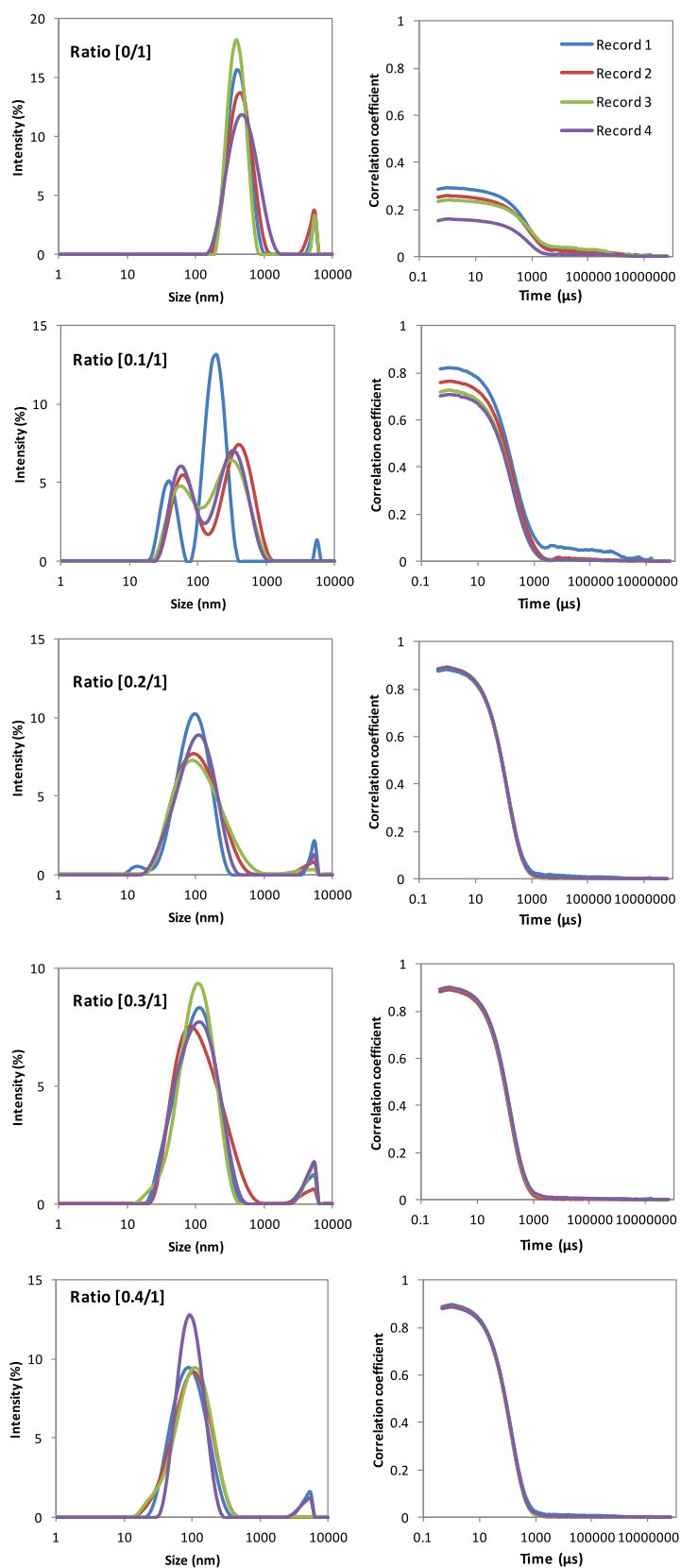


Figure II.1. Size intensity distributions and corresponding correlograms obtained from DLS measurement of $\text{H}_4@$ PEO6-PAA6.5 for $[\text{COO}^-]/[\text{NH}_3^+]$ molar ratio varying from [0/1] to [0.4/1].

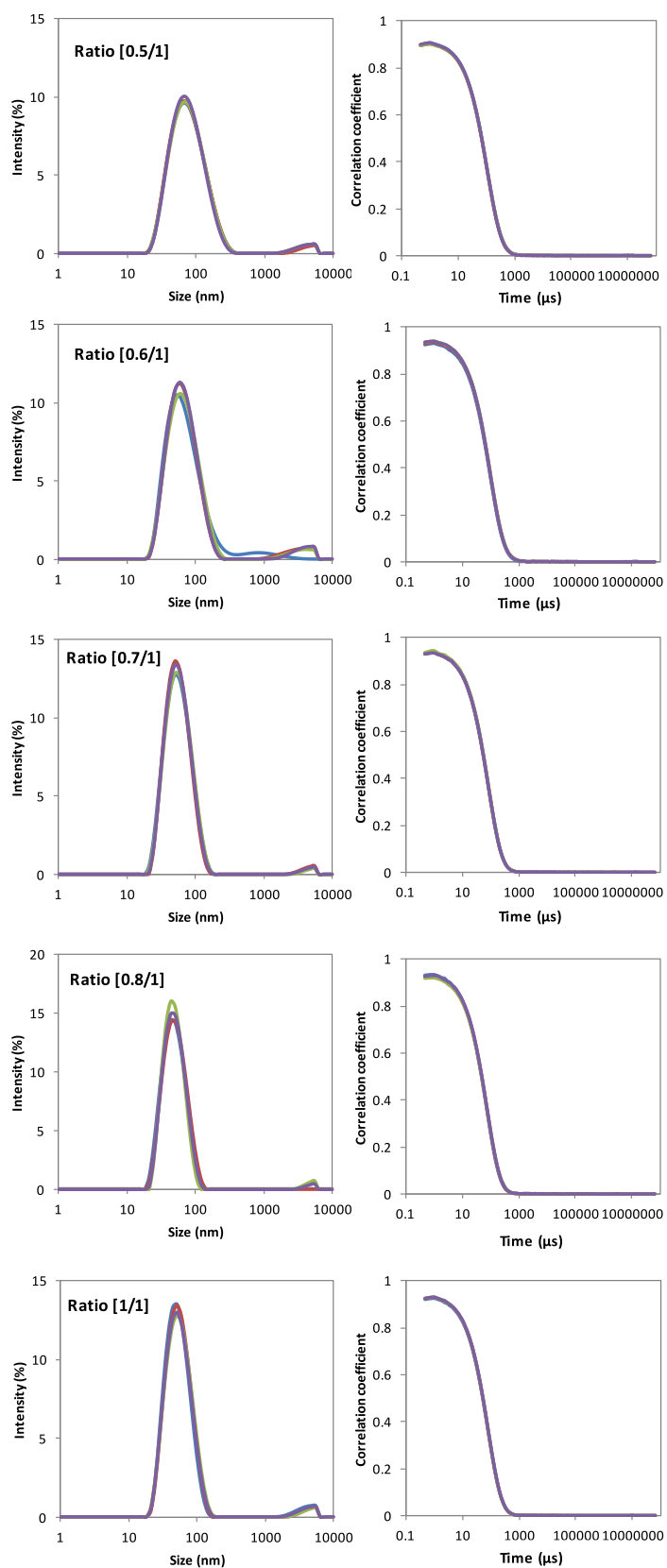


Figure II.2. Size intensity distributions and corresponding correlograms obtained from DLS measurement of H₄@PEO₆-PAA_{6.5} for $[\text{COO}^-/\text{NH}_3^+]$ molar ratio varying from [0.5/1] to [1/1].

As demonstrated by SANS experiments in Chapter 2), H4 exist in solution as a unimolecular object and has a gyration radius of 2.7 nm. Nevertheless DLS experiment performed at 0.1 wt.% does not enable to observe such size, observed distributions might be related to the presence of few aggregates or dust. Formation of complex between H4 and PEO6-PAA6.5 was evidenced after first addition of the diblock. Indeed, whereas low scattered intensity was measured for pristine H4 solution, this intensity significantly increased after addition of PEO6-PAA6.5 to a [0.1/1] charge molar ratio. However monomodal size distributions in intensity were obtained only from [0.2/1] charge ratio with nice reproducible correlograms. Size distributions in intensity of formed PICs had tendency to refine with increasing charge ratio, and they become steady from [0.8/1] charge ratio. This charge ratio value was taken as the value for the formation of well-defined H4@PEO6-PAA6.5 PICs.

Z-averaged value is a hydrodynamic parameter which is defined as a mean particle size. This value is representative for the size of particles in solution when the sample is monomodal (i.e. only one peak), spherical or near-spherical in shape and monodisperse. Count rate value obtained from the number of photons detected from a DLS measurement depends on the concentration of particles as well as measurement position. To get a reliable count rate for a broad range of concentrations, the measurement position was fixed. The count rate needs to be above some minimum values in order to have enough signals for reliable analysis. Unlike in Size Exclusion Chromatography, Polydispersity Index (PDI) in DLS technique is a number calculated from a fit of the correlation data (the cumulants analysis) indicate the difference in size of particles in the sample, values smaller than 0.05 are rarely seen other than with highly monodisperse standards, values greater than 0.7 indicate that the sample has a very broad size distribution and is not suitable for DLS technique.

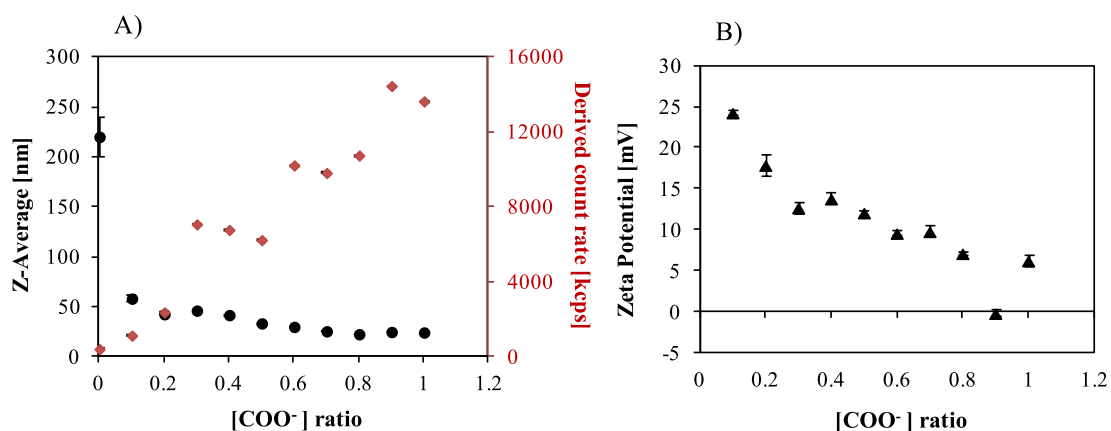


Figure II.3. Evolution of Z-average (r_H nm), derived count rate and zeta potential as a function of [COO⁻/NH₃⁺] molar ratio for H4@PEO6-PAA6.5, [H4] = 0.1 wt.%

As shown in Figure II.3, hyperbranched polymers H4 alone in solution give an unreliable value of Z-average regarding to the corresponding value of derived count rate. As increasing the $[\text{COO}^-/\text{NH}_3^+]$ molar ratio (from 0 to 0.2), the derived count rate increased sharply. This indicates an increase of number or size of aggregates due to formation of PICs assembly. Higher COO^- molar ratio might leads to formation of more defined aggregates (from 0.2 to 0.8) i.e. more densely packed block copolymers around the hyperbranched core. Increasing more the quantity of anionic copolymers however did not make big change in size of the formed PICs (from 0.8 to 1).

Pass up the first points in the Figure II.3.a, Z-average slightly decreases from 45 nm to 31 nm over the increasing $[\text{COO}^-/\text{NH}_3^+]$ molar ratio. As expected, the zeta potential decreases while increasing the molar ratio down to zero. This indicates the formation of objects that are more and more covered by block copolymers.

2. Stability of formed PICs

Stability studies were carried out at a fixed 1/1 charge molar ratio using a fixed concentration of hyperbranched core $[\text{H}_4] = 0.1 \text{ wt.}\%$.

a) Colloidal stability of PIC solutions vs time and dilution

PIC solutions were stable during months: no noticeable change in size of $\text{H}_4@\text{PEO6-PAA6.5}$ complex from DLS measurement was observed after 2 months. Furthermore, these complexes were also revealed to be quite stable upon 6 times dilution by no noticeable change in size. However detected signals decreased due to a decrease of PIC concentration (Figure II.4).

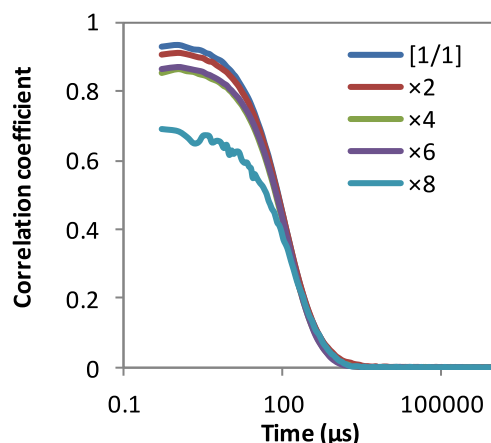


Figure II.4. Correlograms recorded for $\text{H}_4@\text{PEO6-PAA6.5}$ of [1/1] $[\text{COO}^-/\text{NH}_3^+]$ molar ratio at 0, 2, 4, 6 and 8 times dilution. $[\text{H}_4]_{\text{initial}} = 0.1 \text{ wt.}\%$.

b) *Colloidal stability of PIC solutions vs salt addition*

The presence of salt can screen electrostatic interactions between the opposite charges of components, which can initiate the decomposition of PIC micelles.

The tolerance of these micelles against addition of salt was analyzed by DLS (Figure II.5.). Small increase in hydrodynamic radius from 24.9 ± 0.3 to 27.2 ± 0.2 nm and to 35 ± 0.2 nm were observed up to 0.5 M NaCl (H₂O, 25°C). These observations suggest that the structure of the PIC remained constant at low NaCl concentration. At higher concentration of NaCl, PICs might dissociate.

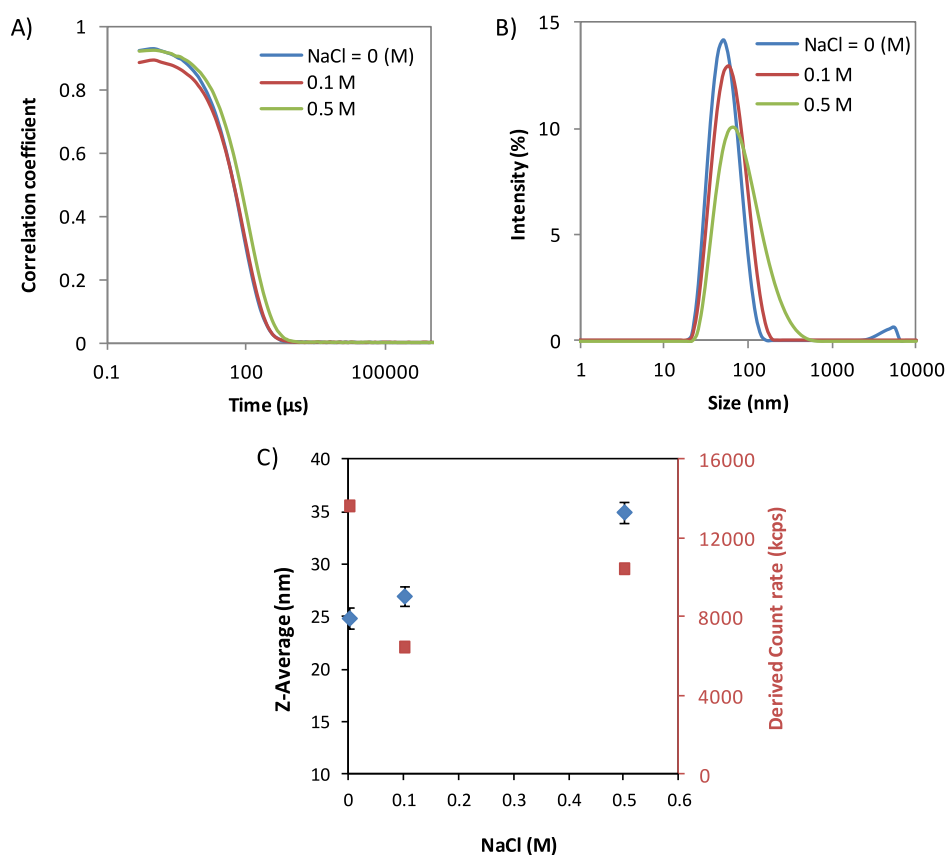


Figure II.5. Correlogram, size distribution in intensity, Z-average and derived count rate of H₄@PEO6-PAA6.5 of [1/1] [COO⁻/NH₃⁺] charge ratio over addition of NaCl at 0.1 and 0.5 mol.L⁻¹. [H₄]_{final} = 0.05 wt.%.

c) *Change of pH*

Since electrostatic interactions are mediated by water molecule both water molecule and ions, PICs formation might be sensitive to variation of pH of the solution. However, study of the stability of hyperbranched PICs was not performed and is expected in the future.

B. Influence of the structural parameters

The influence of the structural parameters of the components on the PICs formation and stability was evaluated. For that, different generations of hyperbranched polyamidoamine polymers (H3, H4 and H5) and PEO-*b*-PAA block copolymers with different chain lengths and composition were used. These copolymers purchased from Polymer Source are listed in Table II.1

Table II.1. Nomenclature of the used block copolymers

Notation\corresponding block chains	PEO (g/mol)	PAA (g/mol)
PEO11-PAA3.7	11000	3700
PEO5-PAA2.7	5000	2700
PEO6-PAA6.5	6000	6500
PEO6-PAA17.5	6000	17500

1. Change of hyperbranched electrolytes

Same experiments than the ones described for H4 core for the formation of PICs were performed with H3 and H5 cores and reported in Figure II.6.

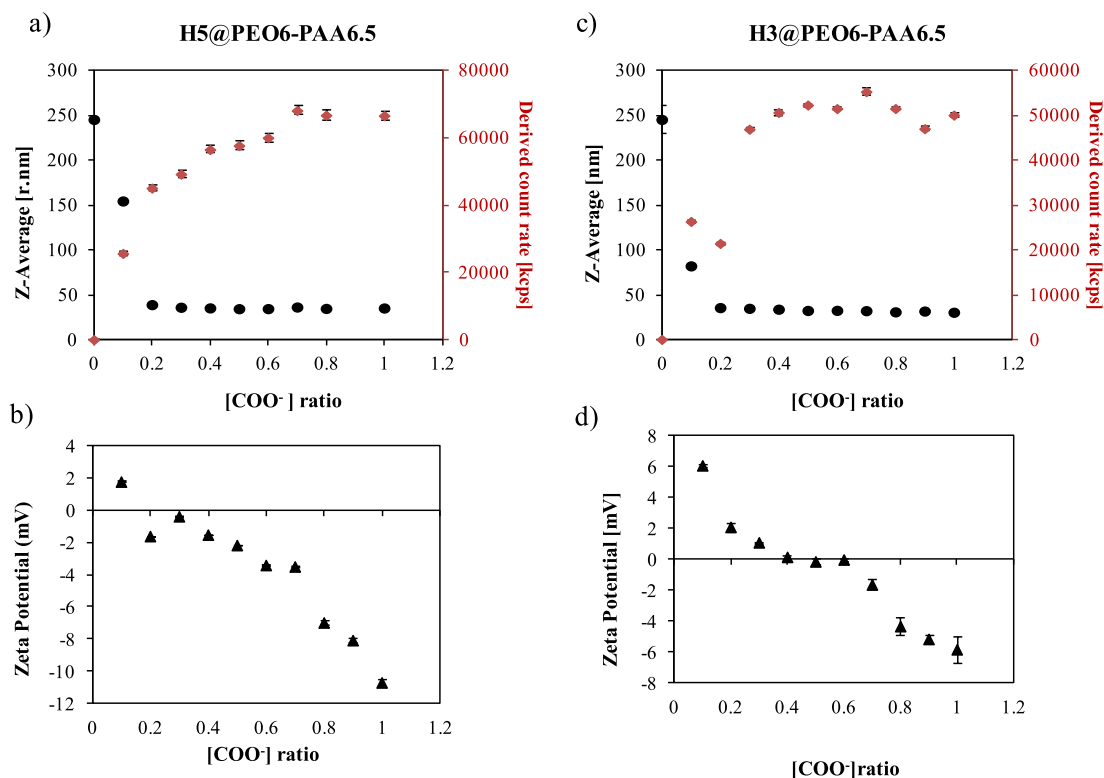


Figure II.6. The change in Z-average (r_H in nm), derived count rate and zeta potential over increasing [COO⁻]/[NH₃⁺] molar ratio of H3@PEO6-PAA6.5 (c,d) and H5@PEO6-PAA6.5 (a,b); [hyperbranched polymers] = 0.1 wt.%.

As shown in Figure II.6 (a,c), the derived count rate increased sharply while increasing the $[\text{COO}^-/\text{NH}_3^+]$ molar ratio (from 0 to 0.2). This indicates an increase of number or size of aggregates due to formation of PICs assembly. The same trends were observed for H3 and H5@PEO6-PAA6.5 systems. As observed for H4@PEO6-PAA6.5, zeta potential values (Figure II.6. (b,d)) decreased with the addition of bloc copolymer. However, the negative zeta potential are unexpected and should be further confirmed.

TEM observations for H3@PEO6-PAA6.5 were performed (Figure II.7). Different morphologies were observed. This might be related to the objects in solution but also can come from drying process. Cryo-TEM analysis must be performed to confirm the morphology of PICs in solution.

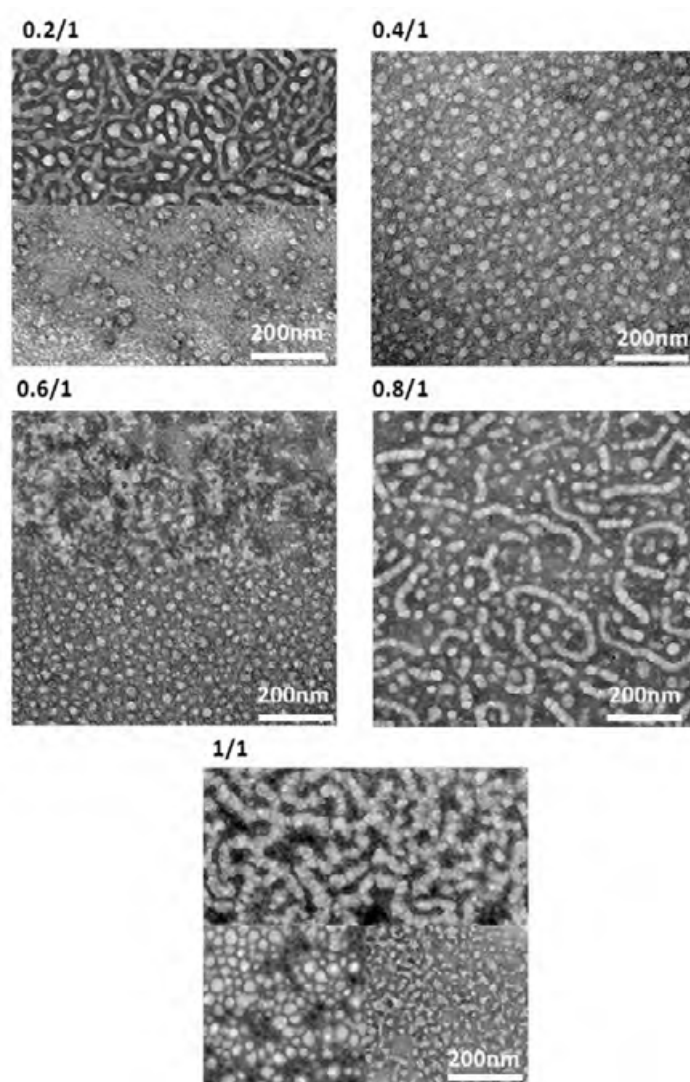


Figure II.7. TEM micrographs for H3@PEO6-PAA6.5 at [0.2 to 0.8/1] $[\text{COO}^-/\text{NH}_3^+]$ molar ratio with negative staining using uranyl acetate; [hyperbranched polymer] = 0.1 wt.%.

Characteristics (minimum molar ratio to form PICs, hydrodynamic radius, zeta potential) of H3@PEO6-PAA6.5, H4@PEO6-PAA6.5 and H5@PEO6-PAA6.5 systems were reported in Table II.2. The minimum molar ratio to obtain well defined PICs was found to be significantly higher for H4 and H5 than for H3@PEO6-PAA6.5. This suggests a more densely packed structure in the formed cases. Nevertheless, hydrodynamic radii remained roughly the same around 30 nm. Considering now the characteristics at a fixed molar ratio ([1/1]), no variation in size was observed. This suggests that excess of block copolymer does not modify the formed object and probably remained free in solution.

Table II.2. Formation and stabilization of H3, H4 and H5@PEO6-PAA6.5.

PICs	Characteristics at minimum molar ratio to obtain well defined PICs			Characteristics at [1/1] [COO ⁻ /NH ₃ ⁺] molar ratio	
	Minimum [COO ⁻ /NH ₃ ⁺] molar ratio	R _h [nm]	ζ [mV]	R _h [nm]	ζ [mV]
H3@PEO6-PAA6.5	0.3/1	31±5	1.0±0.1	31±5	-5.8±0.8
H4@PEO6-PAA6.5	0.8/1	25±5	7.1±0.2	25±5	6.2±0.7
H5@PEO6-PAA6.5	0.6/1	36±5	-3.4±0.4	36±5	-10.7±0.8

2. Change of composition of block copolymers

The effect of PEO-PAA block copolymer length and composition were investigated and main characteristics of the formed PICs were reported in Table II.3.

Table II.3. Characteristic and stability of PICs based on H4 with different PEO-PAA copolymers

N°	PICs	Characteristics at minimum molar ratio to obtain well defined PICs			Characteristics at [1/1] [COO ⁻ /NH ₃ ⁺] molar ratio			
		Minimum [COO ⁻ /NH ₃ ⁺] molar ratio	R _h [nm]	ζ [mV]	ζ [mV]	R _h [nm]		
						0 M NaCl	0.1 M NaCl	0.5 M NaCl
1	H4@PEO11-PAA3.7	0.6/1	91±5	6±0.4	6.7±0.4	92±5	109±5	98±5
2	H4@PEO5-PAA2.7	0.2/1	24±5	4.6±0.1	-2.3±0.1	32±5	54±5	38±5
3	H4@PEO6-PAA6.5	0.8/1	25±5	7.1±0.2	6.2±0.7	25±5	27±5	35±5
4	H4@PEO6-PAA17.5	0.8/1	38±5	-14.2±0.7	-12.1±1.0	38±5	78±5	226±5

PICs formed from the PEO-PAA copolymers of similar PEO block (5000g/mol or 6000g/mol) with increasing size of PAA blocks (entry 2, 3 and 4 in Table II.3) lead to the following observations:

- An increase of the hydrodynamic radius was observed from 24 to 38 nm.
- A longer block of PAA makes the system more sensitive to addition of salt.

Comparison of PICs with PEO-PAA comprising similar PAA block but different length of PEO block (entry 1 and 2 in Table II.3), show that longer PEO block led to PICs with bigger hydrodynamic radius. Furthermore, stability against addition of salt seemed to be more efficient with longer PEO chain.

C. PICs based on dendrigraft polylysine

Dendrigraft polylysine (DGL) were kindly given by Colcom company [6], [7]. The chemical structure of generation 2 was given in Figure II.8. The main characteristics of this polymer were reported in Table II.4.

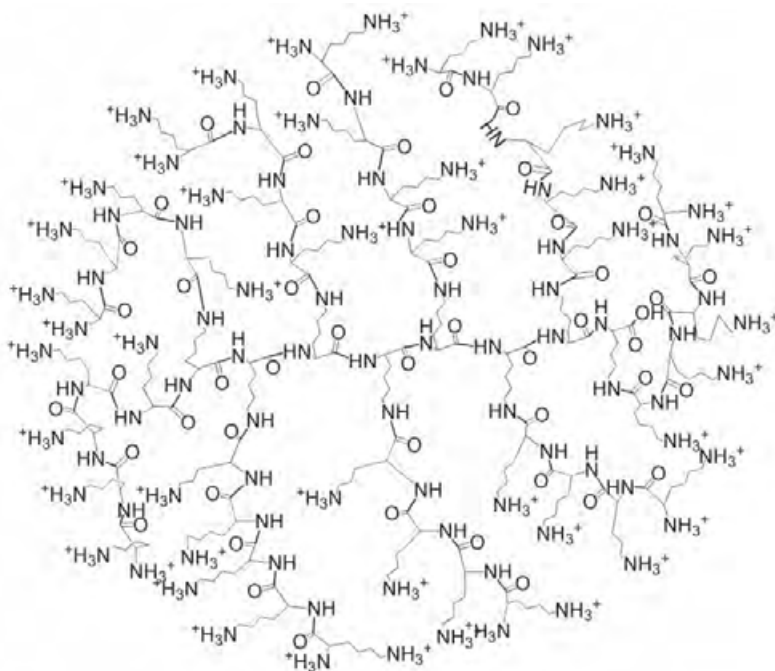


Figure II.8. Dendrigraft polylysine generation G2

Table II.4. Characteristics of DGL G2-3-4

Generation	Mw [g/mol]	PDI (SEC)	R _h [nm]
2	11 800	1.38	1.95
3	32 100	1.46	3.05
4	88 800	1.36	3.7

The effect of PEO-PAA block copolymer length and composition were investigated and main characteristics (minimum molar ratio to form PICs, hydrodynamic radius, zeta potential) of the formed PICs with DGL3 were reported in Table II.5.

Table II.5. Characteristic of PICs based on lysine dendrigraft with different PEO-PAA copolymers

	PICs	Characteristics at minimum molar ratio to obtained well defined PICs			Characteristics at [1/1] [COO ⁻ /NH ₃ ⁺] molar ratio	
		Minimum [COO ⁻ /NH ₃ ⁺] molar ratio	R _h [nm]	ζ [mV]	R _h [nm]	ζ [mV]
1	DGL3@PEO11-PAA3.7	0.7/1	31±5		31±5	
2	DGL3@PEO5-PAA2.7	1.0/1	11±5	0.9±0.2	11±5	0.9±0.2
3	DGL3@PEO6-PAA6.5	1.0/1	20±5	-27±0.2	20±5	-27±0.2
4	DGL3@PEO6-PAA17.5	1.0/1	27±5	17.6±0.4	27±5	17.6±0.4

For similar PEO blocks (see entries 2, 3 and 4 in the Table II.5), increase of PAA block led to bigger hydrodynamic radius PICs as observed in the case of H4 based PICs. It is noticeable that sizes of DGL3@PEO-PAA systems are bigger than the one of H4@PEO-PAA systems. This may be due to the fact that DGL is more monodisperse than hyperbranched polymers.

For similar PAA block (see entries 1 and 2 in the Table II.5), larger PICs were obtained with longer PEO chain as already seen in the case of H4 based PICs.

D. PICs based on PAMAM dendrimers

The formation of PICs based on PAMAM dendrimers was also studied. Two generations PAMAM2 and PAMAM4 were used in this studied. PEO11-PAA3.7 was chosen as block copolymer. As previously, pH of the initial solutions was adjusted to pH7. The main characteristics of the formed PICs are given in Table II.6.

Table II.6. Characteristic of PICs based on PAMAM of generation 2 and 4 with different PEO₁₁-PAA_{3.7} copolymers.

	PICs	Characteristics at minimum molar ratio to obtained well defined PICs		Characteristics at [1/1] [COO ⁻ /NH ₃ ⁺] molar ratio
		Minimum [COO ⁻ /NH ₃ ⁺] molar ratio	R _h [nm]	R _h [nm]
1	PAMAM ₂ @PEO ₁₁ -PAA _{3.7}	0.6/1	28±5	28±5
2	PAMAM ₄ @PEO ₁₁ -PAA _{3.7}	0.7/1	34±5	34±5
3	H ₄ @PEO ₁₁ -PAA _{3.7}	0.6/1	91±5	92±5
4	DGL ₃ @PEO ₁₁ -PAA _{3.7}	0.7/1	31±5	31±5

Increasing the size of the core led to an increase of hydrodynamic radius values from 28 to 34 nm for PAMAM₂ and PAMAM₄ cores respectively. For branched core with similar molecular weights, monodispersed PAMAM₄ enable to obtain smaller PICs as already observed in the case of DGL₃.

E. Conclusion

We have developed PICs systems whose sizes and overall charge can be tuned by changing polymer structural parameters. Preliminary stabilization studies underline good stability of these systems upon addition of salts or dilution. Complete study on the stability of dendrigraft system can give us a toolkit for the formation and stabilization of dendritic PICs. Further structural characterizations of those systems are underway to better understand their overall morphologies in solution (SANS experiments).

III. Thermoresponsive PICs

We aimed in this work at developing a thermoresponsive PICs system by using PNIPAM based block copolymers. For this purpose a diblock copolymer PAA₁₀-PNIPAM₂₄ was used with respective molecular weight of both blocks equal to 10000g/mol and 24000g/mol. The PICs formation was firstly studied on hyper branched H₄, then dendrigraft based PICs will be presented.

A. Thermoresponsive PICs based on hyperbranched polyamidoamine H4

1. Formation and stabilization of PICs

a) *Size measurements by DLS*

Well defined PICs were formed after addition of PAA-PNIPAM polymer solution onto hyperbranched H4 solution with a $[\text{COO}^-/\text{NH}_3^+]$ molar ratio equal to $[0.7/1]$. For this ratio, Z-average was measured at 66 nm (Figure III.1).

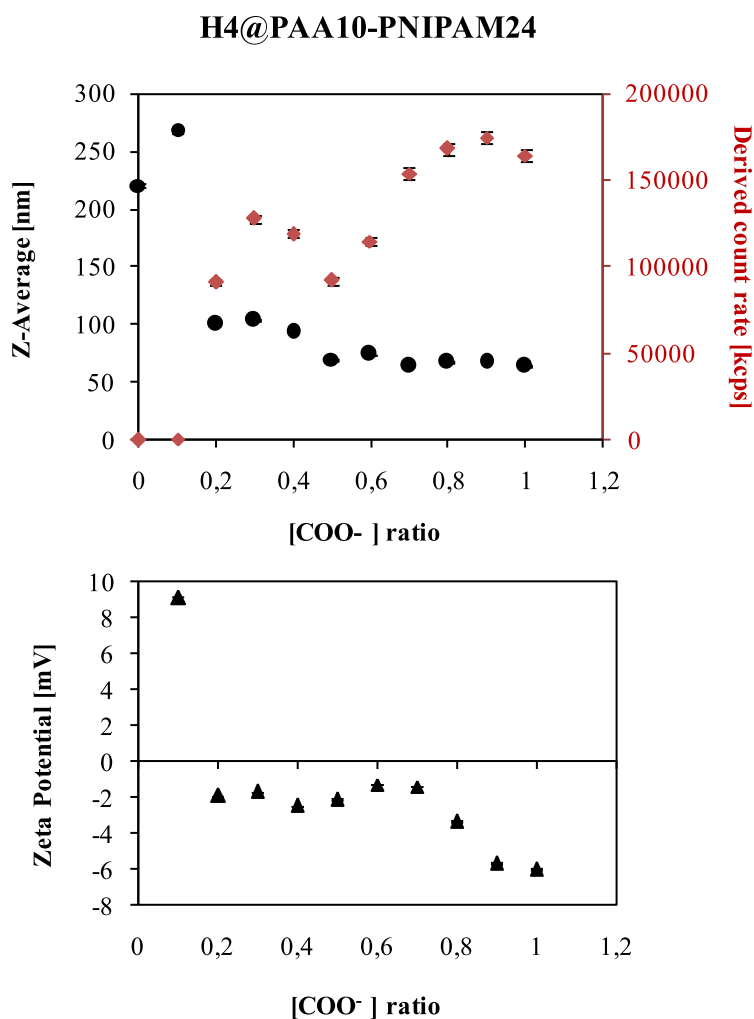


Figure III.1. Evolution of Z-average (radius), derived count rate (top) and zeta potential (bottom) as a function of $[\text{COO}^-/\text{NH}_3^+]$ molar ratio for H4@PAA10-PNIPAM24; [hyperbranched polymers] = 0.1 wt.%.

The main characteristics are given in Table III.1.

Table III.1. Characterization of H4@PAA10-PNIPAM24 by DLS; [H4] = 0.1wt.%; T=25°C

PICs	Characteristics at [1/1] [COO ⁻ /NH ₃ ⁺] molar ratio		Effect of salt addition- R _h [nm]	
	R _h [nm]	ζ [mV]	0.1 M NaCl	0.5 M NaCl
H4@PAA10-PNIPAM24	64±5	-6±0.1	137±10	388±20

H4@PAA10-PNIPAM24 was found highly sensitive to salt addition. At 0.1M NaCl, higher value of Z-average with broaden size distribution were obtained (Figure III.2). At 0.5M NaCl in solution, the PIC assembly aggregated. This may come from the decrease of cloud point temperature of PNIPAM block with the addition of salt.

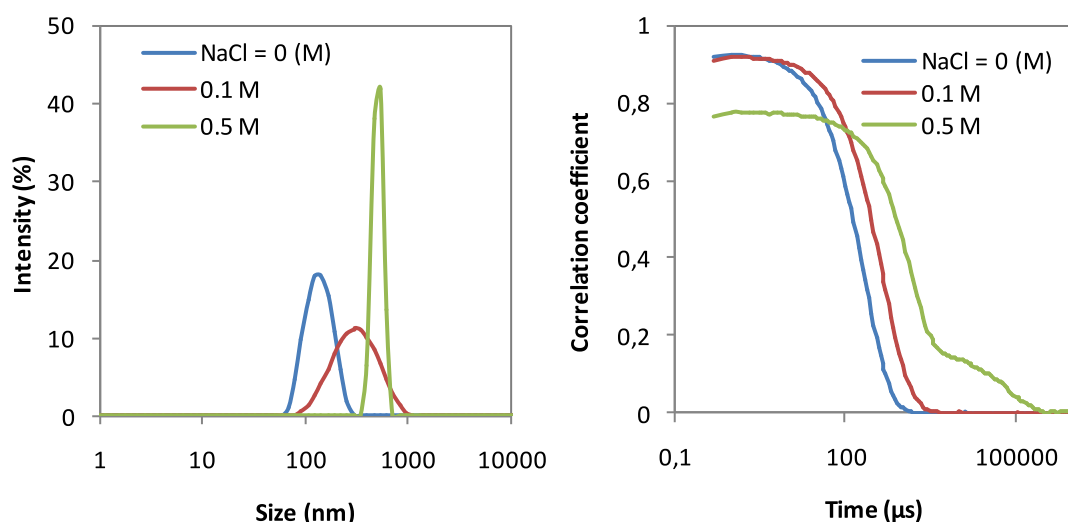


Figure III.2. Correlograms, size distribution in intensity, Z-average and derived count rate of H4@PAA10-PNIPAM24 of [1/1] [COO⁻/NH₃⁺] molar ratio over addition of NaCl at 0.1 and 0.5 M. [H4]_{final}=0.05 wt.%; T=25°C

2. Thermoresponsive properties

a) DLS studies

Due to the presence of PNIPAM block, the PICs displayed a T_c temperature confirmed by a change in size of PICs while increasing temperature (Figure III.3). From 20 to 34 °C, PICs sizes increased very slightly. Above 34°C, Z-average started to increase sharply and from

40°C PICs aggregated into large objects above 1 μ m. T_c was taken at the point where the change in Z-average started to change sharply around 34°C. The results were reported in Table III.2.

Table III.2. Thermoresponsive properties

PICs	DLS			DSC		UV
	T_c	R_h [nm] 20°C	R_h [nm] 40°C	T_c	ΔH [J/g]	T_c
H4@PAA10-PNIPAM24	34	64 \pm 5	386 \pm 5	34.8	23.0 \pm 5.8	34.7

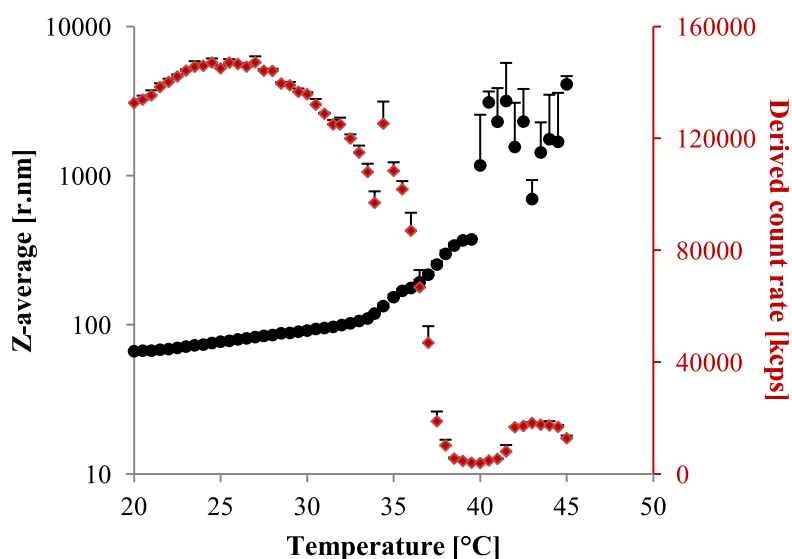


Figure III.3. Evolution in size of H4@PAA10-PNIPAM24 at [0.6/1] [COO-/NH₃⁺] molar ratio with corresponding derived count rate. Values obtained are average of 3 values. [H4]=0.1 wt.%

b) *Turbidity measurements*

Turbidity of H4@PAA10-PNIPAM24 solution was monitored by measuring the absorbance at 500 nm as a function of temperature on both heating and cooling processes (Figure III.4). Different heating and cooling rates were used: 4, 3, 2 and 1°C/min. Transition temperatures were taken at reflection points of each curves and finally extrapolated at zero speed. The extrapolated T_c values for heating and cooling process were found very close at 34.70°C and 34.74 °C respectively.

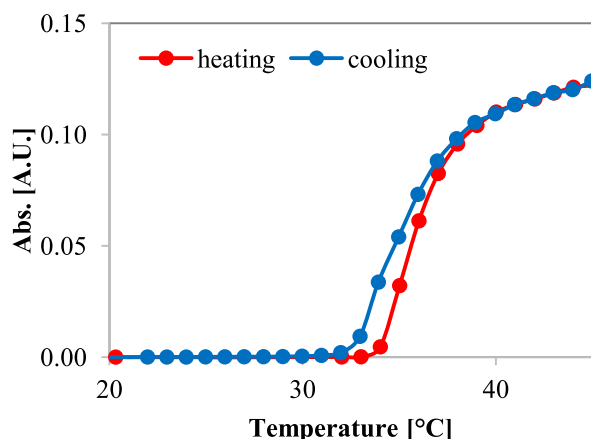


Figure III.4. Evolution of absorbance for H4@PAA10-PNIPAM24 [0.6/1] [COO⁻/NH₃⁺] molar ratio at 500 nm over change of temperature on heating and on cooling at 1°C/min.

c) *DSC measurements*

Transition phenomena were also monitored by DSC experiments, thermograms of H4@PAA10-PNIPAM24 solution were recorded at 4 different heating and cooling rates (4, 3, 2, 1 °C/min). Transition temperature were taken at the top of the peak for each curves and extrapolated to zero speed. As observed in Figure III.5, hysteresis phenomena existed between heating and cooling process which is expected. The extrapolated T_c values for heating and cooling process were found at 34.8°C and 32.6 °C respectively.

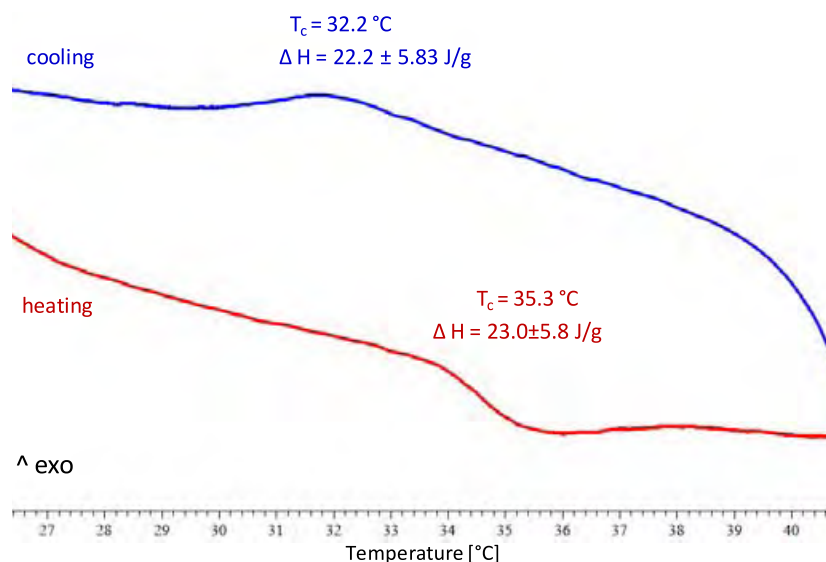


Figure III.5. Thermograms of H4@PAA10-PNIPAM24 [0.6/1] [COO⁻/NH₃⁺] molar ratio recorded on heating and cooling at 1°C/min. T_c values were taken at the top of the peaks, ΔH value is normalized for PNIPAM content (J/g of PNIPAM) and is an average of 4 values obtained from 4 different heating or cooling rates (4, 3, 2, 1 °C/min).

B. Thermoresponsive PICs based on dendrigraft polylysine DGL3

1. Formation and stabilization of PICs

Well defined PICs were formed after addition of PAA-PNIPAM polymer solution onto dendrigraft DGL3 solution with a $[\text{COO}^-/\text{NH}_3^+]$ molar ratio equal to $[0.6/1]$. For this ratio, Z-average was measured at 30 nm. (Figure III.6).

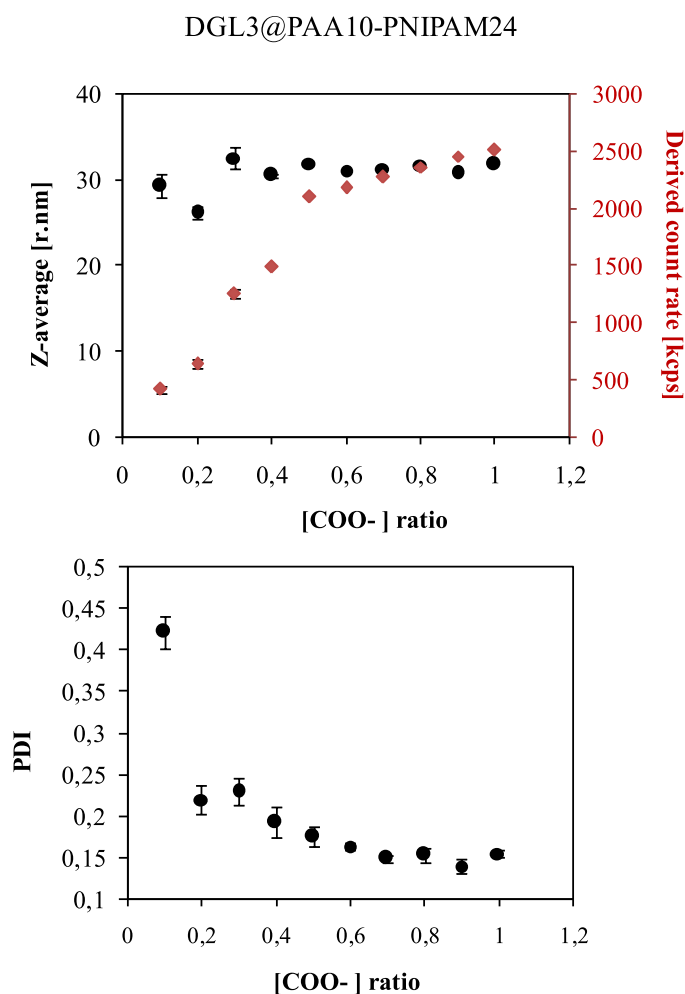


Figure III.6. Evolution of Z-average, derived count rate (top) with corresponding PDI values (bottom) over increasing $\text{COO}^-/\text{NH}_3^+$ ratio of DGL3@PAA10-PNIPAM24. $[\text{DGL3}] = 0.1$ wt.%; $T=25^\circ\text{C}$.

2. Stability of PICs colloidal solution

a) Ionic strength

The systems showed high tolerance against addition of NaCl upon 600 mmol/L confirmed by almost no change in size and PDI. Above 600 mmol/L the size increased and

formed huge aggregates as indicate in figure III.7. Once again, this phenomenon should be related to the decrease of cloud point temperature of PNIPAM when increasing ionic strength.

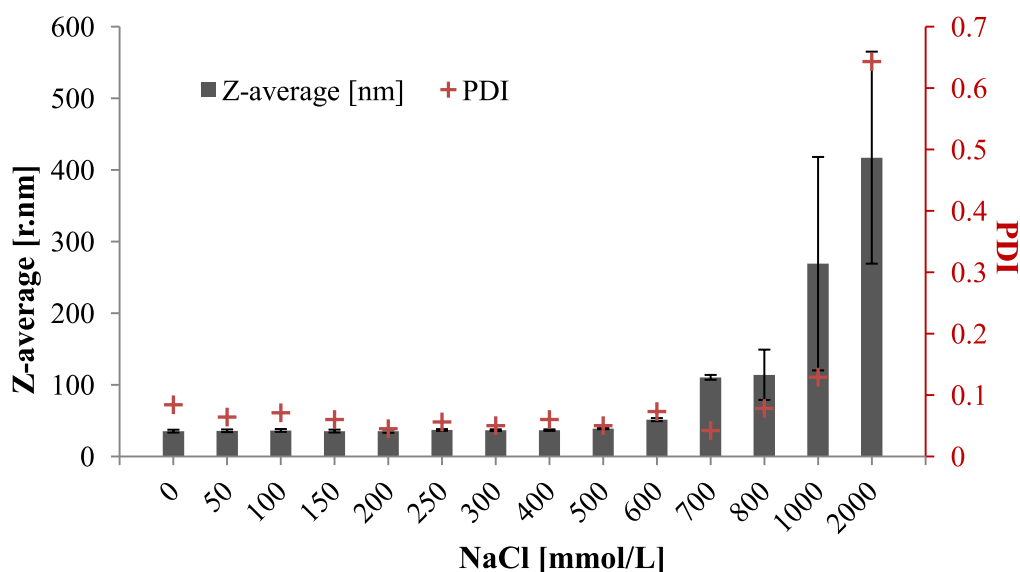


Figure III.7. Evolution of Z-average with corresponding PDI values when increasing of the concentration of NaCl. [DGL3] = 0.05 wt. %; T=25°C.

b) *Change of pH*

Due to the presence of carboxylic functions, PICs assembly can be highly impacted by the change of pH. As shown in Figure III.8, PICs were not stable at low pH value corresponding to protonated form of carboxylate. However, PICs assembly remain stable at higher pH (around 7-8).

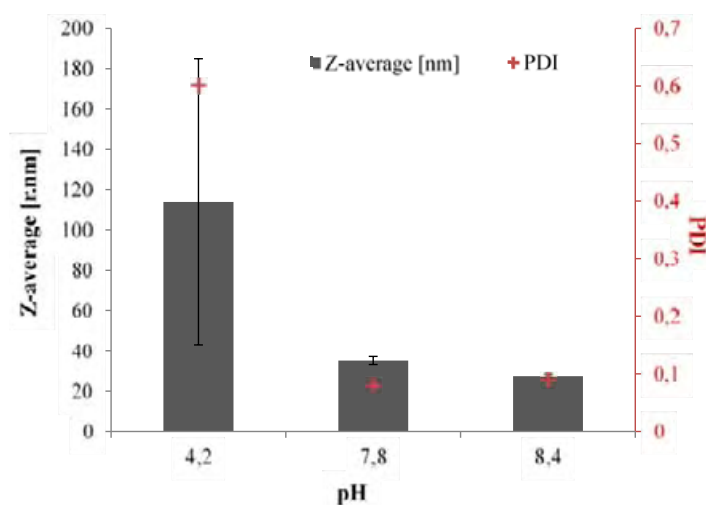


Figure III.8. Evolution of Z-average and PDI as a function of pH; [DGL3]=0.1 wt. %

3. Thermoresponsive properties

Due to the presence of PNIPAM block, the PICs displayed a T_c temperature confirmed by change in size of PICs over increasing of temperature (DLS measurement in Figure III.9). From 20 to 33 °C, PICs sizes increased very slightly. Above 33°C, Z-average started to increase sharply and reached a plateau at 55 nm. T_c was taken at the point where Z-average started to change sharply around 33.2°C.

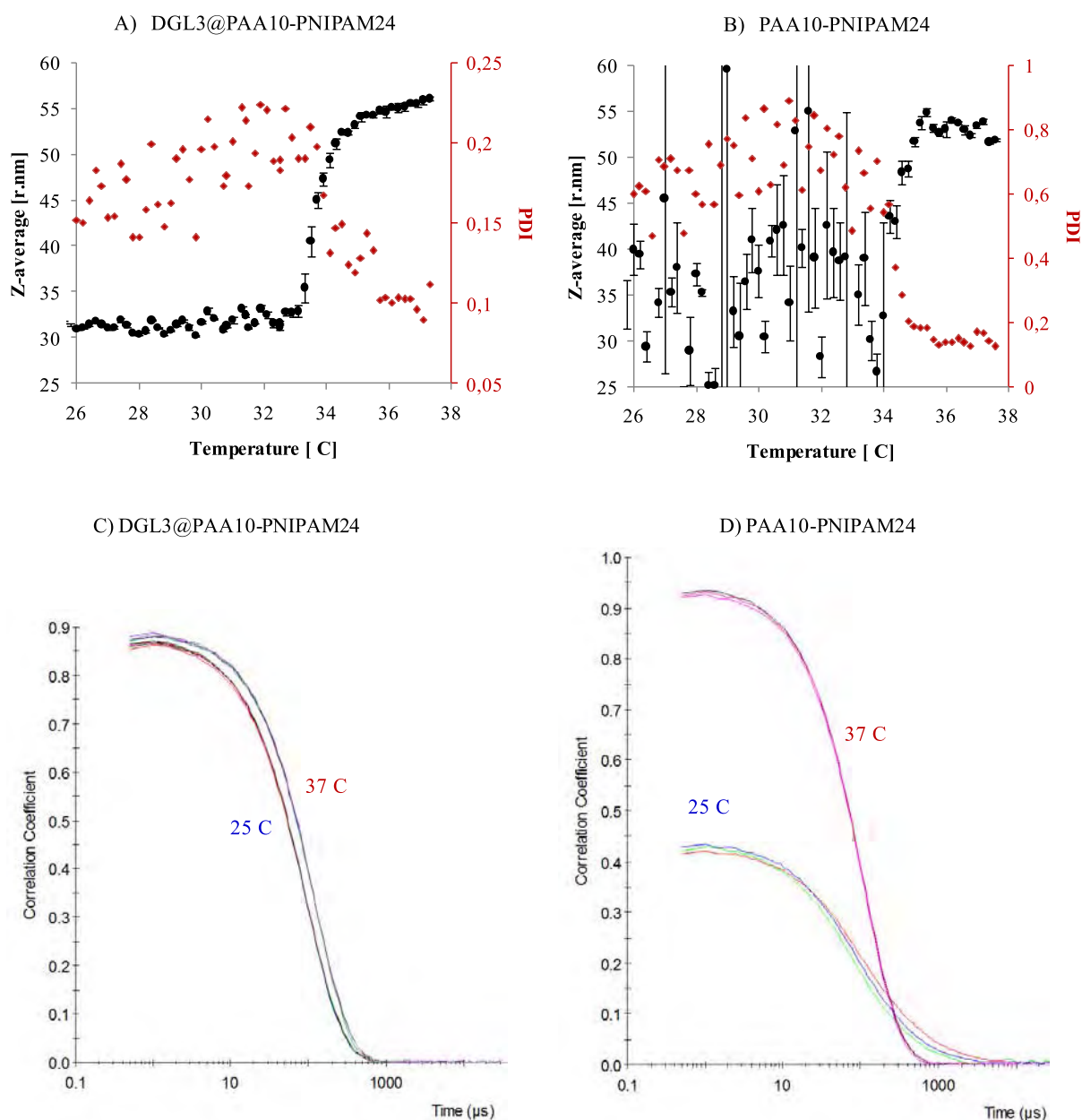


Figure III.9. Evolution of size as a function of temperature with corresponding PDI values for A) DGL3@PAA10-PNIPAM24; [DGL3]=0.1 wt.%, B) PAA10-PNIPAM24; [PAA10-PNIPAM24]=0.01 wt.%. C, D: corresponding correlograms. Values obtained are average of 5 measurements.

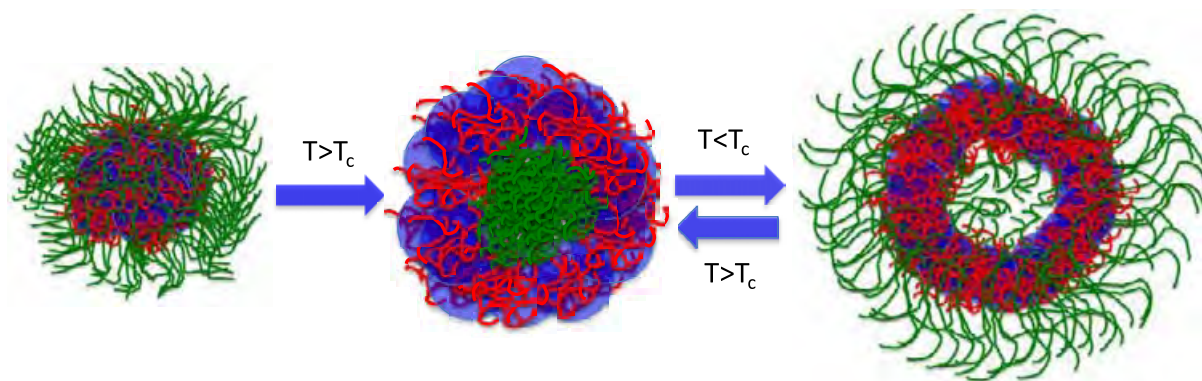
For PAA10-PNIPAM24 a T_c value was measured by DLS technique at 34.2 °C. Below this temperature, PAA10-PNIPAM24 are fully soluble in water as a single chain polymer. Inaccurate Z-average value and very high PDI values are due to the detection limit of DLS measurements. Above T_c , well-defined aggregates are detected, probably corresponding to aggregates of amphiphilic polymers with PNIPAM hydrophobic core. Upon cooling, PAA10-PNIPAM24 aggregates disappeared, the polymer is again fully soluble in water as a single polymer.

For DGL3@PAA10-PNIPAM24, the structure formed above T_c cannot return to its original size while cooling (seen Table III.3).

Table III.3. Z-average and Difusion Coefficient measurement from cycles of heating and cooling at 25 and 40°C of PAA10-PNIPAM24 (0.01wt.%) and DGL3@PAA10-PNIPAM24 ([DGL3]=0.1%)

T °C	PAA10-PNIPAM24		DGL3@PAA10-PNIPAM24	
	Z-average [r.nm]	Z-average [r.nm]	Difusion Coefficient [m ² /s]	
25	n.d.	31.6±0.8	8.3±0.2 x 10 ⁻¹¹	
40	53.3±2.3	79.6±1.2	n.d.	
25	n.d.	98.6±1.8	1.9±0.21 x 10 ⁻¹¹	
40	54.4±1.4	110.6±2.1	n.d.	
25	n.d.	127.2±1.6	1.9±0.21 x 10 ⁻¹¹	
40	54.2±1.2	108.2±1.9	n.d.	

This phenomenon was already observed in the literature in the case of copolymer based PICs [8]–[11]. This may come from the change in the structure of PICs. At low temperature, PAA blocks interact with DGL3 by ionic bonds formed with the hydrophobic core while PNIPAM chains are fully soluble and expose to the solvent therefore leading to a core-shell structure. Above the T_c of PNIPAM, PNIPAM chains lose hydrophilic character and aggregate together to minimize contact with the solvent. PNIPAM might hide inside the structure and form a corona reversed structure stabilized by DGL3. When returning back to low temperature the whole structure is blocked by the GDL3-PAA parts and then cannot return to the original structure below T_c . Suggestion for this transition is illustrated in SchemeIII.1.



Scheme III.1. Suggestion for the transition of PICs above T_c . Color codes : Green : PNIPAM chains, red : PAA chains, blue : DGL.

In addition, NMR experiments were performed (Figures III.10 and III.11). At low temperature, intense PNIPAM signals clearly appeared. Above T_c , the intensity of PNIPAM signals decreased comparatively to the signals of DGL3. When returning to 25°C , the intensities of PNIPAM signals increased back to their initial values.

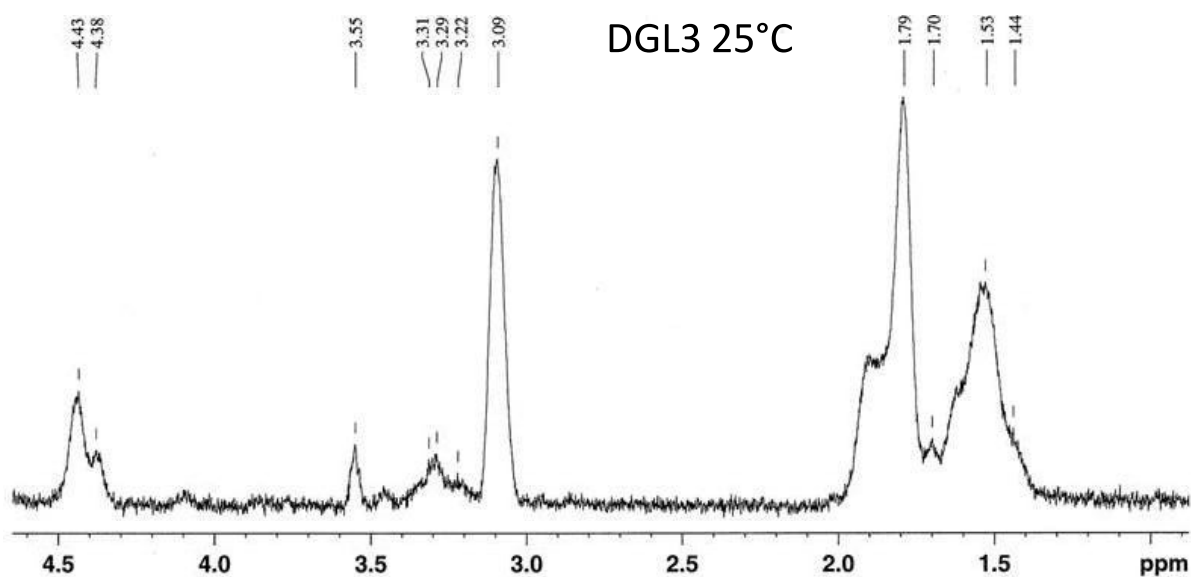


Figure III.10. ^1H NMR spectrum of DGL3 (D_2O , 300Hz, 25°C)

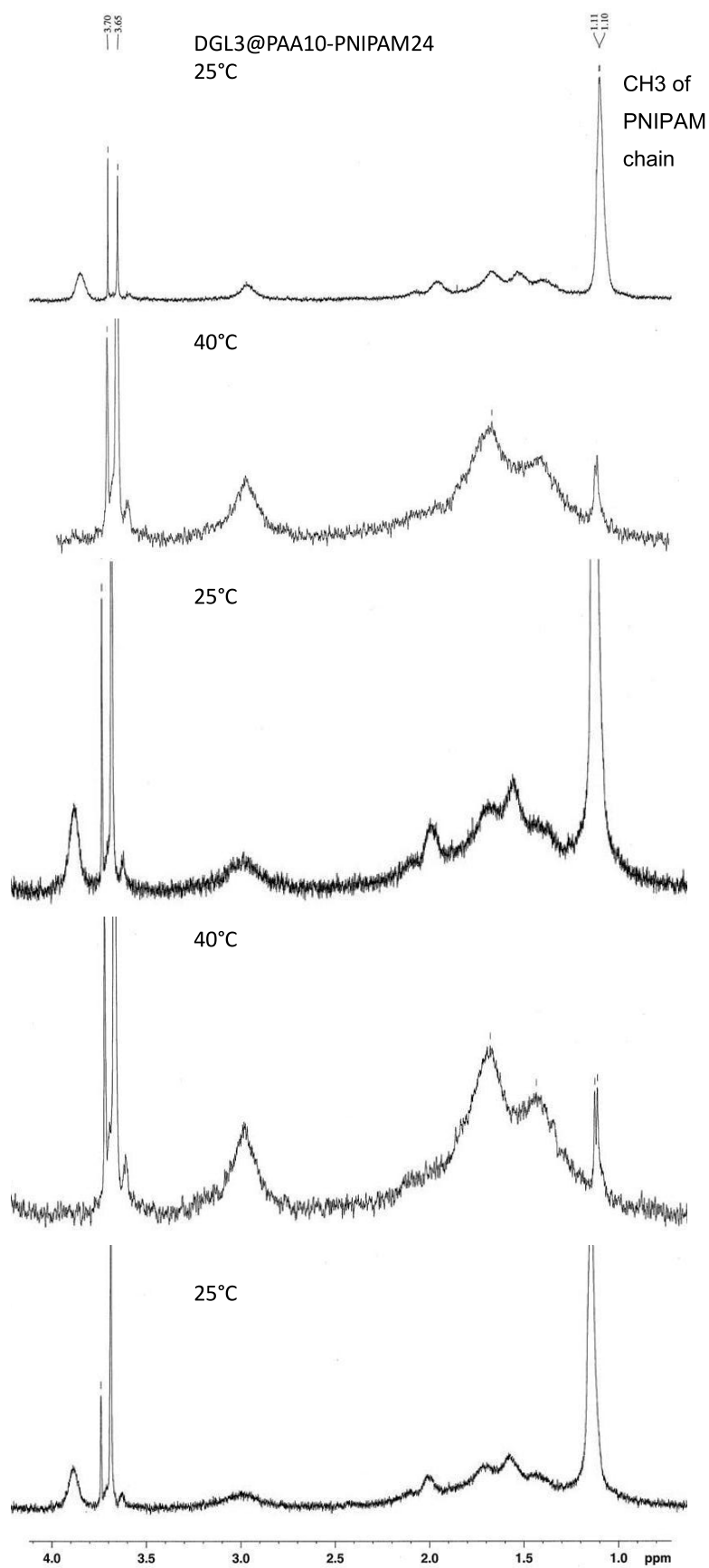


Figure III.11. ^1H NMR spectra of DGL3@PAA10-PNIPAM24 at different heating-cooling cycles at 25 and 40°C, (D_2O , 300Hz).

Diffusion coefficient values calculated from DOSY experiments for DGL₃@PAA10-PNIPAM₂₄ systems over three heating and cooling systems are in agreement with the results from DLS and NMR. Additional experiments are under way to fully characterize the structure proposed in scheme III.1 (SANS and SAXS experiments).

IV. Conclusion

We have developed PICs systems whose sizes and overall charge can be tuned by changing polymer structural parameters. Additionally thermoresponsive PICs have been obtained whose morphology change irreversibly by increasing temperature. Preliminary stabilization studies underline good stability of these systems upon addition of salts or dilution. Further structural characterizations of those systems are underway to better understand their overall morphologies in solution (SANS and SAXS experiments).

V. References

1. Yoon, H., Dell, E. J., Freyer, J. L., Campos, L. M. & Jang, W.-D. Polymeric supramolecular assemblies based on multivalent ionic interactions for biomedical applications. *Polymer* **55**, 453–464 (2014).
2. Kokufuta, E., Ogawa, K., Doi, R., Kikuchi, R. & Farinato, R. S. Geometrical Characteristics of Polyelectrolyte Nanogel Particles and Their Polyelectrolyte Complexes Studied by Dynamic and Static Light Scattering[†]. *J. Phys. Chem. B* **111**, 8634–8640 (2007).
3. Nishiyama, N., Jang, W.-D. & Kataoka, K. Supramolecular nanocarriers integrated with dendrimers encapsulating photosensitizers for effective photodynamic therapy and photochemical gene delivery. *New J. Chem.* **31**, 1074–1082 (2007).
4. Sousa-Herves, A., Fernandez-Megia, E. & Riguera, R. Synthesis and supramolecular assembly of clicked anionic dendritic polymers into polyion complex micelles. *Chem. Commun.* 3136–3138 (2008).
5. Tomalia, D. A. *et al.* A New Class of Polymers: Starburst-Dendritic Macromolecules. *Polym. J.* **17**, 117–132 (1985).
6. Collet, H. *et al.* An Expedient Multigram-Scale Synthesis of Lysine Dendrigrift (DGL) Polymers by Aqueous N-Carboxyanhydride Polycondensation. *Chem. – Eur. J.* **16**, 2309–2316 (2010).
7. Rossi, J.-C. *et al.* Functionalisation of free amino groups of lysine dendrigrift (DGL) polymers. *Tetrahedron Lett.* **53**, 2976–2979 (2012).
8. Grubbs, R. B. & Sun, Z. Shape-changing polymer assemblies. *Chem. Soc. Rev.* **42**, 7436–7445 (2013).

9. Papagiannopoulos, A., Zhao, J., Zhang, G., Pispas, S. & Radulescu, A. Thermoresponsive transition of a PEO-b-PNIPAM copolymer: From hierarchical aggregates to well defined ellipsoidal vesicles. *Polymer* **54**, 6373–6380 (2013).
10. Li, Z. *et al.* Fabrication of an asymmetric hollow particle with a thermo-sensitive PNIPAM inside corona. *Polymer* **50**, 825–831 (2009).
11. Xiong, D. *et al.* Temperature-responsive multilayered micelles formed from the complexation of PNIPAM-b-P4VP block-copolymer and PS-b-PAA core-shell micelles. *Polymer* **49**, 2548–2552 (2008).

Conclusion

Within this study, different families of stimuli responsive polymers have been used to obtain materials (gel structures, hybrid materials,...) whose properties were modified upon application of an external stimulus. More specifically we have been interested in the case of hyperbranched structures which have been extensively studied in the past in our team and have been used, as promising polymers, in literature for many applications as depicted in the literature review. More precisely, the first objective of this work was to understand how the chemical architecture of the studied polymer (molecular weight, level of branching, functionalization,..) can modulate the properties of the studied materials. For this purpose, different families of core-shell polymer obtained from branched cores have been synthesized and characterized. Two main strategies based either on covalent grafting or on ionic interactions between the core and a functional shell have been used. Stimuli responsive materials were thus obtained that were used for the elaboration of (stimuli) thermoresponsive nanohybrid materials.

In a first part, thermoresponsive core-shell structures were obtained from the coupling of poly(N-isopropylacrylamide) PNIPAM of different chain lengths to branched core of different sizes. These polymers are fully soluble in water as aggregates of nanometer size up to their characteristic transition temperature corresponding to dehydration of PNIPAM chains. At low polymer concentrations, the study of their thermoresponsive properties (as the rate of collapse upon transition to hydrated or dehydrated forms) enable to assess a strong relationship between these properties and the macromolecular architecture of the polymers (i.e. structure of the core and length of the PNIPAM shell). Moreover, these core-shell polymers are able to form thermoresponsive gel networks at higher concentration of polymers (above 20% in weight) in water. Microscopic structure of these hydrogels was found to depend strongly on molecular architecture of the polymer. This induces modifications of both thermoresponsive and rheological properties of these gels. Those polymers, either at low concentrations or at higher concentrations in a gel form, were utilized for the stabilization of preformed NPs or the *in situ* synthesis of gold nanoparticles. Once again, we demonstrated that, the macromolecular architectures greatly influence both the growth mechanism of NPs formed *in situ* and the colloidal stability of the obtained nanohybrids. Whereas smaller linear polymers allow a better control on NPs growth, branched structures proved to be better stabilizing agents. Among them, TREN based structures were found to be more efficient than highly branched structures HYPAM. Lastly, in the case of gelified hybrid structures, the presence of AuNPs within the gels acted as cross linking points and improved its gelation properties. Those effects should be modulated by controlling the size/amount of Au NPs within the hydrogel.

Core shell structures were then obtained by using ionic interactions instead of covalent interactions. Firstly, structures resulting from assembly with a small surfactant molecule (sodium dodecylsulfate) were studied. When HYPAM or PAMAM was used as a core, these complexes present columnar rectangular and lamellar thermotropic mesophases as demonstrated by polarizing optical microscopy, differential scanning calorimetry, and small-angle X-ray scattering. The relationships between the structural characteristics of the polymers (size of the hyperbranched core, hyperbranched or dendritic nature of the core, substitution ratio) and the mesomorphic properties were studied. Those ionic structures were then taken into account to interact with an ionic NPs precursor and to localize this one in a specific way within the liquid crystalline structure prior to reduction. The liquid crystalline phase was then used for the *in situ* formation of gold

nanoparticles. The templating effect of the liquid crystal mesophase resulted in the formation of isotropic nanoparticles, the size of which was dictated by the local organization of the mesophase and by the molar mass of the hyperbranched complex. The presence of NPs induced strong changes in local organization of the LCs polymer, nevertheless the obtained hybrid materials remained liquid crystalline. Then, hyperbranched positively charged core (HYPAM, PAMAM, DGL) were put in interaction with block copolymers comprising an anionic part and an hydrophilic polymer (namely polyethylene glycol or thermoresponsive PNIPAM) to obtain polyion complex polymers (PICs). PICs were obtained from PEO-PAA polymers. Whereas they remain rather stable up to high concentration of salt, they dissociate when pH of the solution was decreased below pKa value of the carboxylic function of the interaction block. Moreover, their stability in water solution is dependent on both the average molecular weight and the polymer composition. In the case of thermoresponsive systems based on the use of PAA-PNIPAM block copolymers, well defined nanoobjects were also obtained that can undergo irreversible morphological change upon transition temperature.

In conclusion, all examples described here demonstrated the strong influence of molecular structures on the properties of chosen materials. Hence, branched structures are of special interest to lead to high efficient stabilizing agent form aqueous solutions of metallic NPs, enable the formation of gel with enhanced rheological properties and favor the formation of liquid crystalline highly organized structures. Therefore the polymer described within this study has already been used to mediate the formation of new promising materials:

- Hyperbranched thermoresponsive structures based on PNIPAM and PEG polymers are actually studied for their ability to mediate the formation and stabilization of GdPO₄ NPs in aqueous solution. Their use as magnetic resonance imaging contrast agent was studied.
- Ionic structures (PICs) obtained from ionic interactions between a hyperbranched core and another polymer are studied for their ability to interact with ionic inorganic compounds. They present promising opportunities for the formation of homogeneous hybrid materials used as drug delivery systems or as highly organized hybrid liquid crystalline materials with unprecedented organization (metamaterials).

Experimental section

CONTENTS

I. CHAPTER 2	ES-5
A. MATERIALS	ES-5
B. SYNTHESIS.....	ES-5
1. <i>Polymer synthesis</i>	ES-5
a) Synthesis of tris (2-di (methylacrylate) aminoethyl) amine	ES-5
b) Synthesis of hyperbranched poly(amidoamine) HYPAMx	ES-6
c) The synthesis of core-shell polymers	ES-7
2. <i>Synthesis of gold nanoparticles by NaBH₄</i>	ES-10
3. <i>Gold nanoparticles stabilization by polymer solutions</i>	ES-10
4. <i>Salt adding effect</i>	ES-11
5. <i>In situ synthesis of AuNPs</i>	ES-12
C. CHARACTERIZATION TECHNIQUES.....	ES-12
1. <i>Nuclear Magnetic Resonance</i>	ES-12
2. <i>Fourier transform infra red (FTIR)</i>	ES-13
3. <i>Differential Scanning Calorimetry (DSC)</i>	ES-13
4. <i>Small Angle Neutron Scattering experiments (SANS)</i>	ES-13
5. <i>Transmission electron microscopy (TEM)</i>	ES-14
6. <i>Dynamic Light Scattering (DLS)</i>	ES-14
7. <i>Ultraviolet-visible (Uv-vis)</i>	ES-14
8. <i>Size Exclusion Chromatography (SEC)</i>	ES-15
II. CHAPTER 3	ES-16
A. MATERIALS	ES-16
B. SYNTHESIS.....	ES-16
1. <i>Synthesis of HYPAM core and core-shell polymers</i>	ES-16
2. <i>Synthesis of hydrogels</i>	ES-16
3. <i>In situ synthesis of AuNPs embedded in gels structures</i>	ES-16
C. CHARACTERIZATION TECHNIQUES.....	ES-17
1. <i>Characterization of polymers</i>	ES-17
2. <i>Characterization of hydrogels</i>	ES-17
a) Differential Scanning Calorimetry (DSC).....	ES-17
b) Cryo-Scanning Electron Microscopy (Cryo-SEM)	ES-17
c) Rheology	ES-17
d) UV-vis.....	ES-18
3. <i>Characterization of nanoparticles</i>	ES-18
a) Transmission electron microscopy (TEM).....	ES-18

b) UV-Vis	ES-18
III. CHAPTER 4	ES-19
A. MATERIALS	ES-19
B. SYNTHESIS.....	ES-19
1. <i>Synthesis of hyperbranched polymer surfactant complexes</i>	ES-19
2. <i>Formation of polymeric aggregates in solution</i>	ES-20
3. <i>Synthesis of gold nanoparticles in mesophases</i>	ES-20
C. CHARACTERIZATION TECHNIQUES.....	ES-20
1. <i>SEC</i>	ES-20
2. <i>Nuclear Magnetic Resonance</i>	ES-21
3. <i>Fourier transform infrared (FTIR)</i>	ES-22
4. <i>Differential Scanning Calorimetry (DSC)</i>	ES-22
5. <i>Polarized Optical Microscopy (POM)</i>	ES-22
6. <i>Small Angle X-ray Scattering (SAXS)</i>	ES-22
7. <i>Transmission electron microscopy</i>	ES-22
8. <i>Dynamic Light Scattering (DLS)</i>	ES-23
9. <i>UV</i>	ES-23
IV. CHAPTER 5	ES-24
A. MATERIALS	ES-24
B. SYNTHESIS.....	ES-24
1. <i>Synthesis of HYPAM</i>	ES-24
2. <i>PICs formation</i>	ES-24
3. <i>Dilutions</i>	ES-25
4. <i>Salt adding effect</i>	ES-25
C. CHARACTERIZATION TECHNIQUES.....	ES-26
1. <i>Characterization of HYPAM</i>	ES-26
2. <i>Characterization of PICs</i>	ES-26
a) <i>Dynamic Light Scattering Measurements (DLS)</i>	ES-26
b) <i>Transmission electron microscopy (TEM)</i>	ES-26
3. <i>Thermoresponsiveness characterization</i>	ES-27
a) <i>Differential Scanning Calorimetry (DSC)</i>	ES-27
b) <i>Ultraviolet-visible (UV-VIS)</i>	ES-27
c) <i>Nuclear Magnetic Resonance (NMR)</i>	ES-27
d) <i>Diffusion coefficient measurement by NMR-DOSY (Diffusion Ordered Spectroscopy)</i>	ES-27

I. Chapter 2

A. Materials

Tetrachloroauric acid trihydrate ($\text{HAuCl}_4 \cdot 3\text{H}_2\text{O}$), D-Glucosamine hydrochloride, 1,1'-Carbonyldiimidazole, anhydrous DMSO, carboxylic acid terminated PNIPAM 2000g/mol, 5000g/mol and 7000 g/mol, Pur-A-Lyzer™ Mega Dialysis Kit of MWCO 3.5 kDa, 6-8 kDa and 12-14 kDa were purchased from Aldrich and were used without further purification. Tris(2-aminoethyl)amine (Aldrich) was distilled under reduced pressure and stored under argon atmosphere before use. Ultrapure water ($\rho=18 \text{ M}\Omega \text{ cm}^{-1}$) was obtained from Aquadem apparatus.

B. Synthesis

1. Polymer synthesis

a) *Synthesis of tris (2-di (methylacrylate) aminoethyl) amine*

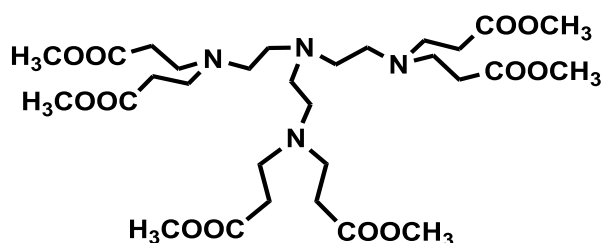


Figure I.1. Tris(2-di(methylacrylate)aminoethyl)amine (TREN)

To 4.092 g of methylacrylate (47.58 mmol) in 6.5 mL of methanol was added dropwise a solution of 1.160 g of freshly distilled tris(2-aminoethyl)amine (7.93 mmol) in 1.5 mL of methanol at 0°C under argon atmosphere. The mixture was then stirred at room temperature during two days. The product (5.16 g, yield=98.2%) was obtained, after elimination of the solvent under vacuum, as slightly yellow oil. The product was then directly used to synthesize HYPAMx Polymer.

$^1\text{H-NMR}$ (300MHz, CDCl_3): $\delta = 2.35$ (t, 12H, $-\text{CH}_2-\text{COOCH}_3$); 2.43 (s, 12H, $-\text{NCH}_2\text{CH}_2\text{N}-$); 2.76 (t, 12H, $-\text{CH}_2\text{CH}_2-\text{COOCH}_3$); 3.65 (s, 18H, $-\text{OCH}_3$) ppm.

b) **Synthesis of hyperbranched poly(amidoamine)
HYPAM_x**

The synthesis of the HYPAM cores were carried out following previously published work by our group [1]. A brief explanation for H3, H4 and H5 is given below.

H3: 2.98 g (20 mmol) of tris(2-aminoethyl)amine were mixed with 1.13 g (1.7 mmol) of tris(2-di(methylacrylate)aminoethyl)amine (ratio trisamine/hexaester=12). The solution was stirred under argon atmosphere at 75°C during two days, at which time the products were dissolved in 5mL CH₂Cl₂ and precipitated into 200mL THF at 0°C. 2.05g of precipitated polymer was obtained as a yellow gum after drying under vacuum during 2 days.

¹H NMR (D₂O, 300 MHz): δ = 2.45 (m, -CH₂-CO-); 2.55-2.77 (br m, -CH₂-NH₂, -N-CH₂-CH₂-N-, -N-CH₂-CH₂-CO-); 3.22 (m, -CH₂-NH-CO-) ppm.

¹³C NMR (D₂O, 300 MHz): δ = 32.7-35.7 (-N-CH₂-CH₂-CO-); 36.9 (-CH₂-NH-CO-); 37.9 (-CH₂-NH₂); 49.3 (-N-CH₂-CH₂-CO-); 50.0-51.4-52.5 (-CO-NH-CH₂-CH₂-N-); 56 (-N-CH₂-CH₂-N-); 174.7 (CONH) ppm.

SEC: $\overline{M}_w = 5200 \text{ g.mol}^{-1}$; DPI = 1.4

H4: 2.50 g (17 mmol) of tris(2-aminoethyl)amine were mixed with 1.13 g (1.7 mmol) of tris(2-di(methylacrylate)aminoethyl)amine (ratio trisamine/hexaester=10). The rest of the procedure is identical to the one for HYPAM₃.

¹H NMR (DMSO-d₆, 500 MHz): δ = 2.24 (m, -N-CH₂-CH₂-N-); 2.45 (m, -CO-NH-CH₂-CH₂-N-); 2.51 (DMSO and m, -CH₂-NH₂); 2.63 (m, -N-CH₂-CH₂-CO-); 2.7 (m, -N-CH₂-CH₂-CO-); 3.1 (m, -CH₂-NH-CO-); 3.45 (NH) ppm.

¹³C NMR (DMSO-d₆, 500 MHz): δ = 33.79 (-N-CH₂-CH₂-N-); 37.34 (-CH₂-NH-CO-); 41.62 (-N-CH₂-CH₂-CO-); 46.15 (-CH₂-NH₂); 47.43 (-N-CH₂-CH₂-CO-); 56.61 (-CO-NH-CH₂-CH₂-N-); 172.0 (CO) ppm.

¹H NMR (D₂O, 300 MHz): δ = 2.45 (m, -CH₂-CO-); 2.55-2.77 (br m, -CH₂-NH₂, -N-CH₂-CH₂-N-, -N-CH₂-CH₂-CO-); 3.22 (m, -CH₂-NH-CO-) ppm.

¹³C NMR (D₂O, 300 MHz): δ = 32.7-35.7 (-N-CH₂-CH₂-CO-); 36.9 (-CH₂-NH-CO-); 37.9 (-CH₂-NH₂); 49.3 (-N-CH₂-CH₂-CO-); 50.0-51.4-52.5 (-CO-NH-CH₂-CH₂-N-); 56 (-N-CH₂-CH₂-N-); 174.7 (CONH) ppm.

IR: $\bar{\nu} = 3345, 3283, 3078, 2943, 2858, 2824, 1645, 1557, 1460, 1354, 1291, 1096, 1062, 946, 915 \text{ cm}^{-1}$.

SEC: $\overline{M}_w = 13000 \text{ g.mol}^{-1}$; PDI = 2.0

H5: 2.44 g (16.7 mmol) of tris(2-aminoethyl)amine were mixed with 1.42 g (2.1 mmol) of tris(2-di(methylacrylate)aminoethyl)amine (ratio trisamine/hexaester=8). The rest of the procedure is identical to the one for HYPAM3.

¹H NMR (D₂O, 300 MHz): $\delta = 2.34$ (m, -CH₂-CO-); 2.5 (m, -N-CH₂-CH₂-N-); 2.55 (m, -N-CH₂-CH₂-CO-); 2.63 (m, -CH₂-NH₂); 2.73 (m, -N-CH₂-CH₂-CO-); 3.22 (m, -CH₂-NH-CO-) ppm.

¹³C NMR (D₂O, 300 MHz): $\delta = 32.7$ -35.5 (-N-CH₂-CH₂-CO-); 36.7 (-CH₂-NH-CO-); 37.8 (-CH₂-NH₂); 49.1 (-N-CH₂-CH₂-CO-); 49.8-51.1-52.5 (-CO-NH-CH₂-CH₂-N-); 56 (-N-CH₂-CH₂-N-); 174.7 (CONH) ppm.

SEC: $\overline{M}_w = 27000 \text{ g.mol}^{-1}$; PDI = 2.3

c) *The synthesis of core-shell polymers*

The synthesis of core-shell polymers were performed using either three-branch molecule TREN (T) or hyperbranched polymer H4 and 5 cores and PNIPAM of different number average molar masses (2000 g/mol, 5000 g/mol and 7000 g/mol noted P2, P5 and P7 respectively). The details of preparation of H4P2 are given below as a typical example. 1g of carboxylic acid terminated P2 (5.10⁻⁴ mol, 1eq.) and 89.2 mg of 1,1'-carbonyldiimidazole (5.5.10⁻⁴ mol, 1.1eq.) were dissolved in 10 mL dry DMSO. The mixture was stirred overnight under argon at room temperature (25°C). Then, 3.63 mL of a 20 mg/mL H4 in DMSO solution (72.6 mg H4, 0.9 eq. of primary amine) was added slowly in the previous mixture. The reaction was continuously stirred for 24 h under argon at room temperature. After the reaction then, the mixture was dialyzed in ultrapure water for 3 days and the final core-shell polymer H4P2 was collected by lyophilization.

TP2 -----

¹H NMR (D₂O, 300Hz): 1.07 (CO-NH-CH-CH₃ PNIPAM), 1.51 (CH-CH₂ PNIPAM), 1.94 (CH-CH₂ main chain PNIPAM), 2.36 (N-CH₂-CH₂-NH-CO), 2.45 (N-CH₂-CH₂-NH-CO), 2.60 (CO-CH₂-CH₂-S PNIPAM), 2.70 (CO-CH₂-CH₂-S PNIPAM), 3.83 (CO-NH-CH-CH₃ PNIPAM)

IR: $\bar{\nu} = 3434, 3289, 3075, 2971, 2932, 2875, 1642, 1543, 1458, 1386, 1366, 1263, 1172, 1130, 1025, 927, 881, 838 \text{ cm}^{-1}$

TP5 -----

¹H NMR (D₂O, 300Hz): 1.06 (CO-NH-CH-CH₃ PNIPAM), 1.51 (CH-CH₂ PNIPAM), 1.93 (CH-CH₂ main chain PNIPAM), 2.35 (N-CH₂-CH₂-NH-CO), 2.45 (N-CH₂-CH₂-NH-CO), 2.60 (CO-CH₂-CH₂-S PNIPAM), 2.70 (CO-CH₂-CH₂-S PNIPAM), 3.83 (CO-NH-CH-CH₃ PNIPAM)

IR: $\bar{\nu}$ = 3426, 3288, 3075, 2972, 2933, 2876, 1634, 1534, 1457, 1386, 1366, 1266, 1172, 1130, 970, 926, 877, 838 cm⁻¹

TP7 -----

¹H NMR (D₂O, 300Hz): 1.03 (CO-NH-CH-CH₃ PNIPAM), 1.90 (CH-CH₂ main chain PNIPAM), 1.51 (CH-CH₂ PNIPAM), 2.36 (N-CH₂-CH₂-NH-CO), 2.45 (N-CH₂-CH₂-NH-CO), 2.60 (CO-CH₂-CH₂-S PNIPAM), 2.71 (CO-CH₂-CH₂-S PNIPAM), 3.83 (CO-NH-CH-CH₃ PNIPAM)

IR: $\bar{\nu}$ = 3433, 3288, 3076, 2972, 2934, 2875, 1538, 1458, 1386, 1366, 1262, 1172, 1131, 1026, 927, 882, 838 cm⁻¹

H4P2 -----

¹H NMR (D₂O, 500Hz): 1.0 (CO-NH-CH-CH₃ PNIPAM), 1.44 (CH-CH₂ PNIPAM), 1.87 (CH-CH₂ main chain PNIPAM), 2.28 (CO-CH₂-CH₂-S PNIPAM), 2.37 (N-CH₂-CH₂-CO), 2.45 (N-CH₂-CH₂-N), 2.53 (CO-NH-CH₂-CH₂), 2.55 (CO-CH₂-CH₂-S PNIPAM), 2.63 (N-CH₂-CH₂-CO), 3.23 (CO-NH-CH₂-CH₂), 3.75 (CO-NH-CH-CH₃ PNIPAM)

¹³C NMR (D₂O, 500Hz): 53.6 (N-CH₂-CH₂-N), 51.1 (N-CH₂-CH₂-CO), 35.09 (N-CH₂-CH₂-CO), 36.51 (CO-NH-CH₂-CH₂), 52.0 (CO-NH-CH₂-CH₂), 37.05 (CO-CH₂-CH₂-S), 27.80 (CO-CH₂-CH₂-S), 42.7 (CH-CH₂ main chain PNIPAM), 35.01 (CH-CH₂), 41.8 (CO-NH-CH-CH₃), 21.7 (CO-NH-CH-CH₃), 174 (CO-NH).

IR: $\bar{\nu}$ = 3434, 3288, 3073, 2972, 2933, 2857, 1641, 1542, 1458, 1386, 1366, 1268, 1172, 1130, 1026, 975, 927, 882, 838 cm⁻¹

H4P5 -----

¹H NMR (D₂O, 500Hz): 1.0 (CO-NH-CH-CH₃ PNIPAM), 1.43 (CH-CH₂ PNIPAM), 1.86 (CH-CH₂ main chain PNIPAM), 2.27 (CO-CH₂-CH₂-S PNIPAM), 2.37 (N-CH₂-CH₂-CO), 2.45 (N-CH₂-CH₂-N), 2.51 (CO-NH-CH₂-CH₂), 2.55 (CO-CH₂-CH₂-S PNIPAM), 2.63 (N-CH₂-CH₂-CO), 3.23 (CO-NH-CH₂-CH₂), 3.75 (CO-NH-CH-CH₃ PNIPAM)

¹³C NMR (D₂O, 500Hz): 53.59 (N-CH₂-CH₂-N), 51.1 (N-CH₂-CH₂-CO), 35.09 (N-CH₂-CH₂-CO), 36.51 (CO-NH-CH₂-CH₂), 52.0 (CO-NH-CH₂-CH₂), 37.04 (CO-CH₂-CH₂-S),

27.80 (CO-CH₂-CH₂-S), 42.7 (CH-CH₂ main chain PNIPAM), 35.01 (CH-CH₂), 41.8 (CO-NH-CH-CH₃),: 21.7. (CO-NH-CH-CH₃), 174 (CO-NH).

IR: $\bar{\nu}$ = 3434, 3283, 3076, 2971, 2933, 2875, 1639, 1583, 1386, 1366, 1270, 1172, 1130, 1025, 973, 927, 882, 839 cm⁻¹

H4P7 -----

¹H NMR (D₂O, 500Hz): 1.0 (CO-NH-CH-CH₃ PNIPAM 1.44 (CH-CH₂ PNIPAM),), 1.87 (CH-CH₂ main chain PNIPAM), 2.28 (CO-CH₂-CH₂-S PNIPAM), 2.37 (N-CH₂-CH₂-CO), 2.45 (N-CH₂-CH₂-N), 2.53 (CO-NH-CH₂-CH₂), 2.55 (CO-CH₂-CH₂-S PNIPAM), 2.63(N-CH₂-CH₂-CO), 3.23 (CO-NH-CH₂-CH₂),: 3.75 (CO-NH-CH-CH₃ PNIPAM)

¹³C NMR (D₂O, 500Hz): 53.61 (N-CH₂-CH₂-N), 51.1 (N-CH₂-CH₂-CO), 35.08 (N-CH₂-CH₂-CO), 36.51 (CO-NH-CH₂-CH₂), 52.01 (CO-NH-CH₂-CH₂), 37.05 (CO-CH₂-CH₂-S), 27.80 (CO-CH₂-CH₂-S), 42.7 (CH-CH₂ main chain PNIPAM), 35.01 (CH-CH₂), 41.8 (CO-NH-CH-CH₃),: 21.7. (CO-NH-CH-CH₃), 174 (CO-NH).

IR: $\bar{\nu}$ = 3434, 3288, 3073, 2972, 2933, 2857, 1641, 1542, 1458, 1386, 1366, 1268, 1172, 1130, 1026, 975, 927, 882, 838 cm⁻¹

H5P2 -----

¹H NMR (D₂O, 500Hz): 1.01 (CO-NH-CH-CH₃ PNIPAM 1.44 (CH-CH₂ PNIPAM),), 1.88 (CH-CH₂ main chain PNIPAM), 2.27 (CO-CH₂-CH₂-S PNIPAM), 2.37 (N-CH₂-CH₂-CO), 2.45 (N-CH₂-CH₂-N), 2.53 (CO-NH-CH₂-CH₂), 2.55 (CO-CH₂-CH₂-S PNIPAM), 2.63(N-CH₂-CH₂-CO), 3.23 (CO-NH-CH₂-CH₂),: 3.75 (CO-NH-CH-CH₃ PNIPAM)

¹³C NMR (D₂O, 500Hz): 53.6 (N-CH₂-CH₂-N), 51.11 (N-CH₂-CH₂-CO), 35.10 (N-CH₂-CH₂-CO), 36.50 (CO-NH-CH₂-CH₂), 52.01 (CO-NH-CH₂-CH₂), 37.05 (CO-CH₂-CH₂-S), 27.80 (CO-CH₂-CH₂-S), 42.7 (CH-CH₂ main chain PNIPAM), 35.01 (CH-CH₂), 41.8 (CO-NH-CH-CH₃),: 21.7. (CO-NH-CH-CH₃), 174 (CO-NH).

IR: $\bar{\nu}$ = 3434, 3288, 3074, 2971, 2933, 2874, 1643, 1542, 1458, 1386, 1366, 1270, 1172, 1130, 1025, 976, 953, 927, 881, 838 cm⁻¹

H5P5 -----

¹H NMR (D₂O, 500Hz): 1.0 (CO-NH-CH-CH₃ PNIPAM), 1.44 (CH-CH₂ PNIPAM), 1.87 (CH-CH₂ main chain PNIPAM), 2.28 (CO-CH₂-CH₂-S PNIPAM), 2.37 (N-CH₂-CH₂-CO), 2.45 (N-CH₂-CH₂-N), 2.53 (CO-NH-CH₂-CH₂), 2.55 (CO-CH₂-CH₂-S PNIPAM), 2.63(N-CH₂-CH₂-CO), 3.23 (CO-NH-CH₂-CH₂),: 3.75 (CO-NH-CH-CH₃ PNIPAM)

^{13}C NMR (D_2O , 500Hz): 53.6 (N- $\text{CH}_2\text{-CH}_2\text{-N}$), 51.1 (N- $\text{CH}_2\text{-CH}_2\text{-CO}$), 35.09 (N- $\text{CH}_2\text{-CH}_2\text{-CO}$), 36.51 (CO-NH- $\text{CH}_2\text{-CH}_2$), 52.0 (CO-NH- $\text{CH}_2\text{-CH}_2$), 37.05 (CO- $\text{CH}_2\text{-CH}_2\text{-S}$), 27.80 (CO- $\text{CH}_2\text{-CH}_2\text{-S}$), 42.7 (CH-CH_2 main chain PNIPAM), 35.01 (CH-CH_2), 41.8 (CO-NH- CH-CH_3), 21.7. (CO-NH- CH-CH_3), 174 (CO-NH).

IR: $\bar{\nu}$ = 3427, 3283, 3076, 2972, 2933, 2875, 1639, 1542, 1458, 1386, 1366, 1274, 1172, 1131, 1023, 953, 928, 882, 839 cm^{-1}

H5P7 -----

^1H NMR (D_2O , 500Hz): 1.02 (CO-NH- CH-CH_3 PNIPAM), 1.45 (CH-CH_2 PNIPAM), 1.87 (CH-CH_2 main chain PNIPAM), 2.27 (CO- $\text{CH}_2\text{-CH}_2\text{-S}$ PNIPAM), 2.37 (N- $\text{CH}_2\text{-CH}_2\text{-CO}$), 2.45 (N- $\text{CH}_2\text{-CH}_2\text{-N}$), 2.53 (CO-NH- $\text{CH}_2\text{-CH}_2$), 2.55 (CO- $\text{CH}_2\text{-CH}_2\text{-S}$ PNIPAM), 2.63 (N- $\text{CH}_2\text{-CH}_2\text{-CO}$), 3.23 (CO-NH- $\text{CH}_2\text{-CH}_2$), 3.76 (CO-NH- CH-CH_3 PNIPAM)

^{13}C NMR (D_2O , 500Hz): 53.6 (N- $\text{CH}_2\text{-CH}_2\text{-N}$), 51.1 (N- $\text{CH}_2\text{-CH}_2\text{-CO}$), 35.09 (N- $\text{CH}_2\text{-CH}_2\text{-CO}$), 36.51 (CO-NH- $\text{CH}_2\text{-CH}_2$), 52.01 (CO-NH- $\text{CH}_2\text{-CH}_2$), 37.05 (CO- $\text{CH}_2\text{-CH}_2\text{-S}$), 27.80 (CO- $\text{CH}_2\text{-CH}_2\text{-S}$), 42.71 (CH-CH_2 main chain PNIPAM), 35.01 (CH-CH_2), 41.8 (CO-NH- CH-CH_3), 21.7. (CO-NH- CH-CH_3), 174 (CO-NH).

IR: $\bar{\nu}$ = 3434, 3288, 3074, 2971, 2933, 2875, 1641, 1542, 1458, 1386, 1366, 1340, 1273, 1172, 1130, 1024, 953, 927, 882, 839 cm^{-1}

2. Synthesis of gold nanoparticles by NaBH_4

For preparing 20 mL of 5.10^{-4} M gold colloid solution: 35 μL of freshly prepared NaOH (1M) solution was added to 18.86 mL of ultrapure water under magnetic stirring. Then 1mL of HAuCl_4 0.01 M solutions was added, the solution became pale yellow. Finally 100 μL of freshly prepared NaBH_4 0.1M was added under vigorous stirring. The solution changed from pale yellow to deep red immediately. The solution was stable for several weeks. $[\text{NaOH}]/[\text{NaBH}_4]/[\text{HAuCl}_4]=3.5/1/1$.

3. Gold nanoparticles stabilization by polymer solutions

AuNps were stabilized with polymer solution whose concentration varied from 5.10^{-2} wt.% to 10^{-6} wt.%. The final gold concentration was fixed at $2.5 \cdot 10^{-4}$ M. The protocol for stabilization with final polymer concentration of 10⁻² wt% was the follow: 10 μL of 0.2 wt.% polymer stock solution of were added to 90 μL of water, finally 100 μL of 5.10^{-4} M gold nanoparticle colloidal solutions was added to the later to yield coated NPs.

Table I.1. Gold nanoparticles stabilization by polymer solutions

<i>Final polymer concentration [wt. %]</i>	<i>V_{water} [μL]</i>	<i>V_{polymers (0.2 wt.%)} [μL]</i>	<i>V_{AuNPs colloid (5.10⁻⁴ M)} [μL]</i>
5×10^{-2}	50	50	100
10^{-2}	90	10	100
5×10^{-3}	95	5	100
		<i>V_{polymers (5.10⁻³wt.%)} [μL]</i>	
10^{-3}	40	60	100
10^{-4}	4	96	100
		<i>V_{polymers (10⁻⁴wt.%)} [μL]</i>	
10^{-5}	20	80	100
10^{-6}	2	98	100

4. Salt adding effect

Final NaCl concentration was fixed at 1M, the protocol for final polymer concentration of 10^{-2} M was the follow: 10 μL of 0.2 wt.% polymer stock solution of were added to 50μL of water, then 100 μL of 5.10^{-4} M gold colloid solutions was added. Finally, 40 μL of 5M NaCl solution were finally added.

Table I.2. Salt adding effect

<i>Final polymer concentration [wt. %]</i>	<i>V_{water} [μL]</i>	<i>V_{polymers (0.2 wt.%)} [μL]</i>	<i>V_{AuNPs colloid (5.10⁻⁴ M)} [μL]</i>	<i>V_{NaCl (5 M)} [μL]</i>
5×10^{-2}	10	50	100	40
10^{-2}	50	10	100	40
5×10^{-3}	95	5	100	40
		<i>V_{polymers (5.10⁻³wt.%)} [μL]</i>		
10^{-3}	20	40	100	40
10^{-4}	56	4	100	40
		<i>V_{polymers (10⁻⁴wt.%)} [μL]</i>		

10^{-5}	40	20	100	40
10^{-6}	58	2	100	40

5. *In situ* synthesis of AuNPs

The final concentration of polymer was fixed at 0.01 wt. %. Typically, 10 μ L of 0.2 wt.% polymer stock solution was added to 180 μ L of water, followed by the addition of 5 μ L of 0.01 M gold colloid solution the solution became pale yellow. Finally, 5 μ L of freshly prepared 0.01M NaBH₄ solution was added to the mixture under manual stirring. The solution color turned into brown, red, or light orange, at different rates, depending on the nature of the polymers. [NaBH₄]/[HAuCl₄]=1/1.

C. Characterization techniques

1. Nuclear Magnetic Resonance

To determine the structural characteristics of the polymers, NMR experiments were performed at 298K in D₂O on a Bruker AVANCE 300 MHz or 500 MHz spectrometer equipped with a 5 mm Z-gradient TCI cryogenic probe. The 90° pulse length was 9 μ s, the sweep width was 10kHz and the acquisition time was 3.5 s. The scan number was adjusted to obtain a sufficient signal to noise ratio and the relaxation delay between transients was 3s. For 1D ¹H experiments, a 30° pulse was used. Attribution of the signals was made by COSY, HSQC and HMBC experiments.

Diffusion coefficient measurements by NMR-DOSY (Diffusion Ordered Spectroscopy). [3] The basic scheme for the characterization of diffusion is the pulse field gradient spin-echo (PFGSE). The measurement was carried out by observing the attenuation of the NMR signals during a delay surrounded by two pulsed field gradients. In practice, a series of NMR diffusion spectra were acquired as a function of the gradient strength (g). The intensities of the resonances follow an exponential decay which depends on the self-diffusion coefficient (D).[4, 5] Their relationship is given by the Stejskal-Tanner relation: $I/I_0 = \exp[\gamma^2 g^2 \delta^2 (\Delta - \delta/3) D]$ where I is the measured signal intensity, I₀ is the signal intensity for a g value of 0 G/cm, γ is the gyromagnetic ratio for the ¹H nucleus, δ is the gradient pulse length, Δ is the time between the two gradients in the pulse sequence.[6] D values are function of temperature and viscosity as indicated from the Stokes-Einstein equation: $D = \kappa T / 6\pi\eta R_h$ (where k = Boltzmann constant, T temperature, η viscosity of the solution and R_h is the

radius of the solvated species). The Z pulsed field gradients were generated with a 10 A GRASP II/P gradient amplifier. Thus, the z-maximum gradient strength (g) was 53.5 G/cm. Experiments were performed by varying g and keeping all other timing parameters constant. Typically, the Δ and the δ durations were 100 ms and 1ms, respectively and g was varied from 2.675 (strength of 5%) to 50.825 (strength of 95%) G/cm by 3% steps. An NMR pulse sequence with a stimulated echo bipolar gradient pulse pair and one spoil gradient was used (pulse program named `stebpgp1s` in the Bruker library). The data were analyzed by maximum-entropy with the DOSY module of NMR notebook software (NMRtec).[7] The DOSY processing algorithm parameter was set to 3 and the data were processed with a diffusion window from 0,1 to 25000 $\mu\text{m}^2/\text{s}$.

2. Fourier transform infra red (FTIR)

Spectra were recorded with a Nexus Thermo Nicolet spectrometer equipped with a detector DTGS, in attenuated total reflection (ATR) mode with a diamond crystal in the spectral region of 600-4000 cm^{-1} with a resolution of 2 cm^{-1} . The physical mixtures were prepared by simple homogenization of HYPAM and PNIPAM as followed: 2 mL of an aqueous solution of HYPAM (5 mg/mL) was prepared. To this solution was added 5 mL, 4.5 mL, 3.75 mL, 2.5 mL of (25 mg/mL) aqueous PNIPAM affording the 1 : 1, 1 : 0.90, 1 : 0.75 and 1 : 0.5 ratios respectively. The obtained solution was then freeze-dried and the spectra of the obtained solids were recorded.

3. Differential Scanning Calorimetry (DSC)

The thermal properties of the polymer (in solution and in bulk) were determined by DSC using a Mettler Toledo DSC 1 STARe System Thermal Analysis calorimeter equipped with a Gas Controller GC200. Solid samples were sealed inside aluminum crucibles of 40 μL , glass transition temperature were taken at inflection points as the temperature increased at different rates: 30, 20, 10 $^{\circ}\text{C}/\text{min}$. Solution samples were sealed in impermeable crucibles of 120 μL . Transition temperatures were taken at the top of the DSC peaks as the temperature increased at different rates; 10, 5, 2 and 1 $^{\circ}\text{C}/\text{min}$, and finally extrapolated to 0 $^{\circ}\text{C}/\text{min}$. The variation of enthalpy was measured as the temperature increased at a rate of 10 $^{\circ}\text{C}/\text{min}$.

4. Small Angle Neutron Scattering experiments (SANS)

SANS experiments were performed with the PACE spectrometer at the Orphée reactor (LLB, Saclay). Polymer solutions in D_2O solvent were put inside quartz cells of 2 mm path length and measured at 20 $^{\circ}\text{C}$. ($[\text{polymer}] = 1 \text{ \%w/v}$). Two spectrometer configurations were used: a neutron wavelength (λ) of 6 \AA with a sample to detector distance of 3 m and a wavelength of 13 \AA with a distance of 4.7 m. The scattering vector range thus reached was

$0.0032 < q \text{ (\AA}^{-1}\text{)} < 0.12$. Scattering intensities have been normalized by the incoherent signal delivered by a 1 mm gap water sample in order to account for the efficiency of the detector. Absolute values of the scattering intensity, $I(q)$ in cm^{-1} , were obtained from the direct determination of the number of neutrons in the incident beam and the detector cell solid angle. No background has been subtracted to the sample scattering, thus a flat incoherent signal has been observed at high q values. Data treatment was done with the PAsiDUR software at the Laboratoire Léon Brillouin.

5. Transmission electron microscopy (TEM)

A drop of the aqueous dispersion was placed on a formvar carbon-coated copper TEM grid (Ted Pella Inc.) and left to dry under air. For samples needing negative staining, the TEM grid was successively placed on a drop of the sample solution for 1min and on a drop of an aqueous solution of uranyl acetate (2 wt %, 10 s), after which the grid was then air dried before introduction into the electron microscope. To visualize mesoglobules, we heated polymer solutions (45°C) for 1 h prior to the deposit. The previously described procedure for preparation of TEM grids was then employed; however, they were dried in an oven at 45°C . The samples were viewed with a MET Hitachi HT7700 transmission electron microscope operating at 80 kV accelerating voltage. Size-distribution histograms were determined by using magnified TEM images. The size distribution of the particles was determined by measuring a minimum of 200 particles of each sample, using WCIF Image J software. The size distributions observed were analyzed in terms of Gaussian statistics ($wc(\sigma)$).

6. Dynamic Light Scattering (DLS)

DLS measurements were carried out with a Malvern Instrument Nano-ZS equipped with a He-Ne laser ($\lambda=633 \text{ nm}$) on 0.1 wt% polymer solution. The correlation function was analyzed via the general purpose method (NNLS) to obtain the distribution of diffusion coefficients (D) of the solutes. The apparent diameter was then determined using the Stokes-Einstein equation. Mean diameter values were obtained from three different runs. Standard deviations were evaluated from diameter distribution.

7. Ultraviolet-visible (Uv-vis)

Transmittance of polymer aqueous solutions was recorded with a HP 8452A diode array spectrophotometer with increasing temperature at different heating rates. The cloud points were then calculated by the extrapolation to 0°C min^{-1} of the cloud points obtained from the inflection point of each transmittance curve.

8. Size Exclusion Chromatography (SEC)

Number average molecular weights (M_n) and polydispersity indexes (PDI) of hyperbranched amidoamine polymers were determined by size exclusion chromatography (SEC) analysis in carbonate buffer solution at pH 10 (Na_2CO_3 and NaHCO_3 0.1M) (flow rate 0.5 mL/min) on an apparatus equipped with a Waters refractive index detector, a Waters column pack (Shodex OHpak SB-802HQ, SB-802.5HQ, SB-804HQ) and a Minidawn Wyatt light scattering detector. The molecular weights were uncorrected from low sensitivity of LS-SEC to lower molecular weights²⁸. The refractive index increments for PAMAM dendrimers were measured in the same eluent at ambient temperature. The values for the hyperbranched polyamides were assumed to be identical. Considering the fact that these polymers have been observed to trap solvent molecules, even after prolonged drying under vacuum, the accuracy for the molecular weight measurement is estimated to be around 20%.

Number average molecular weights (M_n) and polydispersity indexes (PDI) of PNIPAM and PNIPAM grafted polymers were determined by SEC on an apparatus equipped with a Waters 2140 refractive index (RI) detector, using a Waters Styragel HR 4E column (eluent, THF, flow rate, 1 mL·min⁻¹). Typically, samples at a concentration of 5 mg·mL⁻¹ in THF were injected. Alternatively, samples were analyzed with a SEC apparatus comprising a Varian ProStar 325 UV detector (dual wavelength analysis) and a Waters 410 refractive index detector, using two Shodex K-805 L columns (8 mm, 300 mm, 13 μm) and DMF LiCl (1g/L) as the eluent at 40°C (flow rate, 1 mL·min⁻¹).

II. Chapter 3

A. Materials

Tetrachloroauric acid trihydrate ($\text{HAuCl}_4 \cdot 3\text{H}_2\text{O}$), D-Glucosamine hydrochloride, **1,1'-Carbonyldiimidazole**, anhydrous DMSO, carboxylic acid terminated PNIPAM 2000g/mol, 5000g/mol and 7000 g/mol, Pur-A-Lyzer™ Mega Dialysis Kit of MWCO 3.5 kDa, 6-8 kDa and 12-14 kDa were purchased from Aldrich and were used without further purification. Tris(2-aminoethyl)amine (Aldrich) was distilled under reduced pressure and stored under argon atmosphere before use. Ultrapure water ($\rho=18 \text{ M}\Omega \text{ cm}^{-1}$) was obtained from Aquadem apparatus.

B. Synthesis

1. Synthesis of HYPAM core and core-shell polymers

See experimental section of Chapter 2

2. Synthesis of hydrogels

Different concentrations: 5, 10, 15, 20 wt.% of polymers in water were used for this experiment. Typical protocol for 20wt.% polymer solution is the follow: Tubes containing 20 wt.% well dissolved polymers solutions of P7, TP7 and H4P7 were placed in the oven at 40°C for 10 minutes, the sol-gel transition took place resulted in white and turbid gels which did not flow when the tubes was inversed. When the gels were placed in R.T. they returned to the sol state.

3. *In situ* synthesis of AuNPs embedded in gels structures

At room temperature 50 mg of H4P7 polymer was dissolved in 184 μL of water to form a 20% wt. homogeneous solution. Then 10 μL of a solution of HAuCl_4 0.01M was added to the solution following by adding 1 μL of NaOH 1M. Finally, 5 μL of a solution of glucosamine 0.2M was added. The mixture was rapidly vortexed and then the flask was immediately placed in the oven at 40°C for 24 hours. The same procedure was carried out for P7@Au and TP7@Au.

C. Characterization techniques

1. Characterization of polymers

See experimental section of chapter 2.

2. Characterization of hydrogels

a) *Differential Scanning Calorimetry (DSC)*

The thermal properties of the polymer (in solution and in bulk) were determined by DSC using a Mettler Toledo DSC 1 STARe System Thermal Analysis calorimeter equipped with a Gas Controller GC200. Solution samples were sealed in impermeable crucibles of 120 μL . Transition temperatures were taken at the top of the DSC peaks as the temperature increased at $1^\circ\text{C}\cdot\text{min}^{-1}$. The variation of enthalpy was measured as the temperature increased at a rate of $1^\circ\text{C}\cdot\text{min}^{-1}$. The enthalpy variation of the sol-gel transition was normalized to the content of PNIPAM in the copolymers.

b) *Cryo-Scanning Electron Microscopy (Cryo-SEM)*

Cryo-Scanning Electron Microscopy (Cryo-SEM) images were realized with a FEG FEI Quanta 250 microscope (Japan). One drop of the sample was preheated to undergo gel transition just before being frozen in nitrogen slush at -220°C . The frozen sample was transferred under vacuum in the cryofracture apparatus (*Quorum PP3000T Cryo Transfer System*) chamber where it was fractured at -145°C . Then the temperature was decreased to -95°C and maintained at this temperature during 30 min for sublimation. It was then metallized with Pd during 60s and introduced into the microscope chamber where it was maintained at -145°C during the observation operating at 5 kV accelerating voltage.

c) *Rheology*

Measurements have been made with a rheometer AR1000 from TA instruments in cone plate configuration (diameter 2 cm, 2° angle), with Peltier plate. A stress of 1 Pa has been set for viscoelastic measurements. Frequency sweep from 10 to 0.01 Hz provided the viscoelastic "spectrum" of the gel. Variation of the elastic and viscous moduli with temperature has been then monitored at 1 Hz (frequency) and 1 Pa (stress), over a continuous linear temperature ramp at $1^\circ\text{C}/\text{min}$. The inflexion point has been selected as the "transition temperature".

d) ***UV-vis***

Time-dependent turbidity measurements: hydrogels and Au embedded hydrogels pre-formed at 40 °C were placed inside the BMG LABTECH SPECTROSTAR device where the temperature was set at 25°C. The UV spectra were recorded at 720 nm for each 30 seconds during 250 minutes.

3. Characterization of nanoparticles

a) ***Transmission electron microscopy (TEM)***

To analyze the morphology of formed AuNPs, we need to dilute the solution at least 10 times and deposit on TEM grid. A drop of the aqueous dispersion was placed on a formvar carbon-coated copper TEM grid (Ted Pella Inc.) and left to dry under air. The samples were viewed with a MET Hitachi HT7700 transmission electron microscope operating at 80 kV accelerating voltage. Size-distribution histograms were determined by using magnified TEM images. The size distribution of the particles was determined by measuring a minimum of 200 particles of each sample, using WCIF Image J software. The size distributions observed were analyzed in terms of Gaussian statistics (we (σ)).

b) ***UV-Vis***

Au embedded hydrogels were cooled to R.T. prior to perform UV measurements using BMG LABTECH SPECTROSTAR device. The wave length accessible of this device was 300 nm to 1000 nm.

III. Chapter 4

A. Materials

Methylacrylate, tetrachloroauric acid trihydrate ($\text{HAuCl}_4 \cdot 3\text{H}_2\text{O}$), amine-terminated PAMAM dendrimers (G₃ to G₅) as methanol solutions were purchased from Aldrich and were used without further purification. For PAMAM solutions, methanol was removed under vacuum prior to use. Sodium dodecyl sulfate was also purchased from Aldrich and purified by recrystallisation in ethanol/water 95 v/v before use. Tris(2-aminoethyl)amine (Aldrich) was distilled under reduced pressure and stored under argon atmosphere before use. Ultrapure water ($\rho=18 \text{ M}\Omega \text{ cm}^{-1}$) from Aquadem apparatus was used for complex preparation.

B. Synthesis

The synthesis and characterization of the aminoterminated hyperbranched amidoamine : See Experimental section of Chapter 2

1. Synthesis of hyperbranched polymer surfactant complexes

The preparation of hyperbranched polymer surfactant complexes - PAMAM-DS and HYPAM-DS was performed using PAMAM 3, 4 and 5 and HYPAM 3, 4 and 5 cores respectively. The grafted degree of SDS on polymers was calculated using the molar ratio of primary amine groups of the core on sulfate groups of SDS (ie 1:1, 1:0.75, 1:0.5).

For example, the synthesis of HYPAM₄-DS₁₀₀ was carried out as follows: 25 mL of HYPAM₄ acidic aqueous solution (pH 3-4) was prepared by slowly adding an acidic solution (HCl 0.1M and 0.001M) to 100 mg (0.62 mmol of NH_2 groups) of polymer. Then 7.95 mL of an acidic aqueous solution of SDS (0.078 mol.L⁻¹, concentration < cmc) at the same pH was added dropwise to the HYPAM solution under continuous stirring. Progressively, the obtained solution became turbid and the formed precipitate was isolated by centrifugation (8000 rpm, 20°C, 30 min). Then the residue was washed three times with water (3 x 20 mL) and dissolved in a small quantity of DMSO (1 mL). This organic solution was then added dropwise to 50 mL of an acid aqueous solution (HCl, pH3). The formed precipitate was collected by centrifugation (8000 rpm, 20°C, 30 min). The residue was washed by ultrapure water (40 mL) and centrifuged (8000 rpm, 20°C, 30 min) three times before dried under vacuum at room temperature for 3 days (251,22 mg, yield 94.7%).

HYPAM₄-DS₁₀₀:

¹H NMR (500MHz, DMSO-d₆): δ = 0.85 (t, ³J = 6.5 Hz, CH₃ alkyl chain); 1.24 (m, (CH₂)₉); qt (1.51, ³J=6.5 Hz, CH₂ β); 2.51 (DMSO and m, N-CH₂-CH₂-NH-CO); 2.66 (m, N-CH₂-CH₂-N, N-CH₂-CH₂-CO); 2.91 (m, N-CH₂-CH₂-CO-); 3.20 (m, -CH₂-NHCO-); 3.37 (m, -CH₂-NH₃⁺; t, ³J=6.5 Hz, CH₂ α) ; 3.52 (br m, NH) ppm; 3.74 (t, ³J=6.5 Hz, CH₂ α) ppm.

¹³C-NMR (500 MHz, DMSO-d₆): 13.92 (CH₃); 22.15, 25.57, 28.80, 28.92, 29.10, 29.13, 29.16, 34.41 (CH₂ alkyl chain); 29.18 (CH₂ β); 29.44, 50.60 (N-CH₂-CH₂-CO); 36.65, 43.85 (-CH₂-NH-CO-), 36.81 (N-CH₂-CH₂-N); 48.97 (-CH₂-NH₃⁺); 50.61 (N-CH₂-CH₂-CO); 52.01 (N-CH₂-CH₂-NHCO), 60.75 and 66.23 (CH₂ α); 169.33 (CO) ppm

IR (HYPAM4-DS100 complex): $\bar{\nu}$ = 3484, 3291, 3084, 2956, 2924, 2853, 1660, 1557, 1466, 1390, 1379, 1241, 1204, 1057, 983, 804 cm⁻¹.

IR (SDS): $\bar{\nu}$ = 2956, 2918, 2851, 2872, 1468, 1250, 1222, 1096, 1082, 1017, 996, 831 cm⁻¹.

2. Formation of polymeric aggregates in solution

The procedure to form the polymeric aggregates is adapted from the literature.^[2] HYPAM4-DS100 was dissolved in a good solvent DMSO at a concentration of 0.5 wt%. Milli-Q water was then added very slowly (~10 μ L.min⁻¹) to 1.5 μ L of the above solution with slight shaking (final volume water content around 25%). The nature of the formed aggregates was examined by transmission electron microscopy (TEM) with negative staining.

3. Synthesis of gold nanoparticles in mesophases

In situ synthesis of gold nanoparticles inside LC or isotropic HYPAM-DS phase was performed as followed: 500 μ L of a 10⁻² mol.L⁻¹ HAuCl₄ solution in methanol was slowly evaporated in a mortar, after which 10 mg of the HYPAM-4-DS100 ionic complex were added [molar ratio [Au]/[HYPAM] = 120]. The mortar was placed in a thermostated box at the desired temperature and the two components were well crushed with the thermostated pestle to obtain a homogeneous mixture. A flux of hydrogen was added during 60s to assure the reduction of the gold salt (P(H₂) = 1 bar). The formed nanoparticles were analyzed by TEM.

C. Characterization techniques

1. SEC

The average molecular weight of the polymers was determined by size exclusion chromatography (SEC) analysis in carbonate buffer solution at pH 10 (Na₂CO₃ and NaHCO₃

0.1M) (flow rate 0.5 mL/min) on an apparatus equipped with a Waters refractive index detector, a Waters column pack (Shodex OHpak SB-802HQ, SB-802.5HQ, SB-804HQ) and a Minidawn Wyatt light scattering detector. The molecular weights were uncorrected from low sensitivity of LS-SEC to lower molecular weights²⁸. The refractive index increments for PAMAM dendrimers were measured in the same eluent at ambient temperature. The values for the hyperbranched polyamides were assumed to be identical. Considering the fact that these polymers have been observed to trap solvent molecules, even after prolonged drying under vacuum, the accuracy for the molecular weight measurement is estimated to be around 20%.

2. Nuclear Magnetic Resonance

To determine the structural characteristics of the polymers, NMR experiments were performed at 298K (or 308K in dmsO-d6) on a Bruker AVANCE 500 MHz spectrometer equipped with a 5 mm Z-gradient TCI cryogenic probe. The 90° pulse length was 9 μ s, the sweep width was 10kHz and the acquisition time was 3.5 s. The scan number was adjusted to obtain a sufficient signal to noise ratio and the relaxation delay between transients was 3s. For 1D ¹H experiments, a 30° pulse was used. Attribution of the signals was made by COSY, HSQC and HMBC experiments.

Selective 1D ¹H NOESY Experiments. The nuclear Overhauser effect (NOE) between dipolar coupled ¹H nuclei is generally used in structural and conformational analysis of molecules and molecular interactions because its intensity is determined by the internuclear ¹H-¹H distance (r) according to an r^{-6} dependency and by the rotational correlation time (τ_c).^[8] For a rigid spherical molecular complex with radius R and solvent viscosity η , τ_c is determined by the Stokes-Einstein relation: $\tau_c = 4\pi\eta R^3/3k_B T$. Owing to this relation, the NOE intensity signal of the ligand is dependent of its interaction with the macromolecules. The regime of the NOE changes from a small to a large molecule is related to the frequency of the spectrometer (ω) and the mobility of the molecules (τ_c). For $\omega\tau_c = 1.1$, zero intensity for NOE effects; for $\omega\tau_c < 1.1$, positive NOE signals; for $\omega\tau_c > 1.1$, negative NOE signals. In the case of ligand equilibrium between the nanoparticle surface (bound state) and the solution (free state), the NMR Transferred NOESY experiment could give some insights into this exchange rate. Indeed, for a given interaction time, the more the ligand is bound, the more the signal will be intense. Thus, to understand the interaction between ligand and nanoparticles, 1D ¹H selective NOE NMR experiments were used. Selective excitation was performed with double pulsed-field-gradient spin-echo scheme (DPFGSE) with a gaussian pulse shape.^[9] The NOE mixing time was 800 ms. Other parameters were similar to those of 1D ¹H experiments.

3. Fourier transform infrared (FTIR)

Spectra were recorded with a Nexus Thermo Nicolet spectrometer equipped with a detector DTGS, in attenuated total reflection (ATR) mode with a diamond crystal in the spectral region of 600-4000 cm^{-1} with a resolution of 4 cm^{-1} . The physical mixtures were prepared by simple homogenization of HYPAM and SDS as followed: 25 mL of an aqueous solution of HYPAM (100 mg) was prepared. To this solution was added 7.95 mL, 7.15 mL, 6.36 mL, 3.98 mL of 0.078 molL^{-1} aqueous SDS affording the 1:1, 1:0.80, 1:0.5 ratios respectively. The obtained solution was then freeze-dried and the spectra of the obtained solids were recorded. Reflexion IR spectra were recorded in a Microscope IN10MX Thermofisher equipped with a detector MCT and connected to a LINKAM TMS 600. Spectral resolution of 8 cm^{-1} was used and 16 scans were performed.

4. Differential Scanning Calorimetry (DSC)

The crystallizations (T_1 and T_2) temperatures were determined by DSC using a Mettler Toledo DSC 1 STARe System Thermal Analysis calorimeter equipped with a Gas Controller GC200. Samples were sealed inside aluminum crucibles of 40 μL in volume. Transition temperatures were taken at the top of the DSC peaks as the temperature increased at different rates; 10, 5, 2 and 1 $^{\circ}\text{C}/\text{min}$, and finally extrapolated to 0 $^{\circ}\text{C}/\text{min}$. The variation of enthalpy was measured as the temperature increased at a rate of 10 $^{\circ}\text{C}/\text{min}$.

5. Polarized Optical Microscopy (POM)

Observation of LC textures was performed on a hot stage FP 82HT from Mettler Toledo under a polarized light optical microscope BX50 from Olympus. POM observations have been realized after heating samples in the isotropic state and slowly cooling to the aimed temperature. No specific treatment of glass plate was realized.

6. Small Angle X-ray Scattering (SAXS)

SAXS on samples was measured with a Nonius Rotating Anode Instrument (4 kW, Cu $K\alpha$) with pinhole collimation and MARCCD detector (pixel size 79) and a distance of 74.4 cm between detector and sample, covering a range of the scattering vector $q = 4\pi\lambda^{-1} \sin(\theta)$ from 0.25 to 4.5 nm^{-1} (2θ : scattering angle, $\lambda = 0.154 \text{ nm}$). The observed scattering patterns were corrected for empty-beam scattering. The 2D diffraction patterns were transformed into a 1D radial average of the scattering intensity using the Fit2D software.

7. Transmission electron microscopy

TEM was performed on a MET Hitachi HT7700 transmission electron microscope

operating at 200 kV accelerating voltage. To prepare samples for analysis, the mixture of nanoparticles and complex was dissolved in 1mL of DMSO. Samples for TEM were prepared by slow evaporation of droplets of colloidal solution deposited on a carbon-coated 200 mesh copper TEM grid (Ted Pella Inc.). The samples were then carefully dried overnight. The nanoparticle size-distribution histograms were determined by using magnified TEM images. The size distribution of the particles was determined by measuring a minimum of 200 particles of each sample. The size distributions observed were analyzed in terms of Gaussian statistics (wc (σ)).

For polymeric aggregates in solution, samples for TEM were prepared by slow evaporation of droplets of colloidal solution deposited on a carbon-coated 200 mesh copper TEM grid (Ted Pella Inc.). The samples were then carefully air-dried, then negatively staining with uranyl acetate 2wt.% in H₂O. The grid was then carefully dried overnight.

8. Dynamic Light Scattering (DLS)

DLS measurements were carried out with a Malvern Instrument Nano-ZS equipped with a He-Ne laser ($\lambda=633$ nm) on 0.1 wt% polymer solution. The correlation function was analyzed *via* the general purpose method (NNLS) to obtain the distribution of diffusion coefficients (D) of the solutes. The apparent diameter was then determined using the Stokes-Einstein equation. Mean diameter values were obtained from three different runs. Standard deviations were evaluated from diameter distribution.

9. UV

Reflection UV measurements were conducted on an Ocean Optics system (DH 2000 FHS) equipped with Top Sensor Systems optical fibers (FCR-7UV200-2-1.5x100). Data were analyzed with Spectra Win from Ocean Optics.

IV. Chapter 5

A. Materials

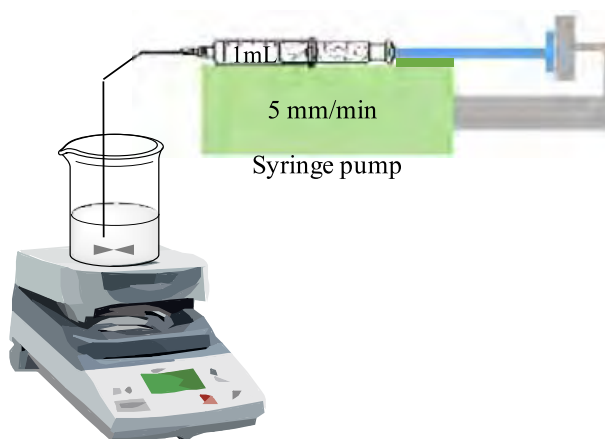
Dendrigraft Polylysine of generation 2, 3 and 4 were provided by Colcom Company as a part of a collaboration project. Diblock copolymers PEO-PAA and PAA-PNIPAM were purchased from PolymerSource and used without further purification. Ultrapure water ($\rho=18 \text{ M}\Omega \text{ cm}^{-1}$) was obtained from Aquadem apparatus.

B. Synthesis

1. Synthesis of HYPAM

See experimental section of chapter 2.

2. PICs formation



Scheme IV.1. Illustration of PICs formation experiments

PICs formation was carried out by slowly adding a block copolymer solution to a dendritic polymer solution using syringe pump. Both stock solutions were adjusted at neutral pH (using HCl and NaOH aqueous solutions). $\text{NH}_3^+/\text{COO}^-$ molar ratio varied from 1/0 to 1/1. Increasing volumes of block copolymer solution were added to a fixed volume of dendritic solution following by adding an adapted amount of water to have a constant concentration of dendritic polymers (0.1 wt.%) in the final mixture. Detailed experiments for the formation of $\text{H}_4@\text{PEO}_6\text{-b-PAA}_{6.5}$ were reported in Table IV.1.

Table IV.1. Establishment of NH_3^+ / COO^- molar ration for PICs formation

$\text{NH}_3^+ / \text{COO}^-$ molar ration	$V_{\text{water}} [\mu\text{L}]$	$V_{\text{H}_4 (0.1\%)} [\mu\text{L}]$	$V_{\text{PEO6-b-PAA6.5 (0.1\%)}} [\mu\text{L}]$
1/0	540	300	0
1/0.1	486	300	54
1/0.2	432	300	108
1/0.3	378	300	162
1/0.4	324	300	216
1/0.5	270	300	270
1/0.6	216	300	324
1/0.7	162	300	378
1/0.8	108	300	432
1/0.9	54	300	486
1/1	1	300	539

3. Dilutions

Dilution experiments were carried out by simple adding of water to preformed PICs solutions. Detailed experiments were reported in Table IV.2.

Table IV.2. Dilution experiments

Dilution ratio	$V_{\text{water}} [\mu\text{L}]$	$V_{\text{H}_4@\text{PEO6-b-PAA6.5 (0.1\%)}} [\mu\text{L}]$
2	100	100
3	133.3	66.6
4	150	50
5	160	40
6	166.6	33.3
7	171.4	28.6
8	175	25
9	177.8	22.2
10	180	20

4. Salt adding effect

In this experiment, 100 μL of preformed PICs solution were diluted with an adapted

amount of 1M NaCl solution following by adding a suitable amount of water to yield final NaCl concentration ranging from 0.1 to 0.5M. Detailed experiments were reported in Table IV.3.

Table IV.3. Salt adding experiments

$[NaCl]_{final} [M]$	$V_{water} [\mu L]$	$V_{H4@PEO6-b-PAA6.5 (0.1\%)} [\mu L]$	$V_{NaCl (1M)} [\mu L]$
0.1	80	100	20
0.2	60	100	40
0.3	40	100	60
0.4	20	100	80
0.5	0	100	100

C. Characterization techniques

1. Characterization of HYPAM

See experimental section of chapter 2.

2. Characterization of PICs

a) *Dynamic Light Scattering Measurements (DLS)*

DLS measurements were carried out at different temperatures with a Malvern Instrument Nano-ZS equipped with a He–Ne laser ($\lambda = 633$ nm). The correlation function was analyzed via the general purpose method (NNLS) to obtain the distribution of diffusion coefficients (D) of the solutes, and then the apparent equivalent hydrodynamic diameter (D_h) was determined using the Stokes–Einstein equation. Mean diameter values were obtained from five different runs. Standard deviations were evaluated from hydrodynamic diameter distribution.

b) *Transmission electron microscopy (TEM)*

A drop of the aqueous dispersion was placed on a formvar carbon-coated copper TEM grid (Ted Pella Inc.) and left to dry under air. For samples needing negative staining, the TEM grid was successively placed on a drop of the sample solution for 1min and on a drop of an aqueous solution of uranyl acetate (2 wt %, 30 s), after which the grid was then air dried before introduction into the electron microscope. To visualize mesoglobules, we heated polymer solutions (45°C) for 1 h prior to the deposit. The previously described procedure for

preparation of TEM grids was then employed; however, they were dried in an oven at 45°C. The samples were viewed with a MET Hitachi HT7700 transmission electron microscope operating at 80 kV accelerating voltage. Size-distribution histograms were determined by using magnified TEM images. The size distribution of the particles was determined by measuring a minimum of 200 particles of each sample, using WCIF Image J software. The size distributions observed were analyzed in terms of Gaussian statistics ($wc(\sigma)$).

3. Thermoresponsiveness characterization

a) *Differential Scanning Calorimetry (DSC)*

The thermal properties of the polymer were determined by DSC using a Mettler Toledo DSC 1 STARe System Thermal Analysis calorimeter equipped with a Gas Controller GC200. Solution samples were sealed in impermeable crucibles of 120 μ L. Transition temperatures were taken at the top of the DSC peaks as the temperature increased at different rates; 10, 5, 2 and 1 °C/min, and finally extrapolated to 0 °C/min. The variation of enthalpy was measured as the temperature increased at a rate of 10 °C/min.

b) *Ultraviolet-visible (UV-VIS)*

Transmittance of polymer aqueous solutions was recorded with a HP 8452A diode array spectrophotometer with increasing temperature at different heating rates. The cloud points were then calculated by the extrapolation to 0 °C min⁻¹ of the cloud points obtained from the inflexion point of each transmittance curve.

c) *Nuclear Magnetic Resonance (NMR)*

To determine the structural characteristics of the PICs, NMR experiments were performed at 298K and 313K on a Bruker AVANCE 500 MHz spectrometer equipped with a 5 mm Z-gradient TCI cryogenic probe. The 90° pulse length was 9 μ s, the sweep width was 10kHz and the acquisition time was 3.5 s. The scan number was adjusted to obtain a sufficient signal to noise ratio and the relaxation delay between transients was 3s. For 1D ¹H experiments, a 30° pulse was used.

d) *Diffusion coefficient measurement by NMR-DOSY (Diffusion Ordered Spectroscopy)*

The basic scheme for the characterization of diffusion is the pulse field gradient spin-echo (PFGSE). The measurement was carried out by observing the attenuation of the NMR signals during a delay surrounded by two pulsed field gradients. In practice, a series of NMR diffusion spectra were acquired as a function of the gradient strength (g). The intensities of

the resonances follow an exponential decay which depends on the self-diffusion coefficient (D). Their relationship is given by the Stejskal-Tanner relation: $I/I_0 = \exp[\gamma^2 g^2 \delta^2 (\Delta - \delta/3) D]$ where I is the measured signal intensity, I_0 is the signal intensity for a g value of 0 G/cm, γ is the gyromagnetic ratio for the ^1H nucleus, δ is the gradient pulse length, Δ is the time between the two gradients in the pulse sequence. D values are function of temperature and viscosity as indicated from the Stokes-Einstein equation: $D = kT/6\pi\eta R_h$ (where k = Boltzmann constant, T temperature, η viscosity of the solution and R_h is the radius of the solvated species). The Z pulsed field gradients were generated with a 10 A GRASP II/P gradient amplifier. Thus, the z-maximum gradient strength (g) was 53.5 G/cm. Experiments were performed by varying g and keeping all other timing parameters constant. Typically, the Δ and the δ durations were 100 ms and 1ms, respectively and g was varied from 2.675 (strength of 5%) to 50.825 (strength of 95%) G/cm by 3% steps. An NMR pulse sequence with a stimulated echo bipolar gradient pulse pair and one spoil gradient was used (pulse program named `stebpgp1s` in the Bruker library). The data were analyzed by maximum-entropy with the DOSY module of NMR notebook software (NMRtec). The DOSY processing algorithm parameter was set to 3 and the data were processed with a diffusion window from 0,1 to 25000 $\mu\text{m}^2/\text{s}$.

References

1. Marty, J.D., et al., Hyperbranched polyamidoamine as stabilizer for catalytically active nanoparticles in water. *Journal of Colloid and Interface Science*, 2008. **326**(1): p. 51-54.
2. Hernandez-Ainsa, S., et al., Nanoobjects coming from mesomorphic ionic PAMAM dendrimers. *Soft Matter*, 2011. **7**(6): p. 2560-2568.
3. Johnson, C.S., Diffusion ordered nuclear magnetic resonance spectroscopy: principles and applications. *Progress in Nuclear Magnetic Resonance Spectroscopy*, 1999. **34**(3-4): p. 203-256.
4. Price, W.S., Pulsed-field gradient nuclear magnetic resonance as a tool for studying translational diffusion .1. Basic theory. *Concepts in Magnetic Resonance*, 1997. **9**(5): p. 299-336.
5. Price, W.S., Pulsed-field gradient nuclear magnetic resonance as a tool for studying translational diffusion: Part II. Experimental aspects. *Concepts in Magnetic Resonance*, 1998. **10**(4): p. 197-237.
6. Stejskal, E.O. and J.E. Tanner, SPIN DIFFUSION MEASUREMENTS: SPIN ECHOES IN THE PRESENCE OF A TIME-DEPENDENT FIELD GRADIENT. *Journal of Chemical Physics*, 1965. **42**(1): p. 288-+.
7. Delsuc, M.A. and T.E. Malliavin, Maximum entropy processing of DOSY NMR spectra. *Analytical Chemistry*, 1998. **70**(10): p. 2146-2148.

8. Fritzing, B., et al., In Situ Observation of Rapid Ligand Exchange in Colloidal Nanocrystal Suspensions Using Transfer NOE Nuclear Magnetic Resonance Spectroscopy. *Journal of the American Chemical Society*, 2009. **131**(8): p. 3024-3032.
9. Stott, K., et al., One-dimensional NOE experiments using pulsed field gradients. *Journal of Magnetic Resonance*, 1997. **125**(2): p. 302-324.

Thesis summary

Thesis summary

Résumé en français

Ces travaux de thèse portent sur la synthèse de copolymères cœur-couronne de cœur hyper-ramifié, l'étude de leur capacité à s'auto-organiser sans solvant et en solutions aqueuses, d'une part diluées et d'autre part, concentrées (gel). Ces différentes phases organisées sont ensuite mises à profit soit pour stabiliser des nanoparticules (NP) d'or préformées, soit pour contrôler leur synthèse *in situ*.

Les polymères dendritiques ont une forme globulaire et possèdent de nombreux groupes fonctionnels sur la surface. Ces groupes fonctionnels peuvent être modifiés de façon covalente ou non-covalente par des polymères, copolymères, tensioactifs ... conduisant à des structures cœur-couronne. Dans le cadre de ce travail, différents types de polymères dendritiques ont été utilisés : des hyperbranchés polyamidoamines (HYPAM), ou dendrimères polyamidoamines (PAMAM) et des dendrigrafts de lysine (DGL).

Sont décrites, tout d'abord, la synthèse et la caractérisation de trois HYPAM de différentes masses molaires (5200, 13000, 27000 g/mol), analogues aux dendrimères PAMAM de trois générations G3, G4 et G5. Sur ces cœurs sont greffés, par des liens covalents, des polymères linéaires thermosensibles, PNIPAM, de différentes longueurs de chaînes (2000g/mol, 5000g/mol et 7000g/mol). Pour une étude comparative, une molécule ayant trois branches (trisamine) est également utilisée comme cœur. Ces polymères cœur-couronne obtenus ont un caractère thermosensible dans l'eau qui peut être modulé en fonction des structures et des concentrations.

En solution à 0,1% en masse, au delà de la température de transition, ils s'auto-organisent pour former des objets de diamètre d'une centaine de nanomètres. La relation entre l'architecture macromoléculaire et ses propriétés thermosensibles a pu ainsi être mise en évidence.

A 20% en masse, au-delà de la température de transition du PNIPAM, des phases gel sont obtenues. L'effet de structure de cœur sur le caractère thermosensible, l'aspect mécanique ainsi que sur la structure des gels formés a été systématiquement étudié.

Dans une deuxième partie, les cœurs HYPAM, DGL, PAMAM ont été modifiés par interactions ioniques avec le tensioactif dodécyle sulfate de sodium (SDS). En fonction de la structure du cœur, les complexes ioniques formés présentent éventuellement un caractère cristallin thermotrope, c'est-à-dire qu'ils s'auto-organisent sans solvant. Des phases lamellaires et colonnaires ont aussi été identifiées pour les complexes HYPAM-sulfate de dodécyle. L'effet de structure du cœur et la balance entre les parties hydrophobe/hydrophile sur le caractère cristallin a été systématiquement étudiés.

Dans une troisième partie, les cœurs HYPAM, DGL, PAMAM ont été fonctionnalisés par des interactions ioniques multiples avec des copolymères poly(éthylène oxyde)-b-poly(acide d'acrylique) (PEO-PAA) de différents longueurs de chaînes ainsi qu'avec des copolymères thermosensibles PNIPAM-PAA. La taille et la stabilité, vis-à-vis d'une augmentation de la force ionique ou sous l'effet de la dilution, des objets formés en solution aqueuse ont été évaluées. La stabilité de ces agrégats appelés « Polyion Complexes » PICs ont été systématiquement étudiés vis-à-vis d'un changement de composition soit du cœur DGLs, HYPAMs, PAMAMs, soit de la couronne (PEO, PAA de différentes longueurs de chaînes), d'une addition de sels, ou de la dilution.

Ces dernières années, de nombreux travaux ont porté sur de nouvelles méthodes

Thesis summary

permettant de contrôler la taille et la forme de matériaux nanostructurés. En particulier, l'utilisation de systèmes auto-assemblés comme « soft-template » pour générer des nanostructures anisotropes et nanomatériaux hybrides ont reçu beaucoup d'attention.

C'est pourquoi, les systèmes auto-assemblés de copolymères hyperbranchés cœur-couronne (micelles, phases gels, cristaux liquides) ont été utilisés pour stabiliser ainsi que pour synthétiser *in situ* des nanoparticules d'or. L'incorporation de ces nanoparticules dans différentes phases (gel, cristal liquide, micelle), l'effet template de ces systèmes sur la taille et la forme des nanoparticules formées ainsi que les propriétés originales des nanohybrides (mécaniques, caractère mésomorphe, stabilité..) ont été étudiés. La synthèse de nanoparticules d'or dans les phases gels a permis notamment la formation d'hydrogels où les nanoparticules agissent comme des points de réticulation.

Ces systèmes auto-organisés de copolymères dendritiques cœur-couronne sont prometteurs pour créer des nanomatériaux hybrides avec d'autres nanoparticules (Ag ...) et ouvrent ainsi des applications dans l'électronique ou l'optique ou la biologie.

English summary

This thesis is focused on the synthesis of hyperbranched core-shell copolymers and the study of their self-organization in mass (liquid crystals), in diluted concentration (lyotropic phase) or concentrated solution (gel). Then, these organized phases are utilized to stabilize gold nanoparticles or control their *in situ* synthesis.

Dendritic polymers have a globular shape and possess numerous functional groups on their surface. These functional groups may be covalently or non-covalently modified by polymers, copolymers or surfactants leading to core-shell structures. As part of this work, different types of dendritic polymers were used: polyamidoamine hyperbranched polymers (HYPAM) or polyamidoamine dendrimers (PAMAM) and polylysine dendrigrafts (DGL).

Hyperbranched polyamidoamine (HYPAM) analogous to PAMAM dendrimer were successfully synthesized by one-step reaction. Stoichiometric adjusting of the reagents led to various polymer molecular weights which are equivalent to the ones of PAMAM dendrimer of generations 2, 3 and 4. Like PAMAM dendrimers, HYPAMs possess plenty of primary amine groups on the surface. Thank to these primary amine groups, the hyperbranched polymers were covalently modified by poly(N-isopropylacrylamide) thermoresponsive polymers (PNIPAM) of different chain lengths. For a comparative study, a molecule with three branches (trisamine) was also used as a core.

These core-shell polymers contain PNIPAM shells and hence they are thermoresponsive in water. At 0.1 weight % solution of polymer, beyond the transition temperature of PNIPAM, they self-assemble to form objects with an average radius of a hundred nanometers. The effect of the hyperbranched and branched cores on the thermoresponsive property was analyzed.

Above 20wt.% of polymers, beyond the transition temperature, the solution forms a gel phase. The effect of the core structure on the thermoresponsive characters, mechanical properties of the gels as well as on the structure of formed gels was systematically studied.

In the second part, HYPAM, DGL, PAMAM cores were also modified by ionic interactions with the surfactant sodium dodecyl sulfate (SDS). Depending on the structure of the cores, ionic complexes present thermotropic liquid crystal character, which means they can self-organize in mesophases without solvent. Lamellar and columnar phases were identified for complex HYPAM dodecyl sulfate. The effect of the core structures and the hydrophobic/hydrophilic composition balance on the liquid crystal properties was systematically studied.

In a third part, HYPAM, DGL, PAMAM core were functionalized by multiple ionic interactions with poly(ethylene oxide)-poly(acrylic acid) (PEO-PAA) block copolymers of different chain lengths as well as with thermosensitive PNIPAM-PAA block copolymers to form dendritic based polyioncomplex (PICs). These aggregates are sensitive to external stimuli such as: dilution, pH, ionic strength, temperature ... Change in the composition of the cores (DGLs, HYPAMs, PAMAMs) or shells (PEO, PAA of different chain lengths, PNIPAM), addition of salts, or dilutions effects on PICs stability are systematically studied.

In recent years, much effort has been made to develop new methods to control the size and shape of nanostructured materials. In this context, the use of self-assembled polymer systems as "soft-template" to generate anisotropic nanostructures and nanomaterial hybrid systems has

Thesis summary

received much attention.

As part of this work, self-assembled systems based on core-shell dendritic copolymers (lyotropic aggregates, phase gels, liquid crystals) were used to *in situ* synthesize gold nanoparticles as well as to stabilize preformed gold NPs.

The objective was not only the synthesis and stabilization of Au NPs within host structures but also to study the effect of Au NPs incorporation on the properties of the hybrid materials. This was achieved using different strategies *in situ* approach or *ex situ* approach. In the *in situ* approach, the reduction of Au^{III} to Au⁰ takes place in the host structure while in the *ex situ* approach preformed Au NPs were introduced in the host structures; the choice of which depended on the desired properties of the final materials.

The self-assembled structures of core-shell polymers showed ability to act as soft-template for the formation of AuNPs and also as stabilizers for preformed AuNPs. Conversely, this work has also demonstrated that the presence of AuNPs affects the properties of the hybrid structures.

In diluted solution, *in situ* and *ex situ* approaches were successfully adopted to synthesize thermoresponsive nanoparticles. Linear, branched and hyperbranched PNIPAM based polymers modify the size of the *in situ* synthesized Au NPs. In *ex situ* approach, they showed the ability to protect the preformed AuNPs against salt addition up to 1M at very low concentration of polymers (down to 10⁻⁴ wt. %).

The synthesis of gold nanoparticles in the gel networks allowed the formation of hydrogel hybrids where the nanoparticles act as crosslinking points and thus increase the mechanical properties of the hydrogels. Inversely, the sizes of the Au NPs were governed by the structure of the gels related to the linear branched or hyperbranched structure.

Homogeneous gold nanoparticles/liquid crystals hybrid was successfully synthesized where the sizes of AuNPs were governed by the liquid crystal phases and the structure of the hyperbranched core. Inversely, liquid crystal phases were disturbed by the presence of the Au NPs.

These self-organized dendritic core-shell copolymers systems are promising for the elaboration of hybrid nanomaterials with other nanoparticles (Ag ...) and thus open the way to applications in electronics, optics or in the biological field.

Appendix

A.1. Liquid Crystal Optics: the principles

An incident ray passing through an isotropic medium follows Snell's law of refraction. In addition, the refractive index of the medium is independent of the direction of the incident beam. However crystalline solids and liquid crystals are optically anisotropic and therefore their refractive indices do depend on the polarization of the incident ray.

The majority of LC phases such as nematic and smectic-A LCs are optically positive materials. This means that the refractive index parallel (n_{\parallel}) to the optical axis is larger than the perpendicular one (n_{\perp}). Therefore $\Delta n = n_{\parallel} - n_{\perp} > 0$. In contrast, LC phases such as most cholesteric phases are said to be optically negative ($\Delta n = n_{\parallel} - n_{\perp} < 0$). The case of an optically positive material can be represented by an *indicatrix*, an ellipsoid with its long and short axes equal to the parallel and perpendicular refractive indices, respectively (See Figure A.1. Left). The reverse is true for an optically negative material, thus is represented by an ellipsoid with its long and short axes equal to the perpendicular and parallel refractive indices.

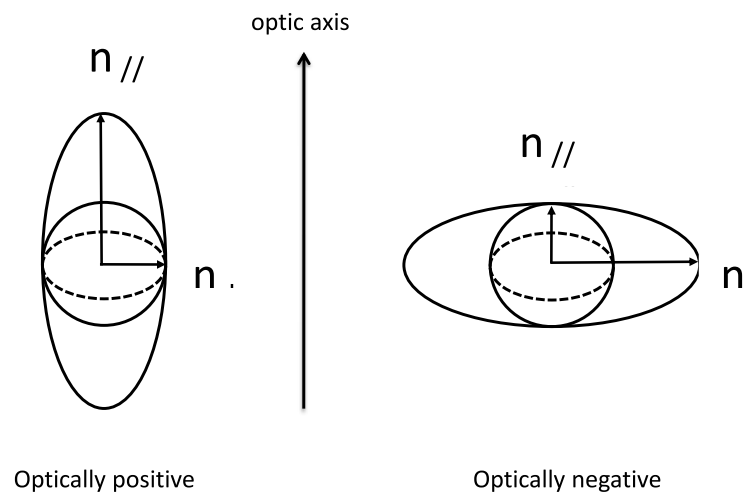


Figure A.1. Indicatrix for a uniaxial, optically positive material (left-hand side) and an optically negative material (right-hand side).

Light incident on a liquid crystal is split into two components; the ordinary and extraordinary rays (*birefringence*). The former is one that follows Snell's law and the latter does not. These two rays travel through the material at different velocities because they experience different refractive indices, n_o and n_e , therefore creating a phase difference δ , given by

Eqn. 1

$$\delta = \frac{2\pi}{\lambda} (n_e - n_o)d$$

where λ is the wavelength and d is the distance travelled in the medium. The refractive indices n_o and n_e are related to n_{\parallel} and n_{\perp} by

Eqn. 2

$$n_o = n_{\perp}$$

and

Eqn. 3

$$n_e = \frac{n_{\parallel} n_{\perp}}{\sqrt{n_{\parallel}^2 \cos^2 \phi + n_{\perp}^2 \sin^2 \phi}}$$

where ϕ is the angle between the optic axis and the direction of light propagation. When linearly polarized light is incident on a liquid crystal it is elliptically polarized and can go through crossed polarizers. The transmitted intensity is given by

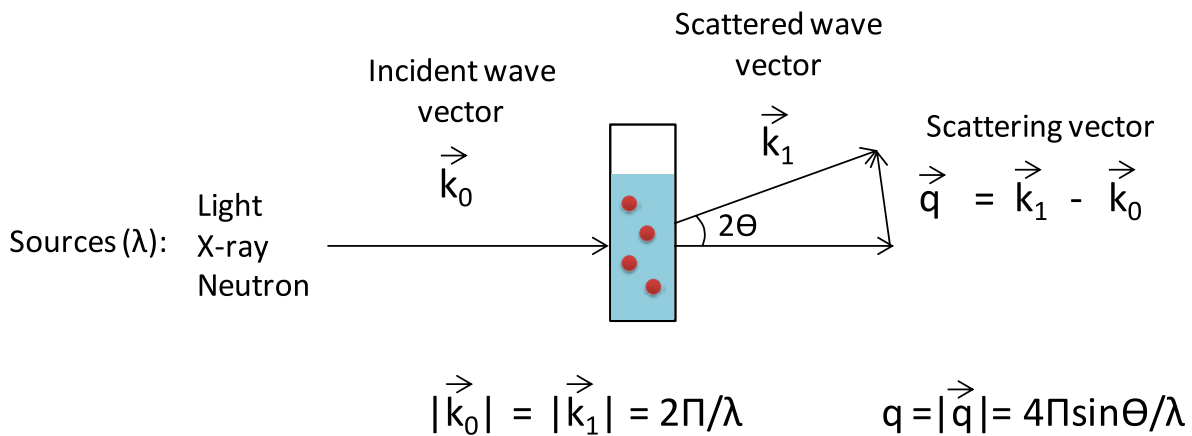
Eqn. 4

$$I = I_o \sin^2 2\phi \sin^2 \frac{\delta}{2}$$

where I_o is the light intensity after the polarizer and ϕ is the angle between the analyzer and the projection of the optic axis onto the sample plane. The first term is responsible for the changes in intensity when turning a LC sample between crossed polarizers, while the second is responsible for the variety of colours observed in LC textures.

Other LC phases such as the smectic-C involve a tilted organization of mesogens in the structure. These do not have a rotational symmetry around the optic axis and are said to be biaxial phases. In this case, three refractive indices are present and the optics become more complicated. Biaxiality is not discussed herein since such phases will not be encountered throughout this project.

A.2. Scattering techniques



In simple case:

Scattering intensity: $I(\mathbf{q}) = K \cdot F(\mathbf{q}) \cdot S(\mathbf{q})$

$F(\mathbf{q})$: form factor

$S(\mathbf{q})$: structure factor

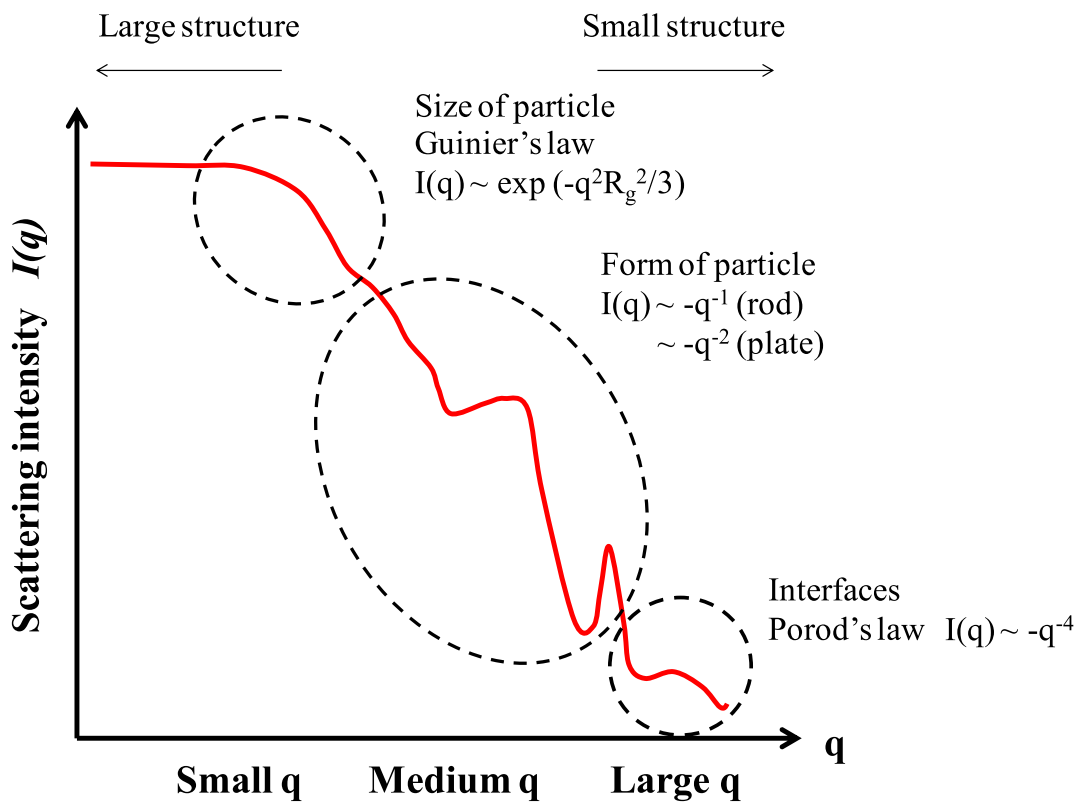


Figure A.2. $I(q) \sim q$ for scattering techniques, $q=2\pi/d$

A.2.1. Small angle neutron scattering (SANS): Calculation of R_g

The fit at small value of q by following Guinier's law permit to calculate the R_g

Regardless of particle shape, in conditions listed below:

- $q \cdot R_g < 1$
- Diluted solution, or no interaction between object
- Matrix or solvent scattering is removed

From Guinier's law :

Eqn 5

$$I(q) = I(0)\exp[-(q^2 R_g^2)/3]$$

Eqn 6

$$\ln I(q) = \ln I(0) - (R_g^2)/3 q^2$$

Tracing $\ln I(q)$ in function of q^2 , the slope of the fitted line at small q value is equal to $-(R_g^2)/3$, then the value of R_g can be induced.

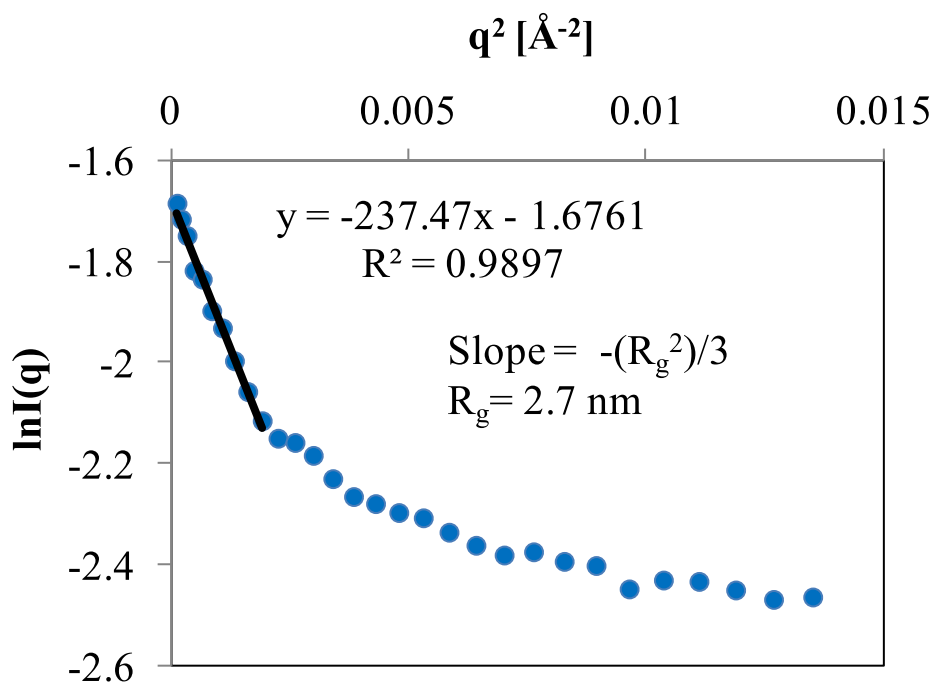


Figure A.3. $\ln I(q) \sim q^2$ of H4 at 0.1 wt% solution in D_2O

A2.2 SANS: Fractal model

Models for monodisperse spheres were used

DESCRIPTION

The scattering from fractal-like aggregates built from spherical building blocks was calculated following the Teixeira reference.

A commercially available routine was used to calculate the number density, aggregation number, and other parameters based on the volume fraction and polydisperse articles volume (weighted using the 3 rd moment of the radius).

VARIABLES

Input variables (default values):

Point	Parameters-fra	Coef-fra
1	Volume fraction (scale)	0.05
2	Block radius (A)	5
3	Fractal dimension	2
4	Correlation length (A)	100
5	SLD block (A-2)	2×10^{-6}
6	SLD solvent (A-2)	6.5×10^{-6}
7	bkgd ($\text{cm}^{-1} \text{sr}^{-1}$)	0

USAGE NOTES

The returned value is scaled to units of [$\text{cm}^{-1} \text{s r}^{-1}$]

The scattering intensity $I(q)$ is calculated by:

$$I(q) = P(q) S(q) + \text{bkgd}$$

Where $P(q)$ is the scattering from randomly distributed spherical “building block” particles, having radius $R_0 = w[1]$, volume fraction $\Phi = w[0]$, scattering length density $\Delta\rho = w[4] - w[5]$ and bkgd stands for the residual background.

$$P(q) = \Phi V_p \Delta\rho^2 F(qR_0)^2$$

Where $V_p = 4/3\pi R^3$ and

$$F(x) = \frac{3[\sin(x) - x\cos(x)]}{x^3}$$

The spherical building blocks aggregate to form fractal-like clusters. The clusters have a correlation length $\xi = w[3]$ corresponding to their overall size, and self-similarity dimension $D_f = w[2]$. From Teixeira reference, the interference from building blocks of fractal-like cluster can be calculated from expression:

$$S(q) = 1 + \frac{\sin [(D_f - 1)\tan^{-1}(q \xi)]}{(qR_0)^{D_f}} \frac{D_f \Gamma(D_f - 1)}{[1 + 1/(q^2 \xi^2)]^{(D_f - 1)/2}}$$

The macro “NumberDensity_Fractal” calculates the number density of building blocks $N_o = \Phi/V_p$, and the mean number of blocks per cluster, aggregation number $G = S(0) = r(D+1)(\xi/R_o)^D$, and the Guinier radius of cluster, $R_g^2 = D(D+1)\xi^2/2$

$W[0]$ (scale) and $(w[4]-w[5])^2$ (contrast) are multiplicative factors in the model and are perfectly correlated. Only one of these parameters should be left free during model fitting.

Reference: J. Teixeira, (1988) J. Appl. Cryst., vol. 21 p781-785

A.2.3 Calculation for SAXS

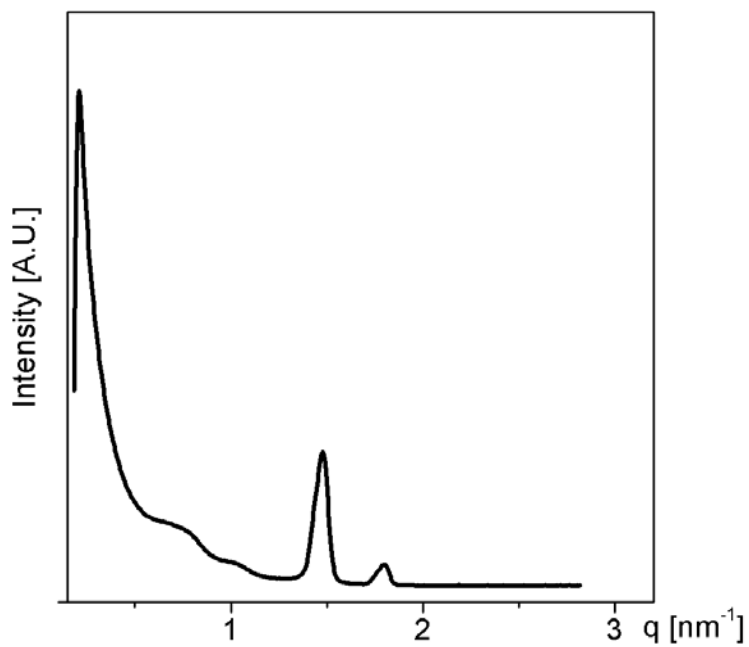
Table 16.1. Lyotropic liquid crystalline mesophases that are currently recognized; the ratio s of spacings between allowed (reciprocal) lattice Bragg reflections are listed

Class	Mesophase	Descriptor (homogeneity index, γ , g)	Symmetry (dimensionality)	Peak ratios (observed reciprocal spacings) or (hk) (2D), (hkl) (3D) reflections	Notes All phases have diffuse ca. 4.2 \AA^{-1} wide-angle scattering peaks, except L_{β}
<i>Smectic</i>	Lamellar	L_{α}, L_{β}	Smectic (1D)	1:2:3:4... etc.	Gel phase, L_{β} , also has 2D chain (wide-angle) lattice
<i>Mesh</i>	Rhombohedral	R_1, R_2	(1D)	1:2:3:4... etc.	Turbostratic (no in-plane register between sheets) Dependent on a cell parameters ^d
	Tetragonal	T_1, T_2	$R\bar{3}m$ (3D) (1D) I422 (3D)	(003), (101), (012)... (006) (most intense reflections only) 1:2:3:4... etc. (002), (101), (110)... (103), ... (004)	Turbostratic Dependent on α, c cell parameters. $d^{-2} = (h\alpha^*)^2 + (k\alpha^*)^2 + (lc^*)^2$
<i>Sponge</i>	Bicontinuous cubics (V_1, V_2)	P ($Q^{229}, Im\bar{3}m$) (0.716,3,3)	$Im\bar{3}m$ (3D)	$\sqrt{2}:\sqrt{4}:\sqrt{6}:\sqrt{8}:\sqrt{10}$... etc. (most intense reflections only)	Other structures have been suggested: I-WP ($Im\bar{3}m$) (0.742,4,4)
		D ($Q^{224}, Pn\bar{3}m$) (0.750,2,3)	$Pn\bar{3}m$ (3D)	$\sqrt{2}:\sqrt{3}:\sqrt{4}:\sqrt{6}:\sqrt{8}$: ... etc.	F-RD ($Fm\bar{3}m$) (0.658,4,6)
		G ($Q^{230}, Ia\bar{3}d$) (0.766,5,3)	$Ia\bar{3}d$ (3D)	$\sqrt{6}:\sqrt{8}:\sqrt{14}:\sqrt{16}:\sqrt{18}:\sqrt{20}$ etc.	C(P) ($Im\bar{3}m$) (0.664,9,9)
<i>Columnar</i>	Hexagonal (H_1, H_2)	$p6m$	(2D)	$\sqrt{3}:\sqrt{4}:\sqrt{7}:\sqrt{12}$	-
	Ribbon	cmn (centred rectangular)	(2D)	(11):(20):(22):(31):(40):... etc.	“Intermediate” spacings depend on α, β parameters: $d^{-2} = (h\alpha^*)^2 + (k\beta^*)^2$
		$pmm, pgg, p2$	(2D)	-	Primitive rectangular and oblique phases also reported
<i>Micellar</i>	Discrete cubic (I_1, I_2)	-	bcc packing $Im\bar{3}m$ (3D)	$\sqrt{2}:\sqrt{4}:\sqrt{6}:\sqrt{8}:\sqrt{10}$... etc.	Bilayer lines the faces of the Kelvin foam
		-	fcc packing $Fm\bar{3}m$ (3D)	$\sqrt{3}:\sqrt{4}:\sqrt{8}:\sqrt{11}:\sqrt{12}$... etc.	-
		-	$Pm\bar{3}n$ (3D)	$\sqrt{2}:\sqrt{4}:\sqrt{5}:\sqrt{6}:\sqrt{8}$: ... etc.	Clathrate
		-	$Fd\bar{3}m$ (3D)	$\sqrt{3}:\sqrt{8}:\sqrt{11}:\sqrt{12}:\sqrt{16}$	Clathrate (two distinct micelles)
	Hexagonal micellar	-	$P6_3mmc$ (3D)	$\sqrt{(4/3)}:\sqrt{(4/R^2)}:\sqrt{(4/3 + 1/R^2)}:$ $\sqrt{(4/3 + 4/R^2)}:\sqrt{4}$	One case reported to date ($R = 1.6$) ^b

For H4-DS100 compound:

$$q=2\pi/d$$

At 20°C



20°C

q- measured	hk^b	d^a	q- calculated
0.77	10	8.06	0.78
1.05	11	5.93	1.06
1.47	02	4.33	1.45
1.8	21	3.51	1.79

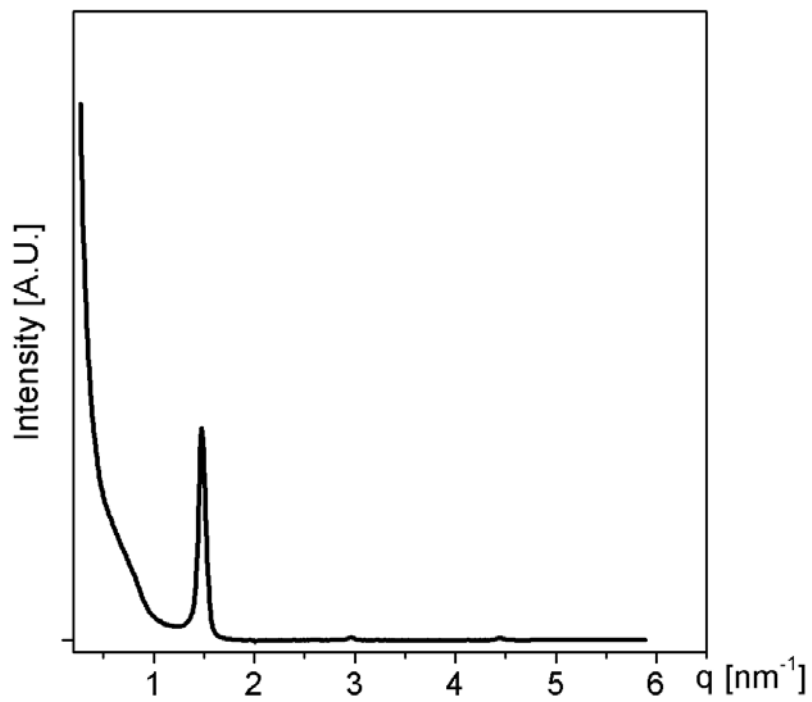
^a calculated using $d = 2\pi/q$

^b hk=Miller indice

structure

p2mg	a	8.06
	b	8.67

At 40°C



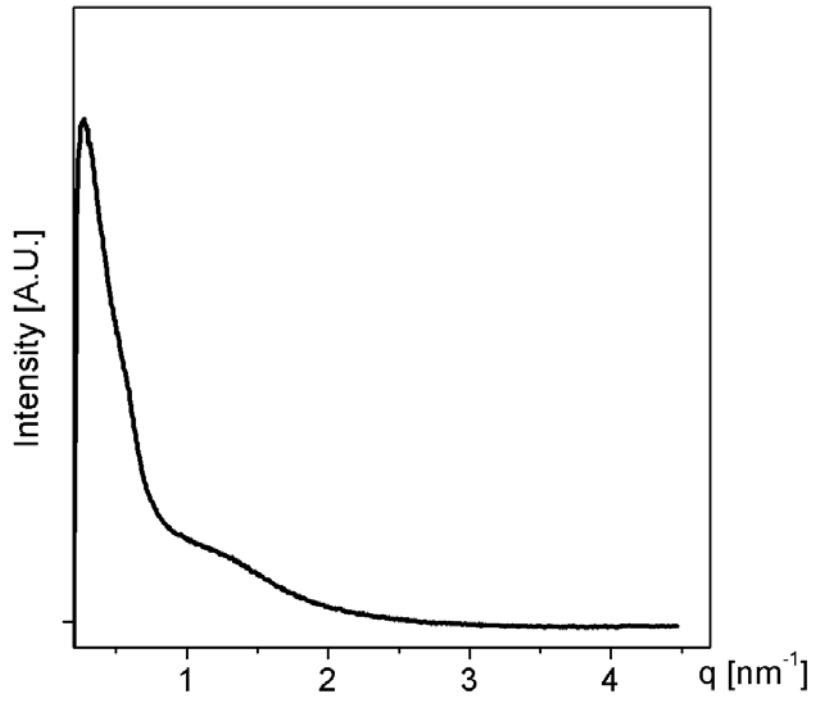
40°C

q- measured	hk	d
1.49	10	4.22
2.98	20	2.11
4.47	30	1.41

structure

lamellar	a	4.22
-----------------	----------	------

At 63°C

**63°C****isotropic**

Hong Hanh NGUYEN

Core-shell structures based on dendritic polymers sensitive to external stimuli: applications to the synthesis of gold nanohybrid materials

Supervisors : Prof. Nancy LAUTH-de-VIGUERIE and Dr. Jean-Daniel MARTY

Defended on 28th October 2014 in Toulouse

The work presented in this manuscript describes the design and synthesis of core-shell architectures based on dendritic polymers, as well as the different assemblage states of those polymers (lyotropic phases, hydrogels, liquid crystals) and finally the incorporation of gold nanoparticles inside such systems. Different types of cores were used in this project: polyamidoamine hyperbranched polymers, polyamidoamine dendrimers and polylysine dendrigrafts. These cores were functionalized either with thermoresponsive poly(N-isopropylacrylamide) via an amide coupling, or with sodium dodecyl sulfate surfactant by ionic interactions, or with ionic block copolymers also by ionic interactions. The core-shell polymers organized into aggregates in aqueous solution, gels or liquid crystals depending on their architectures and their environment. All the phases formed by these structures were used to *in situ* synthesize gold nanoparticles as well as to stabilize preformed gold nanoparticles. The changes in these phases induced by the incorporation of nanoparticles as well as the properties of the hybrid systems (mechanical, liquid crystal character, stability ...) were presented. Furthermore, the « soft-template » effect of these systems on the size of the *in situ* formed nanoparticles was studied. The size of gold nanoparticles was governed by the nature of the assembled phase related to the structure of the hyperbranched polymer.

Keywords : Hyperbranched polymer, hydrogel, liquid crystal, thermoresponsive, gold nanoparticle, nanohybrid.

Laboratoire des Interactions Moléculaire et Réactivité Chimique et Photochimique, UMR5623, Université Paul Sabatier, Bât 2R1, 118 route de Narbonne, 31062 Toulouse.

Hong Hanh NGUYEN

Structures cœur-couronne répondant à un stimulus à base de polymères dendritiques : applications à la synthèse de matériaux hybride

Directeurs de thèse : Prof. Nancy LAUTH-de-VIGUERIE et Dr. Jean-Daniel MARTY

Soutenue le 28 Octobre 2014 à Toulouse

Le travail présenté dans ce manuscrit décrit la conception et la synthèse d'architectures cœur-couronnes à base de polymères dendritiques, ainsi que les différents états d'assemblage de ces polymères (phases lyotropes, hydrogels, cristaux liquides) et enfin l'incorporation de nanoparticules d'or dans ces systèmes. Différents types de cœurs ont été utilisés dans ce projet: des polymères hyper-ramifiés polyamidoamine, des dendrimères de polyamidoamine et des dendrigrafts de polylysine. Ces cœurs ont été fonctionnalisés soit avec un polymère thermosensible de type poly(N-isopropylacrylamide) via un couplage amide, soit avec un tensio-actif comme le dodécyl sulfate de sodium ou avec des copolymères présentant des séquences ioniques, ces deux derniers cas via des interactions ioniques. Les polymères cœur-couronne s'organisent en phases organisées lyotropes ou thermotropes en fonction de leurs architectures et de leur environnement. Les différentes phases formées par ces structures ont été utilisées pour stabiliser des nanoparticules d'or préformées ou pour les synthétiser *in situ*. L'influence de la présence de nanoparticules sur l'organisation du polymère et sur les propriétés des systèmes hybrides (mécaniques, stabilisation ...) a été étudiée. En outre, l'influence de ces systèmes sur la croissance de nanoparticules formées *in situ* a été évaluée. La taille des nanoparticules d'or est dictée par la nature de la phase organisée qui est elle-même liée à la structure du polymère hyper-ramifié.

Keywords : Polymère hyper-ramifié, hydrogel, cristal liquide, thermosensible, nanoparticule d'or, nanohybride.

Laboratoire des Interactions Moléculaire et Réactivité Chimique et Photochimique, UMR5623, Université Paul Sabatier, Bât 2R1, 118 route de Narbonne, 31062 Toulouse.